Inducing structural changes in biological polymers

Joanna Glab

Submitted in partial fulfillment of the requirements for the degree of
Doctor of Philosophy

School of Optometry and Vision Sciences, Cardiff University

May 2009

ProQuest LLC
789 East Eisenhower Parkway
P.O. Box 1346
Ann Arbor, MI 48106-1346

Declaration

This work has not previously been accepted in substance for any degree and is not concurrently submitted in candidature for any degree.

Signed ..... (candidate) Date 29th May 2009

STATEMENT 1

This thesis is being submitted in partial fulfilment of the requirements for the degree of PhD

Signed ..... (candidate) Date 29th May 2009

STATEMENT 2

This thesis is the result of my own independent work/investigation, except where otherwise stated.

Other sources are acknowledged by explicit references.

Signed ..... (candidate) Date 29th May 2009

STATEMENT 3

I hereby give consent for my thesis, if accepted, to be available for photocopying and for inter-library loan, and for the title and summary to be made available to outside organisations.

Signed ..... (candidate) Date 29th May 2009

Table of Contents

List of Figures

List of Tables

Abbreviations

DOPA – Dihydroxyphenylalanine

ECM – Extracellular Matrix

EM – Electron Microscopy

ESRF – European Synchrotron Research Facility

FTIR – Fourier Transform Infrared Spectroscopy

FWHM – Full Width at Half Maximum

MAGP – Microfibril-Associated Glycoprotein

MMP – Matrix Metalloproteinases

PBS – Phosphate Buffered Saline

RTT – Rat Tail Tendon

SAXS – Small-angle X-ray Scattering

SRS – Synchrotron Radiation Source

STEM – Scanning Transmission Electron Microscopy

TAMD – Theoretical Axial Mass Distribution

WAXS – Wide-angle X-ray Scattering

W-H – Williamson-Hall

X-FEL – X-ray Free Electron Laser

XPCS – X-ray photon correlation spectroscopy

Acknowledgements

I would like to thank Prof Tim Wess for his supervision during three years of this PhD project and my colleagues from the School of Optometry for their help and support: Lee Gonzalez, Dr Donna Lammie, Dr Clark Maxwell, Kate Thomas, Dr Carlo Knupp and Dr Linda Wess.

I would also like to thank Dr Chris Hall for his supervision during the early part of this project and all collaborators involved in the studies presented in this thesis: Dr Sarah Pearson, Dr Oscar Paris, Dr Lorenz-Mathias Stadler and Prof Peter Fratzl.

Since this project involved data collection at the synchrotron radiation sources, I would like to acknowledge the support of beamline scientists: Dr Guenter Grossmann and Dr Tina Geraki (station 2.1 SRS Daresbury) and Dr Anders Madsen (ID10, ESRF).

The support of The Science and Technology Facilities Council is gratefully acknowledged.

Abstract

The aim of the project is to investigate disorder induced into molecular structure of biological polymers by various extrinsic factors. This study focuses on two major proteins found in the extracellular matrix of connective tissues – collagen and fibrillin. Collagen is the most abundant protein in mammals and can be found in connective tissues providing the all important structural scaffolding for cells. It is mostly found in a highly ordered fibrillar form; however, various extrinsic factors can lead to its degradation and transformation into disordered gelatine. During degradation, the ordered structure of collagen is lost; triple helical molecules unfold into gelatine, however, it has been proposed that this process may involve different intermediate states depending on the treatment. The aim of this project is to identify and characterize these potential metastable states that occur during collagen transformation. Understanding of the underlying molecular transformations can be beneficial in medicine where gelatinisation of collagen is observed in malignant breast tissues (induced by metalloproteinases) or can be induced by heat during surgical treatment (e.g. laser based) or an intense X-ray beam (i.e. used as a sophisticated treatment of cancer). Investigation of induced alteration in biological tissues and other materials that contain collagen (historical parchment, leather) can also benefit biomaterial production and future designs in implant surgery and pharmacy, e.g. tissue-engineered skin substitutes.

The results presented in this thesis proved that the nature of collagen transformations varies depending on the treatment and the main findings, which were previously unobserved include: (1) identification of a novel collagen structure with an 80 nm axial periodicity (recorded during an intensive X-ray irradiation), (2) a novel 20 nm periodic structure (formed during UV irradiation) and (3) changes in collagen fibril diameter and interfibrillar spacing (observed in breast cancer tissues).

The second of the studied proteins, fibrillin, is a main component of fibrillin-rich microfibrils and plays a crucial role in providing elasticity to the majority of connective tissues. The study described here was designed to investigate the elastic response of fibrillin-rich microfibrils during controlled tissue extension, and hence the effect of the external factor – mechanical stress. The results gave a further insight into the basis of the elastic properties of fibrillin and have major implications for understanding the functionality and extensibility of fibrillin in connective tissues.

Thesis outline

Chapter One of this thesis introduces general information about collagen and fibrillin, examples of the external factors that can modify their molecular structure and possible molecular rearrangements found so far. The principles of X-ray radiation, small angle X-ray scattering and Fourier Transform Infrared spectroscopy (FTIR) techniques that were used in this work are described in Chapter Two. Chapter Three contains experimental details of the experiments performed.

Chapters Four to Six are detailed descriptions of five conducted studies: examining the effects of intensive X-ray dose (Chapter Four), UV-radiation (Chapter Five), Matrix Metalloproteinases (Chapter Six), temperature and *in-situ* metastasis (Chapter Six) on collagen molecular structure. Chapter Seven contains examination of effects of controlled tissue extension on the elastic properties of fibrillin-rich microfibrils. Each chapter contains brief introduction, material and methods, results and discussion. A results summary and conclusions are given in Chapter Eight.

1. Introduction

1.1. Connective tissues and the extracellular matrix

Connective tissue comprises a diverse group of several tissues that provide structure and support in living organisms. The specialized tissue types include: tendon, cartilage, bone and ligaments. A characteristic feature of connective tissue is the abundance of the extracellular matrix (ECM), a structure that surrounds connective tissue cells. The ECM is built by a large number of molecules that can be divided into four major classes (Hay, 1991): (1) collagens, (2) elastic fibres, (3) proteoglycans and (4) other structural glycoproteins. Together, these components provide support and elasticity to connective tissues. Apart from this role, ECM components are also thought to control cell growth and differentiation and to participate in cell migration (Bard, 1990). This section provides information about two of the major ECM macromolecules: collagen and a component of elastic fibres – fibrillin microfibrils.

1.1.1. Collagen

Collagen is the most abundant protein in mammals and can be found in connective tissues building structural scaffolding for cells. It is a main component of tissues such as skin, tendon, cornea and ligament where it is found mostly in a fibrillar form (Metcalfe and Ferguson, 2007). There are over 27 genetically different types of collagen (Kim et al., 2005), which are explained in section 1.1.1.1. The most abundant type is type I collagen, and the

collagen species mainly used in the studies presented here, therefore the information presented in this chapter will be focused on its structure and organization.

1.1.1.1. Types of collagen

Depending on the tissue source collagen occurs in different forms known as collagen types. Collagen types can be divided into three groups: (1) fibrillar collagens, (2) fibril-associated collagens and (3) network-forming collagens (Linsenmayer, 1991). Fibril-forming collagens such as type I-III, V and XI are found in most connective tissues (Metcalfe and Ferguson, 2007). For example, tendons consist mostly of Type I collagen (Bass et al., 1992) while in tissues such as skin, Type I collagen is accompanied by Type III collagen (approximately 20%) (Burgeson and Nimni, 1992). Type V collagen can be found in corneal stroma, while type XI is characteristic for cartilage (Holmes and Kadler, 2005; Ricard-Blum and Ruggiero, 2005). Several types of collagen form structures other than fibres. These include types: IV, VI, VIII, X and XIII, which are part of structures such as basement membranes or beaded microfilaments (Rest and Garrone, 1991; Metcalfe and Ferguson, 2007). Collagen types IX, XII and XIV are members of a group of fibril-associated collagens with interrupted triple helices (FACITs). They do not form fibrils but they participate in fibrillogenesis and accompany fibrils of other collagen types (e.g. type I) (Saika et al., 2001).

1.1.1.2. Levels of organization in type I collagen

Type I collagen is the most abundant among fibril forming collagens. It has a highly hierarchical structure which is responsible for visco-elastic properties of connective tissues

(Fratzl, Misof and Zizak, 1997). In the experiments described in this thesis, rat tail tendon was used as a source of collagen, since it is a useful model tissue that consists of >95% Type I collagen (Bass et al., 1992).

Figure 1.1 shows the hierarchical levels of organization in tendon. Collagen molecules (explained in section 1.1.1.3) are packed in an organized structure and form collagen fibrils. Fibrils, which are almost parallel to the tendon axis, are grouped into primary bundles (fibres), secondary bundles (fascicles) and in some cases tertiary bundles (Wang, 2006). Tendons are surrounded by the epitendon, a fine connective tissue sheath that reduces the friction during tendon movements (Kannus, 2000). Individual collagen fibres are bound together by a thin connective tissue network, endotendon. This structure is also responsible for carrying blood vessels and nerves to the deeper layers of tendon (Jozsa et al., 1991).

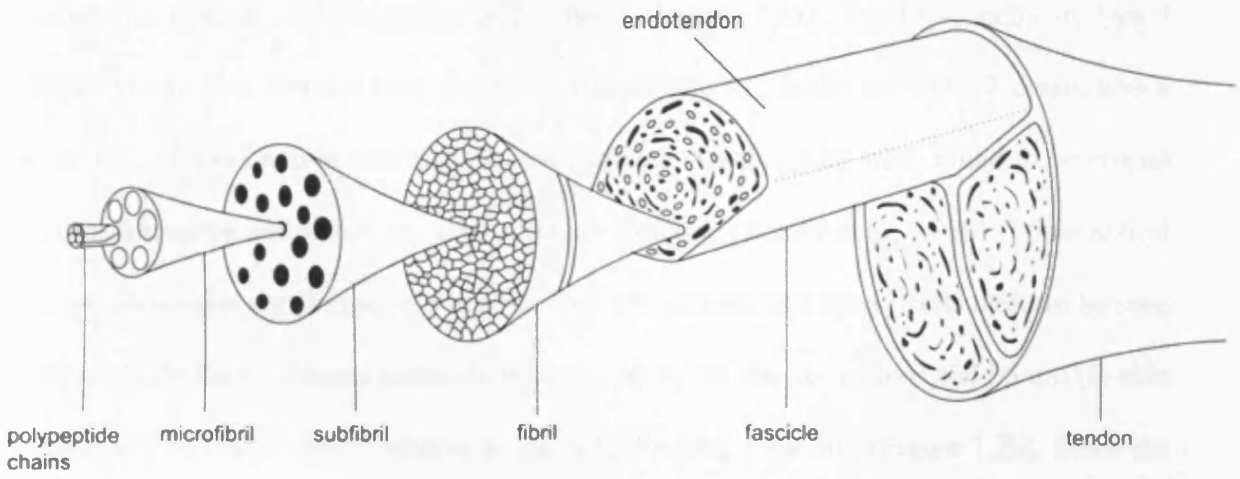

Figure 1.1. Levels of organization in tendon (adapted from (Kastelic, Galeski and Baer, 1978)). From left to right: parallel collagen molecules (triple helices) are aligned forming microfibrils, which then form subfibrils and fibrils. Collagen fibrils are grouped into fascicles, which are covered by a fine connective tissue network –the endotendon.

A characteristic crimp structure can be observed in the tendon fascicles. The wavy pattern has been observed using techniques such as X-ray diffraction, electron microscopy (EM) and optical coherence tomography (OCT) (Hansen, Weiss and Barton, 2002) and was characterized by a crimp period and a crimp angle (104 μm and ~26 degrees, respectively) which can be measured using polarizing optics (Kastelic, Palley and Baer, 1980; Nicholls et al., 1983). The collagen crimp was reported to disappear after about 3 % of strain application (Hansen et al., 2002).

1.1.1.3. Type I collagen molecular structure

The fundamental structural units of the fibrous collagen are collagen molecules, helical structures consisting of three polypeptide chains (Figure 1.2a). The triple helix of type I collagen is typically 300 nm long and it consists of two α1 chains and one α2 chain, which are flanked by short non-helical regions, telopeptides. Telopeptides were found to be crucial for fibril formation and stabilization of collagen structure (Kadler et al., 1996). Triple helical collagen molecules are aligned in a head-to-toe arrangement and form fibrils that can be seen in Figure 1.2b. Each collagen molecule is staggered by 67 nm (in tendon) and 65 nm (in skin (Stinson and Sweeny, 1980)) relative to the neighbouring molecule (Figure 1.2b). Since the length of a single collagen molecule is 300 nm, and a characteristic D-period is 67 nm, it can be easily calculated that each molecule consists of ~4.4D (Burgeson and Nimni, 1992). The non-integer length of the collagen molecule and the characteristic staggering gives rise to regions of low and high electron density (gap and overlap – Figure 1.2c) (Petruska and Hodge, 1964). This leads to the characteristic axial D-period that has been observed using various physical techniques (Worthington and Tomlin, 1955; Meek, Chapman and

Hardcastle, 1979). The 'gaps' are the low electron density zones between the neighbouring molecules and in negative stained electron micrographs these are the regions where stain accumulates (Chandross and Bear, 1973). Because there is no stain accumulation in 'overlap' zones, this leads to a characteristic banding pattern that can be observed using electron microscopy (Figure 1.3). Also, each gap-overlap repeat has a fixed size - in the native fibrils the overlap region is approximately 30 nm long (which correspond to 0.46D), and the gap region is approximately 36 nm long (=0.54D) (Chandross and Bear, 1973). The dimensions of a collagen molecule and gap and overlap regions are shown in Figure 1.2c.

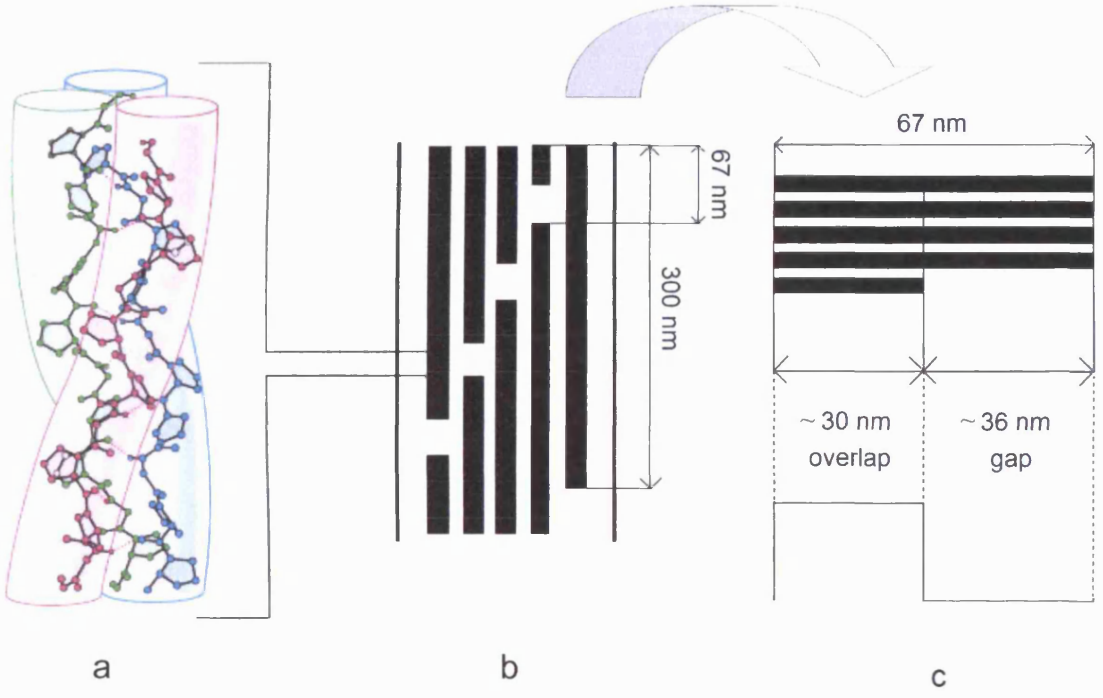

Figure 1.2. Molecular organization of collagen: (a) collagen triple helix, (b) collagen molecules staggered within the fibril (each line corresponds to an individual collagen molecule triplex). The 67 nm staggering and the non-integer length of the collagen molecule (300 nm = ~4.4D) leads to overlap and gap regions. (c) a D-period, built by four complete

segments (67 nm = 1D) and one, which corresponds to 0.46D (~30 nm). This arrangement produces a characteristic step function of electron density.

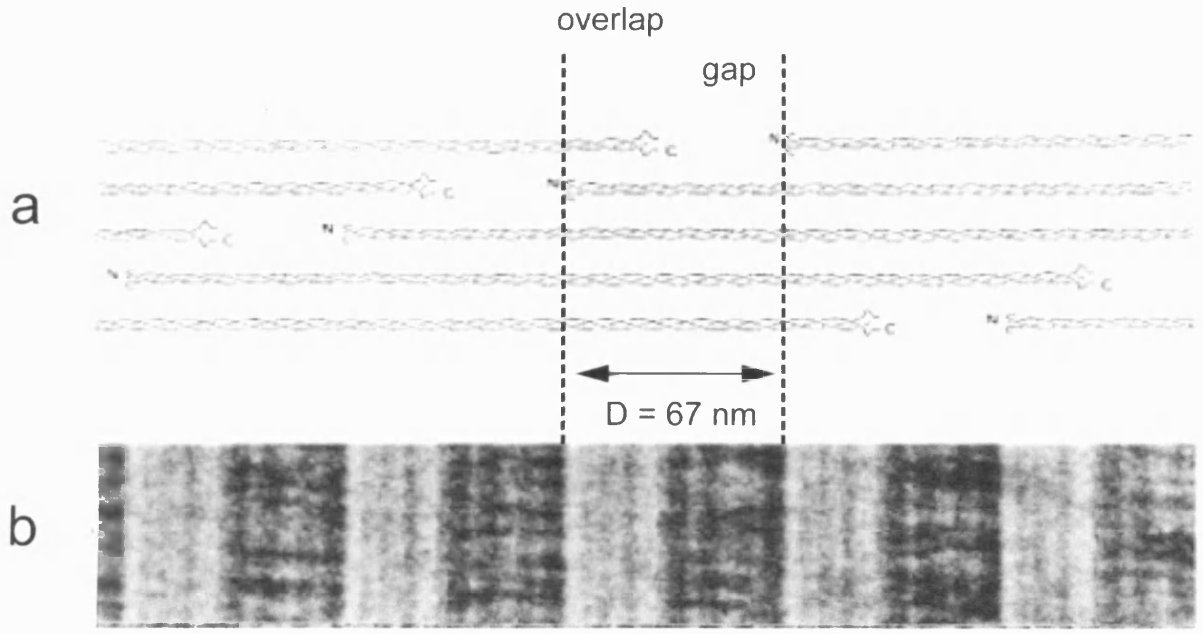

Figure 1.3. A schematic model of staggered collagen molecules with indicated gap and overlap regions (a), which give rise to a characteristic periodic banding pattern revealed by negatively stained EM micrograph (adapted from (Kadler et al., 1996)).

Several thousand collagen molecules are packed together forming fibrils, which are approximately cylindrical with 10-500 nm diameters (Hulmes et al., 1995). In some tissues, such as skin and cornea, where Type I collagen is also accompanied by Type III (skin) or Type V collagen (cornea) fibril diameters are highly regulated, i.e. ~ 90 and ~ 35 nm, respectively (Stinson and Sweeny, 1980; Newsome, Gross and Hassell, 1982). In tendon, which primarily consist of Type I collagen, fibril diameters are less uniform.

1.1.1.4. Collagen-water interactions

Water plays an important role in the formation of stable collagen structures. Collagen-rich tissues consist of approximately 50% water. There are subsets of water populations that surround individual triple helices, fill the gap zone in the hydrated state and surround the fibrils (Lees, 1986; Price, Lees and Kirschner, 1997). There are believed to be three main water fractions in collagen: (1) intrahelical water, the most tightly bound fraction that form water bridges and link the three helical strands, (2) intermolecular bound water, which can be found on the surface of fibrils and (3) bulk water, the mobile fraction that freezes at about 0°C (Price et al., 1997). The interaction with water is thought to be caused by the highly repetitive structure of collagen molecules and the high content of hydroxyproline (Bella, Brodsky and Berman, 1995). The removal of water from collagen results in a number of structural changes: a decrease of the axial period from 67 nm to 64 nm, alterations in the electron density distribution and an increase in the variability of molecular packing (Worthington and Tomlin, 1955; Chandross and Bear, 1973; Wess and Orgel, 2000). Detailed information about the effects of drying on collagen structure are provided in section 1.3.3.

1.1.2. Fibrillin microfibrils

The second extracellular matrix component used in the studies presented in this thesis, fibrillin-rich microfibrils have unique extensible properties and play a crucial role in providing elasticity to elastic and non-elastic connective tissues (Mecham and Heuser, 1991; Kielty et al., 2005). Microfibrils are built by several molecules; however the major component is a complex glycoprotein – fibrillin (Sakai, Keene and Engvall, 1986). The

importance of microfibrils has been highlighted by linking the mutations in the fibrillin gene to a Marfan syndrome, a severe heritable disorder.

1.1.2.1. Distribution and function

Fibrillin-rich microfibrils are widely distributed in elastin-containing tissues such as major blood vessels, lung, muscle and skin (Sakai et al., 1986; Davis, 1994). In these tissues they provide a structural lattice for elastin deposition; they were also reported to join elastic fibres together as well as link them to other extracellular matrix components, and are thought to be responsible for normal skin and muscle development (Mecham and Heuser, 1991; Kielty and Shuttleworth, 1993; Kielty and Shuttleworth, 1995). Microfibrils can also be found in elastin-free tissues such as ciliary zonules in the eye, a structure that plays a crucial role in the suspensory system of the lens (Bourge et al., 2007) (Figure 1.4). Mutations in the fibrillin-1 gene are linked to Marfan syndrome, a severe connective tissue disorder, which indicates a key role of microfibrils in providing reinforcement and elasticity (Dietz and Pyeritz, 1995) (Figure 1.4). In the ocular system, the symptoms of Marfan syndrome include dislocation of the ocular lens (Ectopia lentis – Figure 1.4) and a detachment of the retina, which results from the weakened connective tissue (Judge and Dietz, 2005). Other features of Marfan syndrome are associated with the skeletal system (overgrowth of the bones, scoliosis) and cardiovascular system (thickening of the valves) (Nollen and Mulder, 2004; Judge and Dietz, 2005).

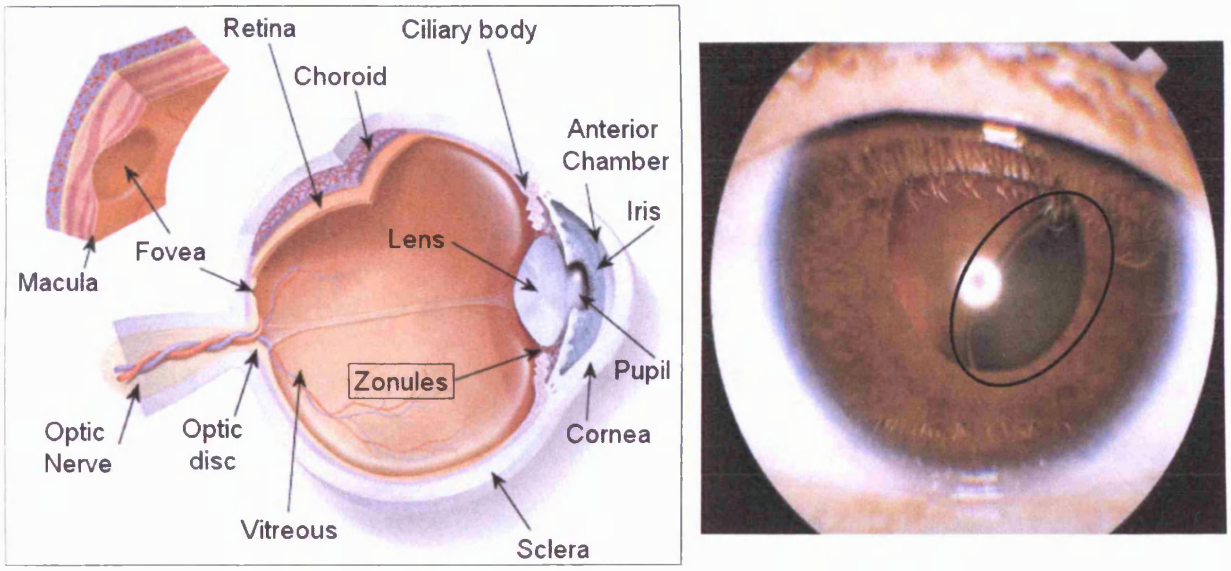

Figure 1.4. Zonular fibres in the eye (left panel) secure the lens in the optical axis and play an important role in the eye accommodation (source: www.gimbeleyecentre.com). Right: the eye of a person with Marfan syndrome – a genetic disorder that along with skeletal and cardiovascular abnormalities can result in lens dislocation – Ectopia lentis (the dislocated lens has been indicated on the image) (source: www.medstudents.com.br).

1.1.2.2. Fibrilin microfibril molecular structure

Electron microscopy studies revealed the structure of individual microfibrils as 'beads on a string' (Figure 1.5a). These regular beaded structures have a resting axial periodicity of approximately 56 nm, which is the generally accepted value (Wess, Purslow and Kielty, 1997; Sherratt et al., 2001; Kielty et al., 2002). A detailed study using Scanning Transmission Electron Microscopy (STEM) mass distribution analysis of microfibrils showed that there are characteristic minima and maxima along microfibrils that correspond to the observed interbead and bead regions (Sherratt et al., 1997). The authors suggested that the mass maxima that occur at the beads could be a result of macromolecules attached to the

microfibrils at regular intervals (every 56 nm) or that the molecules that build microfibrils are periodically folded (Figure 1.5b).

The diameter of microfibrils has been observed to vary from 10 to 40 nm depending upon the technique used (Sakai et al., 1986; Keene et al., 1991; Wallace, Streeten and Hanna, 1991; Hanssen, Franc and Garrone, 1998; Sherratt et al., 2003). It is unclear whether the difference is the result of changes in fibrillin diameter or sensitivity of the technique and different methods of microfibril extraction, hydration and sample preparation. It is therefore important to analyze those complex structures in their intact and native state.

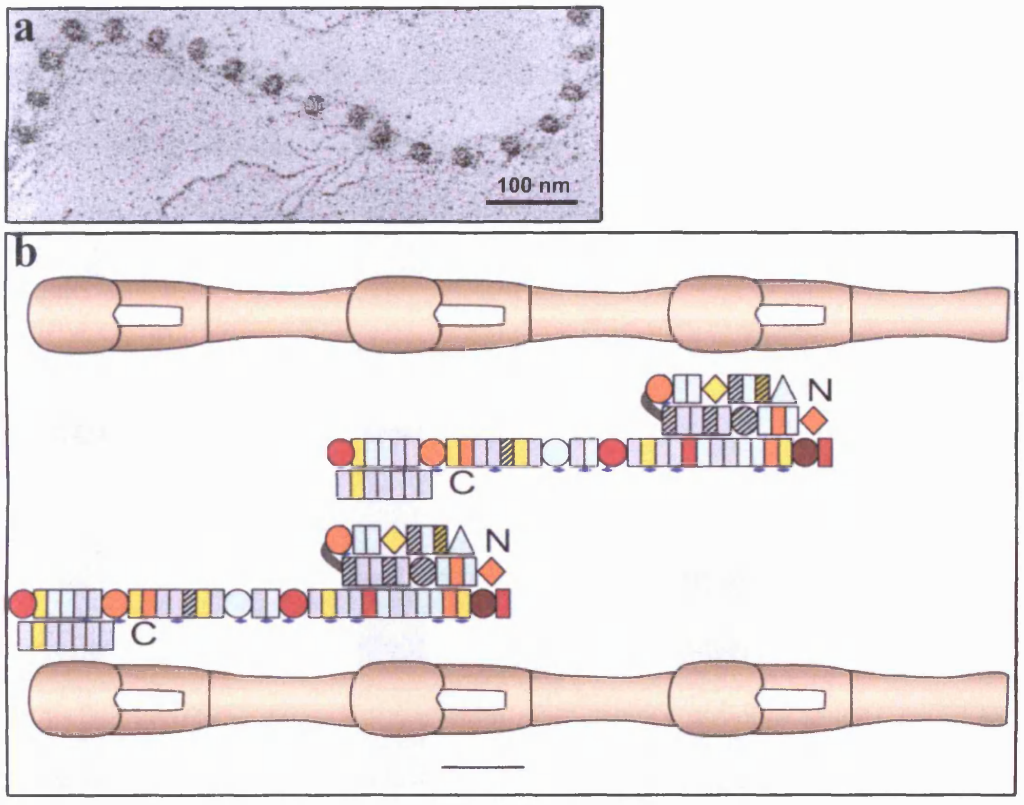

Figure 1.5.(a) Electron Micrograph of fibrillin-rich microfibrils that are characterized by a repeating "beads-on-a-string" appearance (reproduced from (Kuo et al., 2007)); (b) a schematic model of the microfibril with highly folded fibrillin molecules, based on a model proposed by (Baldock et al., 2001) (reproduced from (Cain et al., 2006)).

1.1.2.3. Fibrillin-1

The major component of fibrillin-rich microfibrils is a large multidomain glycoprotein, fibrillin-1 (Reinhardt et al., 1996; Handford et al., 2000). A single fibrillin molecule has been found to have a length of approximately 148 nm (Sakai et al., 1991), 143 nm (Sherratt et al., 2003) and 160 nm (Baldock et al., 2001) and was reported to contain specific sites of variable flexibility (Yuan et al., 2002; Lee et al., 2004). It is still poorly understood how fibrillin monomers are arranged within a microfibril; one of the models proposes that fibrillin monomers are highly folded within the microfibrils and that the reversibility of this folding arrangement is responsible for its elastic properties (Baldock et al., 2001). A simplified diagram of this alignment is shown in Figure 1.5b. This and other models that were proposed to explain the molecular organization of fibrillin within a microfibril are discussed in detail in Chapter Seven.

1.1.2.4. Other Microfibril Associated Molecules

Several other molecules apart from fibrillin-1 were identified to be associated with microfibrils. Fibrillin-2 and fibrillin-3 were found, however their expression was reported to be limited mainly to foetal tissues (Cain et al., 2006). Another protein found in the majority of fibrillin-rich tissues is MAGP-1 (Microfibril-Associated Glycoprotein) (Mecham and Heuser, 1991). Although it is an elastin-binding protein, it was also found in non-elastin zonular fibrils where it was specifically localized within the beads of the microfibrils (Gibson et al., 1996; Henderson et al., 1996). A recent study using mass spectroscopy showed that MAGP-1 is the only molecule observed in the fundamental microfibrillar structure in addition

to fibrillin (Cain et al., 2006). It was suggested that MAGP-1 may play a role in the stabilization of the head-to-tail organization of fibrillin molecules and also may be involved in lateral aggregation of microfibrils (Gibson et al., 1996). A study using quick-freeze deep-etch (QFDE) microscopy revealed a realistic view of the microfibril ultrastructure and showed small lateral filaments connecting microfibrils at regular intervals (Davis et al., 2002). These filaments were suggested to be aggregates of MAGP-1 which play an important role in the lateral organization of microfibrils. Another member of MAGP family is MAGP-2, however this glycoprotein is not distributed as widely as MAGP-1. MAGP-2 was found to be attached to microfibrils in the bead and a part of the interbead region and was suggested to take part in the stabilization of microfibrils (Hanssen et al., 2004).

1.2. External factors that can affect collagen and fibrillin structure

1.2.1. Alterations to collagen structure

Collagen-based materials are widely used in medicine, pharmacy, engineering and everyday life. Characteristic biomechanical properties of collagen that derives from its complex fibrillar structure makes it an important biomaterial used for implant surgery and a diagnostic tool for aberrant cell matrix remodelling. It is also a main component of parchment and leather and as gelatine it is widely used in photography, cosmetic and food industries. Collagen is commonly used in biomaterial production due to its easy availability (it is a main protein found in a mammalian body) and also low toxicity, low immune response, the ability to regulate cellular behaviour and promote cellular growth. Another advantage is the ability of collagen solutions to reconstitute into fibrillar structure *in vitro* (Sionkowska, 2000; Wang,

Li and Yost, 2005). These properties make collagen a useful material that can be used in various forms such as sponges, films and membranes (Rosso et al., 2005; Metcalfe and Ferguson, 2007).

Various external factors can cause a loss of structural integrity of collagen and lead to its transformation into disordered gelatine. It is important to understand changes that occur within collagen structure during degradation, since this knowledge can be used to control the process of transformation, e.g. in designing new materials. It is possible that degradation of collagen occurs via an intermediate, metastable state i.e. a novel structure that can potentially have improved properties. When the process of gelatinization is fully understood, potentially it can also be controlled, which would be of great benefit in biomaterial production.

The following subsections describe the factors that can cause various effects on long range order in collagen structure:

1.2.1.1. Effects of high temperature

Heating therapies are often used in cardiology, dermatology, neurosurgery, oncology, ophthalmology, orthopaedics and urology (Wright and Humphrey, 2002). Here, high temperatures are used to treat various injuries and diseases and during this process surrounding tissues such as skin are also affected. High temperature can cause denaturation of collagen molecules, i.e. unfolding of the triple helical structure into disordered gelatine. Thus it is essential to understand underlying molecular transformations to know how exposure to heat damage will alter the function and properties of collagen-rich tissues.

During the heating therapies, collagen subjected to high temperatures is present in a hydrated state. However, high temperatures can also be applied to the protein in a dry state. This

procedure (i.e. approximately 120°C dry heat) is called dehydrothermal treatment and it is used in medical sterilisation procedures for implant surgery or surgical practices that involve lasers. It has also been used as a non-toxic and inexpensive method of inducing crosslinks into collagen which improve its strength and stabilization (Gorham et al., 1992). In the studies of historical parchment and leather it also can be used as a simulation of accelerated ageing (Wess and Orgel, 2000).

1.2.1.2. Effects of X-ray radiation

X-rays are widely used in medicine e.g. in medical imaging and diagnosis (radiography) or as a part of cancer treatment (radiotherapy). The use of synchrotron X-ray radiation has been proposed as a sophisticated treatment of tumours (Blattmann et al., 2005). It was suggested that patients receive single exposures of the radiation, which is thought to suppress the clonogenicity of tumour cells (Blattmann et al., 2005). By using the synchrotron sources it is possible to generate X-ray beams of small widths that can be focused on a reduced tissue volume. This in turn enables the use of higher radiation intensities, which can target the tumour more effectively (Slatkin et al., 1995). The X-ray microbeams were reported to have a preferential effect on tumour tissues, i.e. tumour tissues fail to repair after the treatment, as opposed to the normal surrounding tissues that had higher tolerance for the dose (Dilmanian et al., 2003; Dilmanian et al., 2005). The effects of an intensive X-ray dose on the collagen axial structure have been investigated in Chapter Four of this thesis.

1.2.1.3. Effects of Metalloproteinases

Collagenases are a group of the Matrix Metalloproteinases (MMP) family that catalyze the degradation of native fibrillar collagen into thermally-unstable triple-helical fragments, which denature into gelatine (Ala-aho and Kahari, 2005). MMPs are involved in the degradation of extracellular matrix proteins and in normal tissues, the activity of collagenases is strictly controlled and they are usually expressed at low levels. However, their abnormal expression in breast tissue can lead to tumour growth, invasion and metastasis (Overall and Lopez-Otin, 2002). Breast cancer is a major cause of death in middle-aged woman hence understanding the specific pattern of collagen degradation in the tissue may be crucial for early diagnosis and prevention of cancer (Duffy et al., 2000). Detailed information on MMPs is provided in Chapter Five.

1.2.1.4. Effects of UV radiation

UVA (λ = 400 nm – 315 nm) and UVB (λ = 315 nm – 280 nm) radiation is a constant challenge to the skin and the most important factor in premature aging of this tissue (Giacomoni and D'Alessio, 1996; Rittie and Fisher, 2002). UVC (λ = 280 nm – 100 nm) treatment is also used as a cross linking agent in biomaterials (Sionkowska, 2000). It has also been used as a method of inducing cross-links and hence increasing stiffness into corneal collagen as a treatment in keratoconus (Spoerl, Huhle and Seiler, 1998; Wollensak, Spoerl and Seiler, 2003; Mencucci et al., 2007). The effects of UV irradiation (λ=254 nm) on collagen molecular structure have been investigated in Chapter Six of this thesis.

1.2.2. Mechanical effects on fibrillin structure

The abundance of collagen in connective tissues of animals makes it a model protein that can be easily studied. The understanding of its degradation and the effects of various external factors is beneficial in many fields, such as biomaterial production and medicine. The second studied protein, fibrillin, is rarely found in its pure form (it is usually accompanied by elastin – see section 1.1.2.1). An example of the elastin-free tissue is the zonular filament of the eye, where fibrillin microfibrils play a specific and a crucial role in providing elasticity to the connective tissue. Therefore, this study was focused on the understanding of the basis of fibrillin elasticity and the only external factor used here was a mechanical distortion (i.e. a controlled tissue extension). In the study described here alterations were induced into fibrillin molecular structure and in structural hierarchies. These changes were monitored *in-situ* and can provide new insights into understanding the functionality and extensibility of fibrillin in connective tissues.

1.3. Molecular alterations in collagen axial and fibrillar structure induced by external factors

Various external factors can cause alterations within the highly ordered collagen molecular structure. These factors, such as temperature, UV irradiation or mechanical stress that were explained in detail in the previous section, can be a constant challenge to collagen present in connective tissues of animals. They also affect other materials that contain collagen such as historical parchment or leather. Modifications induced in collagen structure can potentially

lead to its degradation; however, it is also possible that when collagen structure is altered it can result in the formation of structures with improved properties that can be used as novel biomaterials. It is therefore essential to identify and describe molecular alterations that occur in collagen structure. Understanding novel disordered states is also important in future design and development of drugs and in fundamental protein chemistry for better understanding of the molecular rearrangements.

This section provides a list of possible rearrangements within the collagen molecular structure; the following subsections describe potential changes that may occur at different levels of collagen organization, i.e. helical, molecular and fibrillar lengthscale.

1.3.1. Alteration in axial rise per residue

The characteristic axial periodicity of collagen in rat tail tendon is 67 nm which corresponds to 234 amino acid residues, i.e. the axial distance between amino acid residues in the collagen helix is 0.286 nm (Meek et al., 1979). Application of strain might however cause elongation of amino acids.

If the residues elongate all in the same way (for example to 0.299 nm) then it leads to an increase in pitch of the collagen helix, although the relative position of amino acids will not be altered. In this case the intensity values will remain unchanged and the only effect would be an alteration in D-period (increase in this example) and the lattice. The elongation of triple helices was suggested to be responsible for the initial increase of the D-period during the stretching of rat tail tendon (Folkhard et al., 1987; Fratzl et al., 1997; Puxkandl et al., 2002). On the other hand, processes such as dehydration might cause shortening of the helix pitch

which results in a reduced periodicity. This rearrangement was suggested as one of the mechanisms that caused a decrease of the D-period in dry tendons (Wess and Orgel, 2000).

1.3.2. Breakage of hydrogen bonds and/or polypeptides chains

The triple helical collagen molecules are stabilized by weak hydrogen bonds. These bonds are stable at low temperatures; however, when collagen is heated, it results in breakage of the bonds and unfolding of the protein (Miles, Burjanadze and Bailey, 1995; Wright and Humphrey, 2002). The unfolded triple helical structure is unstable and therefore can be transformed into a more random coiled structure (Sandler and Wyler, 2000). Further thermal denaturation results in hydrolysis of collagen into a gelatin (mixture of disordered polypeptides that consist of helical conformations). Differential scanning calorimetry (DSC) studies provided characteristics of the thermal denaturation of collagen (i.e. transition into gelatine); it was shown that the process is irreversible and that during denaturation a specific region of a collagen molecule unfolds first (i.e. 'thermally labile domain') (Miles et al., 1995; Miles and Ghelashvili, 1999). After the initial unfolding of the thermally labile domain, the whole collagen molecule becomes unstable and unfolds completely (Miles et al., 1995). A DSC technique has also been used to identify an intermediate state that was formed during collagen degradation induced by UV light; Miles et al (Miles et al., 2000) reported a new structure that consists mainly of triple helices; however the triple helix was partly destabilized. A schematic model of local unravelling of collagen structure is shown in Figure 1.6.

Another modification to collagen structure could be a hydrolysis of the polypeptide chains, which can result in formation of local disordered regions and loss of axial crystallinity. This

modification has been observed in collagen after the liming treatment of parchment; in this study an increase in the variation of a helical rise per residue distance was observed (see also section 1.3.1) and was suggested to be caused by a partial hydrolysis of the polypeptide chains and local relaxation of the collagen structure (Maxwell, Wess and Kennedy, 2006).

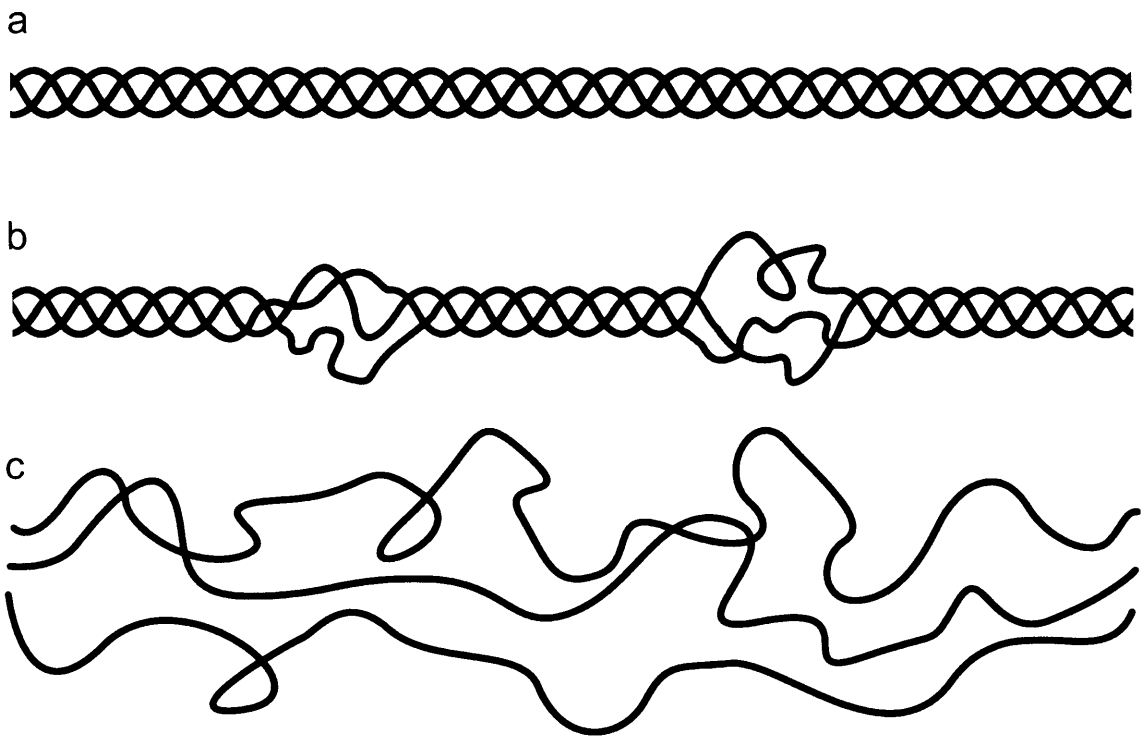

Figure 1.6. Unfolding of collagen molecule. (a) shows an intact triple helical molecule; breaking of hydrogen bonds (e.g. induced by high temperatures) can result in destabilization and local unfolding of collagen molecule (b) and can lead to a complete transformation of ordered structure into random coiled structure of gelatine (c).

1.3.3. Alteration in the size of gap and overlap regions

The characteristic gap-overlap repeat that can be observed in hydrated collagen structure has a fixed size (see section 1.1.1.3). The removal of water from collagen leads to the increase of the overlap region from the original 0.46D (30 nm) in the native fibrils up to 0.78D (50 nm). This is accompanied by a decrease in the gap region from 0.54D (36 nm) down to 0.22D (14 nm). This rearrangement results in a change in the electron density distribution along the unit cell of collagen (Chandross and Bear, 1973; Bigi et al., 1987). Figure 1.7 shows a model proposed by Chandross and Bear to explain observed molecular rearrangements. It can be seen that in the proposed model for the hydrated fibrils, there is a distinct border between gap and overlap regions, which is lost upon the transition from hydrated to dry state. These rearrangements lead to a decrease in the axial D-periodicity of collagen from 67 nm to approximately 64 nm (Worthington and Tomlin, 1955).

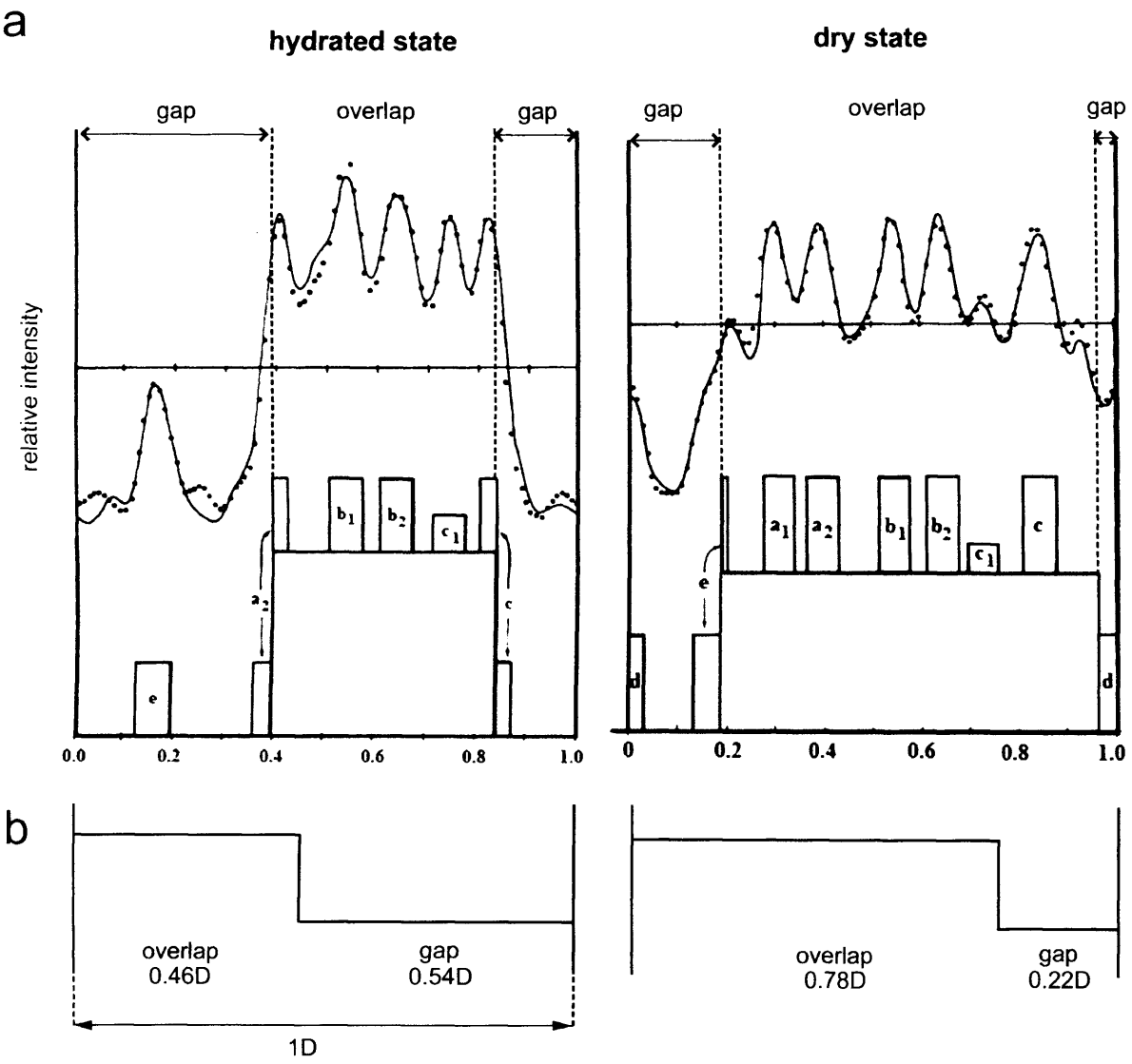

Figure 1.7. (a) Electron density distribution models proposed by Chandross and Bear for hydrated (left) and dry (right) kangaroo tail tendon (KTT). The density profile is shown on the top, while the bottom of the picture represents the strips of the model that are present in the gap and overlap zones of the unit cell (adapted from (Chandross and Bear, 1973)). (b) shows a simplified projected step function of the above.

1.3.4. Local strain within fibril and axial relative sliding of collagen molecules within a fibril

Local strain within fibrils can be potentially caused by local movements of the mobile water fraction. These local water movements can cause a relative motion of the collagen chains and therefore may lead to changes in the electron density profile. This can result in an increase in the variation of the D periodic lattice, e.g. a formation of several subpopulations of fibrils with various axial D-periodicities.

A relative motion of the collagen triple helices (i.e. relative slippage) has also been suggested to explain the increase of the D stagger during mechanical stretching of collagen fibres (Mosler et al., 1985). In that experiment relative slippage caused stretching of the telopeptides which are cross-linked to neighbouring molecules. Figure 1.8 shows a schematic explanation of relative sliding. (a) shows a normal set of 5 collagen molecules staggered by the characteristic 67 nm and (b) molecules that slide relative to each other. If each molecule slides relative to its neighbour by a distance c then the unit cell content will change. The length of the unit cell will increase by a fixed value, which would lead to the increase periodicity. Although it can be conceived that a sample could therefore contain a number of different D periodic structures, this has been hitherto unobserved by a number of techniques.

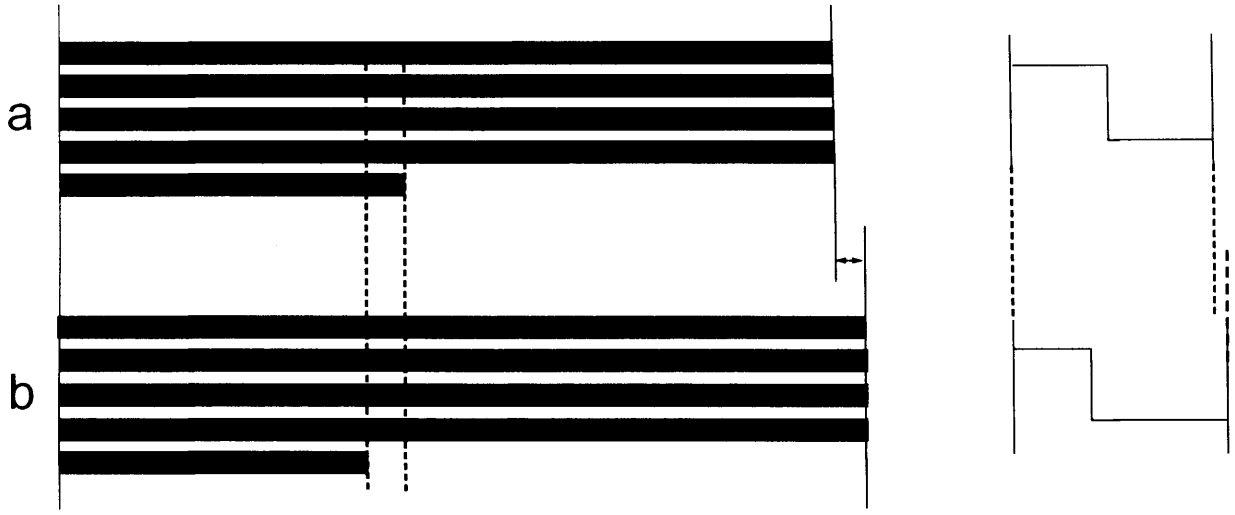

Figure 1.8. A simplified model of relative molecular slippage (adapted from (Mosler et al., 1985)). (a) One D-period, which consists of five segments of collagen molecules from normal, untreated collagen, (b) the D-period after the relative slippage of neighbouring triple helices. In (b) the fundamental periodicity is increased, which also results in an alteration of the projected step function (shown on the right).

1.3.5. Interfibrillar gliding and fibril misorientation

Interfibrillar gliding is an example of the rearrangement of the collagen structure that occurs on the fibrillar level. This mechanism was suggested by Fratzl et al to explain elongation of the tendon (Fratzl et al., 1997). The molecular rearrangement involves movement of entire fibrils where water and proteoglycans play an important role in the process (Figure 1.9). As a result of the process axial D-period does not change, however the fibrillar order is lost.

Rearrangements on the fibrillar level can also involve fibril misorientation. In tendon collagen fibrils are aligned with respect to the fibre axis. However in various tissues, fibrils can be oriented in all directions within the plane of the fibre (Figure 1.9) (see section 2.3.1).

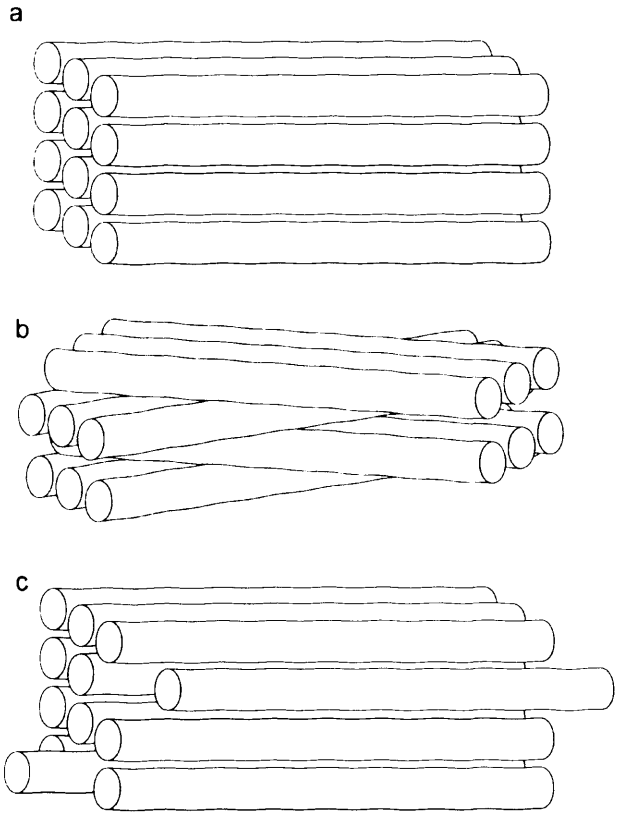

Figure 1.9. Examples of collagen fibril orientation: (a) shows fibrils that are aligned with respect to the fibre axis and can be found in tendons, while in (b) fibrils are oriented in various directions. (c) shows an interfibrillar gliding where entire fibrils are involved in the movement.

1.4. Summary

This chapter has provided general information about collagen and fibrillin, as well as various alterations that can be induced into their molecular structure. These alterations can potentially lead to a formation of intermediate, metastable states and their identification and description is one of the main aims of this thesis. Molecular rearrangements within collagen and fibrillin structure can be observed using X-ray diffraction, which is explained in the next chapter.

2. Principals of X-ray diffraction and Fourier Transform Infrared Spectroscopy (FTIR)

2.1. X-ray diffraction

X-ray diffraction is a technique widely used to determine the structure and organization of objects on a nanometer and an atomic scale. This chapter provides general information about X-rays and their interactions with matter, and focuses on the scattering of X-rays from ordered objects such as crystals and fibrous materials. It describes the mathematical methods used in diffraction studies (Fourier transform) and the collection of diffraction data. Finally, synchrotron radiation is explained, which is a source of X-rays used in the experiments described here.

2.1.1. X-ray scattering and diffraction

X-rays are electromagnetic waves with a wavelength (λ) in the range of 10nm to 0.1nm. When a photon interacts with matter it causes an oscillation of the charged particles and results in the eventual release of a photon. When oscillations within the matter are of the same frequency as the incident radiation and no energy is lost from the system, this form of interaction is coherent scattering. Incoming X-rays that are scattered by matter can interfere destructively (majority of X-rays) or constructively. The constructive interference occurs when X-rays are in phase and they combine after an interaction with matter, increasing the

amplitude of the resultant wave (Figure 2.1). Reinforced waves form diffracted beams that can be observed on the diffraction pattern.

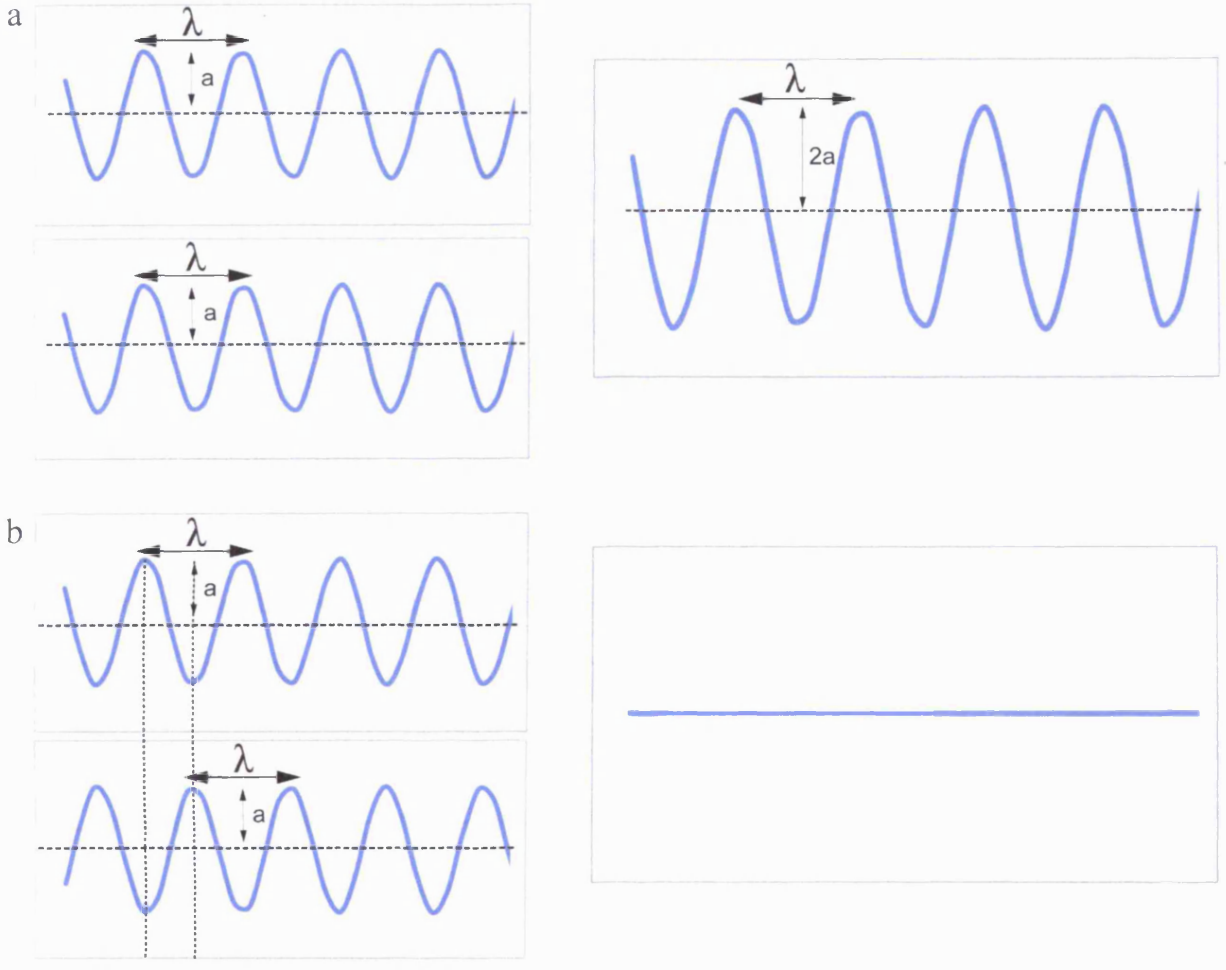

Figure 2.1. Interference of waves:(a) two waves in phase (left), which have the same wavelength (λ) and amplitude (=a) interfere constructively and produce a wave with greater amplitude (=2a) and the same wavelength (right), while waves out of phase (b) interfere destructively and the result is a decrease of the amplitude.

2.1.2. X-ray scattering and diffraction patterns

The angle dependent intensity profile of the recorded scattering pattern depends on the state of matter within the studied system. Figure 2.2 shows examples of scattering curves collected from various systems; in Figure 2.2a particles are in a gas-phase and therefore they are separated widely enough in order to make independent contributions to the scattering curve. Gas particle interacts with X-rays to give a scattering profile (Figure 2.2b). When particle concentration is increased, e.g. in the liquid or solid state (Figure 2.2 c, d), an interference effect occurs, which result in distinctive reflections on the scattering pattern.

In the case of highly ordered structures (i.e. samples that contain a high regularity in the material lattice) a scattering curve consists of sharp peaks (Figure 2.2e). These peaks are produced by strong diffracted beams, which are generated when X-rays interact with the ordered lattice (see Bragg's law in section 2.1.3). Figure 2.3 shows an example of a diffraction pattern collected from collagen, which is one of the most crystalline tissues known. Its diffraction pattern consists of a series of sharp peaks that reflect a highly regular lattice, which will be described in section 2.1.7.1.

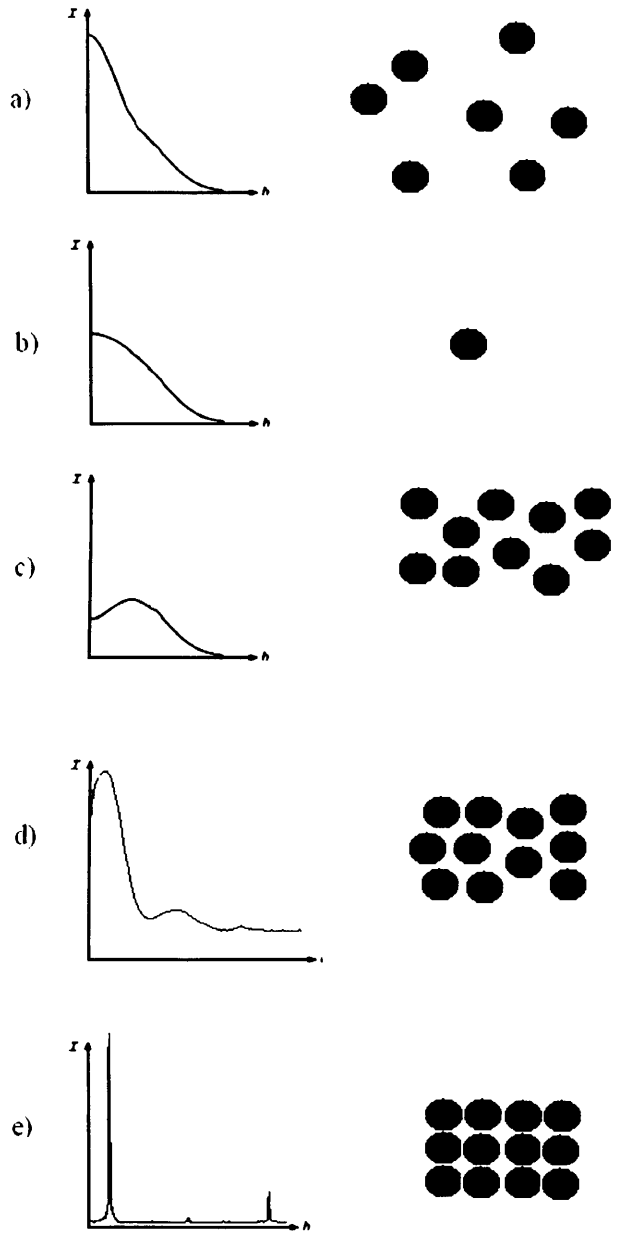

Figure 2.2. Left panels: scattering curves generated from various states of matter: (a) gas-type sample, (b) single particle, (c) liquid-type, (d) quasi-crystalline, (e) solid state. Right panels: corresponding models showing the arrangement of particles within the sample (adapted from (Glatter and Kratky, 1982)). The y-axis on the graphs is a scattering intensity, while the x-axis is a scattering vector.

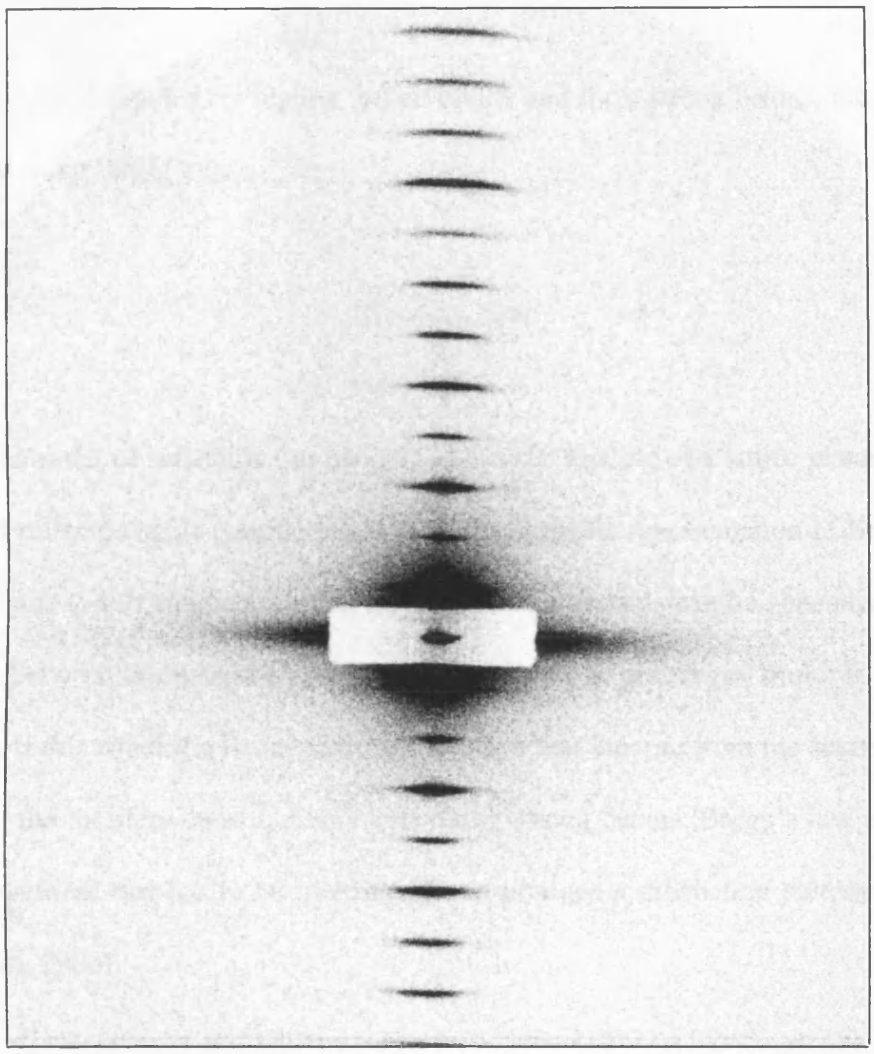

Figure 2.3. An example of the X-ray diffraction pattern from collagen (from rat tail tendon). The pattern consists of a series of sharp peaks generated by reinforced diffracted beams that were produced by interaction of incoming X-rays with ordered collagen lattice.

Even when samples are highly ordered, there is usually some degree of disorder found in their structure. These imperfections, such as a displacement in an ordered plane, cause a diffuse scatter, i.e. diffuse radiation that can reduce the intensity of the reinforced, diffracted beams produced by a perfect crystalline lattice.

2.1.3. Bragg's law

When X-rays are diffracted by regular lattice points and form strong beams, the process can be expressed using Bragg's law:

$$n\lambda = 2d_{hkl} \sin\theta$$

where n is the order of reflection (an integer), d_{hkl} is the spacing of a lattice plane and θ is the incident and reflected angle (Hammond, 1997). A schematic representation of Bragg's law is shown in Figure 2.4. It can be seen that strong diffracted beams can be generated only when the distance between the successive lattice planes is equal to an integral multiple of the X-ray wavelength. If this condition is satisfied then the rays that emerge from the successive planes are in phase and interfere constructively generating strong beams. Bragg's law is therefore a necessary condition that has to be met in order to produce a diffraction pattern (Hammond, 1997; Rhodes, 2000).

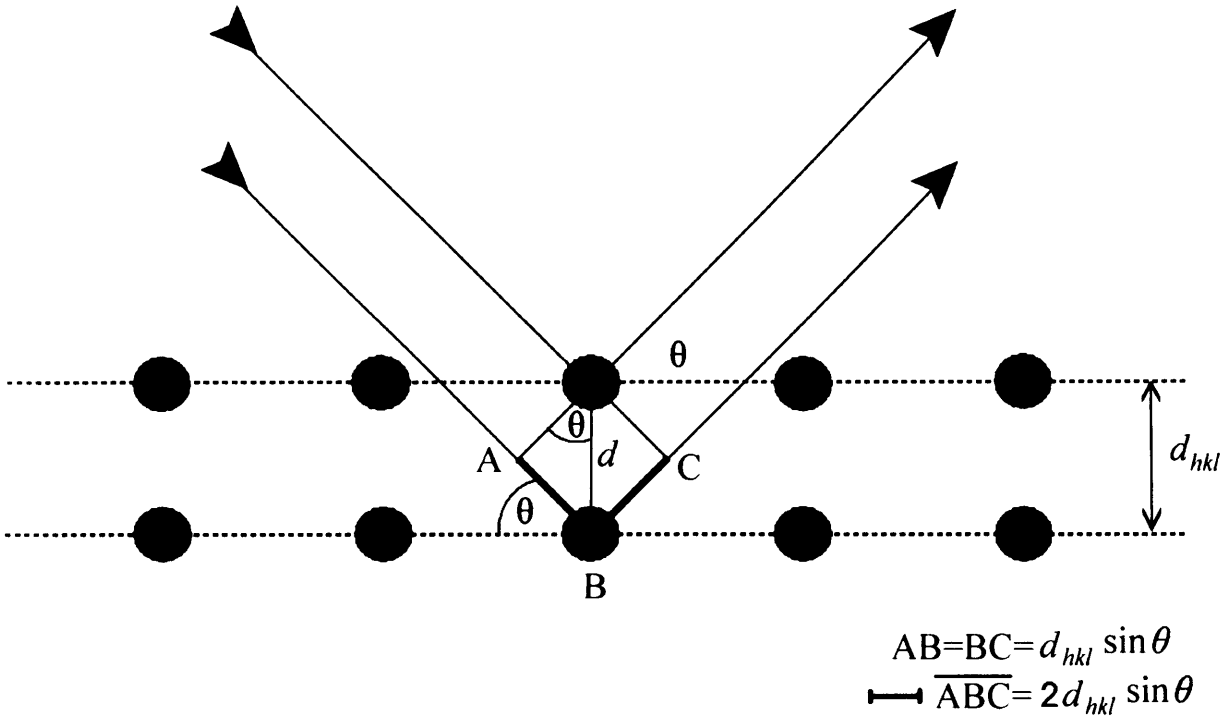

Figure 2.4. Diffraction of X-rays by two planes of atoms separated by the distance dhkl: if Bragg's law conditions are satisfied (i.e. the difference in the path length between two waves (marked as a blue line) is equal to $2d_{hkl}$ sinθ)) then the reflected waves interfere constructively.

2.1.4. Reciprocal space

Generated diffracted beams can be recorded as characteristic reflections on the diffraction pattern. The spacing of these reflections is inversely proportional to the dimensions of the crystalline lattice. Because of this inverse relationship, spacings recorded on the diffraction pattern correspond to the reciprocal lattice, as opposed to the real lattice of the studied crystalline material (Rhodes, 2000). Detailed information about the reciprocal lattice can be found in (Hammond, 1997).

2.1.5. Fourier Transform

Since crystalline materials are highly ordered, the array of molecules in the lattice produces a characteristic, periodic electron density distribution. This pattern can be very complex and depends on the shape and the size of the molecules that build unit cells (Hammond, 1997). The electron density distribution consists of maxima, which arise from the molecules, and minima, which correspond to the spaces between them. The internal content of the periodic distribution can be described using Fourier series (Rhodes, 2000). This mathematical method is used to approximate complex periodic functions using many simple sine and cosine functions; an example of Fourier series is shown in Figure 2.5.

Fourier transformation can be express by the equation:

$$F(h) = \int f(x)\, e^{2\pi i(hx)}\, dx$$

where *F(h)* is a Fourier transform of the original function *f(x)* and *h* is a reciprocal variable of the original variable *x* (e.g. the distance in the object) (Hammond, 1997; Rhodes, 2000). This transformation is a crucial part of the diffraction process, since a diffraction pattern of a studied object is its Fourier transform (Fraser and MacRae, 1973; Senechal, 1995). By using this relationship it is therefore possible to obtain information about the object (real lattice) from its diffraction pattern (reciprocal lattice).

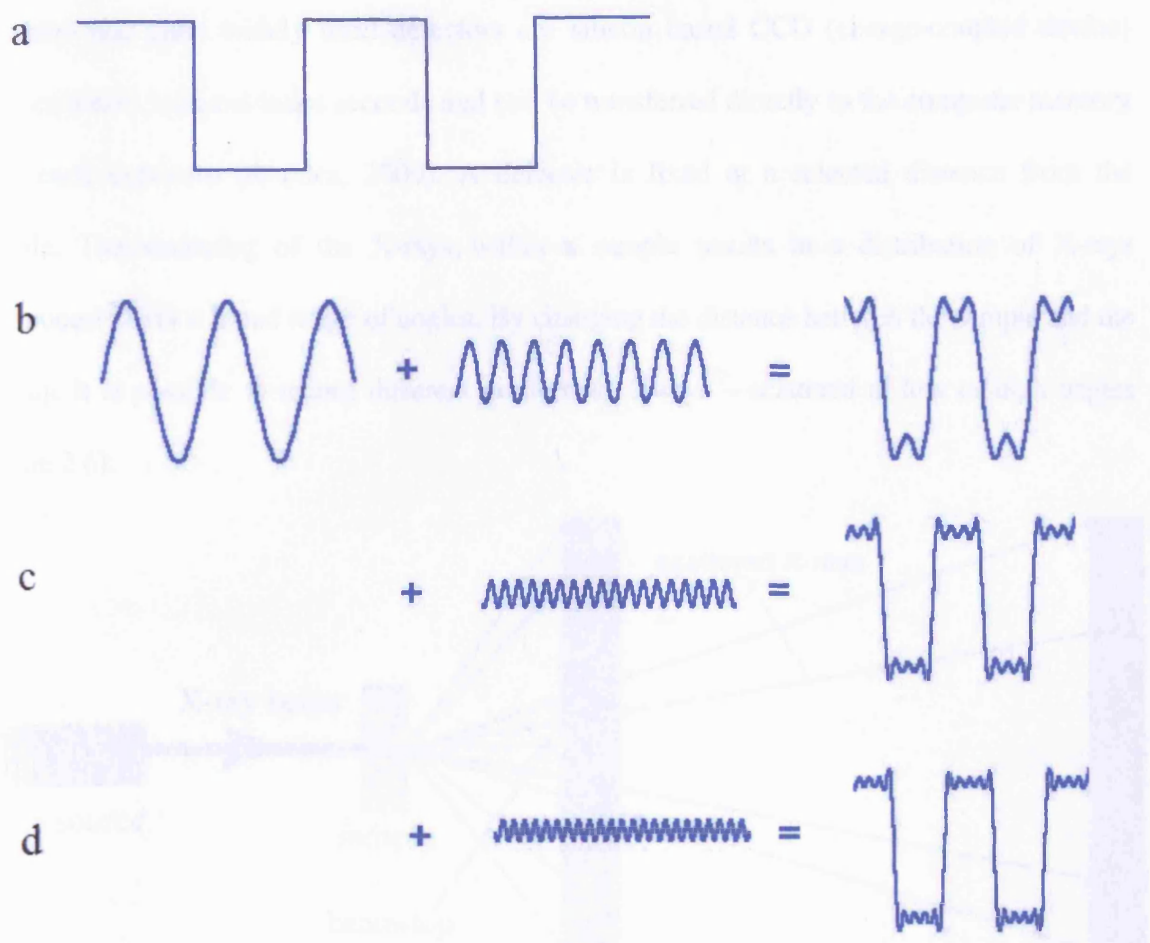

Figure 2.5. Fourier series: a periodic function, such as step function (a) can be described as a sum of many simple sine and cosine functions (Fourier terms) (b-d). When all Fourier terms are added together they form the original wave (adapted from www.intmath.com).

2.1.6. Data collection

Figure 2.6 shows a simplified model of an X-ray diffraction experiment. It consists of a selected X-ray source that generates radiation, a detector and specimen (e.g. a crystal or a fibrous material) which is mounted between those devices. Emitted X-rays are diffracted by

the regions of different electron density and a characteristic pattern is recorded on a selected detector. The most widely used detectors are silicon based CCD (charge-coupled device) devices where read-out takes seconds and can be transferred directly to the computer memory after each exposure (Rhodes, 2000). A detector is fixed at a selected distance from the sample. The scattering of the X-rays within a sample results in a distribution of X-rays continuously over a broad range of angles. By changing the distance between the sample and the detector it is possible to record different portions of X-rays – scattered at low or high angles (Figure 2.6).

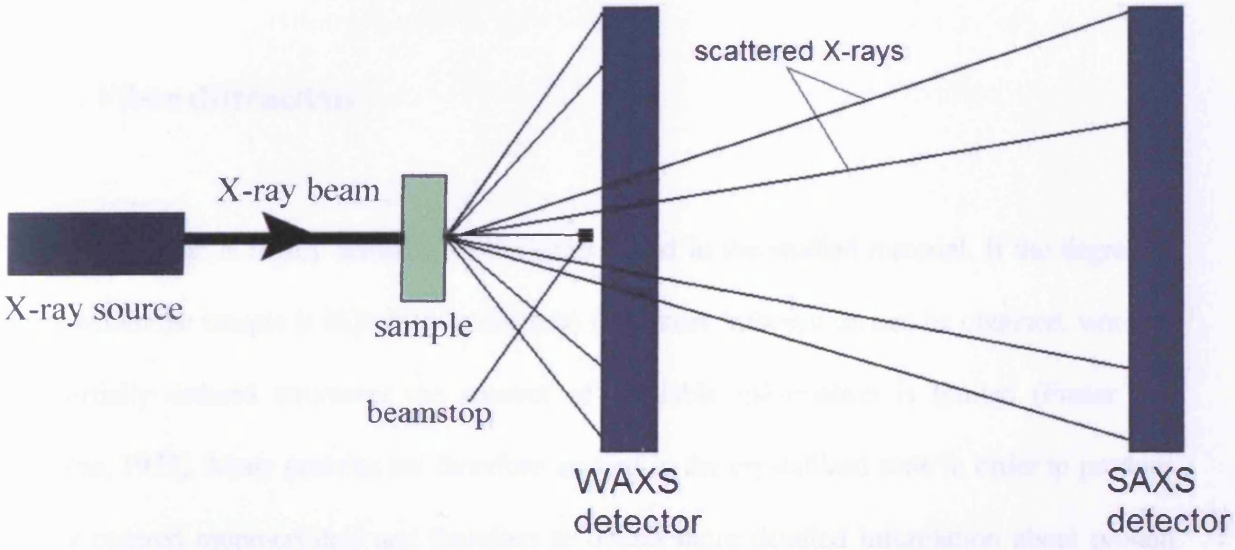

Figure 2.6. Experimental set up for X-ray diffraction: x-ray beam, generated by an X-ray source, hits the sample and the scattered waves are recorded on the detector. A lead beamstop prevents the non-scattered radiation from striking the detector. Low or high angle reflections can be recorded by changing the distance between the specimen and the detector (adapted from (Maxwell et al., 2006)).

As most of the X-rays do not interact with matter and pass through the specimen it is necessary to prevent the direct beam from striking the detector. As a result a lead beamstop is

mounted between the specimen and the detector directly in line with emitted radiation and absorbs direct beam rays (see Figure 2.6).

Characteristic diffraction patterns are usually accompanied by scattered X-ray radiation that was a result of optics and camera design. This background radiation needs to be subtracted from the original data to obtain correct intensity values. Usually this can be done by recording a diffraction pattern of an empty cell (without a specimen) which then can be subtracted from the collected data. The methods of data reduction and analysis are described in detail in Chapter 3.

2.1.7. Fibre diffraction

X-ray diffraction is highly sensitive to the order found in the studied material. If the degree of order within the sample is high (e.g. in crystals) then more information can be obtained, whereas for partially ordered structures the amount of available information is limited (Fraser and MacRae, 1973). Many proteins are therefore studied in the crystallized state in order to produce highly ordered mono-crystals and therefore to obtain more detailed information about protein structure. Many biological substances do not form monolithic crystals, however they may still contain long or short-range order regions and can generate distinctive diffraction patterns characteristic of preferentially aligned poly crystallites. An example can be fibrous materials such as collagen, muscle fibres or fibrillin (Worthington and Tomlin, 1955; Lowy and Poulsen, 19821990; Wess et al., 1997). In the case of fibrous proteins the high degree of crystallinity is often present in the direction parallel to the fibre axis. This long-range order gives rise to the meridional reflection observed on the diffraction pattern; for example, in collagen the axial packing is caused by the characteristic D-periodicity along the fibril axis, which produces a series

of meridional reflections (i.e. diffraction orders). The lateral packing in fibrous proteins (i.e. in the direction perpendicular to the fibre axis) is often less crystalline and therefore produces more diffuse scatter. The lateral packing of the molecules gives rise to an equatorial pattern (Meek and Quantock, 2001).

Using X-ray diffraction in the study of fibrous proteins has many advantages: (1) the technique is non-destructive, (2) it does not require any specific sample preparation prior to measurements (e.g. staining, dehydration), which can induce artefacts into the final image, (3) it enables the examination of samples in their native state, e.g. specimens can be kept hydrated during the measurements. It also allows dynamic studies to be conducted, such as the measurement of the molecular structure of the protein during mechanical stretching or drying.

2.1.7.1. Collagen small-angle diffraction

In small-angle X-ray diffraction the scattering at very low angles from the direct beam (typically 0.1 – 10°) is recorded, which requires a longer sample to detector distance (Figure 2.7). It allows the examination of large scale structures from one to several hundred nanometers.

Collagen structure is highly ordered, the molecules are regularly staggered by a fixed distance (tissue specific D-period), moreover in some tissues (e.g. cornea and breast tissue), collagen fibrils have a uniform diameter and a fixed centre-to-centre distance (Meek and Quantock, 2001; Fernandez et al., 2002). This high level of organization can produce scattering of the incoming X-rays and generate characteristic reflections on a diffraction pattern. A small-angle X-ray scattering pattern of rat tail tendon collagen consists of sharp reflections which

correspond to the characteristic, axial periodicity present due to the electron density fluctuations along the fibrils (Bear, 1944). The predominance of odd orders can be observed on the diffraction pattern, which results from a broad overlap zone in the molecular structure that occupy 0.46 of the 67 nm period (approximately 30 nm) (Chandross and Bear, 1973). This characteristic predominance indicates that the density distribution along the fibrils consists of a nearly consinusoidal fluctuations (Figure 2.7b) and the diffraction pattern corresponds to the Fourier transform of a step function (Figure 2.7c).

In tissues such as rat tail tendon, fibrils are mostly oriented parallel to the fibre axis. This arrangement produces a pattern with a series of sharp arcs (Figure 2.8a and b). However in many tissues collagen fibrils are randomly oriented as a feltwork which means that they lie in all directions, thus the diffraction pattern consists of rings (Figure 2.8c and d) (Purslow, Wess and Hukins, 1998; Fernandez et al., 2002; Fratzl, 2003).

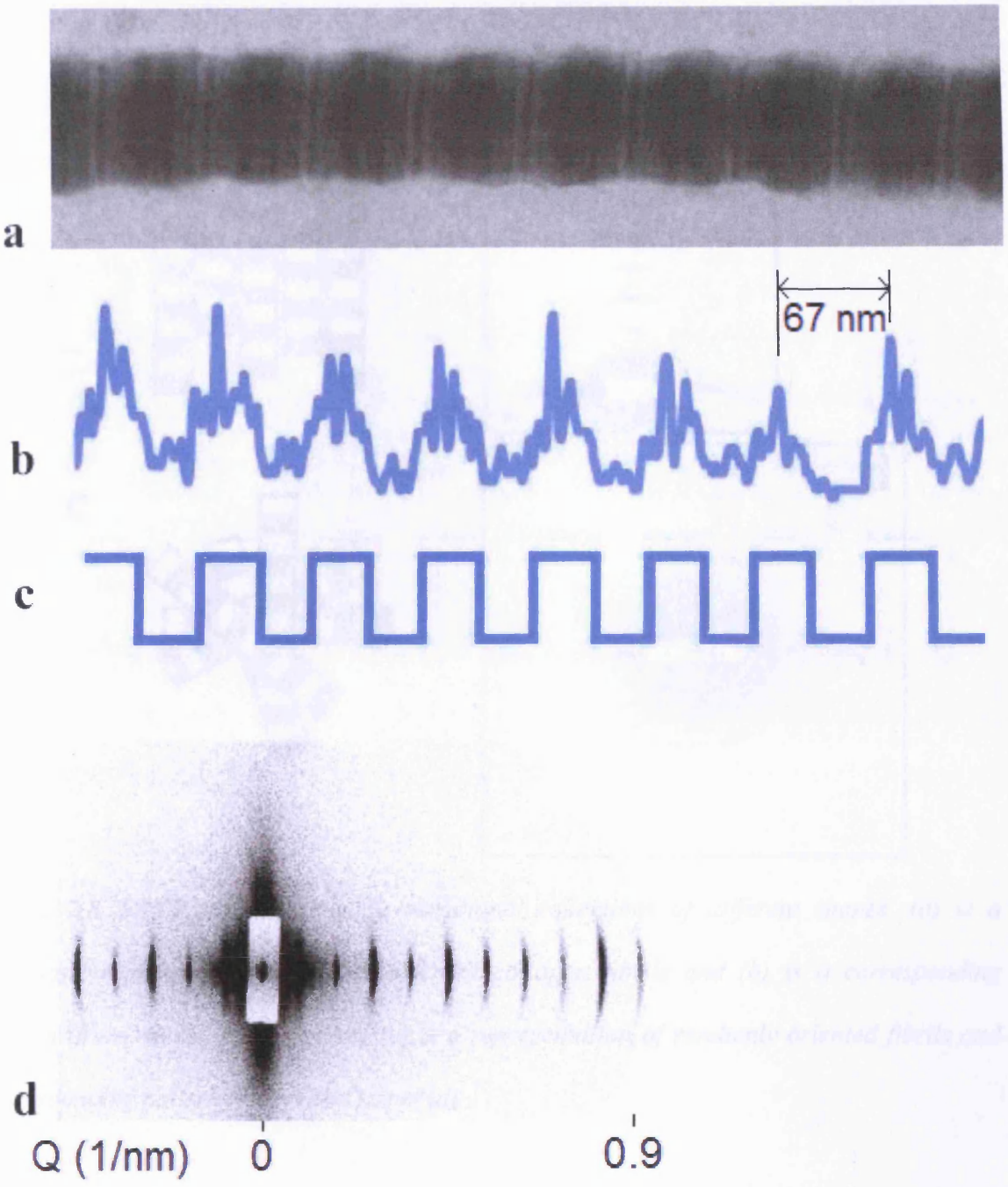

Figure 2.7. Electron micrograph of a single collagen fibril (a) and corresponding variation in electron density obtained using ImageJ software (b), which resembles a step function (c). These fluctuations give rise to the series of meridional reflection on the small-angle X-ray scattering pattern (d). Q is an angular position ($Q = 4\pi\sin\theta/\lambda$).

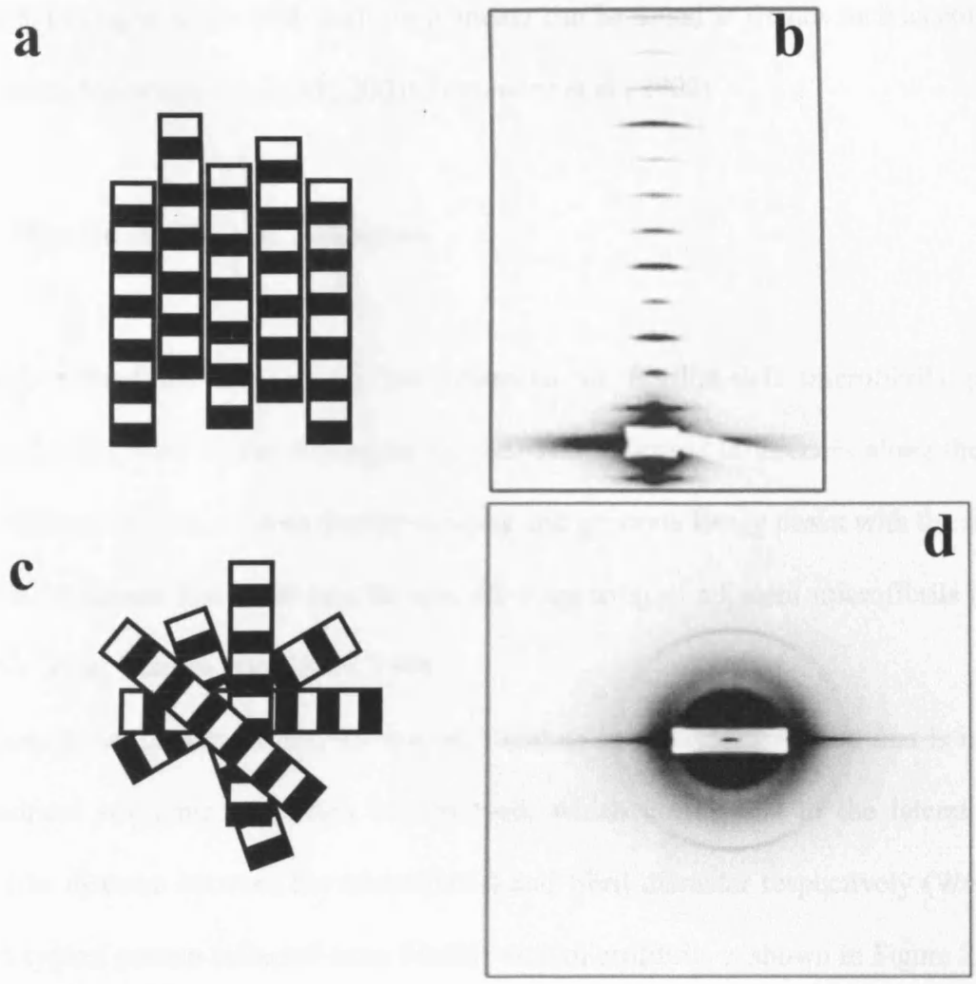

Figure 2.8. SAXS patterns showing meridional reflections of different shapes. (a) is a schematic representation of highly oriented collagen fibrils and (b) is a corresponding pattern (from rat tail tendon) while (c) is a representation of randomly oriented fibrils and corresponding pattern from breast tissue (d).

The equatorial pattern provides information about fibril diameter and the interfibrillar distance. However, in order to produce a scattering function on the diffraction pattern, the diameter of collagen fibrils must be uniform. When this condition is satisfied, the scattering from such a system can be described using the Bessel function, which is described in detail in

Chapter 3. Collagen fibrils with uniform diameter can be found in tissues such as cornea and breast tissue (Meek and Quantock, 2001; Fernandez et al., 2002).

2.1.7.2. Fibrillin small-angle diffraction

The bead-to-bead distance of 56 nm observed in fibrillin-rich microfibrils produces meridional reflections on the diffraction pattern. The structural differences along the beaded microfibrils result in an electron density contrast and generate Bragg peaks with the strong 3rd order. This suggests that there may be specific staggering of adjacent microfibrils (Wess et al., 1997; Wess, Purslow and Kielty, 1998).

On the equatorial pattern an interference peak and an intensity distribution that is indicative of cylindrical scattering can often be observed, which correspond to the lateral packing density (the distance between the microfibrils) and fibril diameter respectively (Wess et al., 1998). A typical pattern collected from fibrillin-rich microfibrils is shown in Figure 2.9.

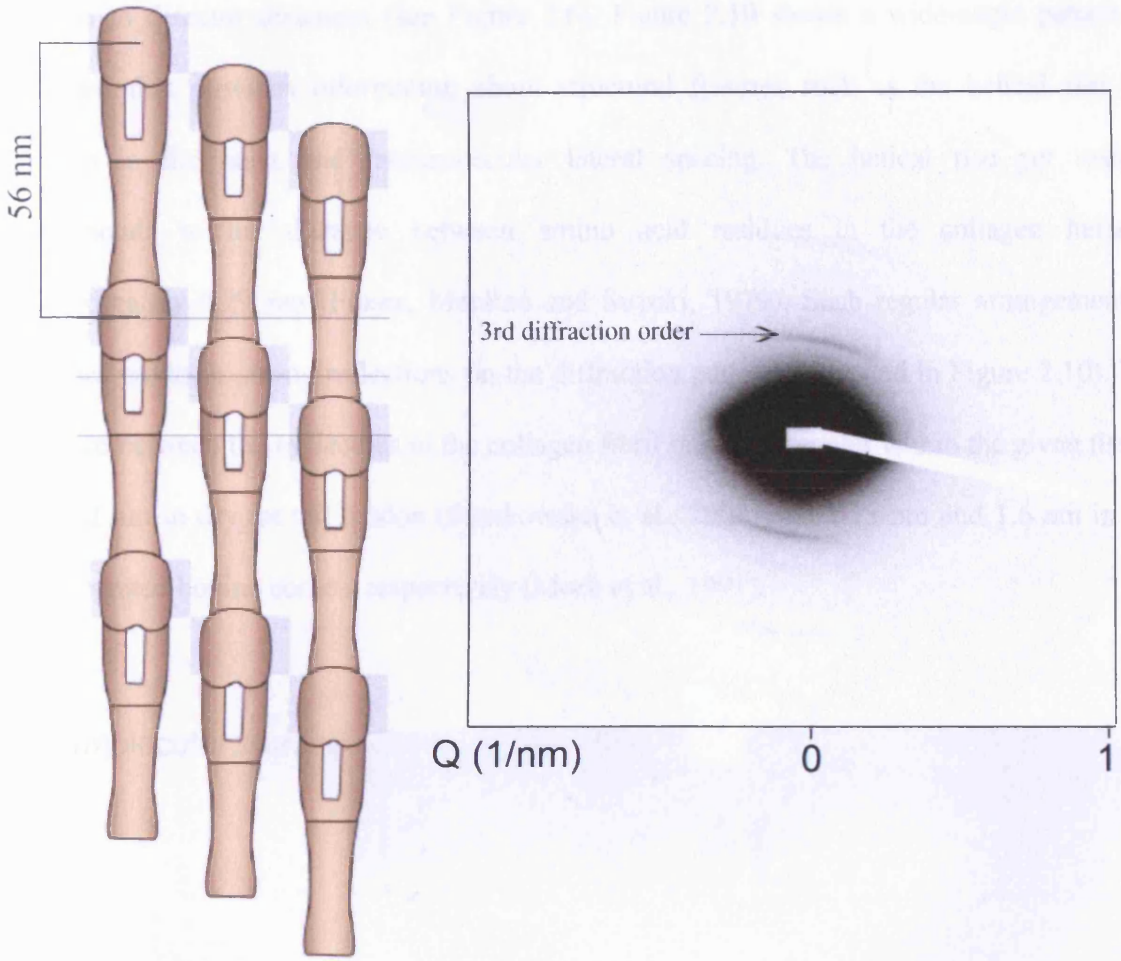

Figure 2.9. Left: A schematic arrangement of fibrillin microfibrils. A 56 nm bead-to-bead distance produces a series of meridional reflections and a specific 1/3 staggering generates a scattering pattern with strong 3rd order – adapted from (Cain et al., 2006). Right: small-angle scattering image collected from zonular filaments.

2.1.7.3. Collagen wide-angle diffraction

In wide-angle X-ray diffraction the scattering at higher angles from the direct beam is recorded (typically 5-60°) and it provides information about much smaller structural features than those observed using SAXS. The collection of wide angle reflections requires very short

sample to detector distances (see Figure 2.6). Figure 2.10 shows a wide-angle pattern of collagen that provides information about structural features such as the helical rise per residue in the helix and intermolecular lateral spacing. The helical rise per residue corresponds to the distance between amino acid residues in the collagen helix – approximately 0.29 nm (Fraser, MacRae and Suzuki, 1979). Such regular arrangement of residues produces strong reflections on the diffraction pattern (indicated in Figure 2.10). The distance between the molecules in the collagen fibril is highly regular within the given tissue: e.g. 1.2 nm in dry rat tail tendon (Sionkowska et al., 2004) and 1.15 nm and 1.6 nm in dry and hydrated bovine cornea, respectively (Meek et al., 1991).

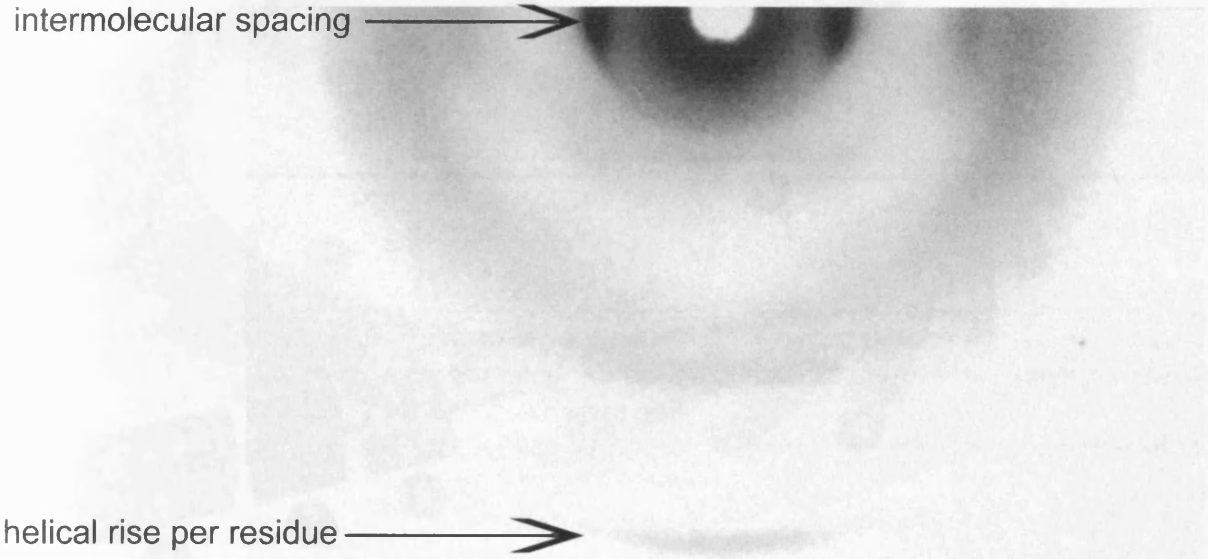

Figure 2.10. Wide-angle X-ray scattering pattern collected from rat tail tendon. Positions of helical rise per residue (0.29 nm) and intermolecular spacing reflections are indicated by arrows. Image has been reproduced from (Meek et al., 1991).

2.1.8. Synchrotron radiation

Synchrotron radiation was used as a source of X-rays in the experiments described in this thesis. A synchrotron is a specific type of cyclic particle accelerator that can produce electromagnetic radiation at wavelengths from X-rays to the far infra-red (Helliwell, 2006). In synchrotrons a magnetic and an electric field are used to circulate and accelerate particles. Synchrotrons consist of (1) an electron source (electron gun), (2) a linear accelerator which accelerates electrons close to the speed of light (LINAC), (3) a booster ring where electrons intensities are enhanced and (4) an outer storage ring (shown in Figure 2.11).

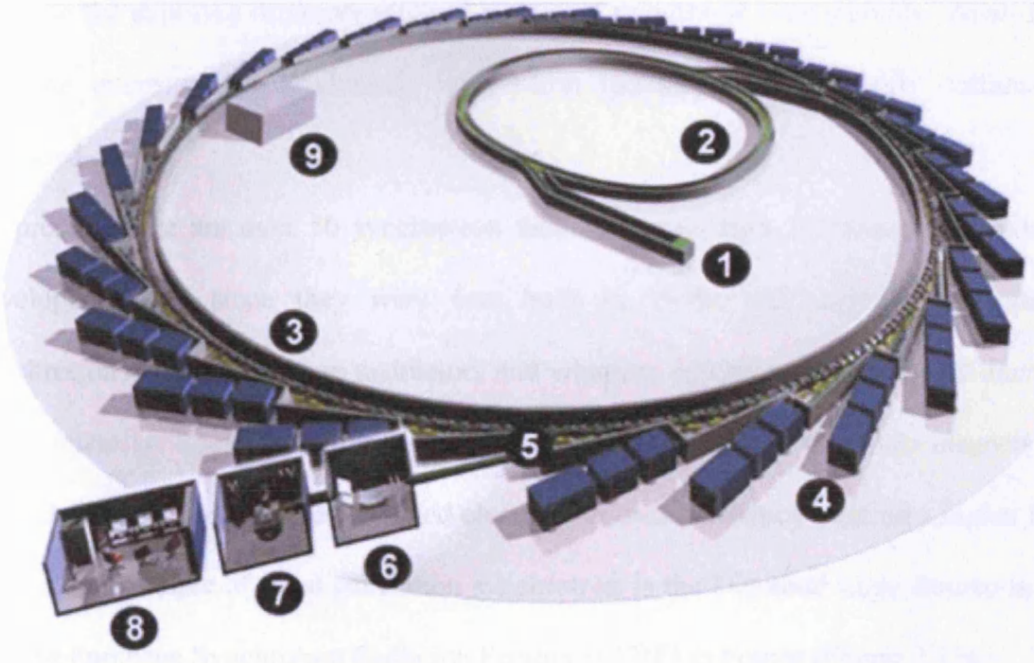

Figure 2.11. A schematic representation of a synchrotron. LINAC (1) accelerates electrons near the speed of light. Electrons are transferred to the booster ring that consists of bending and focusing magnets (2) and then to the outer storage ring where they are forced to travel in the nearly-circular trajectory (3). Emitted photons can be focused and transferred to the beamlines (4-8) where experiments can be conducted. Copyright: Diamond Light Source Ltd.

The electrons travel in ultrahigh vacuum. The beam of light is produced when the electrons are deflected through the magnetic field generated by the bending magnets in the storage ring. When electrons travel at relativistic velocities (near the speed of light) photons are emitted in a narrow cone in a forward direction. Emitted beams can be then be focused so the beam is kept small and well-defined and used for the appropriate technique in the beamlines (e.g. SAXS beamline), straight tubes that depart from the storage ring and lead to the stations. Synchrotron radiation consists of a wide energy spectrum and it is possible to obtain radiation of a selected wavelengths for a specific purpose. X-rays generated using synchrotron radiation sources are hundreds of thousands of times more intense than conventional X-ray tubes so the exposure times are reduced to several minutes or even seconds. Apart from the extreme intensity and brightness, synchrotron radiation is also highly collimated and polarised.

At present there are over 50 synchrotron facilities worldwide. Synchrotron facilities have developed vastly since they were first built in 1930s and currently 3rd generation synchrotrons are built that use undulators and wigglers, insertion devices, which increase the beam intensity. These synchrotrons differ from previous ones as they use magnets located around the ring causing the accelerated electrons to oscillate hence creating a higher intensity beam. An example of a 3rd generation synchrotron is the Diamond Light Source in the UK and the European Synchrotron Radiation Facility (ESRF) in France (Figure 2.12).

Synchrotron radiation has been used as a source of X-rays in the experiments described here and further information about specific beamlines can be found in the next, Experimental chapter.

Figure 2.12. Synchrotron facilities: (a) Daresbury Radiation Facility, UK, (http://www.srs.ac.uk) (b) Diamond Light Source, UK; Copyright: Diamond Light Source Ltd. (c) European Synchrotron Radiation Facility (ESRF) in Grenoble, France. (http://www.esrf.eu) (d) shows a laboratory based X-ray scattering system – NanoSTAR (at the School of Optometry and Vision Sciences, Cardiff University).

2.2. Fourier Transform Infrared Spectroscopy (FTIR)

X-ray diffraction has been used in the studies described in this thesis to examine molecular and fibrillar structure of collagen and fibrillin e.g. the distances between molecules, characteristic axial periodicity, lateral packing and fibril radius, in response to the various external factors. In order to gain more understanding into possible modification of the proteins, the technique of FTIR was used to provide information about the protein backbone. The technique has already been proved useful for examining conformational changes in collagen structure as a result of denaturation, UV-irradiation and as an assessment of degradation in historical parchment (Liu et al., 1994; Yakimets et al., 2005; Sionkowska, 2006; Gonzalez and Wess, 2008).

2.2.1. Principals of FTIR

Infrared light has a wavelength between 2.5 μm and 25 μm and is absorbed by chemical bonds in the molecules. Molecules absorb infrared light which has the same frequency as the vibrating bond; those molecules are known to be infrared active (Pavia, Lampman and Kriz, 1996). Bond motion is governed by steric restrictions within the polyatomic molecule and the mass of the vibrating atoms. There are distinct modes of motion known as normal modes. Figure 2.13 illustrates the modes of motion seen in molecules when they absorb infrared radiation.

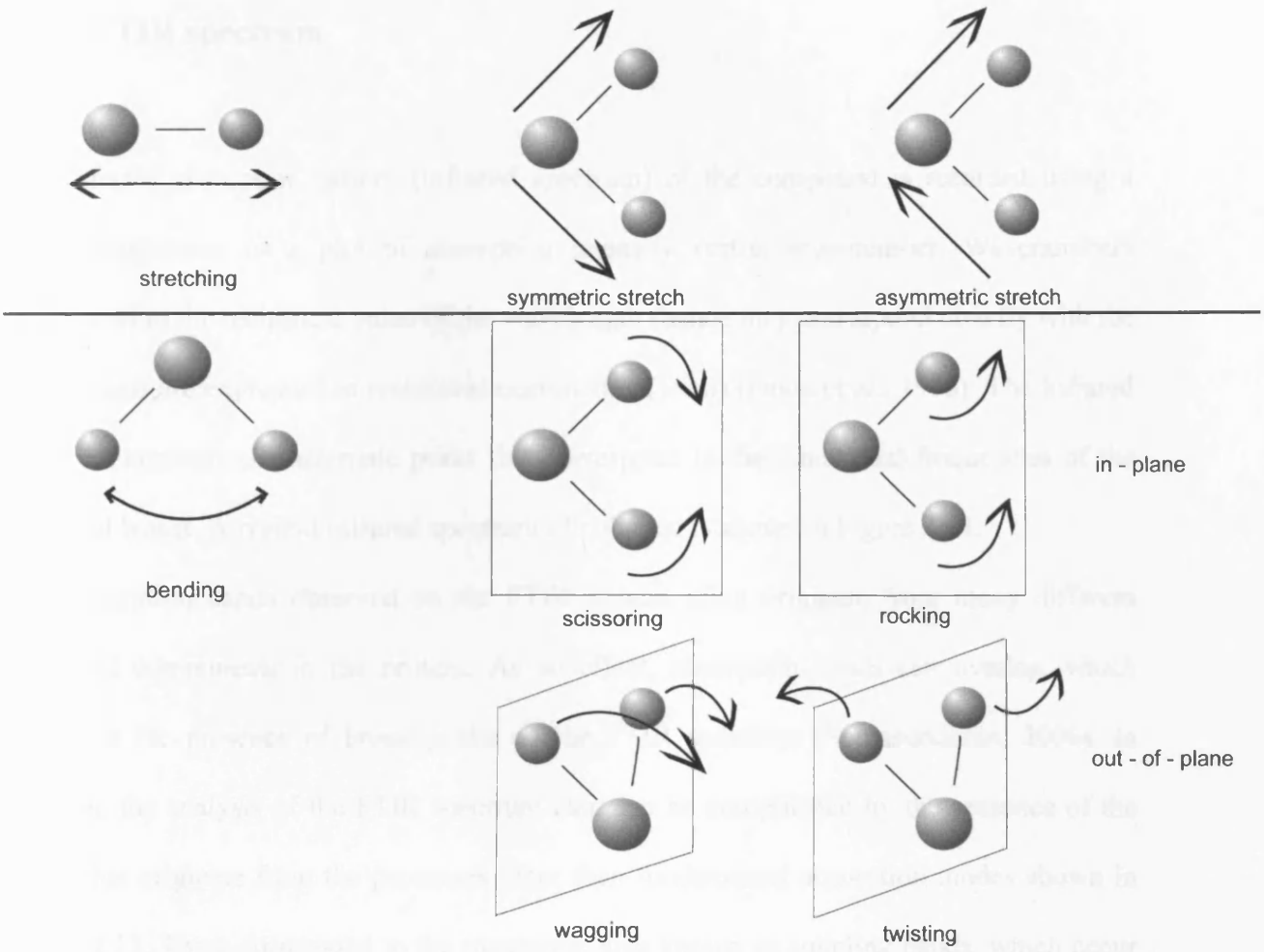

Figure 2.13. Vibrational modes induced by infrared radiation (adapted from (Pavia et al., 1996)). Top panel: stretching modes involve a change in a distance along the bond axis and can be symmetrical or asymmetrical. Bottom panel: bending modes occur when the angle between two bonds is changed. Each of these vibrations occurs at different frequencies.

Only bonds that contain a dipole moment can absorb infrared energy; the energy can be transferred when an electrical dipole is oscillating at the same frequency as the infrared radiation.

2.2.2. FTIR spectrum

The infrared absorption pattern (infrared spectrum) of the compound is recorded using a spectrophotometer as a plot of absorption intensity versus wavenumber. Wavenumbers correspond to the reciprocal value of the wavelength (hence they correspond directly with the energy) and are expressed in reciprocal centimetres (1/cm) (Pavia et al., 1996). The infrared spectrum contains characteristic peaks that correspond to the vibrational frequencies of the chemical bonds. A typical infrared spectrum of collagen is shown in Figure 2.14.

The absorption bands observed on the FTIR spectra often originate from many different structural components in the protein. As an effect, absorption bands can overlap, which results in the presence of broad peaks on the FTIR spectrum (Somasundaran, 2006). In addition, the analysis of the FTIR spectrum can also be complicated by the presence of the bands that originate from the processes other than fundamental absorption modes shown in Figure 2.13. These correspond to the overtones, also known as coupling bands, which occur at twice the frequency of the fundamental vibration (Crews, Rodriguez and Jaspars, 1998). An example of a coupling band can be an Amide B band present in the collagen FTIR spectrum, which is an overtone of the Amide II band (Figure 2.14) (Hasegawa, Umemura and Yamada, 2005).

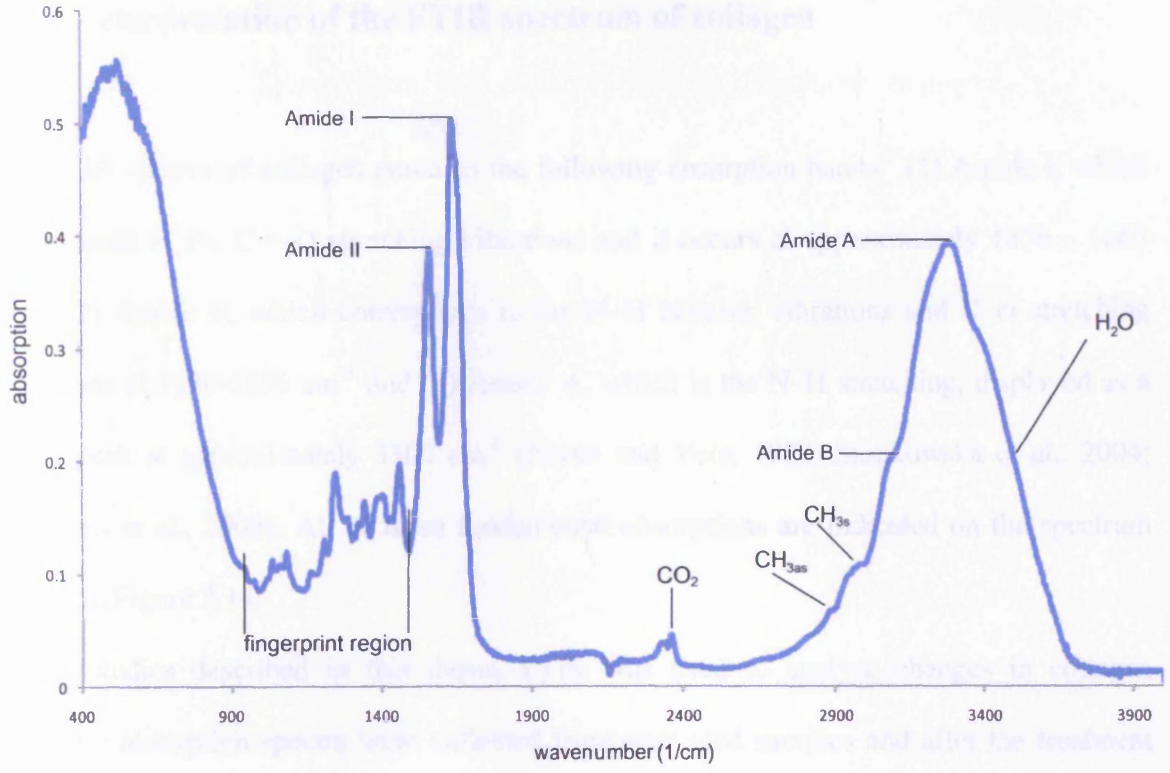

Figure 2.14. The FTIR spectrum of collagen taken from rat tail tendon. The fundamental absorptions are indicated on the graph: Amide I (CO stretching), Amide II (NH bending and CN stretching), Amide A (NH stretching), Amide B (Amide II overtone), CO_2, symmetric and asymmetric CH_3 vibrations. The fingerprint region indicated on the left side of the spectrum originates from the absorptions of chemical groups from the side chains of glycine and proline. A broad band on the side of the Amide A peak is attributed to the water absorption.

2.2.3. Interpretation of the FTIR spectrum of collagen

The FTIR spectra of collagen contains the following absorption bands: (1) Amide I, which corresponds to the C = O stretching vibrations and it occurs at approximately 1650 – 1665 cm^{-1}, (2) Amide II, which corresponds to the N–H bending vibrations and C–N stretching vibrations at 1530-1550 cm^{-1} and (3) Amide A, which is the N–H stretching, displayed as a broad peak at approximately 3300 cm^{-1} (Payne and Veis, 1988; Sionkowska et al., 2004; Yakimets et al., 2005). All of these fundamental absorptions are indicated on the spectrum shown in Figure 2.14.

In the studies described in this thesis, FTIR was used to analyse changes in collagen structure; absorption spectra were collected from untreated samples and after the treatment and the positions of each absorption band were compared. The frequency shift in the wavenumber of the bands corresponds to the strength of the hydrogen bonds in the collagen molecule and can provide information about the formation or breaking of hydrogen bonds.

2.2.4. FTIR measurements

FTIR analysis was performed using Attenuated Total Reflectance-FTIR (ATR-FTIR) at The National Archives, London. The ATR technique provides high resolution data and allows measurement of solid specimens without any sample preparation, which is a great advantage over a transmission IR. The measurements are performed using an optically dense ATR crystal, which is held in contact with the sample. As infrared beam passes through the crystal, it creates an evanescent wave that extends beyond the crystal and into the sample; the created wave interacts with the sample and the regions of IR that match the natural vibrational

frequency of the bonds are absorbed. The altered evanescent wave exits the crystal and is then collected by a detector. Figure 2.15 shows a schematic diagram of the process.

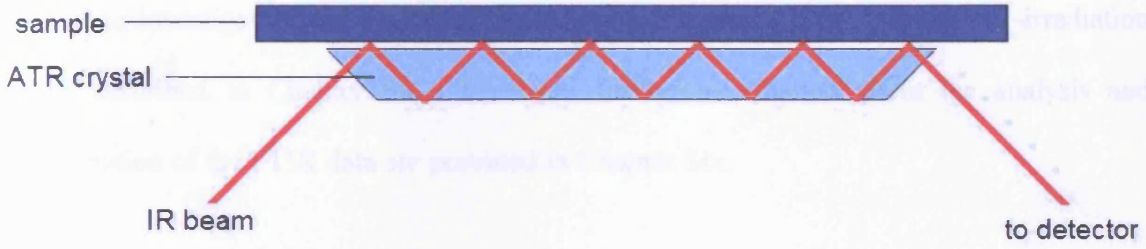

Figure 2.15. ATR-FTIR system (adapted from Perkin Elmer Life and Analytical Sciences (2005)). During the measurements, the IR beam passes through the ATR crystal, creating the evanescent wave that interacts with the sample. The evanescent wave typically penetrates less than 1μm inside the sample (Gonzalez and Wess, 2008). The altered wave is then collected by a detector.

2.3. Summary

This chapter has provided general information about X-ray diffraction and Fourier Transform Infrared Spectroscopy, two techniques that have been used in this thesis to examine molecular and conformational alterations induced in collagen and fibrillin structure by various external factors. It is important to understand the general principles of the techniques in order to correctly interpret collected data. In this chapter, the scattering of X-rays by matter has been explained, as well as the relationship between the structure of the sample (i.e. crystalline lattice) and its diffraction pattern and distinctive features that are produced on the

diffraction pattern by an ordered structure of collagen and fibrillin. The next chapter provides information about the collection of X-ray diffraction data and methods of data analysis.

While X-ray diffraction has been used to examine collagen and fibrillin structure in all four studies presented in this thesis (Chapters Four to Seven), the FTIR technique was only applied to investigate conformational changes in collagen in a response to UV-irradiation (study described in Chapter Six). Therefore further information about the analysis and interpretation of the FTIR data are provided in Chapter Six.

3. Methods

3.1. Data collection

X-ray diffraction experiments presented in this thesis were conducted using synchrotron radiation and a laboratory based X-ray source (NanoSTAR). This section provides information about the collection of the scattering data, their analysis and interpretation.

3.1.1. SAXS

SAXS experiments were performed at the synchrotron facilities: Daresbury Laboratory (UK), European Synchrotron Radiation Facility (ESRF-France) and Diamond Light Source (UK). Data were collected on the following beamlines:

3.1.1.1. Station 2.1 - X-ray scattering of non-crystalline materials at the Daresbury Radiation Facility, UK

The station (Figure 3.1) enables SAXS and fibre diffraction measurements. The sample to detector distance can vary from 1 to 8.25 m and provides spatial resolution in the range of 0.8 to 150 nm. The station operates at a fixed wavelength of λ=1.54 Å. The X-ray beam cross section is approximately 1 mm x 5 mm at the specimen position. Technical details of the 2.1 station can be found in Towns-Andrews et al (Towns-Andrews et al., 1989) and on the website: http://www.srs.ac.uk/srs/stations/station2.1.htm

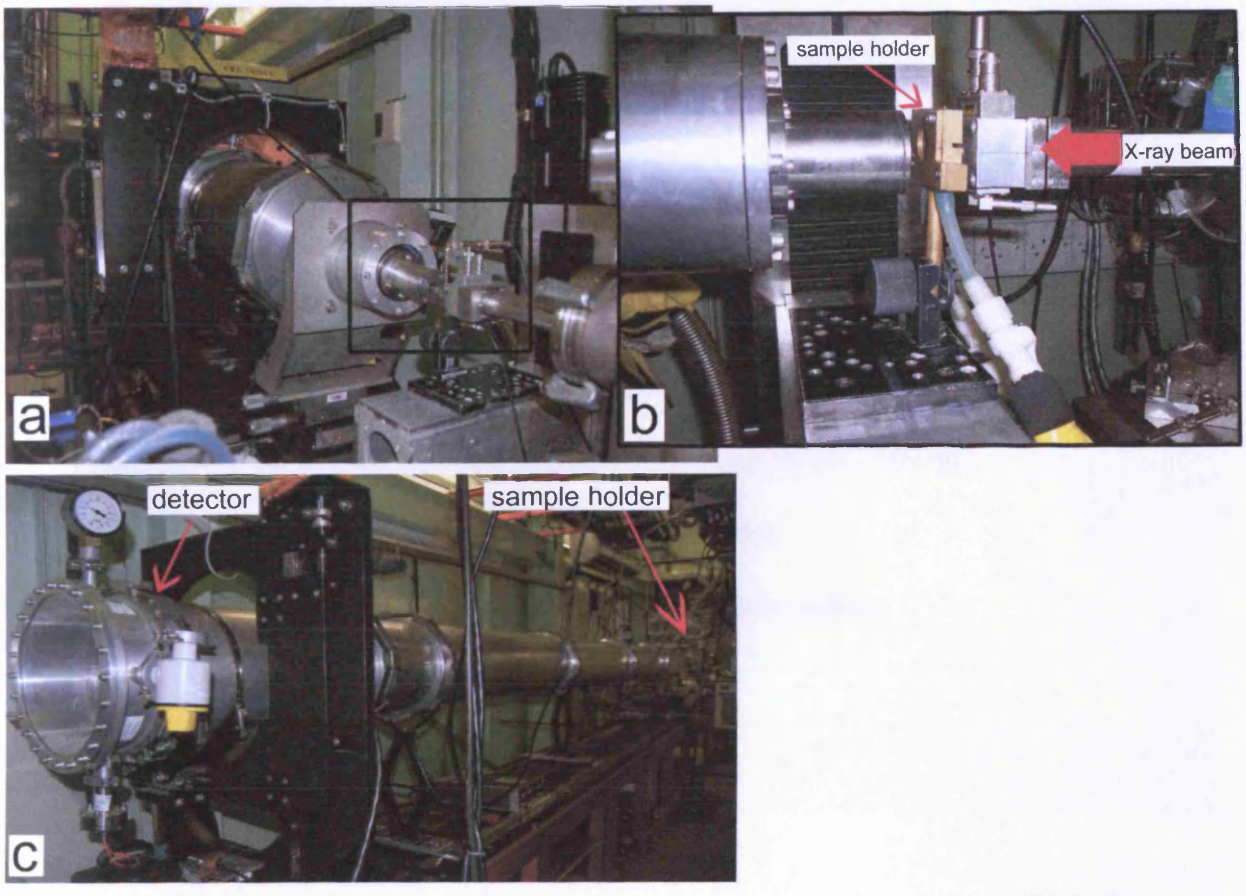

Figure 3.1. The inside of the experimental hutch at SAXS station 2.1 at the Daresbury Laboratory. (a) a sample holder, (b) is a zoomed in section of a and shows a sample holder and the direction of X-rays. The scattered radiation is collected on a detector showed in (c).

3.1.1.2. Beamline ID10C (Troika) at the European Synchrotron Radiation Facility (ESRF) in Grenoble, France

The station enables high resolution X-ray scattering (XD) and X-ray photon correlation spectroscopy (XPCS) experiments to be conducted. The main features of the beamline are high coherent flux (> 10^9 ph/sec/100mA) and a small beamspot size (10x10 μm^2).

Technical information about ID10 station can be found on the website:

http://www.esrf.eu/UsersAndScience/Experiments/Beamlines

3.1.1.3. Station I22 at the Diamond Light Source, UK

This station is the non-crystalline diffraction beamline at the newly built third generation 3 GeV synchrotron light source. It provides spatial resolutions of 0.1 - 500 nm.

Technical information about I22 can be found on the website:

http://www.diamond.ac.uk/Beamlines/Beamlineplan/I22/index.htm

3.1.2. WAXS

Wide-angle X-ray scattering was performed using the laboratory based NanoSTAR (Figure 3.2). In this device X-rays with a wavelength of $\lambda = 0.154$ nm are generated by a Kristalloflex 760 X-ray generator (Bruker AXS, Germany). The size of the resultant X-ray beam is 0.4 mm x 0.8 mm. The X-ray beam is focused using cross-coupled Göbel mirrors and defined by a series of pinholes that produce a beam of 50 micron diameter; a two-dimensional HI-STAR detector is used to collect data. Similarly to the synchrotron beamlines, it is possible to change the sample to detector distance; the NanoSTAR provides spatial resolution in the range from 1-70 nm.

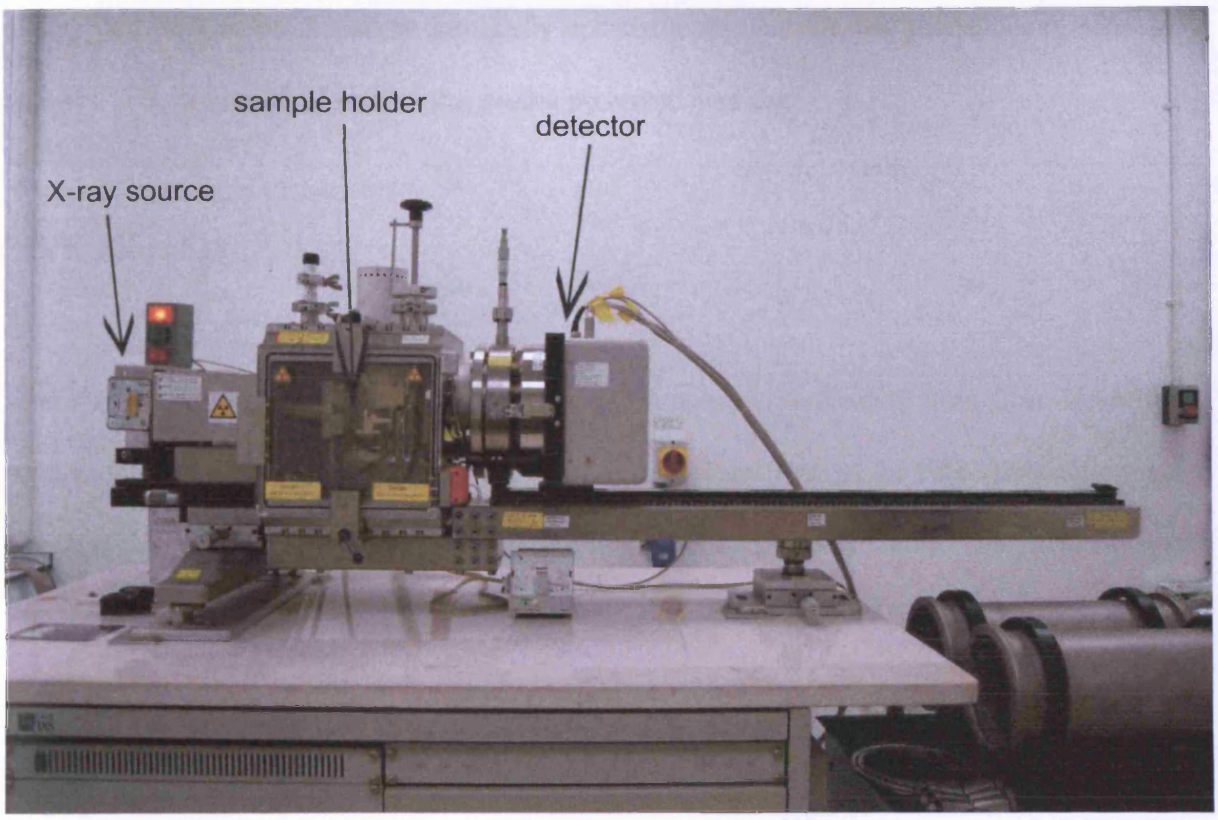

Figure 3.2. Bruker NanoSTAR – a laboratory based X-ray source at the School of Optometry and Vision Sciences, Cardiff University. The X-ray source, the sample holder and the detector are indicated by the arrows.

3.2. Data reduction

X-ray diffraction data were collected as two-dimensional images. They were reduced by the conversion from two-dimensions into one-dimensional linear plots of scattering intensity against angular position ($Q = 4\pi\sin\theta/\lambda$, or $q=2\sin\theta/\lambda$). This was done by integrating the diffraction signal over the whole angular distribution of the detector, using computer programmes. Various programmes are currently available for data reduction and processing. These change on an

almost year by year basis and are frequently updated to account for new modalities of software analysis. The programmes used in the studies presented here are:

3.2.1. FibreFix

FibreFix is a software package created to determine specific parameters from fibre diffraction patterns (created by the former Collaborative Computational Project for Fibre Diffraction and Solution Scattering – CCP13). This user friendly program contains various analytical features that allow the raw data to be read in and displayed as a two-dimensional image. It also has many additional features, for example, it allows (1) adjustment of the intensity scale and the contrast of the image, (2) estimation and removal of the background radiation (radiation derived both from the machine and disorder within the sample), (3) calculation of the image centre, (4) calculation of any specimen tilt and (4) generation of one-dimensional intensity profiles from the integration of two dimensional data. The user can also choose the type of linear intensity plot, for example an intensity profile along a line or a scan around an arc. A screenshot from the FibreFix software is shown in Figure 3.3.

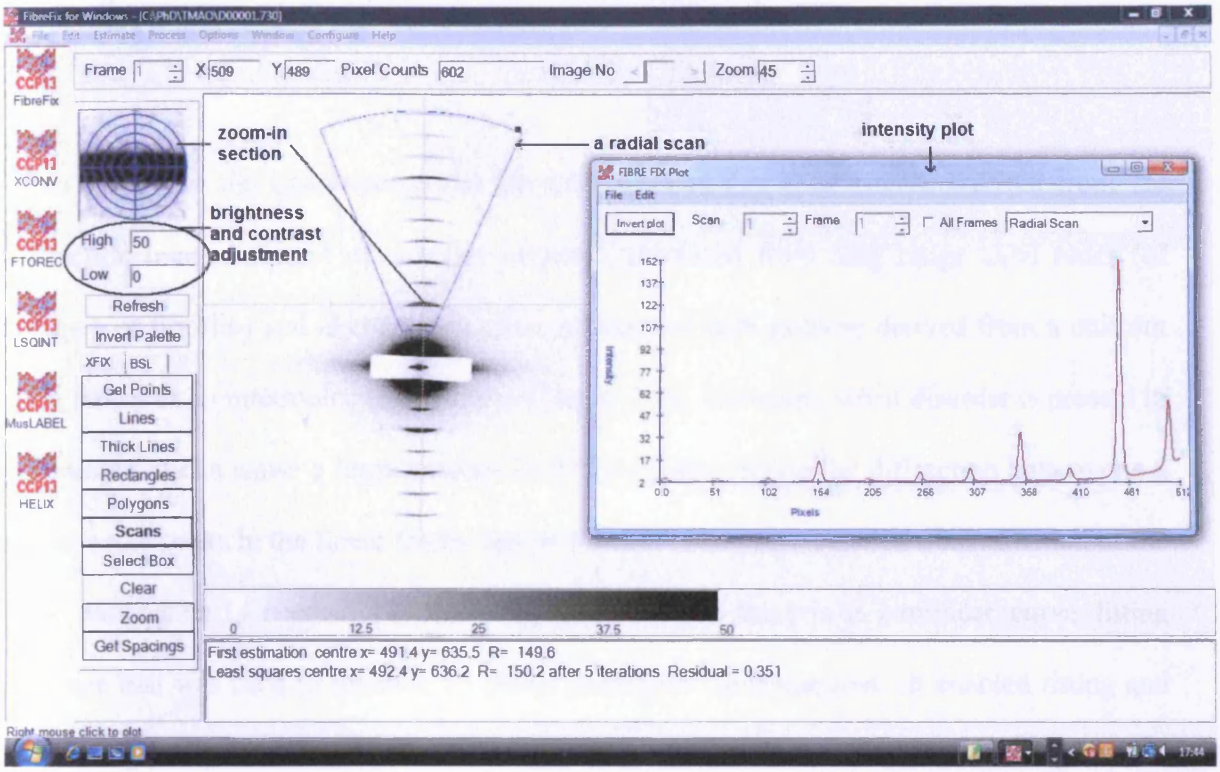

Figure 3.3. A screenshot from FibreFix software displaying a SAXS pattern of rat tail tendon collagen. The software enables users to convert 2D diffraction images into linear profiles (shown on the screen as an intensity plot converted from a scan indicated by an arrow). The window on the left shows a detailed section at any point on the diffraction image chosen by the user – here, it is a zoomed-in section of one of the diffraction peaks.

3.2.2. Fit2D

This software program performs mathematical operations and geometrical transformations such as background subtraction. Fit2D can also be used to analyze powder diffraction data and performs such manipulations as centre estimation, polar transformation of the data and generation of 1D intensity profile as a function of azimuth (Hammersley, 1997).

3.2.3. Peak Fit (Systat Software Inc.)

In an ideal case the one-dimensional intensity profiles that have been converted from 2D diffraction images consist of a series of peaks produced from long range axial order (of collagen or fibrillin) and also contain other reflections such as those derived from a uniform fibril radius or an intermolecular distance (Figure 3.4). However, when disorder is present in the sample, it can cause a large amount of diffuse scattering on the diffraction pattern. As a result, some peaks in the linear traces can be hidden. Therefore detailed determination of the peak parameters is needed. PeakFit (Systat Software Inc.) is a nonlinear curve fitting software that was used to separate all peaks present in the linear plot. It enabled fitting and subtracting a baseline from the traces using different characteristic models for each different data set (e.g. exponential or logarithmic). It also allowed the peaks to be mapped and fitted and the calculation of the peak parameters such as the peak position, the peak amplitude, the integral area and the peak width (full width half maximum, FWHM). A screenshot from PeakFit software is shown in Figure 3.4, while Figure 3.5 shows the peak parameters.

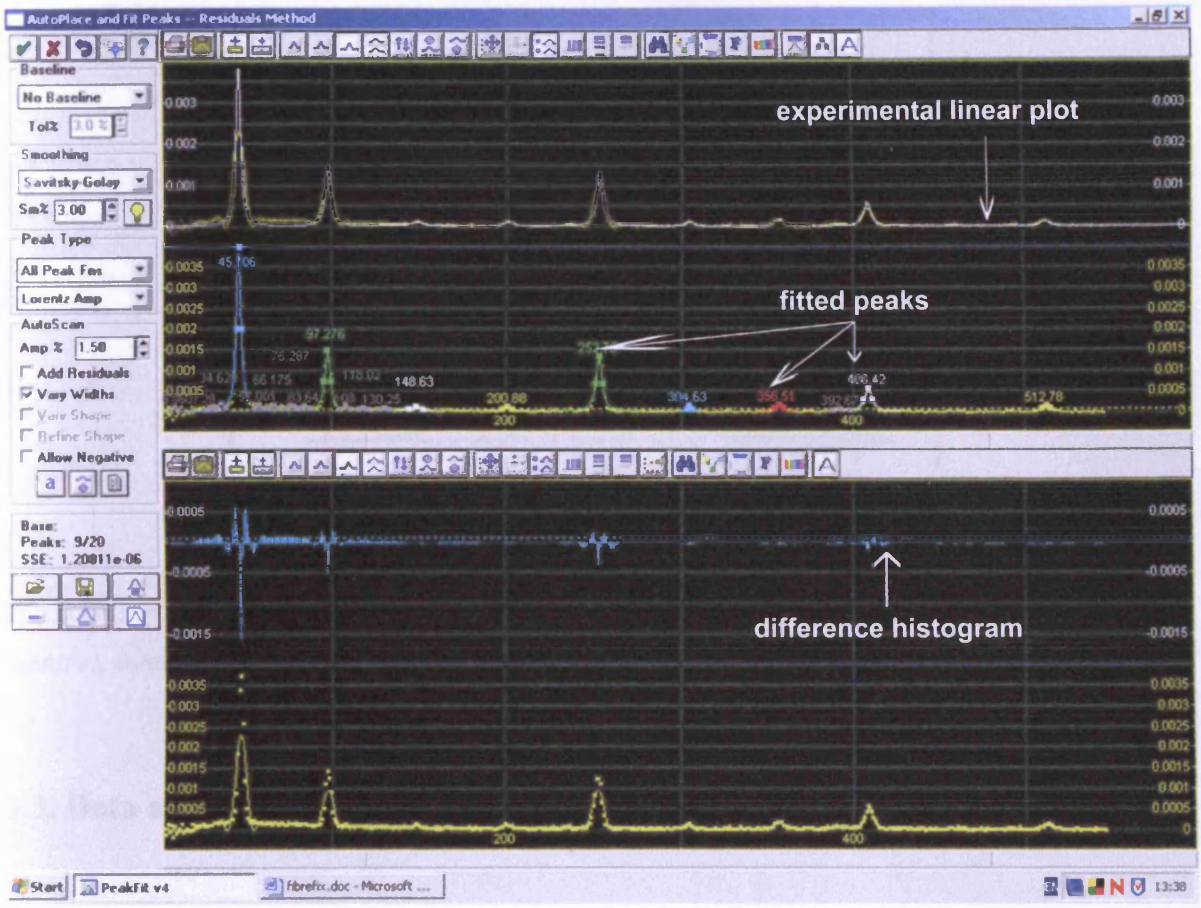

Figure 3.4. A screenshot from PeakFit software. The linear profile displayed on the screen has been converted from the 2D diffraction images collected from rat tail tendon. Peaks correspond to the meridional reflections on the diffraction pattern. The software enables users to fit the peaks (indicated by arrows) and obtain parameters such as peak intensity, position and FWHM. The lower panel shows the residual difference between experimental data and peaks fitted by the software.

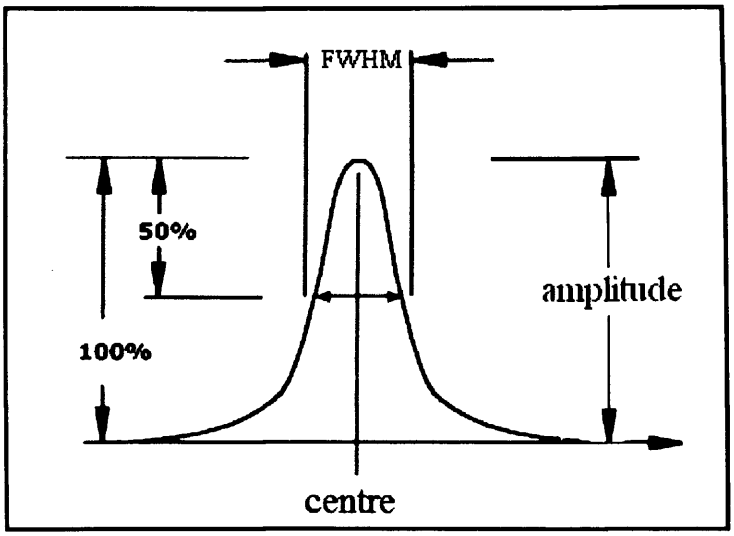

Figure 3.5. Diffraction peak parameters. PeakFit software enables to measure a position (centre), intensity (amplitude) and breadth (full width half maximum – FWHM) of a peak.

3.3. Data analysis

X-ray diffraction patterns from fibrous proteins such as collagen and fibrillin contain meridional and equatorial planes (see section 2.1.7). Reflections on the meridional plane originate from the axial long-range order, while equatorial reflections are produced as a result of ordered (or partially ordered) lateral packing of the protein. By analyzing the position, intensities and the breadth of all these reflections, it is possible to obtain information about structural features of the biological system at the nanoscale. The following parameters can be obtained from the fibre diffraction pattern: (1) from the meridional pattern – the position, intensity and a shape of diffraction peaks (providing information about the axial periodicity, e.g. characteristic D-period in case of collagen) and in case of collagen the helical rise per residue (distance between amino acid residues in the collagen helix), (2) from the equatorial pattern – intermolecular spacing (relative distance between collagen molecules), interfibrillar

spacing (distance between collagen fibrils or fibrillin microfibrils) and fibril radius (Figure 3.6).

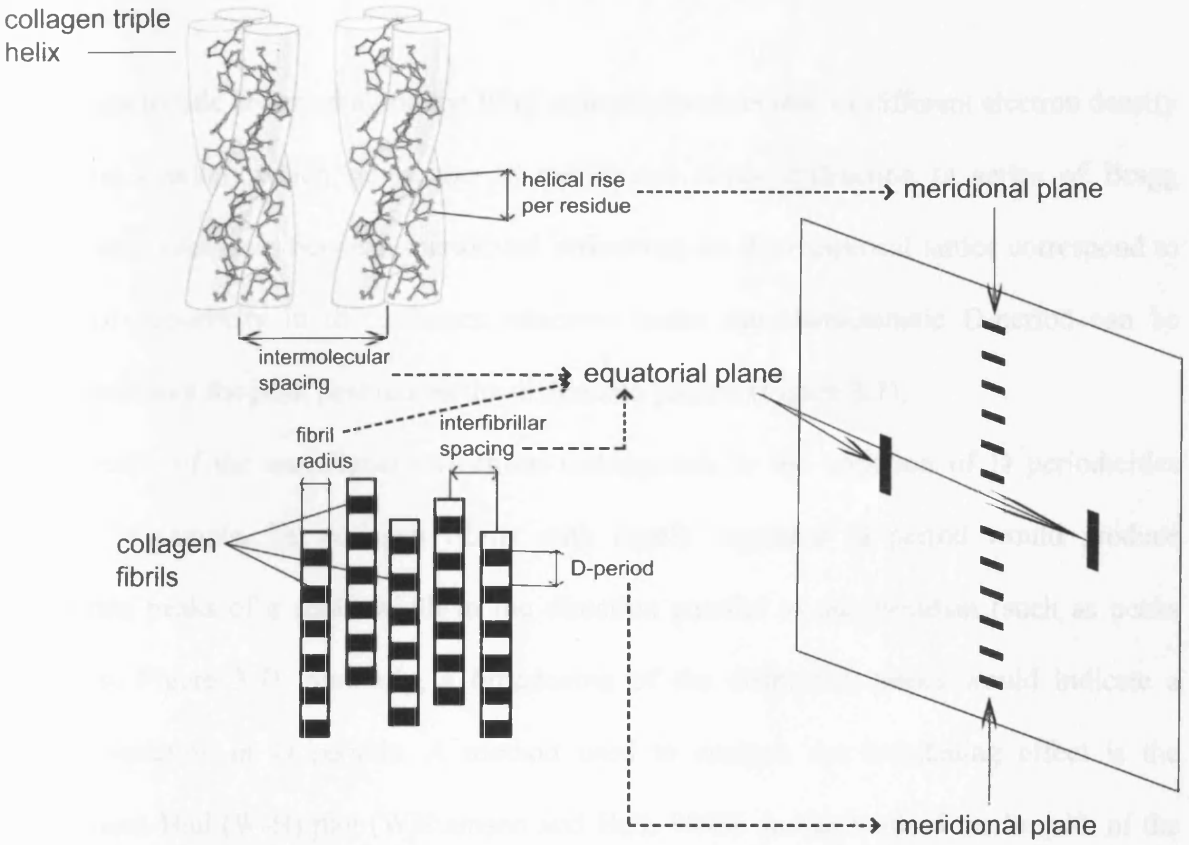

Figure 3.6. A schematic diagram of structural features of collagen (left panel) that give rise to the characteristic X-ray diffraction pattern (right panel). The axial packing of collagen (i.e. helical rise per residue and the D-periodicity) produces meridional reflections, while the lateral packing of collagen (i.e. intermolecular and interfibrillar spacing and fibril radius) gives rise to the equatorial pattern.

3.3.1. Meridional diffraction pattern

3.3.1.1. Axial periodicity

The characteristic D-period along the fibril axis produces regions of different electron density (gap and overlap) which gives rise to meridional X-ray diffraction (a series of Bragg reflections). Distances between meridional reflections on the reciprocal lattice correspond to the axial periodicity in the collagen structure hence the characteristic D-period can be calculated from the peak position on the diffraction pattern (Figure 3.7).

The breadth of the meridional reflections corresponds to the variation of D periodicities within the sample, i.e. collagen fibrils with highly regulated D period would produce diffraction peaks of a small width in the direction parallel to the meridian (such as peaks shown in Figure 3.7). Similarly, a broadening of the diffraction peaks would indicate a greater variation of D periods. A method used to analyze the broadening effect is the Williamson-Hall (W-H) plot (Williamson and Hall, 1953). In this method the breadth of the reciprocal lattice points (i.e. the breadth of the meridional peaks) is plotted against the scattering vector ($Q = 4\pi\sin\theta/\lambda$). The W-H plot allows estimation of two parameters that change within the samples: strain and the finite crystal size (Williamson and Hall, 1953). The slope of the W-H plot is used to estimate the strain and the intercept is used to estimate the crystal size (Figure 3.8). Therefore, this method can be used to discriminate between the influence of finite crystal size from that of lattice strain.

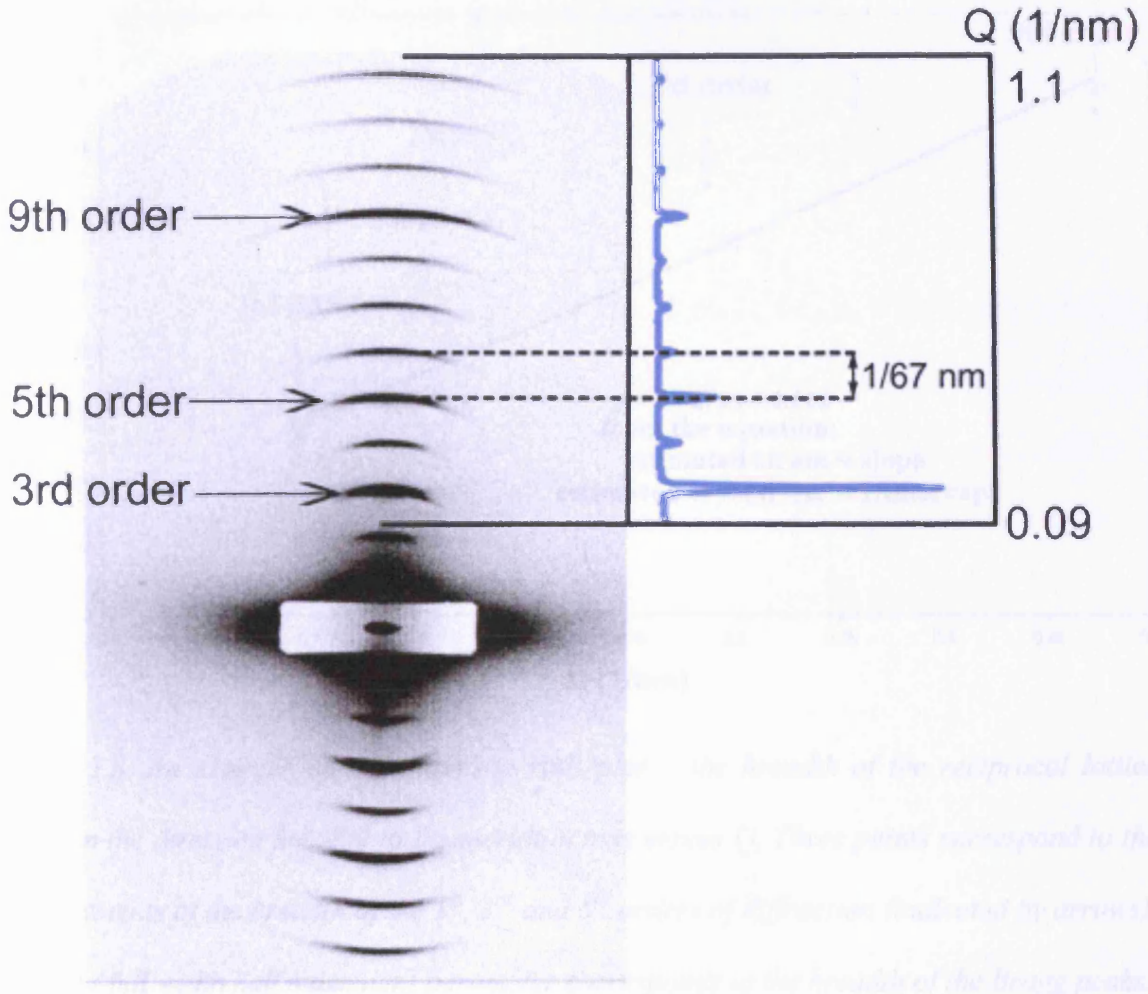

Figure 3.7. Meridional X-ray diffraction pattern of rat tail tendon (D-periodicity = 67nm) and the corresponding linear plot. A two dimensional pattern consists of a series of equidistant Bragg reflections; the D-period can be calculated from the distance between two peaks. The 3rd, 5th and 9th diffraction orders of collagen have been indicated by arrows.

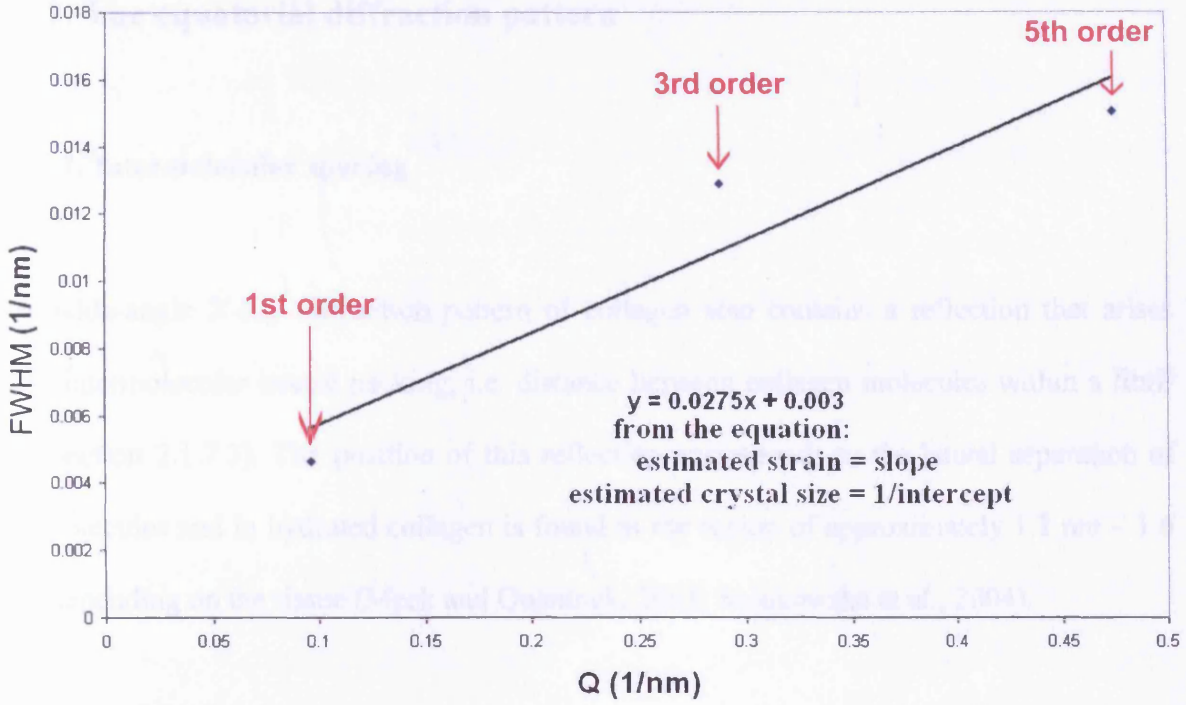

Figure 3.8. An example of a Williamson-Hall plot – the breadth of the reciprocal lattice points in the direction parallel to the meridian axis versus Q. Three points correspond to the measurements of the breadth of the 1st, 3rd and 5th orders of diffraction (indicated by arrows). FWHM (full width half maximum) parameter corresponds to the breadth of the Bragg peaks.

3.3.1.2. Helical rise per residue

The reflection that originates from a helical rise per residue (i.e. a distance between amino acid residues in the collagen helix – see section 2.1.7.3) can be observed on the wide angle diffraction pattern. In normal collagen from rat tail tendon its position corresponds to the value of approximately 0.29 nm (Meek et al., 1979) (Figure 3.6).

3.3.2. The equatorial diffraction pattern

3.3.2.1. Intermolecular spacing

The wide-angle X-ray diffraction pattern of collagen also contains a reflection that arises from intermolecular lateral packing, i.e. distance between collagen molecules within a fibril (see section 2.1.7.3). The position of this reflection corresponds to the lateral separation of the molecules and in hydrated collagen is found in the region of approximately 1.2 nm – 1.6 nm, depending on the tissue (Meek and Quantock, 2001; Sionkowska et al., 2004).

3.3.2.2. Interfibrillar spacing

Fibrils found in connective tissues (i.e. collagen fibrils or fibrillin microfibrils) can be conveniently described as cylinders. Therefore, if the fibrils are arranged in an ordered manner (i.e. at regular distances), an interference function will occur, which gives rise to a characteristic reflection on a low angle equatorial pattern. If the fibrils are not placed on a regular lattice, then an interference function will have reduced intensity.

The position, intensity and the width of this reflection depends on the scattered amplitude of X-rays from a single cylinder (i.e. collagen fibril or fibrillin microfibril) and the relative position of the cylinders. It can be expressed by the equation:

$$I(K) = F^2 * G(K)$$

where F^2 is the scattered intensity for a single collagen or fibrillin fibril (assumed to have a cylindrical shape) and G(K) is the interference function (Glatter and Kratky, 1982; Meek and Quantock, 2001). The position of the first maximum of the interference function provides a value for the mean centre-to-centre distance between fibrils.

Collagen or fibrillin fibrils are usually placed at fixed distances, which can be conveniently described using a Lennard-Jones potential. In this model, fibrils are attracted at large distances but repulsed when they approach too close, which leads them to be situated in an equilibrium position that corresponds to the minimum of the Lennard-Jones potential (Hulmes et al., 1995). The graph of the potential can be seen in Figure 3.9. The minimum of the Lennard-Jones that can be seen on the graph corresponds to the equilibrium distance between two objects (e.g. collagen fibrils or fibrillin microfibrils).

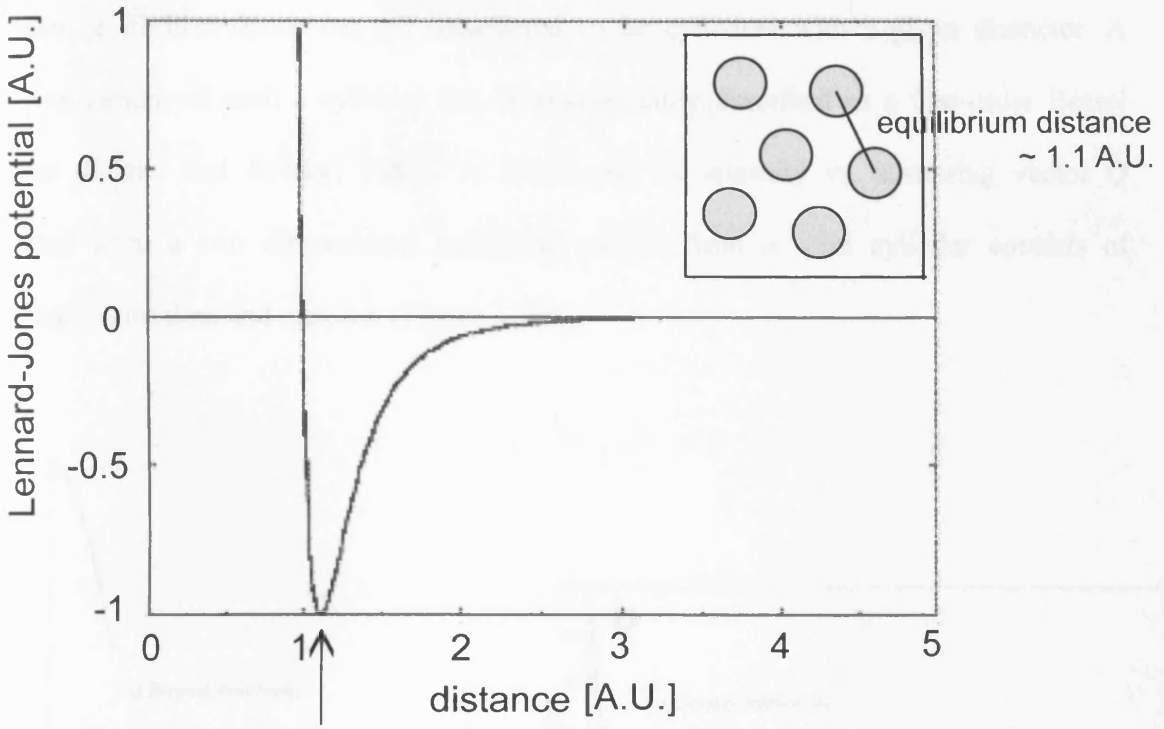

Figure 3.9. The Lennard-Jones potential. The minimum on the graph (indicated by an arrow) corresponds to the equilibrium distance between two objects (e.g. cylindrical objects such as collagen fibrils or fibrillin microfibrils) and in this example it has a value of approximately 1.1 [A.U. – arbitrary units]. The insert shows a simplified situation where objects are situated at the equilibrium position.

3.3.2.3. Fibril diameter

Collagen or fibrillin fibrils can be considered to be cylinders with a given diameter. A scattering pattern of such a cylinder can be conveniently described as a first-order Bessel function (Glatter and Kratky, 1982). A linear plot of intensity vs. scattering vector Q converted from a two dimensional scattering pattern from a solid cylinder consists of characteristic minima and maxima (Figure 3.10a).

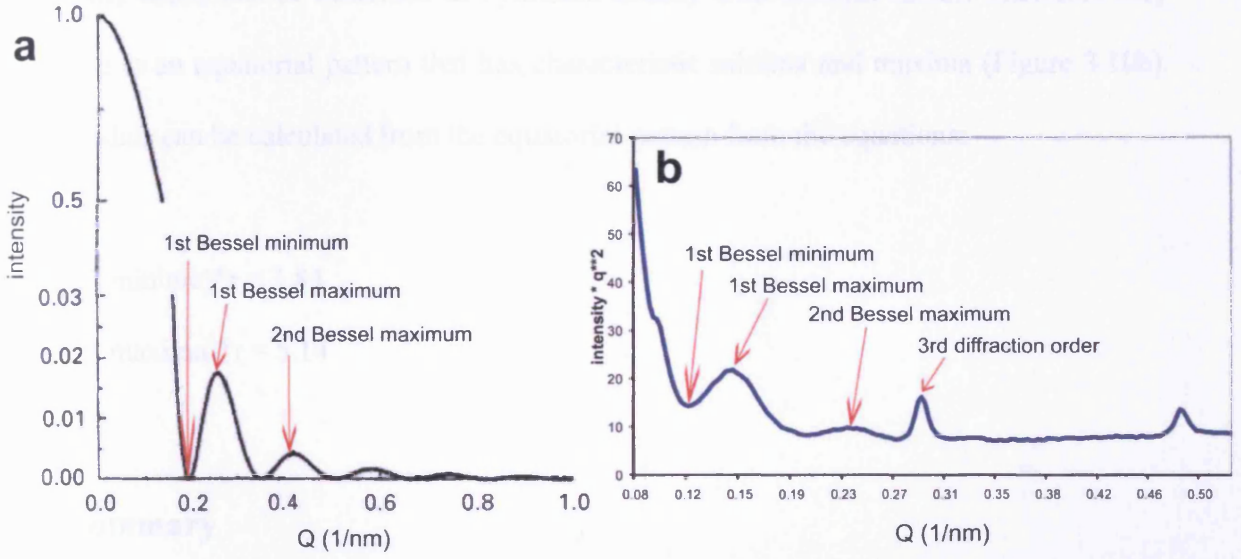

Fiure 3.10. (a) A simulated scattering pattern from a cylinder of 20 nm radius (adapted from (Meek and Quantock, 2001)); the intensity profile consists of characteristic maxima and minima (indicated on the graph) – their position depends on the cylinder radius; (b) an example of a diffraction pattern of collagen where 1st and 2nd maximum can be seen (tumour breast tissue, linear plot converted from 2D diffraction image).

Their positions are related to r (fibril radii) and can be used to estimate its value. Intensity of the scattered X-rays is given by equation:

$$F(Q) = \rho A \frac{2J_1(Qr)}{Qr}$$

where J_1 is the first order Bessel function of the first kind, A is a cross-section area of the cylinder (πr^2) and Q is the coordinate in reciprocal space on the X-ray diffraction pattern ($Q = 4\pi\sin\theta/\lambda$) (Glatter and Kratky, 1982; Goh et al., 2005).

Connective tissues in animals and wood tissue in plants are built from firbril forming molecules which can be described as cylinders usually with uniform radius. Therefore they give rise to an equatorial pattern that has characteristic minima and maxima (Figure 3.10b). Fibril radius can be calculated from the equatorial pattern from the equations:

Q (at 1st minima)*r = 3.84

Q (at 1st maxima)*r = 5.14

3.4. Summary

This chapter provided information about the collection of fibre diffraction data from collagen and fibrillin. Methods of data reduction and analysis have been described, which are used to obtain information about structural features of two biopolymers e.g. the axial periodicity, intermolecular and interfibrillar distance and fibril diameter. The examination of collagen and fibrillin structure on the molecular and fibrillar level is crucial to fully understand the underlying mechanisms and structural transformations that are induced by external factors. The methods of data analysis and interpretation described here provide statistically

significant results since the incoming X-rays interact with thousands of fibrils present in the sample. Therefore, the resulting diffraction pattern represents the structural features from the majority of fibrils. These methods have been used in all four studies presented in the following chapters Four – Six.

4. Introduction of local strain defects in collagen axial structure.

4.1. Introduction

The study described in this chapter presents changes observed within collagen structure that were induced by an intense X-ray photon dose. X-ray beams generated at synchrotron sources have been used in medicine as a treatment of cancer (see section 1.2.1.2). In such therapies only beams of very small sizes are used to reduce the volume of the tissue that is being irradiated (i.e. to only irradiate the tumour cells). However, during surgery there is a risk that healthy, collagenous tissues that surround the tumour are also exposed to an intensive X-ray dose. Therefore, in the study presented here, a model collagenous tissue was used (rat tail tendon) to examine the possible molecular rearrangements within the collagen structure in response to X-ray irradiation. The understanding of the alterations in collagen structure induced by extreme conditions is also beneficial in biomaterial production; it can aid the design of new materials with controlled biodegradative properties.

The X-ray radiation damage of biological samples is a known problem in studies conducted at synchrotron facilities. In the 4^{th} generation light sources that are currently under development (i.e. X-ray free-electron lasers, X-FEL), where an extremely intense and coherent X-ray beams will be generated, the radiation damage will potentially become an increasing problem that requires to be understood. The experiment described in this chapter is an initial study of radiation damage on collagen and collagen dynamics. A partially coherent X-ray beam, used for X-ray photon correlation spectroscopy (XPCS) was applied in order to obtain an extremely intense X-ray dose. The high coherence of the X-ray beam, combined

with its extreme brightness enable to conduct dynamic studies over very short time scales. The results from this initial study of collagen dynamics could lead to further experiments where even shorter time scales are used (i.e. on a femtosecond scale at X-FEL).

The measurements were taken at 8 different temperature settings: -20, -15, -10, -5, 0, +5, +10 and +20°C, to examine the effects of an X-ray dose at various environments and to see if the observed effects are temperature dependent. As a result, the small-angle meridional X-ray diffraction patterns showed novel molecular alterations in the collagen axial structure. Williamson-Hall plots, a method used to analyze the broadening effects observed on the diffraction pattern, were used to understand the nature of the novel alterations and the results suggest that they can be explained by the local strain variation. The local strain was found to be dose dependent and the resulting Arrhenius plot (i.e. the dose-dependent strain change plotted against the temperature) was used to examine the effect of temperature on the rate of the observed process.

4.2. Materials and methods

4.2.1. Sample preparation

The X-ray diffraction data presented in this chapter were collected prior to the commencement of this PhD project by Oskar Paris, Lorenz-Mathias Stadler, Anders Madsen, Peter Fratzl and Tim Wess.

The collagen used in this experiment was obtained from rat tail tendon. Single fibres with a thickness of about 100 μm were used. Fibres were kept under slight tension to remove the macroscopic crimp, and were fully hydrated during the experiment in sealed capillaries.

4.2.2. Small-angle X-ray scattering (SAXS)

The measurements were conducted at the European Synchrotron Radiation Facility (ESRF) in Grenoble, France. Beamline ID10C (Troika) was used for the experiments and a partially coherent X-ray beam (defined by a 10 micron pinhole about 20 cm upstream of the sample) was employed. The X-ray energy was 12.9 keV with a relative energy resolution of about 10^{-4} and a corresponding wavelength of λ=0.096 nm. The flux was ~ 10^{13} ph/sec/mm^2 which amounts to 10^9 ph/sec in the primary beam (10 micron diameter). The scattered intensity was recorded by a directly illuminated CCD detector (Princeton Instruments, 1242x1152 pixels, 22.5x22.5 μm^2 pixel size) mounted in a distance of 3.2 m from the sample. In order to speed up the CCD read-out, only the region of interest (341x1041 pixels) was used for the measurements, since the dynamics of collagen are faster than the average read-out time of a CCD detector (Figure 4.1). With an exposure time of typically one second the repetition rate was then 2 s per frame. This allowed the Q-range ($Q = 4\pi\sin\theta/\lambda$) for a single setting to be 0.069 – 0.544 nm^{-1}. The intensity patterns of collagen displayed strong speckle features which is a clear indication of coherent illumination. Hydrated rat tail tendon was used as a calibration standard.

Eight different sample environment temperatures were used in the experiment: -20, -15, -10, -5, 0, +5, +10 and +20°C. Samples at each temperature were exposed to the intense synchrotron X-ray beam and a series of frames were collected. The number of collected frames was 600 (which correspond to 20 minutes of exposure), except the samples from -20°C (1200 frames – 40 minutes) and -15°C (248 frames – 8 minutes 26 seconds).

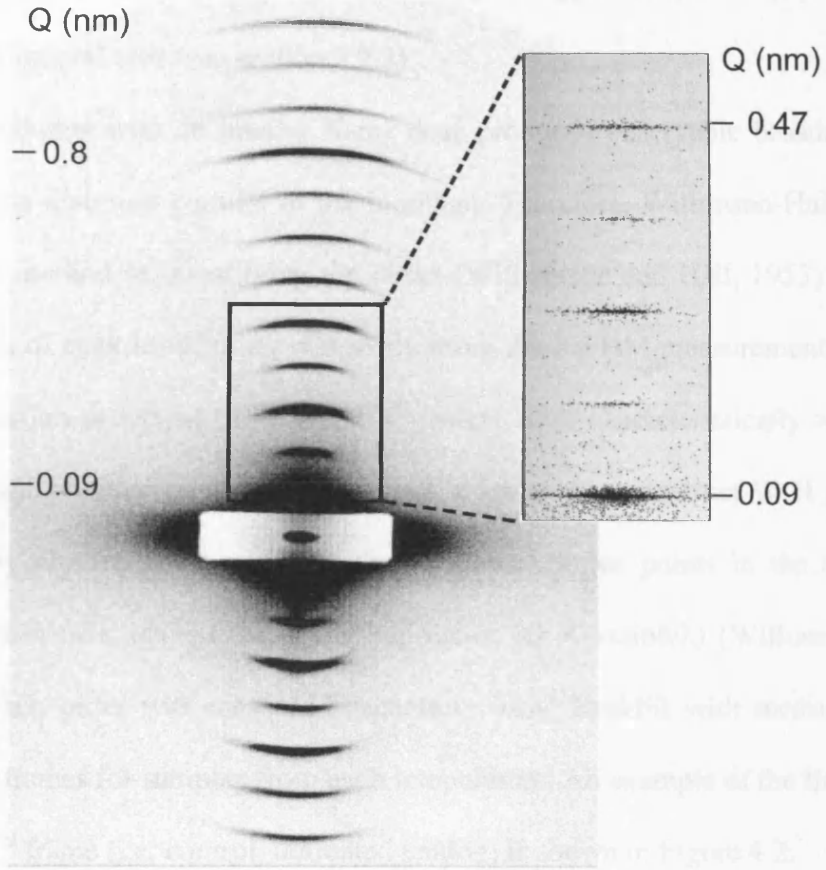

Figure 4.1. A region of interest selected from the X-ray diffraction pattern from rat tail tendon collagen. An insert shows a zoomed-in section used in the measurements in order to speed up the detector read-out time.

4.2.3. Data analysis

X-ray diffraction data of collagen fibrils were analyzed as described in Chapter 3 using CCP13 FibreFix software and PeakFit software. The first five orders of collagen were observed on the small-angle meridional X-ray diffraction patterns (Figure 4.2a). PeakFit

software allowed determination of peak parameters – amplitude, position, FWHM (full width at half-maxima) and integral area (see section 3.2.3).

The irradiation of collagen with an intense X-ray dose produced observable broadening of axial reflections in the direction parallel to the meridian. Therefore, Willimson-Hall (W-H) plots were used as a method of quantifying the effect (Williamson and Hall, 1953) (section 3.3.1.1). The analysis of peak broadening was made using the FWHM measurements for the 1^{st}, 3^{rd} and 5^{th} diffraction orders as the 2^{nd} and 4^{th} orders were characteristically relatively weak. The FWHM and position data for these orders were used to construct W-H plots for successive frames by plotting the breadth of the reciprocal lattice points in the direction parallel to the meridian axis against the scattering vector ($Q = 4\pi\sin\theta/\lambda$) (Williamson and Hall, 1953). Here each order was measured separately using PeakFit with measurements made for successive frames for samples from each temperature. An example of the linear plot converted from the 1^{st} frame (i.e. control, untreated tendon) is shown in Figure 4.2.

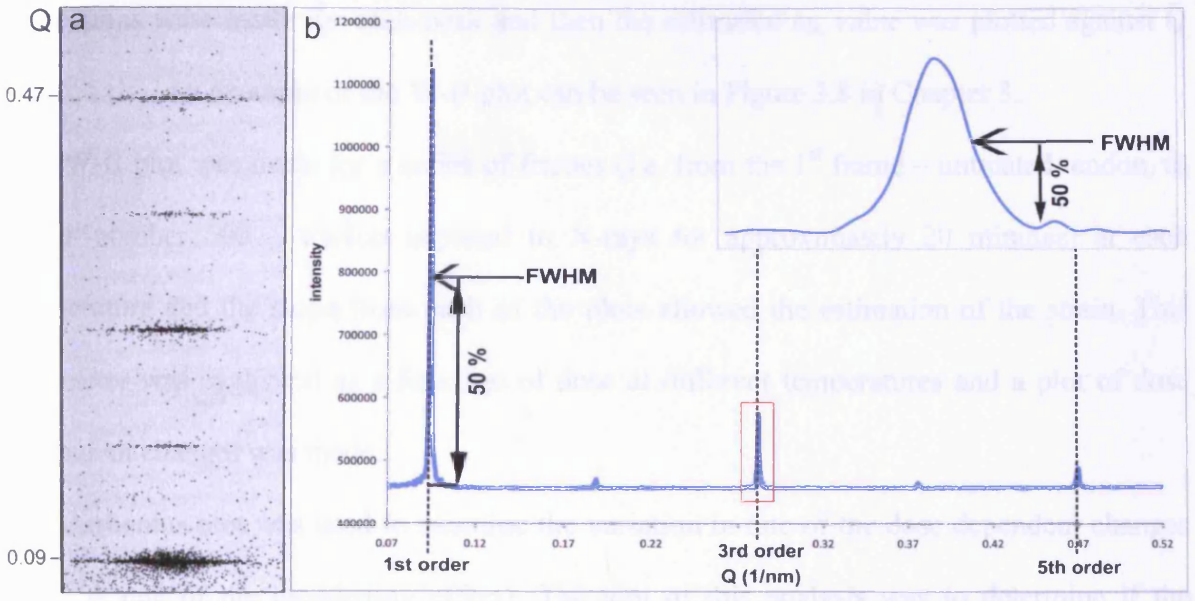

Figure 4.2. (a) an X-ray diffraction pattern, collected from control tendon at -5°C, where five diffraction orders of collagen can be observed. (b) a corresponding linear plot. The positions of the 1st, 3rd and 5th diffraction order (indicated on the plot) were measured, as well as the full width at half-maxima of all three orders. These parameters were used to construct each Williamson-Hall plot. An insert corresponds to the 3rd diffraction order, highlighted on the graph by a red box (the position where FWHM was measured is indicated by an arrow for the 1st diffraction order and 3rd diffraction order in a zoomed-in section).

The FWHM value calculated from the corresponding order in the first frame (i.e. untreated sample) was used here as a correction for instrumental broadening, due to the initial high coherence of the collagen. The y-axis of the W-H plot (i.e. corresponding to the breadth of the diffraction peaks in the direction parallel to the meridian axis), ω_k, was estimated from the equation $\omega_k=\sqrt{\omega^2-\omega_0^2}$, where ω is the FWHM of an observed diffraction order in the sample [nm^{-1}] and ω_0 is the FWHM [nm^{-1}] of the corresponding order in the first frame. The

corrections were made for each peak and then the estimated ω_k value was plotted against Q (the x-axis). An example of the W-H plot can be seen in Figure 3.8 in Chapter 3.

The W-H plot was made for a series of frames (i.e. from the 1st frame – untreated tendon, to frame number 600 – tendon exposed to X-rays for approximately 20 minutes) at each temperature and the slope from each of the plots allowed the estimation of the strain. This parameter was evaluated as a function of dose at different temperatures and a plot of dose dependent changes was made.

The Arrhenius plot was used to examine the variation in rate of the dose dependent changes (i.e. the rate of the broadening effect). The aim of this analysis was to determine if the changes in the lattice strain are temperature dependent. To achieve this, the dose dependent change (i.e. the rate of the broadening process) was plotted against 1000/T, creating the Arrhenius plot (see Result section below). By using the Arrhenius plot it is possible to see if the process (broadening due to the strain in this case) is temperature dependent: if there is no relation to the temperature, then there is a large scatter of data points on the Arrhenius plot. However, if the points produce a straight line, it indicates the Arrhenius relation and the temperature dependence of the process.

4.3. Results

Meridional reflections of the X-ray diffraction pattern of collagen can be used to investigate the characteristic axial packing of collagen molecules. Effects induced by an intense X-ray photon dose to the X-ray diffraction pattern can be seen in Figures 4.3-4.11. The main effects observed here are:

The dose dependent broadening of the diffraction peaks in the direction parallel to the meridian axis which increases with diffraction order

A change in the position of the diffraction peaks, which indicates variation in the characteristic axial periodicity of collagen

A change in the relative intensity of the meridional diffraction orders indicating an alteration in axial electron density within a fibril

4.3.1. Peak broadening

The analysis of the breadth of the Bragg reflections in the successive time frames showed the broadening of all diffraction peaks in the direction parallel to the fibre axis (Figures 4.3-4.10). The broadening increased with diffraction order; typically here, the fifth order often became increasingly difficult to measure after 50-100 frames of exposure as it merged into the background, while the 1st order remained measurable until the end of each experiment. At temperatures above -10°C, the diffraction orders split into two peaks in the direction parallel to the fibre axis, (two separate peaks that appear at both lower and higher Q are indicated on Figures 4.5-4.10). The splitting occurred in all diffraction orders and the distance between two peaks increased with the reciprocal lattice position. This specific effect was best observed in the 3rd diffraction order, as the separate peaks of the first order were relatively close to each other, and the fifth order merged into the background and was increasingly difficult to resolve.

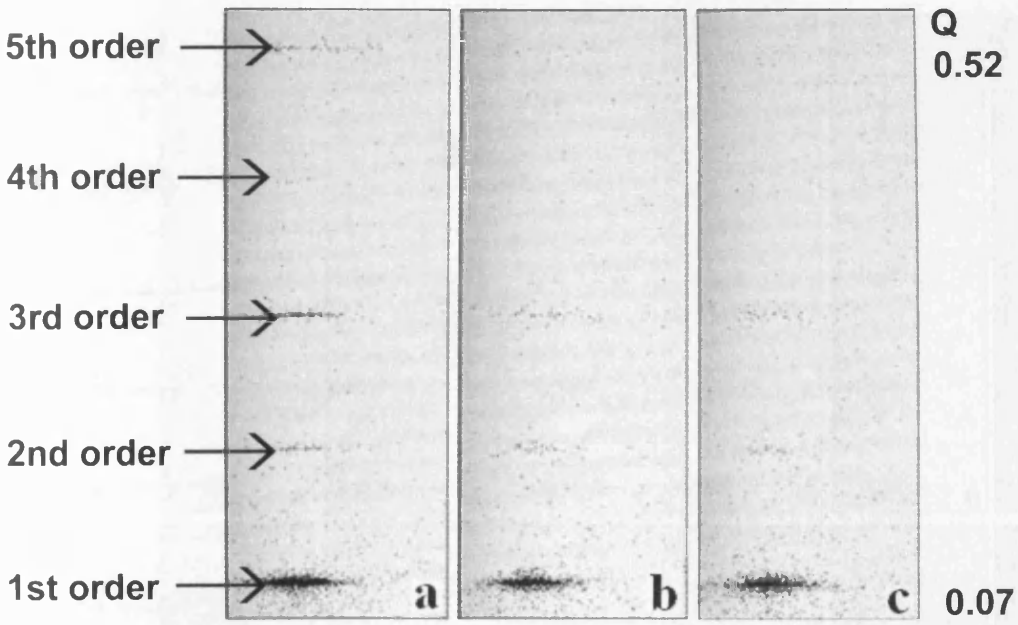

Figure 4.3. Small-angle X-ray diffraction images collected at -20 °C. The image (a) was collected from a control tendon, while images (b) and (c) correspond to tendons after 23 and 40 minutes of exposure, respectively.

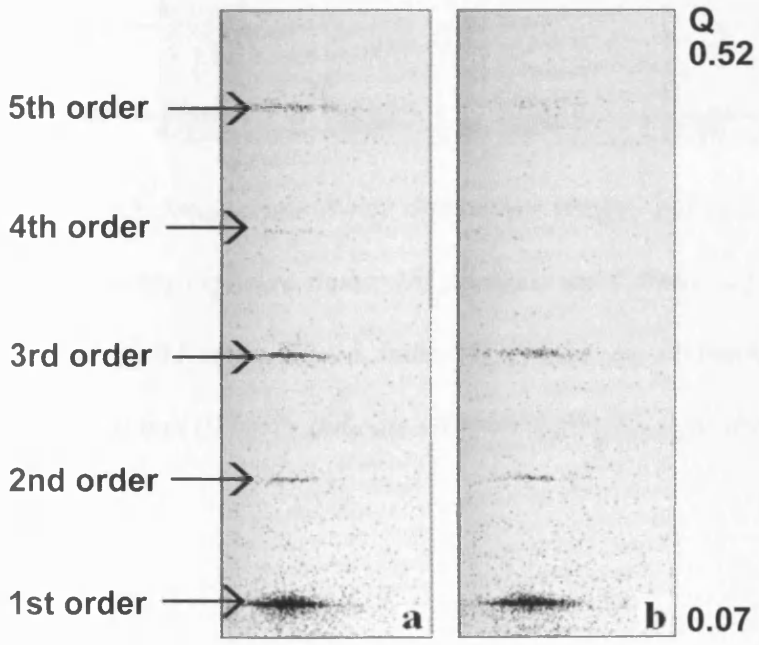

Figure 4.4. Small-angle X-ray diffraction images collected at -15°C. The image (a) was collected from a control tendon; (b) corresponds to tendon after 8.2 minutes of exposure.

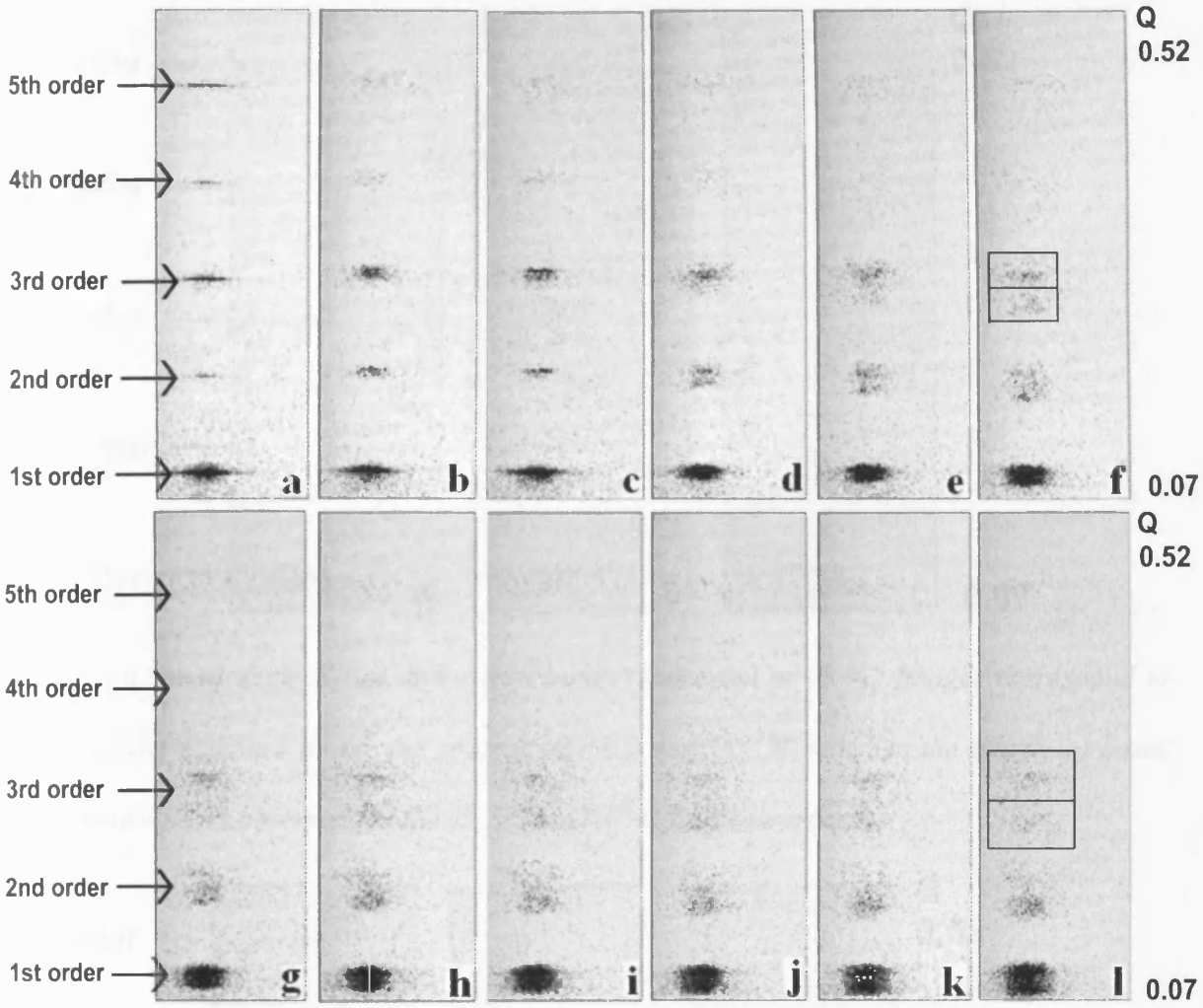

Figure 4.5. Small-angle X-ray diffraction images collected at -10°C. Images correspond to the following exposure times: (a) control, (b) 3.3min; (c) 5min; (d) 6.6min; (e) 8.3min; (f) 10min; (g) 11.6min; (h) 13.3min; (i) 15min; (j) 16.6min; (k) 18.3min; (l) 20min. On the images (f) and (l) boxes indicate two peaks observed for the 3rd diffraction order.

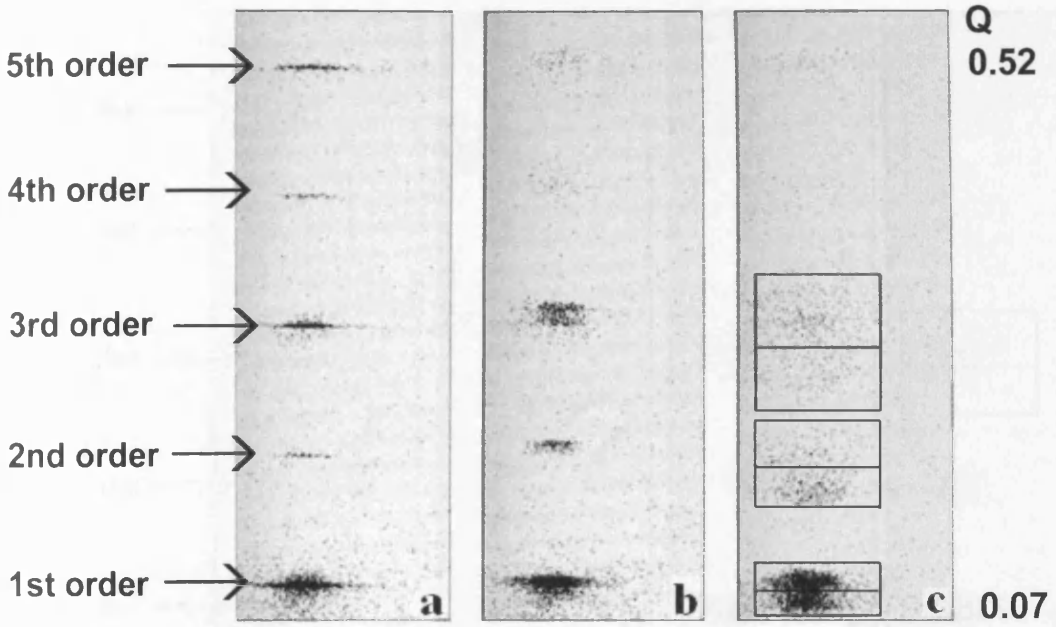

Figure 4.6. Small-angle X-ray diffraction images collected at -5 °C. Images correspond to the following exposure times: (a) control; (b) 3.3 min; (c) 20 min. On the image (c) boxes indicate two peaks observed for the 1st, 2nd and 3rd diffraction order.

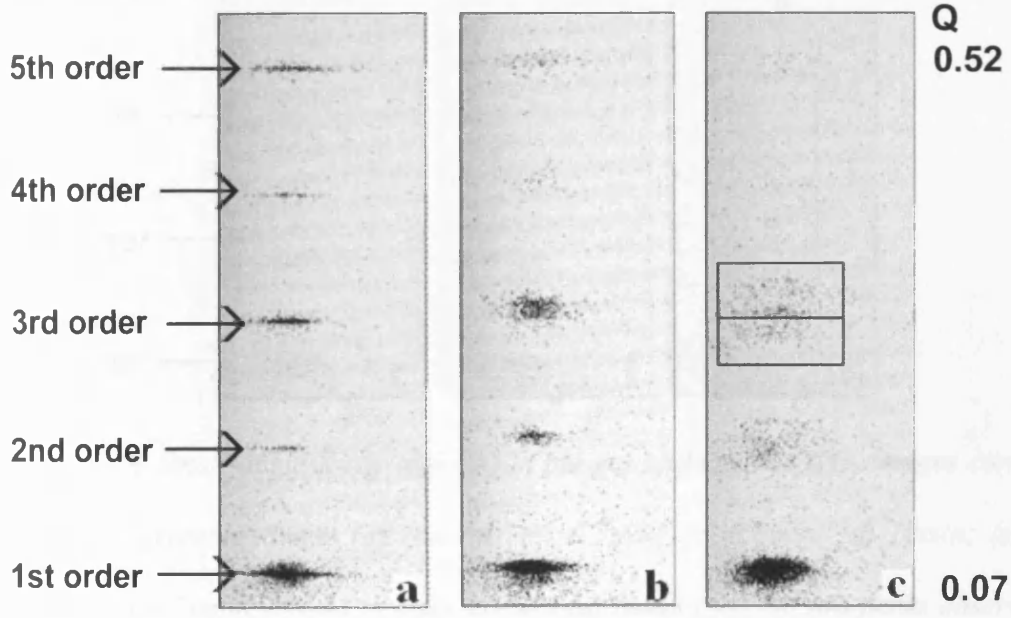

Figure 4.7. Small-angle X-ray diffraction images collected at 0°C. Images correspond to the following exposure times: (a) control; (b) 3.3 min; (c) 20 min. On the image (c) boxes indicate two peaks observed for the 3rd diffraction order.

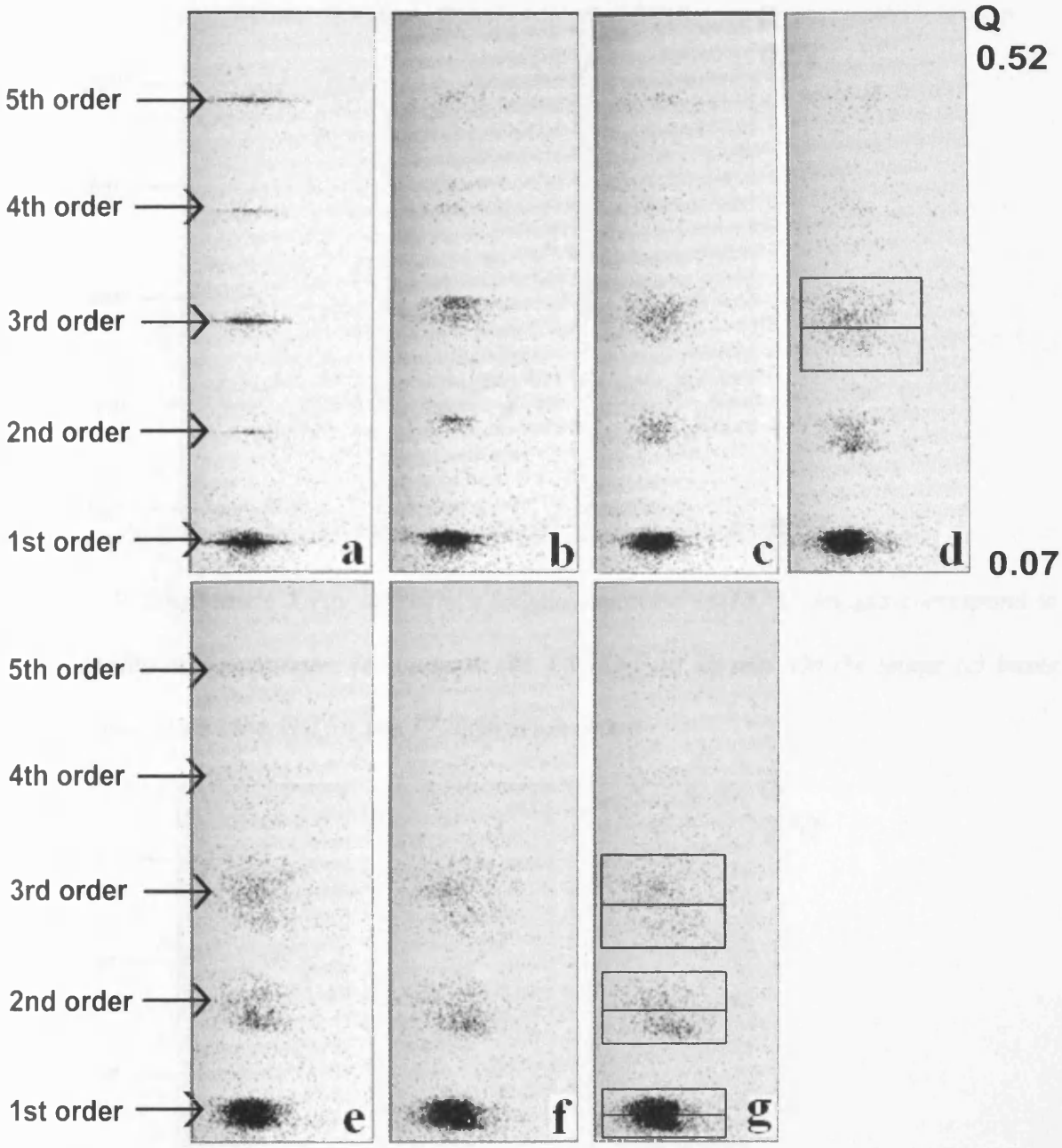

Figure 4.8. Small-angle X-ray diffraction images collected at 5°C. Images correspond to the following exposure times: (a) control; (b) 3.3min; (c) 6.6min; (d) 10min; (e) 13.3min; (f) 16.6min; (g) 20min. On the images (d) and (g) boxes indicate two peaks observed for the 1st, 2nd and 3rd diffraction order.

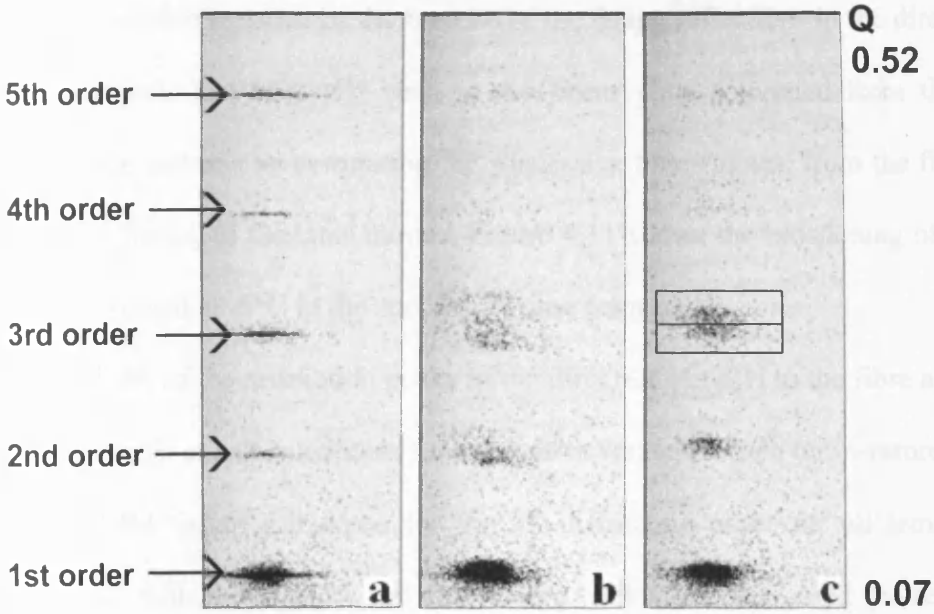

Figure 4.9. Small-angle X-ray diffraction images collected at 10 °C. Images correspond to the following exposure times: (a) control; (b) 3.3 min; (c) 20 min. On the image (c) boxes indicate two peaks observed for the 3rd diffraction order.

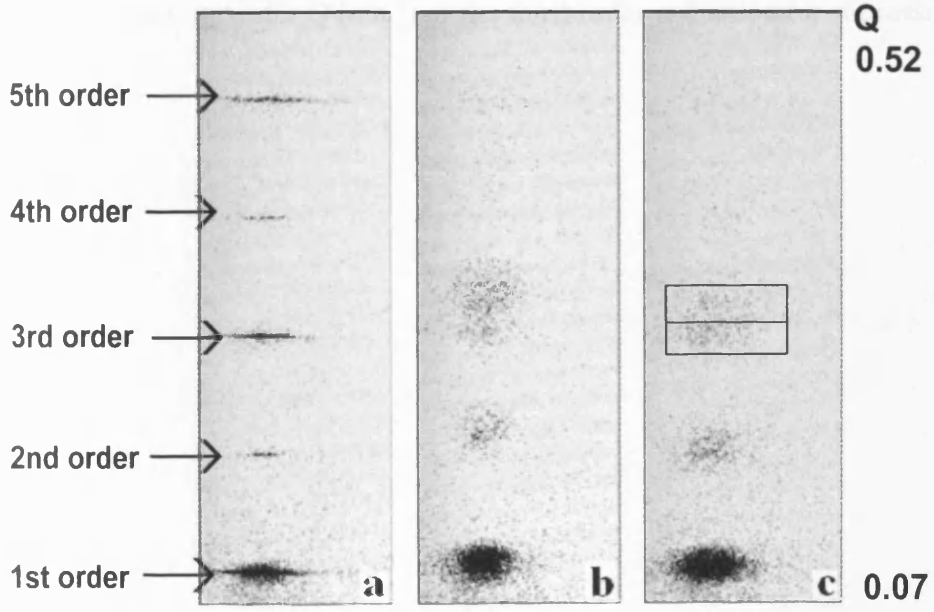

Figure 4.10. Small-angle X-ray diffraction images collected at 20°C. Images correspond to the following exposure times: (a) control; (b) 3.3 min; (c) 20 min. On the image (c) boxes indicate two peaks observed for the 3rd diffraction order.

The remarkable increase of the breadth of the Bragg reflections in the direction parallel to the meridian axis can be easily seen in the linear plots converted from the two dimensional diffraction patterns by comparing the successive time frames: from the first frame (untreated collagen fibrils) to the later frames. Figure 4.11 shows the broadening of the first diffraction order observed at -5°C in the successive time frames.

The breadth of the diffraction peaks in the direction parallel to the fibre axis was measured as the full width at half-maximum for successive frames at each temperature. Figure 4.12 shows the FWHM values calculated for the 3rd diffraction order for all temperatures. It can be observed that the breadth of the Bragg reflection increased more rapidly at higher temperatures. It should be noted, that all environment temperatures were below the melting temperature of collagen.

The broadening is also demonstrated in Figure 4.13 which shows the linear plot of intensity versus scattering vector Q (nm^{-1}) of the third-order reflection for successive time frames.

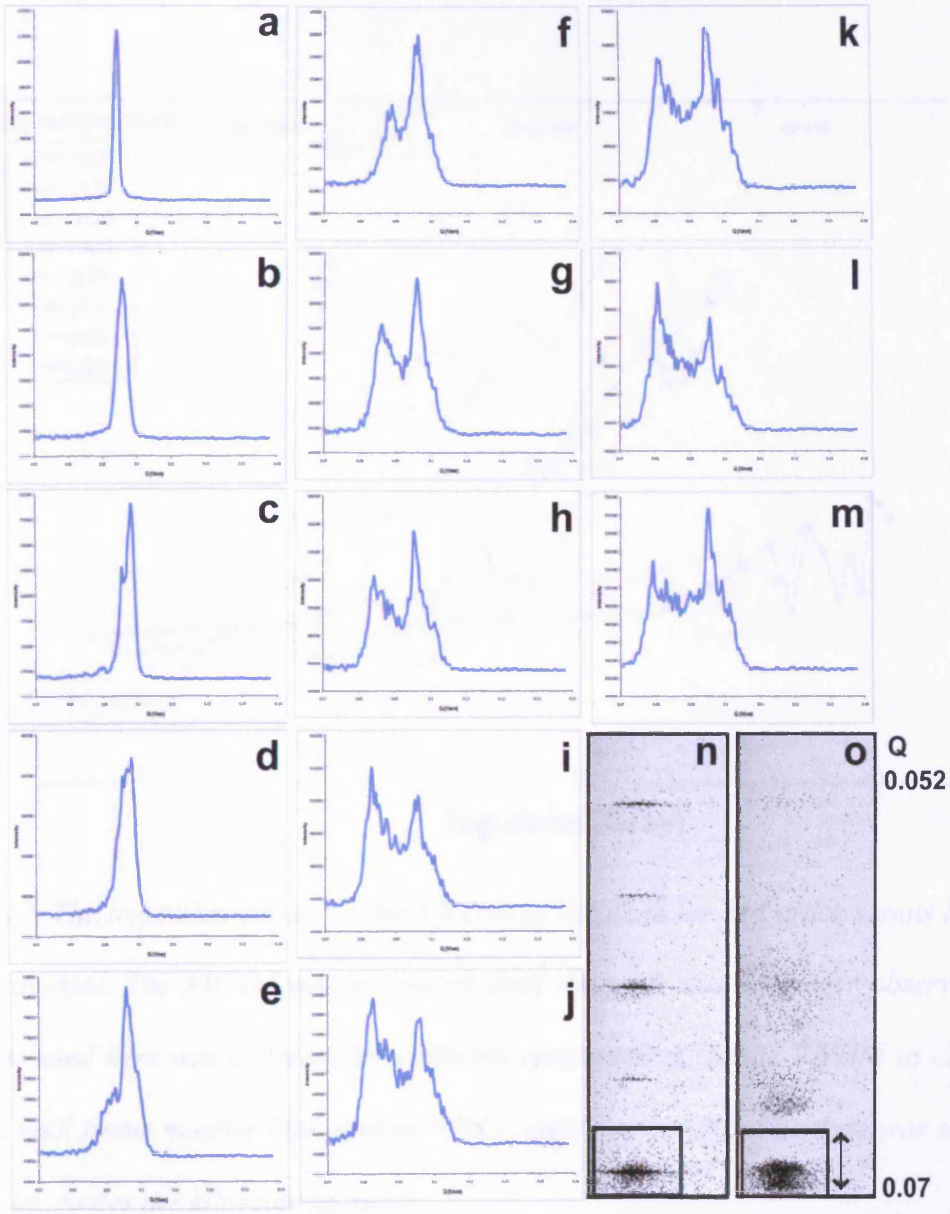

Figure 4.11. Linear plots converted from diffraction images collected at -5°C. The sections show the position and the shape of the 1st diffraction order. Graphs correspond to the following exposure times: (a) control (b) 1.6min (c) 3.3min (d) 5min (e) 6.6min (f) 8.3min (g) 10min (h) 11.6min (i) 13.3min (j) 15min (k) 16.6min (l) 18.3min (m) 20min. (n) and (o) show diffraction images collected from control tendon and tendon irradiated for 20 minutes, respectively; the 1st order region presented on the graphs (a)-(m) is highlighted and arrows indicate the direction of linear profiles.

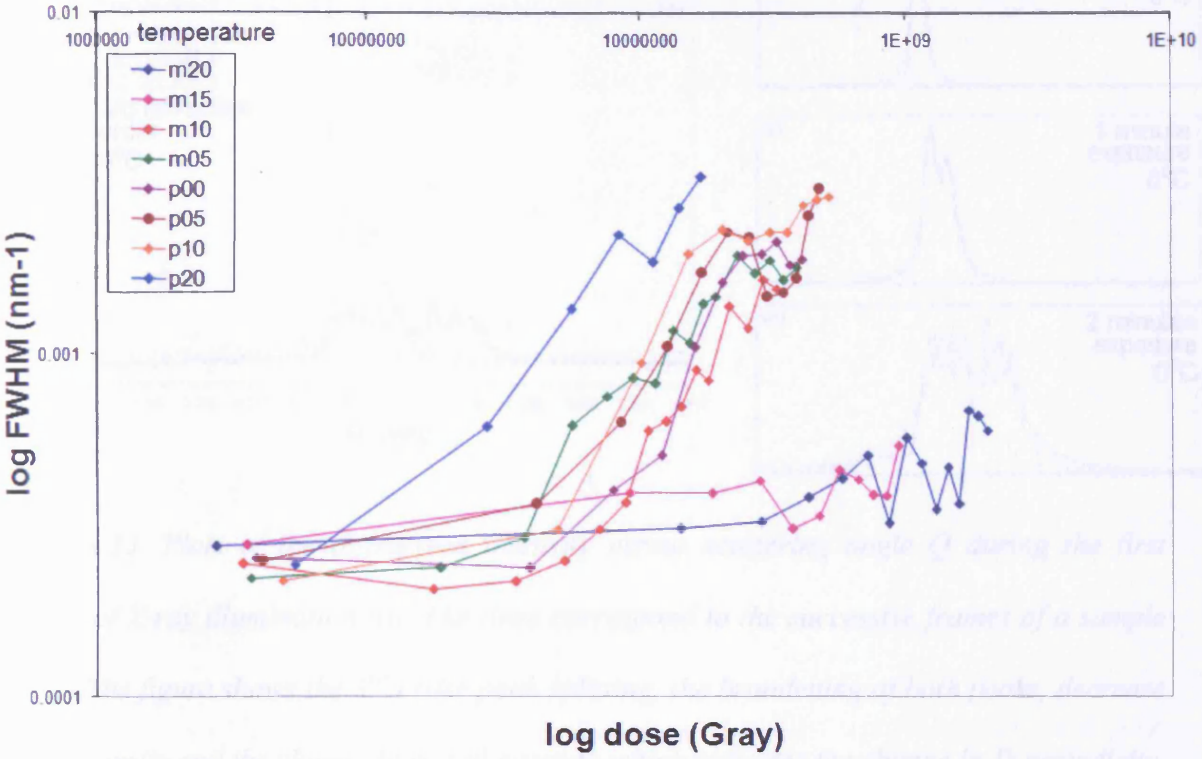

Figure 4.12. The logarithm values of the FWHM of the peak for 3rd order versus logarithm of the X-ray dose. The FWHM was measured until the peak was no longer observable (the final frame used here was different for different temperatures, hence FWHM in -20°C was measured until frame number 700, and in +20°C until number 30). The dose was calculated in Grays, i.e. Joules per kilogram of mass.

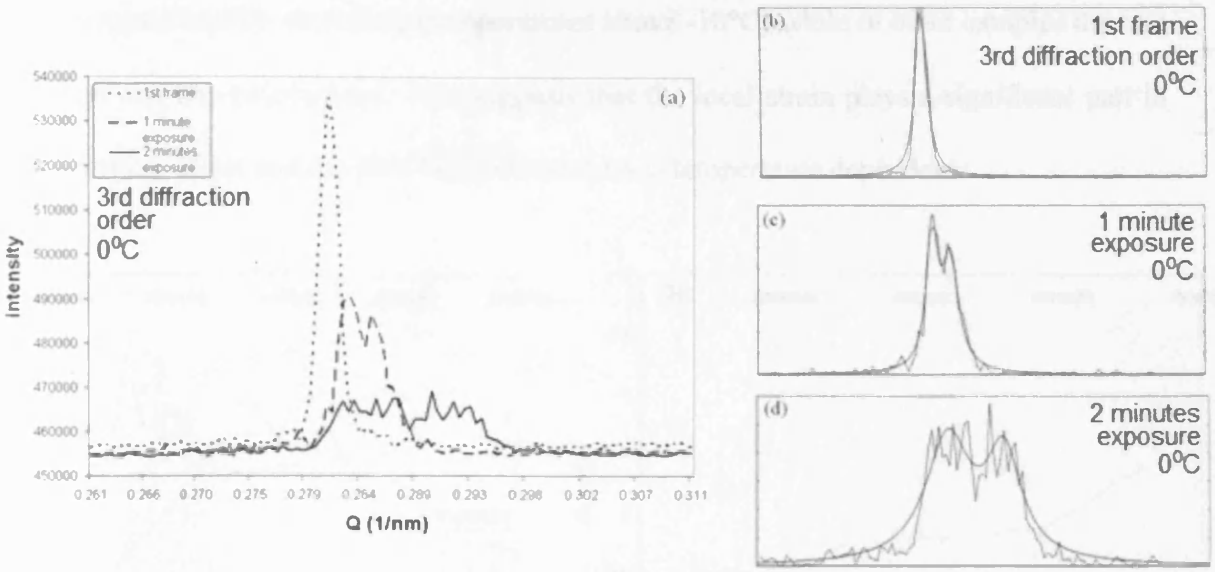

Figure 4.13. Plots of the diffraction intensity versus scattering angle Q during the first minutes of X-ray illumination (a). The lines correspond to the successive frames of a sample at 0°C. The figure shows the 3rd order peak splitting, the broadening of both peaks, decrease of the intensity and the change in radial position which indicates the change in D-periodicity. (b), (c) and (d) show the peak fitting used in the data analysis; the red line corresponds to the experimental data and the blue line is the fitted peak.

4.3.2. Evidence of lattice strain

The local lattice strain was estimated by taking the slope in the Williamson-Hall plots for successive time frames. The breadth of the reciprocal lattice was plotted against the scattering vector Q, and measurements for the 1st, 3rd and 5th orders of diffraction were used to obtain the plot (see section 3.3.1.1). This allowed the estimation of the strain (as a slope from a W-H plot) and crystal size (1/intercept). The obtained slope values were then plotted against the X-ray photon dose, which is demonstrated in Figure 4.14. The graphs show that in some cases

strain increases rapidly with dose (temperatures above -10°C) while in other samples the rate of change was less pronounced. This suggests that the local strain plays a significant part in the broadening effect and the physiological process is temperature dependent.

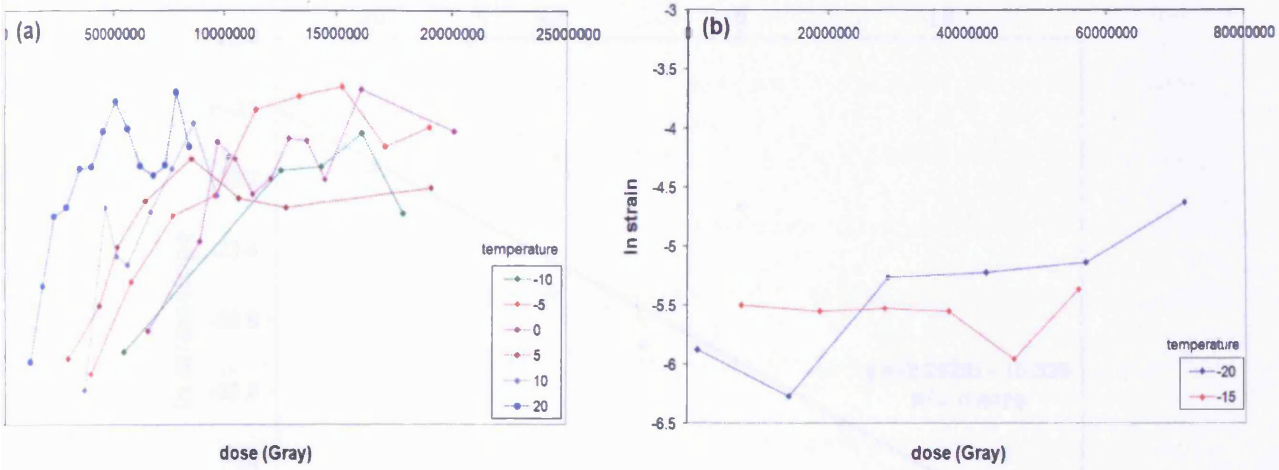

Figure 4.14. The natural logarithm values of strain, estimated from a Williamson-Hall plot, versus the dose. Each line corresponds to a different temperature. The graph shows that the strain changes only slightly with dose in lower temperature (b) and it increases more rapidly in higher temperatures (a). The slope of each line (strainslope) was used to make an Arrhenius plot.

As can be seen in Figure 4.14 (a) each strain curve from temperatures above -10°C shows an initial linear and then a saturation regime with respect to the X-ray dose. The first few points from the initial linear regime of each curve were used to make an Arrhenius plot, where the natural logarithmic base (ln) of the dose dependent change in strain was plotted against 1000/T (see Data Analysis section – 4.2.3). It is clearly visible (Figure 4.14b) that strain curves for -15 and -20°C are different from the curves for higher temperatures which may be due to the water freezing inside the fibrils (see Discussion). It suggests a different water and

phase-dependent mechanism responsible for molecular rearrangements at lower temperatures, hence these curves were not used in the Arrhenius plot. The Arrhenius plot for the strain change (i.e. strainslope) is shown in Figure 4.15.

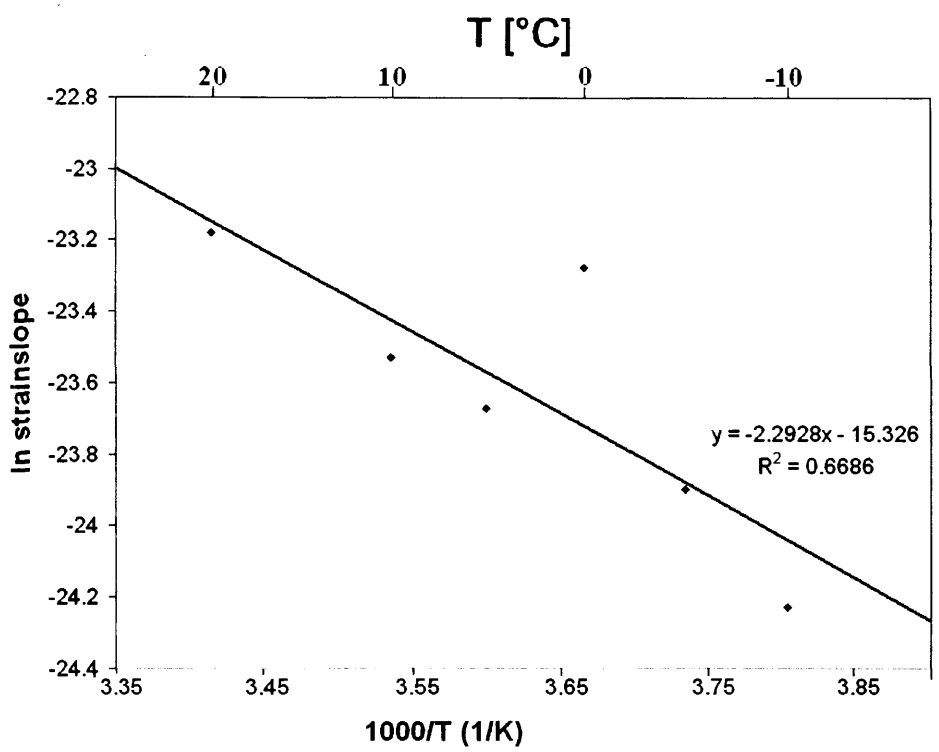

Figure 4.15. Arrhenius plot – the ln of the strainslope against 1/temperature [K]. The scatter of the data points is small and forms a straight line, which indicates an Arrhenius relation (i.e. a temperature dependence of the process).

4.3.3. Variation in D-period

Table 4.1 shows the changes in the D-periodicity observed during the experiment. The columns show the periodicity in the first frame, after 3.5 minutes of X-ray illumination (frame number 100, where the 3rd order was still above the background radiation) and frame number 600 (corresponding to ~ 20 minutes of irradiation); the D-period was calculated using the Q value of the 1st diffraction order. The D-periodicity decreased with dose at each temperature in the first stage of the experiment (first 3.5 minutes of exposure). At lower temperatures the change was relatively slight (to about 66 nm); in higher temperatures the periodicity decreases to a mean value of 63 nm. In samples exposed to X-ray dose at temperatures above -10°C the diffraction orders split into two peaks in the direction parallel to the fibre axis (as shown in Figures 4.5-4.10). The two peaks correspond to two populations of collagen fibrils, each with the different axial periodicity: i.e. the first peak appears at the lower Q values, therefore it corresponds to the collagen fibril population with the higher D-periodicity (population number 1 in Table 4.1), while the second peak appears at higher Q values and corresponds to the population with the lower D-periodicity (population number 2 in Table 4.1). The graphical representation of the D-periodicity values is shown in Figure 4.16. The first and the second peak (shown as blue and red lines, respectively) correspond to the collagen fibril populations #1 and #2.

temp [°C]	mean D-periodicity [nm]				
	1st frame	frame #100		frame #600	
		population #1	population #2	population #1	population #2
-20	67.06 +/- 0.21	66.74 +/- 0.24	n/a	67.15 +/- 0.44	n/a
-15	66.83 +/- 0.21	66.41 +/- 0.23	n/a	n/a	n/a
-10	66.92 +/- 0.18	66.07 +/- 0.78	64.66 +/- 0.26	79.18 +/- 5.56	65.76 +/- 3.59
-5	66.89 +/- 0.17	66.25 +/- 0.8	64.23 +/- 0.48	77.49 +/- 6.06	65.64 +/- 3.07
0	67 +/- 0.19	66.08 +/- 0.65	64.38 +/- 0.69	70.82 +/- 1.62	65.49 +/- 1.89
5	66.99 +/- 0.19	66.51 +/- 0.92	66.31 +/- 0.85	75.95 +/- 3	67.92 +/- 3.31
10	67.06 +/- 0.16	66.29 +/- 1.12	63.33 +/- 0.9	66.19 +/- 2.75	61.01 +/- 0.83
20	67 +/- 0.18	65.55 +/- 1.79	60.52 +/- 1.52	66.8 +/- 2.93	62.23 +/- 2.62

Table 4.1. Observed D-periodicity and its variation (calculated from the FWHM values) in the collagen samples exposed to an intense X-ray dose, obtained from measuring the lattice position of meridional reciprocal reflections. Frames number 100 and number 600 correspond to ~3.5 and 20 minutes of exposure, respectively. In samples from temperatures above -10°C the 3rd diffraction order consist of two peaks, which correspond to two collagen fibril populations; therefore two values of D-periodicity are shown. (n/a) corresponds to the absence of the second peak in the temperatures -20 and -15°C.

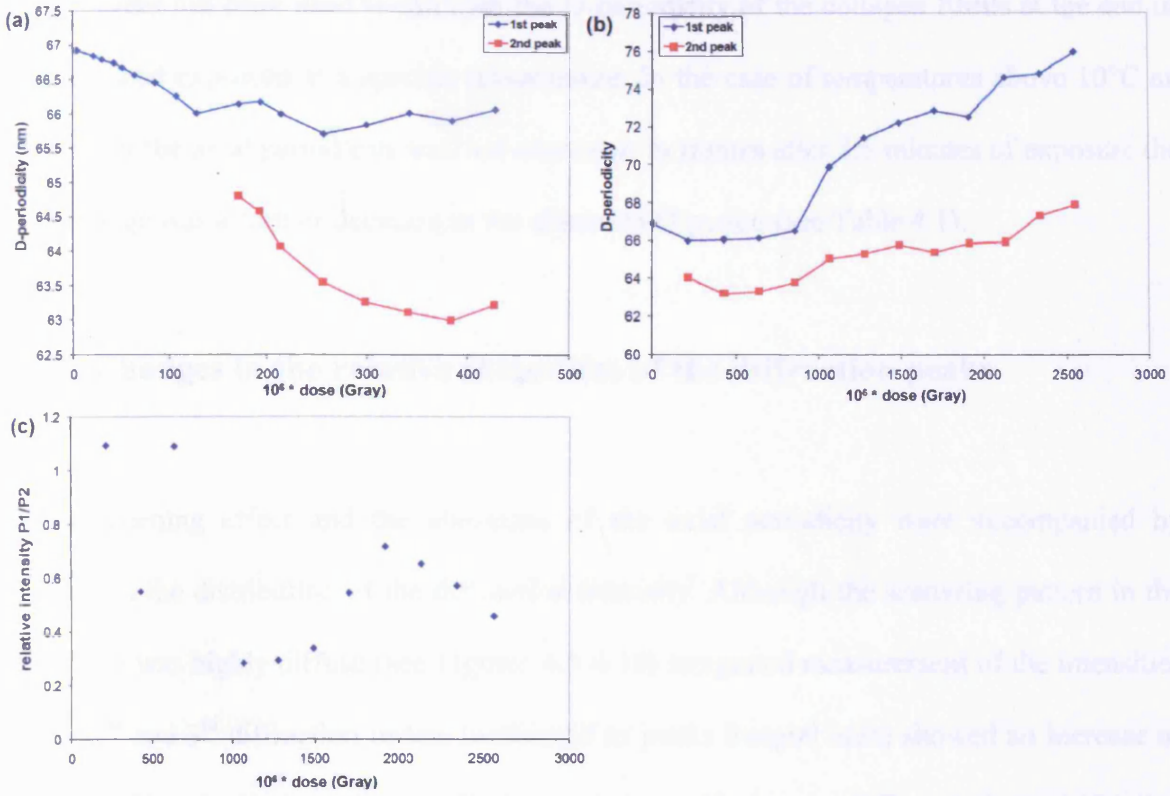

Figure 4.16. D-periodicity values calculated for samples irradiated at +5°C. (a) shows the D-periodicity in the first stage of the experiment (first 3.5 minutes of exposure) where the 1st order splits into two peaks with different periodicity. (b) shows the later stage of the experiment where an increase of the D-period can be seen. The dotted part of the (b) graph corresponds to the plot in (a). (c) shows the relative intensity plot of two peaks (P1 and P2).

The analysis of the frames after 3.5 minutes of exposure (using the remaining 1st diffraction order) showed the increase of lattice D-periodicity but only in temperatures between -10°C and 5°C, suggesting that this specific change is temperature dependent. The peak broadening was observed and the change in periodicity from 66.5 nm (after 3.5 minutes) to 75.9 nm (the first peak) and from 63.3 to 67.9 nm (the second peak) after 20 minutes of X-ray irradiation (at 5°C).

The 1st order has been used to estimate the D-periodicity of the collagen fibrils at the end of each planned exposure at a specific temperature. In the case of temperatures above 10°C an increase of the axial periodicity was not observed. In frames after 3.5 minutes of exposure the only change was a further decrease in the observed D-period (see Table 4.1).

4.3.4. Changes in the relative intensities of the diffraction peaks

The broadening effect and the alteration of the axial periodicity were accompanied by changes in the distribution of the diffraction intensity. Although the scattering pattern in the last frame was highly diffuse (see Figures 4.5-4.10) integrated measurement of the intensities of the 2nd and 3rd diffraction orders (estimated as peaks integral area) showed an increase of the I(2)/I(3) ratio in the collagen fibril population with increased D-periodicity indicating changes in the underlying molecular transform. The I(2)/I(3) ratio increased from ~0.11 in unaltered fibrils to above 1.0 in fibril populations with axial periodicity higher than 70 nm, up to the mean value of 2.9 at -10°C where the periodicity is ~79.18 nm.

4.4. Discussion

The results presented here represent two major perturbations to collagen structure not previously observed: (1) broadening of the diffraction peaks along the meridian axis due to the lattice strain, (2) alteration in the characteristic D-period up to ~ 80 nm. In addition to this changes in the electron density distribution (as indicated by the I(2)/I(3) ratio) were observed, which has been reported before during mechanical stretching and drying (Mosler et al., 1985; Bigi et al., 1987). This results from the experiment conditions i.e. very high X-ray dose and a

long exposure time at exactly the same sampling point, which normally is avoided, but requires to be understood for both medical and experimental purposes.

Potential alterations to collagen structure have been listed in Chapter 1; in case of the broadening effect observed here it is possible that one of the following occurred: (1) alteration in finite crystallite size, (2) microfibrillar shear within a fibril, (3) local strain within fibrils / within a fibril population. It is also possible that a combination of the above effects could take place.

To understand the nature of these novel molecular rearrangements it is important to compare the effects observed here to the previously published studies; the variation of axial periodicity in collagen fibrils between tissues and after heating was previously reported for many tissues by using X-ray diffraction and /or microscopic techniques. A search through the literature revealed that the axial periodicity may vary between tissues (67 +/- 0.5 nm in wet and 64 +/- 0.5 nm in dry rat-tail tendon; 65 +/- 0.5 nm in wet cornea and wet and dry skin (Worthington and Tomlin, 1955; Stinson and Sweeny, 1980; Marchini et al., 1986; Bigi et al., 1987). However within a specific tissue the D periodic value is regarded as being a highly regulated parameter (the measured variance is never higher than +/- 0.5 nm), since the periodicity is governed by the sequence specific alignment of collagen molecules within the fibril. All previous diffraction experiments point to minimal changes in the variance of D periodicities within the sample induced by heating, drying and mechanical testing as judged by the change in the breadth of the meridional diffraction peaks in the axial direction.

The characteristic 67 nm D-period of wet rat tail tendon decreased to 63.5 nm upon drying (Worthington and Tomlin, 1955). Wess and Orgel also reported a change in axial periodicity in rat-tail tendon from 67.2 to 64.7 nm during air drying (Wess and Orgel, 2000). The diffraction patterns of altered collagen fibrils showed the broadening of the meridional

diffraction peaks in the direction perpendicular to the meridian. They also reported the reduction of the spacing of the meridional reflections in dry skin from 64.5 to 60 nm upon dehydrothermal treatment (i.e. dry heat at ~120°C). Apart from these alternations in diffraction patterns, no significant change in peak breadth in the direction parallel to the meridian axis was observed. Bigi et al. also reported a reduction in the axial periodicity with increasing temperature (up to 190°C where the value reached 47 nm) which was accompanied with the decrease in the I(2)/I(3) ratio (Bigi et al., 1987). The I2/I3 ratio is a measure often used to describe deviations in the collagen axial structure from a step function to less well defined disorganized regions. Its variation corresponds to the change of the electron density distribution within the unit cell. As explained by the authors these alterations in the molecular packing were due to the loss of water and were divided into three steps of progressive removal of free, bound and structural water.

An increase of the axial D-periodicity has been previously observed during stretching of collagen. Mosler et al observed stress-induced increase of the D-periodicity in human finger flexor tendon and rat-tail tendon, from 67 to 68.3 nm (Mosler et al., 1985). The authors also reported the change of the intensity of the second and third diffraction order (increase in the I(2)/I(3) ratio with elongation) and suggested an explanation for this based on the alteration of the overlap/gap region ratio (the increase in the length of the gap region and the decrease in the length of the overgap region). These alterations in the collagen structure were explained by the authors as an effect of the relative sliding of the triple helices. Similar changes (increase in D-periodicity and alteration in I(2)/I(3) ratio due to applied force) were also reported by other groups where relative slippage of lateral molecules was suggested as an explanation of the process (Sasaki and Odajima, 1996; Fratzl et al., 1997; Sasaki et al., 1999).

Other unusual values for the D-period were reported using a variety of techniques. The greatest reported type I collagen axial periodicity was measured using electron / atomic force microscopy and was described as fibrous long spacing collagen (FLS) fibrils. The FLS is a significantly different collagen based structure; these fibrils displayed periodicity between 120 and 240 nm and were found in normal tissues, tumours and tissues treated with collagenase (Cravioto and Lockwood, 1968; Miki et al., 1993). The FLS fibrils are suggested to be the product of collagen enzymatic biodegradation or/and a result of immature collagen microfibrils association with acid mucopolysaccharides present in tumoural tissues (Paige, Rainey and Goh, 1998; Paige, Lin and Goh, 2002). The FLS can be also formed *in vitro* from type I collagen with α_1-acid glycoprotein (AAG) addition (Lin and Goh, 2002). However, the experimental conversion to FLS from normal "quarter staggered" fibril is unreported as the FLS formation requires a complete fibril reassembly. Therefore, it seems unlikely that an unusual 80 nm periodicity observed during the experiments presented here correspond to the FLS structure.

Examination of the diffraction profiles showed that the major effect observed on irradiation of the samples was the change in the breadth of reflections in the direction parallel to the meridian axis. This effect was angular dependent (i.e. Q dependent) and in many cases the fifth order of diffraction became sufficiently broad to be immeasurable. The broadening in the direction parallel to the meridian axis observed here can be explained by two processes: (1) change in finite crystallite size or (2) lattice strain. It is possible to discriminate between the two processes by using the Williamson-Hall plot; in the case of the broadening observed in this study the W-H plots showed that the estimated size of the crystallites remained very large, i.e. in the micron range; this may however be in part due to the potentially very large

coherence length of the collagen fibrils and the subsequent insensitivity of the technique for large crystallites, where the finite axial length may change significantly yet remain in the micron range. The strain effects as judged by the angle dependent broadening of the Bragg peaks are more pronounced. This points to local strain being the major contributor to alteration in the diffraction pattern. The measurements of the lattice strain in the series of frames showed that there was an initial linear and then a saturation regime with the irradiation dose (see Figure 4.14a). The analysis using the Arrhenius plot showed that the broadening process due to the lattice strain is temperature dependent. The changes in the diffraction profile observed here are novel and point to changes in collagen structure within a population of collagen fibrils or within regions of a single fibril.

Collagen-rich tissue fibrils consist of approximately 50% water with subsets of water populations that surround individual triple helices and fill the gap zone in the hydrated state and water that surrounds fibrils (Lees, 1986; Price et al., 1997). It can be imagined that the local change in lattice parameters may be induced by the local movement of water within the fibrils. One of the changes observed in the diffraction profile was the alteration of the mean lattice value from 67 nm to 64 nm, which was reminiscent of the diffraction pattern from dry collagen. This, however, is usually not accompanied by the measurable broadening of the Bragg reflections process. Changes induced by the X-ray photon dose may be the result of more selective movements of water populations from within the gap region of a fibril.

Unbound water which is the mobile fraction in collagen has the ability to form large clusters, which can behave as ice and undergo a phase transition (Pineri, Escoubes and Roche, 1978). The interfibrillar unbound water fraction freezes close to 0°C, while intermolecular unbound water undergoes freezing-point depression between 0°C and -30°C (Price et al., 1997). This

transition arises from the storage of the intermolecular water fraction in small areas, which results in its inability to assume clustering characteristic of bulk water fraction (Dehl, 1970; Price et al., 1997). It can be observed in the experiments presented in this Chapter that the strain curves for -15°C and -20°C are different from the curves for higher temperatures (see Figure 4.14). It can therefore be speculated that in tendons exposed to an X-ray dose at the lowest temperatures, the freezing of the unbound water fractions has caused the reduction of the peak broadening effect. It is possible that when unbound water is frozen within the fibrils, its movements are greatly reduced; therefore the effect on the axial structure of collagen (i.e. induction of local strain) is limited. The broadening effect is still observed at temperatures -10°C and -5°C, even though the interfibrillar unbound water fraction is expected to be frozen at these temperatures (thus limiting the effect). However, considering the freezing-point depression of the intermolecular unbound water, it could be speculated that this water fraction is still mobile at -10°C and -5°C and therefore its movements lead to local strain effects.

Effects of irradiation treatment on collagen structure have been investigated before using electron microscopy (Grant, Cox and Kent, 1970). The ionizing radiation was reported to cause the rupture of inter- and intramolecular hydrogen bonds, collagen chain scission and the random formation of a large number of intermolecular cross-linking which might be a result of free radical reactions (Bailey, Rhodes and Cater, 1964; Bailey and Tromans, 1964; Grant et al., 1970). It was observed that water played an important part in irradiation damage: the loss of order within the collagen fibrils was suggested to be due to the penetration of water to the regions which were disorganized by ionizing radiation (Bailey and Tromans, 1964); however, there is little evidence for this. Also, the mechanism of the crosslinking formation was suggested to be dependent on the presence of water (Bailey et al., 1964).

As the samples were kept fully hydrated during the X-ray photon treatment, rearrangements in the axial packing of collagen may be explained by the local movement of a mobile water fraction. It can be speculated that an intensive X-ray dose causes molecular bond scissions and therefore a local unravelling of collagen triple helical structure. It is possible that local movements of mobile water fraction result in local stretching of collagen molecules and local deviations of structure may result in the variation of lattice parameters (i.e. variation in D-period). Although water movement and more specifically loss of water are obviously connected with structural alterations in dehydration of fibrillar collagen, the changes in broadening and periodicity observed here may also be a result of drastic alterations in local water population that facilitate local strain of collagen molecules previously unobserved.

5. The effect of Matrix Metalloproteinases on the long and the short range order of collagen.

5.1. Introduction

This chapter presents two studies that were conducted to monitor the effects of Matrix Metalloproteinases (MMPs) on two collagenous tissues – rat tail tendon and breast tissue. MMPs are collagen degrading enzymes that are present at high levels in breast tumour tissues (Overall and Lopez-Otin, 2002) (see section 5.2 below) and it is believed that during tumour invasion and metastasis they affect tissues that surround the tumour site. Understanding the molecular alterations induced by MMPs in collagen structure may lead to the development of a simple method to distinguish between normal and tumour tissue, and can be crucial for early prognosis and prevention of cancer. It has been proposed that SAXS can be potentially used as a method to monitor changes induced in collagen molecular structure by MMPs; previous studies have shown clear differences between diffraction patterns from malignant and normal tissues (Fernandez et al., 2002; Fernandez et al., 2004; Round et al., 2005). Therefore, it has been suggested that SAXS can be used as a potential diagnostic test to diagnose cancer by biopsy. However, previous studies were focused on the examination of the axial structure of collagen e.g. the differences of the D-periodicity and the intensity of diffraction peaks between normal and tumour tissue. The study presented in this chapter concentrates on the analysis of the equatorial pattern of collagen and therefore the analysis of the lateral packing: fibril radius and interfibrillar spacing. This project is a comparison of normal and malignant (therefore potentially subjected to the high levels of MMPs) breast

tissues and the analysis of the effect of elevated temperature on the tissues. Different temperature settings were used during the measurements (i.e. 5, 20, 37 and 60°C) to monitor the potential differences between the two types of tissues at various environments.

The second study described in this chapter involves monitoring the changes in rat tail tendon collagen axial structure after incubation with MMPs for various amounts of time. RTT was used here as a well characterized model tissue to examine potential rearrangements that can occur within its ordered molecular structure as the effect of degrading enzymes. The results provide information about the diffraction intensity and the axial periodicity of collagen after the treatment.

5.2. Matrix Metalloproteinases (MMPs)

The matrix metalloproteinases (MMPs) are a family of endoproteinases involved in the degradation of extracellular matrix proteins (Duffy et al., 2000). Collagenases are one of the group of MMPs. The first purified collagenase was human fibroblast collagenase (MMP-1). Similar to many other collagenases (MMP-8 or MMP-13), this enzyme catalyzes the degradation of native fibrillar collagen into thermally-unstable triple-helical fragments, which denature into gelatine (Ala-aho and Kahari, 2005). Collagenases have different catalytic activities depending on the collagen type e.g. type I collagen is most efficiently degraded by MMP-8 while type III collagen is cleaved by MMP-1 (Egeblad and Werb, 2002). Collagenases are also involved in the degradation of other matrix and non-matrix proteins (Pardo and Selman, 2005). The ability to cleave fibrillar collagen and other proteins by MMPs plays an important part in tissue remodelling processes such as embryonic development, ovulation and wound healing (Duffy et al., 2000; Pardo and Selman, 2005). In

normal tissues, the activity of collagenases is strictly controlled and they are usually expressed at low levels; however, abnormal expression has been connected to tumour growth, invasion and metastasis (Overall and Lopez-Otin, 2002).

It has been suggested that some of the MMPs are critical to the onset of breast cancer and are responsible for tumour growth and metastasis (Duffy, 1987). Previous studies showed that there is a correlation between specific MMPs levels and metastatic states in the tissue, and a potential use of MMPs as markers in human breast cancers has been proposed (Bernhard, Gruber and Muschel, 1994).

5.3. Effects of temperature on the short range order in breast tissue collagen

5.3.1. Material and methods

X-ray diffraction data of the normal and tumour breast tissue were obtained from the collaboration with Sarah Pearson from University of New England, Australia. Samples were excised from breast tissue, frozen in liquid nitrogen and stored at -80°C. They were then heated (4 different temperatures were applied: 5, 20, 37 and 60°C) and placed in a liquid cell with Phosphate Buffered Saline (PBS, pH=7). Different temperature settings were used to examine the differences between normal and tumour tissues at various environments. SAXS images were taken at 4 different points with a 300 s exposure at each point. The experiments were conducted at the 2.1 station at the Daresbury Laboratory, UK, using a 6.25 m camera length (see section 3.1.1.1).

The two-dimensional SAXS images were converted into linear plots using in-house software and analyzed as described in Chapter 3. The equatorial peak corresponding to the interfibrillar spacing was observed as well as the intensity distribution corresponding to the central section of cylindrically averaged scattering of a rod-like object, hereafter called the cylindrical scattering intensity, which were used to estimate collagen fibril diameter (see Figure 5.1).

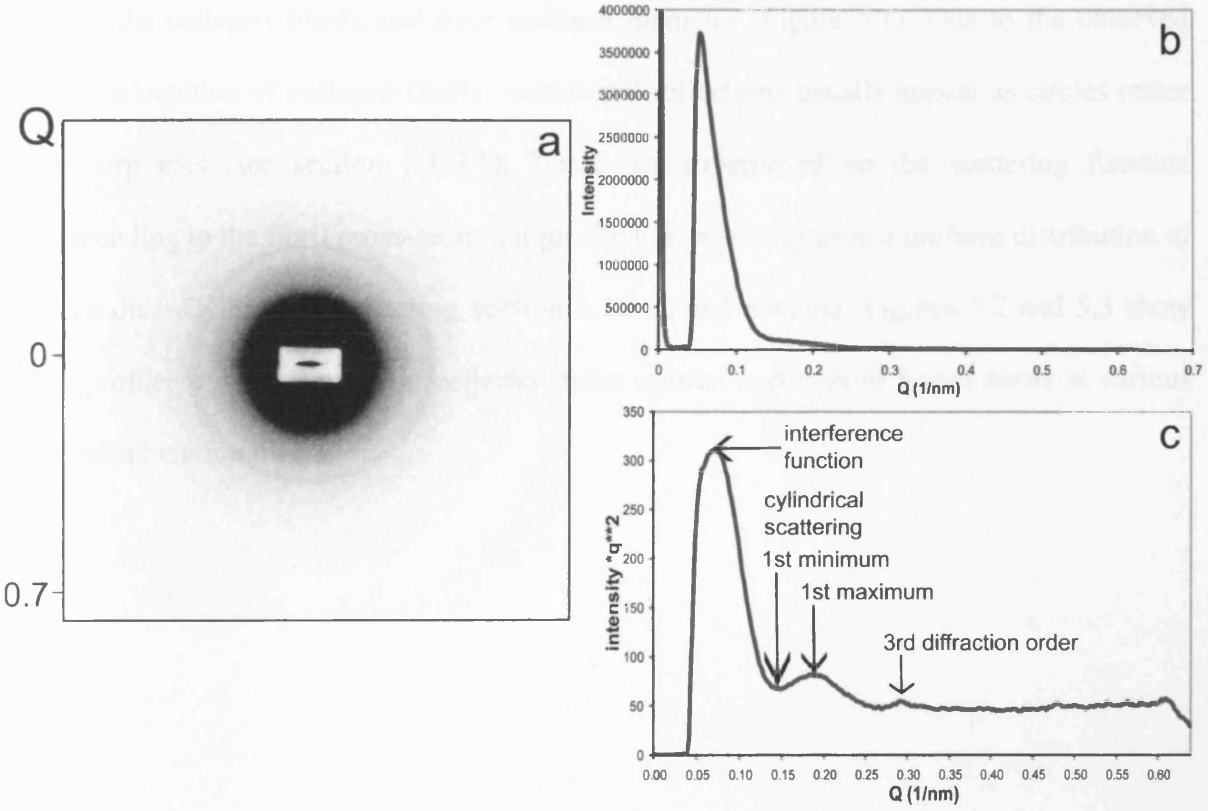

Figure 5.1. An example of an X-ray diffraction image from breast tissue: tumour tissue at 5°C (a). The right panels illustrate linear plots converted from the diffraction pattern: (b) is a linear trace of intensity vs. the momentum transfer vector Q. On the graph (c) the diffraction intensity was multiplied by a distance squared in order to enhance the signal, which allowed observation of an interference function, cylindrical scattering intensity and the 3rd diffraction order (all indicated by arrows).

5.3.2. Results

Small angle X-ray scattering patterns from breast tissue consist of characteristic meridional and equatorial reflections; the meridional reflections result from the axial periodicity of collagen fibrils and the equatorial reflections (i.e. an interference function and the cylindrical scattering intensity) result from lateral packing of collagen fibrils – an average distance between the collagen fibrils and their uniform diameter (Figure 5.1). Due to the observed random orientation of collagen fibrils, meridional reflections usually appear as circles rather than sharp arcs (see section 2.1.7.1). These are superposed on the scattering function corresponding to the fibril cross-sectional profile (i.e. resulting from a uniform distribution of fibrils radii – Cylindrical scattering section 3.1.3.2) and packing. Figures 5.2 and 5.3 show linear profiles of SAXS patterns collected from normal and tumour breast tissue at various temperature environments.

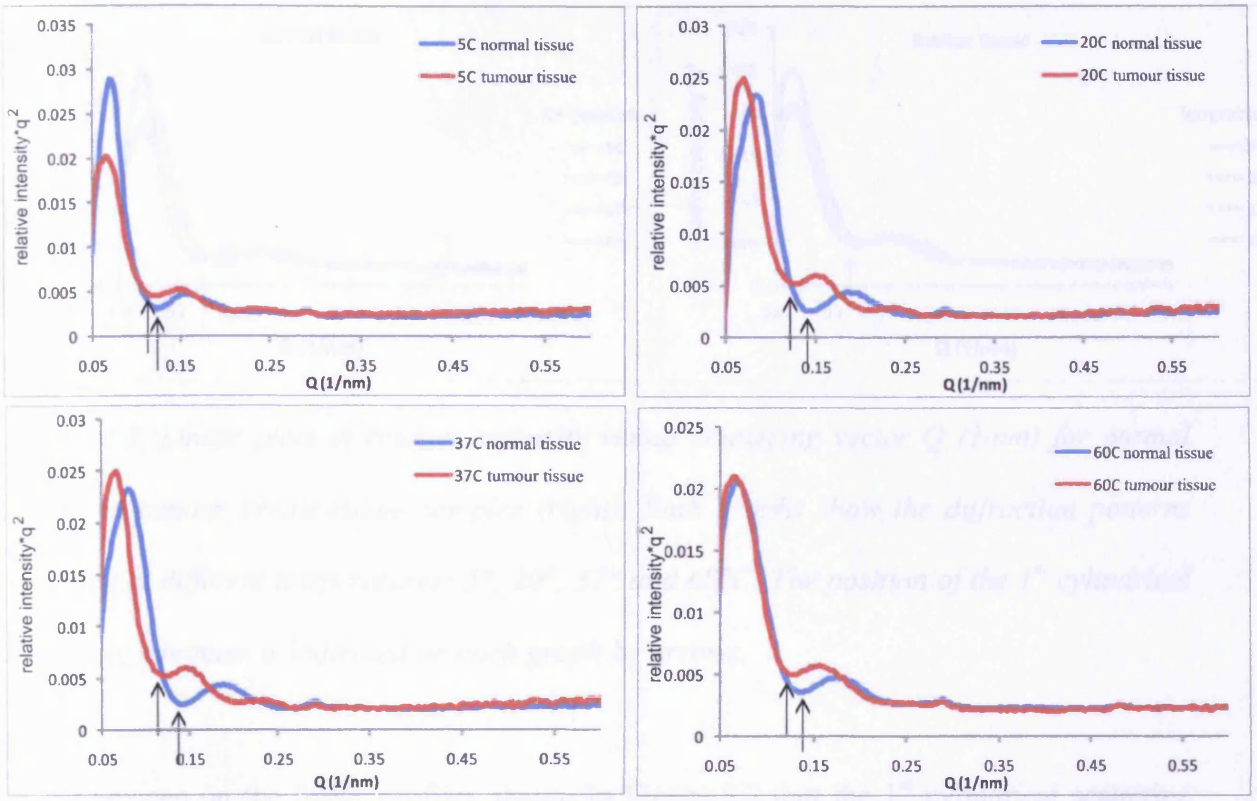

Figure 5.2. Linear plots of relative intensity versus scattering vector Q (1/nm) for normal (blue lines) and tumour breast tissue samples (red lines). Each graph corresponds to the measurements collected at different temperatures: 5°, 20°, 37° and 60°C. The position of the 1st cylindrical scattering minimum (Bessel function), which can be used to calculate fibril radius, is indicated on each graph by arrows.

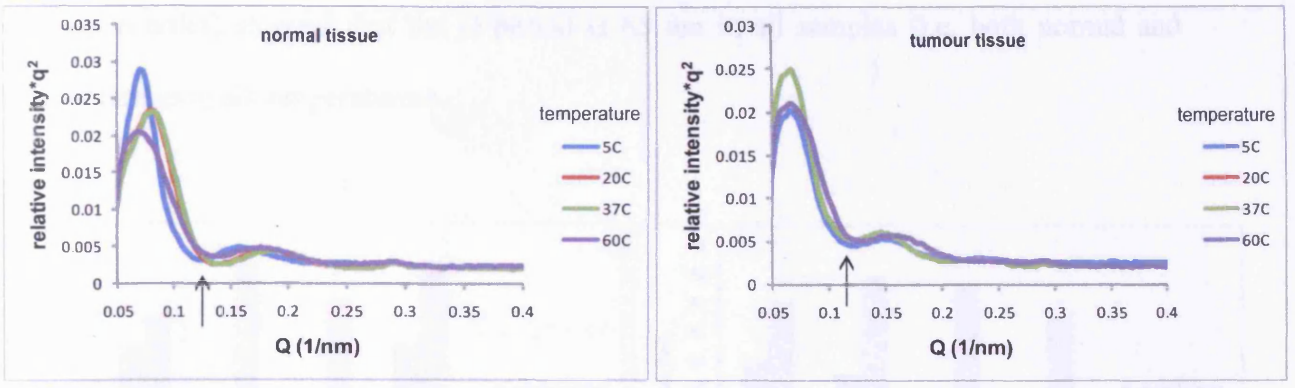

Figure 5.3. Linear plots of relative intensity versus scattering vector Q (1/nm) for normal (left) and tumour breast tissue samples (right). Both graphs show the diffraction patterns collected at different temperatures: 5°, 20°, 37° and 60°C. The position of the 1st cylindrical scattering minimum is indicated on each graph by arrows.

It can be seen on the linear profiles shown in Figure 5.2 that the 1st cylindrical scattering minimum, which can be used to calculate fibril radius (see section 3.1.3.2), appears at higher angles in normal tissues compared to the tumour samples. This indicates that there are differences between fibril radii in the measured samples. The values for both fibril radius and interfibrillar spacing obtained for normal and tumour breast tissue samples are shown in Figure 5.4. It can be seen that the lateral spacing between collagen fibrils (i.e. the distance between centres of two neighbouring fibrils) is higher in tumour samples than in normal tissues, which is especially evident in temperatures above 20°C (Figure 5.4a). Also fibril radii values were observed to be greater in tumour samples (Figure 5.4b). In addition, the surface-to-surface distance between fibrils was calculated (i.e. as a difference between centre-to-centre distance and fibril diameter, shown in Figure 5.5) and the obtained values can be found in Figure 5.4c. The measurements of the axial periodicity (based on the position of the 3rd

diffraction order) showed that the D-period is 65 nm in all samples (i.e. both normal and tumour tissues at all temperatures).

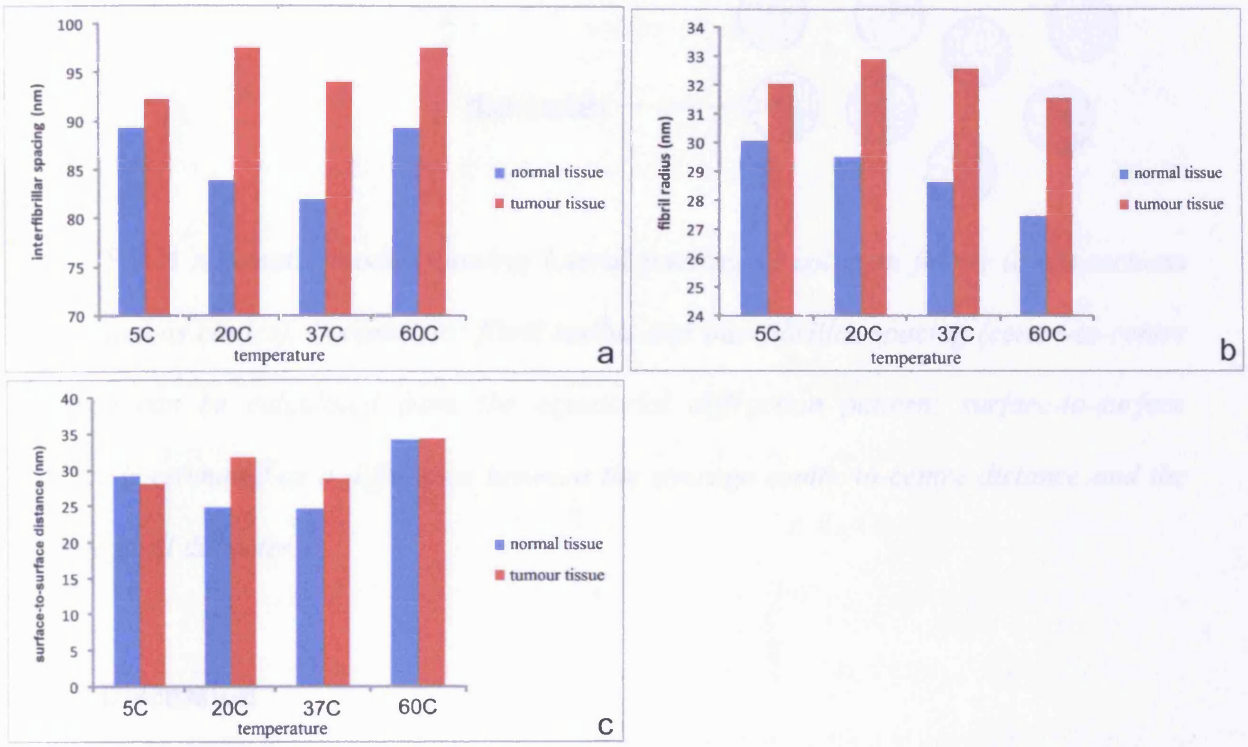

Figure 5.4. Bar charts derived from the analysis of equatorial pattern: (a) interfibrillar spacing values from normal (blue charts) and tumour (red) samples at different temperatures; (b) fibril radii values; (c) surface-to-surface distance between fibrils.

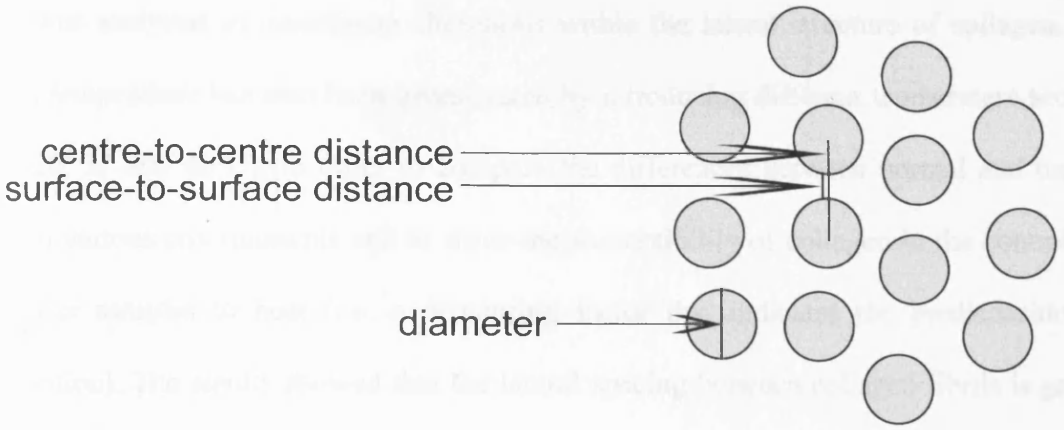

Figure 5.5. A schematic model showing lateral packing of collagen fibrils (cross-sections represented as circles). Parameters: fibril radius and interfibrillar spacing (centre-to-centre distance) can be calculated from the equatorial diffraction pattern; surface-to-surface distance is estimated as a difference between the average centre-to-centre distance and the average fibril diameter.

5.3.3. Discussion

Collagens types I and III are present in the connective tissue of the breast. The axial periodicity in healthy tissue is approximately 65 nm. Collagen fibrils from breast tissue have an average radius of about 35 nm and an interfibrillar spacing of about 100 nm (Fernandez et al., 2002). Previous analysis of normal and pathologic breast tissues showed that diffraction patterns from those samples are clearly different (Fernandez et al., 2002; Fernandez et al., 2004; Round et al., 2005). It was reported that tumour tissue samples gave rise to less intense diffraction peaks suggesting a loss of crystallinity within the collagen structure. Also, an increase in D-periodicity has been reported for cancer tissues (0.2 and 0.3 nm increase; (Fernandez et al., 2002; Fernandez et al., 2004)). In the study presented here, the equatorial

pattern was analyzed to investigate alterations within the lateral structure of collagen. The effect of temperature has also been investigated by introducing different temperature settings (i.e. 5, 20, 37 and 60°C), in order to compare the differences between normal and tumour tissues in various environments and to show the susceptibility of collagen in the control and the tumour samples to heat (i.e. a denaturing factor that indicates the predisposition to gelatinisation). The results showed that the lateral spacing between collagen fibrils is greater in malignant breast tissues compared to the healthy samples. Differences were also observed in fibril radius where its value was higher in fibrils from malignant tissues. These differences were observed at all temperatures, which may indicate that tumour invasion (and therefore potentially high levels of MMPs) affects collagenous tissues in a similar way at all various environments investigated in this study. It should also be noted, that the calculated surface-to-surface distance between fibrils was similar for normal and tumour tissues at all temperatures (see Figure 5.4c). This result suggests that the differences in interfibrillar spacing between both types of tissue (i.e. greater spacing observed in tumour samples) are mainly due to an increase in fibril radius.

The observed increase in fibril radius in tumour samples might be explained by a swelling of collagen fibrils. It is possible that MMPs penetrate fibrils and cause the local gelatinization of collagen structure; as a result collagen molecules might move apart causing an increase in fibril radius. It should be noted, that alterations in collagen structure observed in breast cancer tissues are not only caused by a MMPs enzymatic degradation; Pucci-Minafra et al reported a new type of collagen found in tumour samples (Pucci-Minafra et al., 1993; Pucci-Minafra et al., 1998). It was suggested that the modified collagen was newly synthesised as a result of tumour invasion, as opposed to a modification of collagen already present in the tissue. The altered collagen was reported to have modifications within the α2(I) chains; moreover, the

α2(I) chain was absent in some samples which resulted in the formation of an unusual collagen homotrimer, composed of three α1(I) chains (Pucci-Minafra et al., 1993; Pucci-Minafra et al., 1998). This finding may lead to the conclusion that the increase in collagen fibril radius in tumour tissues, reported in this thesis, may be explained by the presence of the novel, modified collagen. However, the modified fibrils, when viewed under an electron microscope, were reported to be thinner than normal collagen fibrils (Pucci-Minafra et al., 1998). It is therefore more likely that an increase in fibril radius is caused by the swelling of collagen fibrils as a result of partial gelatinization induced by high levels of MMPs.

Although analyses presented in this study were based only on a few data sets, these initial results may suggest that there is a clear difference between the interfibrillar spacing and the fibril radius in normal and malignant breast tissues. Further studies have to be conducted to explain underlying molecular alterations. However, if the results presented here are confirmed by a study with a larger number of specimens, the two parameters (interfibrillar spacing and the fibril radius) will have a great potential to be used as markers in breast cancer diagnosis. It should be noted here, that the differences between the axial periodicity in normal and tumour breast tissues that were reported previously were only in the range of 0.2 – 0.3 nm (Fernandez et al., 2002; Fernandez et al., 2004). The differences in parameters measured here are much greater, e.g. at 37°C the fibril radius is ~28 nm in normal and ~32 nm in tumour tissues, while interfibrillar spacing is ~82 nm and ~94 nm in normal and tumour samples, respectively (also at 37°C – see Figure 5.4). Therefore, the healthy and tumour tissues can be more easily distinguished.

5.4. Effects of MMPs on rat tail tendon collagen

5.4.1. Material and methods

X-ray diffraction data were obtained from the collaboration with Sarah Pearson from the University of New England, Australia. Samples were prepared as follows: rat tail tendons were incubated with collagenases (1.86 mg/mL) for a specific, fixed amount of time (i.e. 7 minutes, 15 minutes, 30 minutes and 1 hour). Samples were placed in DMEM (Dulbecco's Modified Eagle Medium) with collagenase and then placed in a water bath at 37°C. They were then placed in EDTA (Ethylenediaminetetraacetic Acid) for approximately 30 minutes to stop degradation by removing calcium ions and deactivating the collagenase. The degradation was terminated in order to examine the effects of collagenase activity for a specific time (7 min, 15 min, 30 min and 1 hour, depending on the sample). Finally, samples were washed again in buffer and placed in 1 mm capillary tubes with PBS (Phosphate Buffered Saline, pH=7), to conduct SAXS data collection. The measurements were made using the Bruker Nanostar SAXS device (see Chapter 3 for details). The camera length was 106 cm and the wavelength was 1.54 Å. The meridional and equatorial sectors of the two-dimensional images were integrated into linear plots as described in Chapter 3 using FibreFix software.

Six different samples were compared: normal rat tail tendon (in phosphate buffer), control – the same sample environment but no collagenase added (water bath, washing with buffer), and samples incubated with collagenase for 7 minutes, 15 minutes, 30 minutes and 1 hour.

Numerical analyses were performed using the Statistica package. Due to the high values, standard deviation values were included in the graphs showing parameters calculated from the diffraction images.

5.4.2. Results

Figure 5.6 shows small-angle X-ray scattering images collected using the Bruker Nanostar device. It can be seen that the intensities of the corresponding orders of diffraction are lower in samples incubated with collagenase for a longer time. Thus, in the samples exposed to the collagenase treatment for an hour, only the 3rd and 5th diffraction orders can be observed, as the intensities of the other orders are too weak to measure. The values for the 3rd and 5th order intensity are shown in Figure 5.7. However, the relative intensity distribution between reflections was not altered (Figures 5.8 and 5.9). The width of the meridional diffraction peaks, measured as a full width at half-maximum (FWHM) was not found to increase. The results are shown as graphs in Figure 5.10. The graphs show the breadth of the 3rd and 5th diffraction orders as only these orders could be measured in the 1 hour sample. The broadening of the diffraction peaks in the direction parallel to the fibre axis could indicate the possible changes in the local strain as explained in Chapter 4.

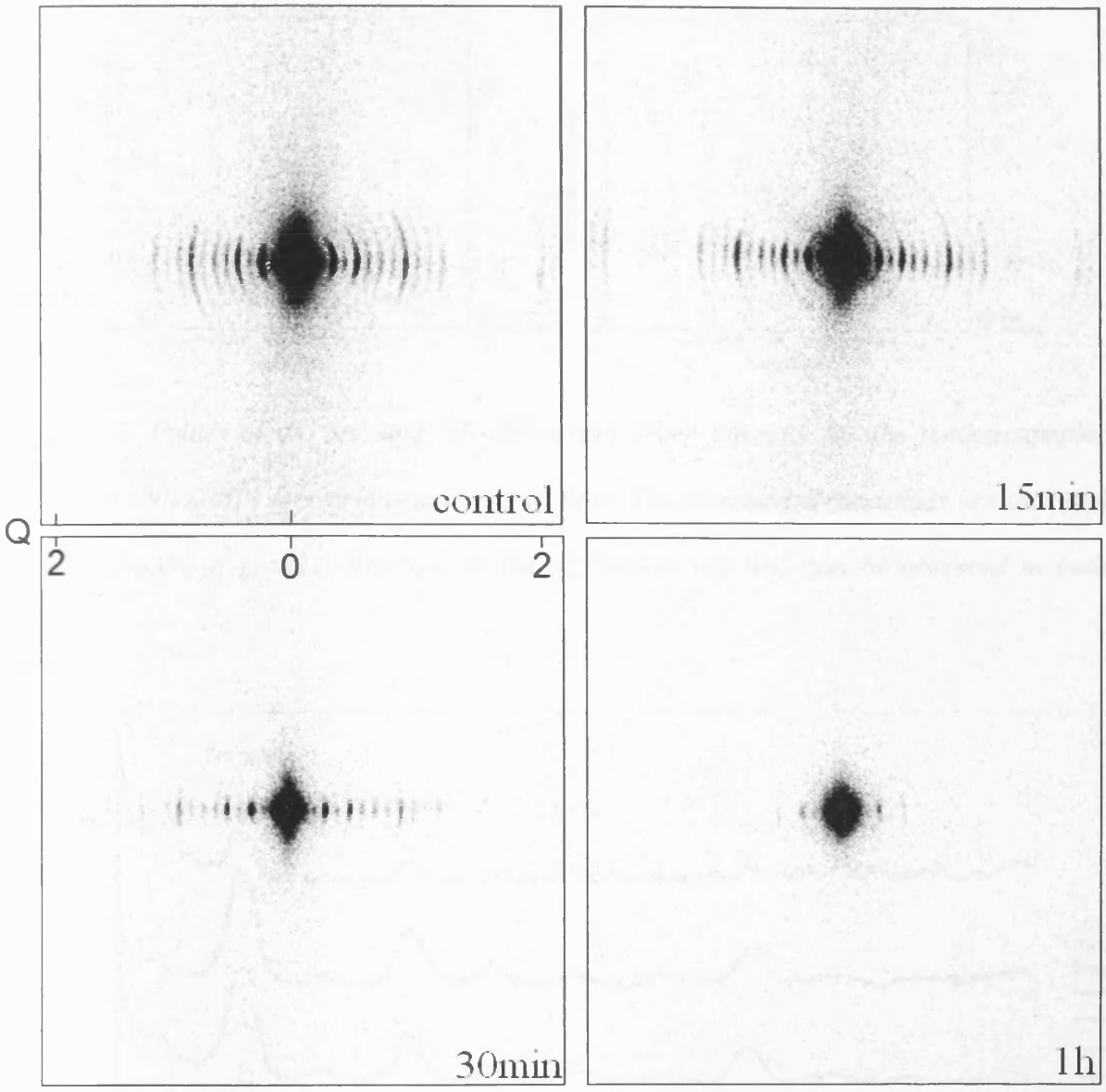

Figure 5.6. Small angle X-ray diffraction images collected from control tendons and tendons treated with MMPs for 15 min, 30 min and 1 hour (sample axis has been placed horizontally). A decrease in the diffraction intensity can be observed in samples incubated with the enzyme for longer times; in case of the sample treated for 1 hour only weak 3rd and 5th diffraction orders remain visible.

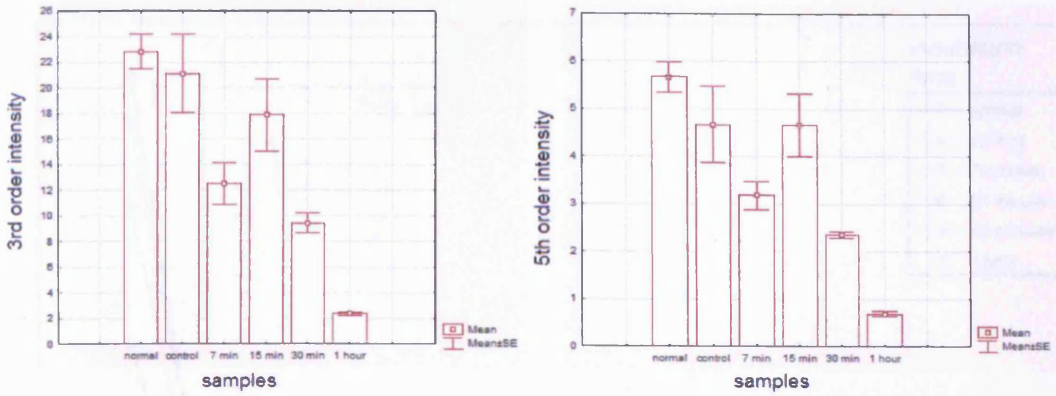

Figure 5.7. Values of the 3rd and 5th diffraction order intensity for the tendon samples incubated with MMPs for various amounts of time. The standard error values are included on both graphs. A gradual decrease in the diffraction intensity can be observed in both graphs.

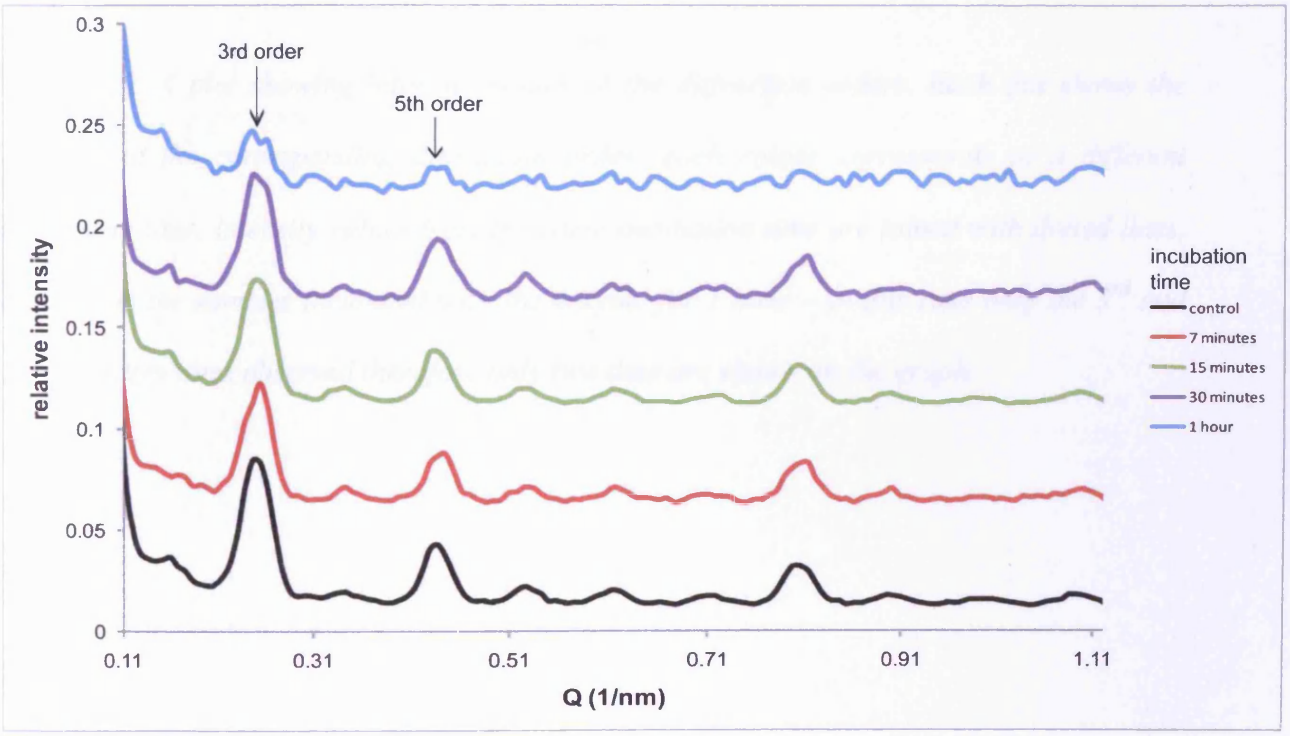

Figure 5.8. Linear profiles converted from 2D small-angle X-ray diffraction images of tendons incubated in MMPs, showing the position and intensities of the diffraction peaks. The 3rd and the 5th diffraction orders are indicated on the graphs.

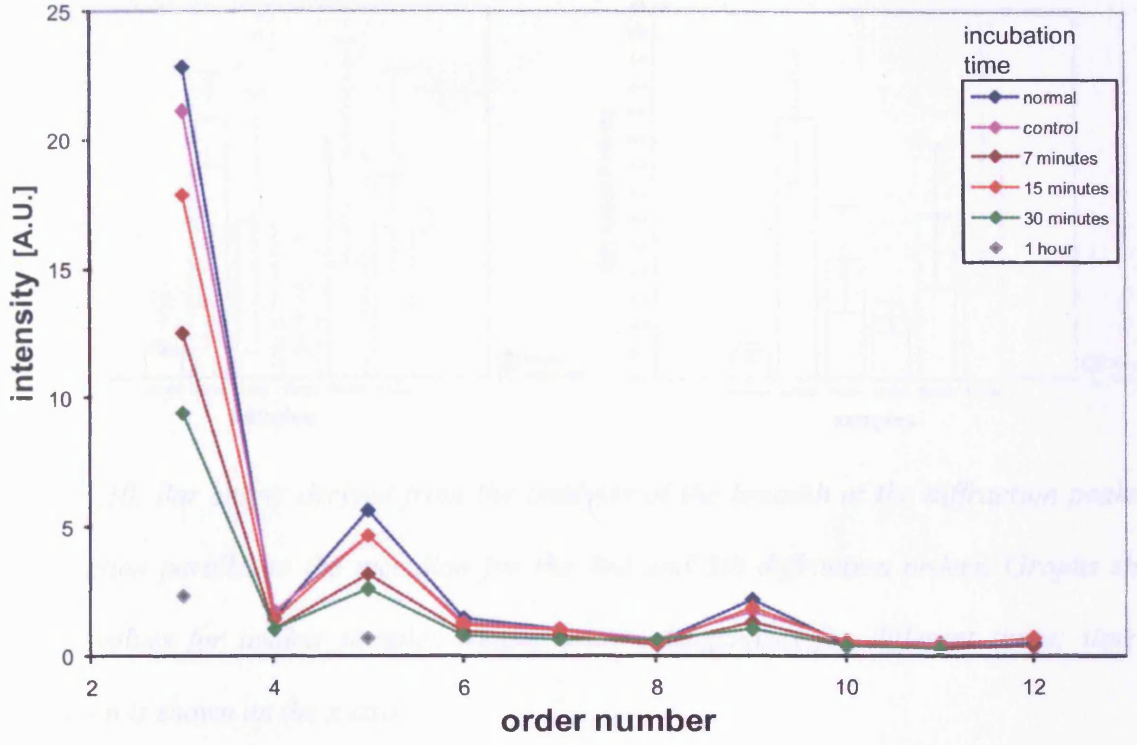

Figure 5.9. A plot showing intensity values of the diffraction orders. Each dot shows the intensity of the corresponding diffraction order; each colour corresponds to a different incubation time. Intensity values from the same incubation time are joined with dotted lines, apart from the samples incubated with the enzyme for 1 hour – in this case only the 3rd and the 5th orders were observed therefore only two dots are shown on the graph.

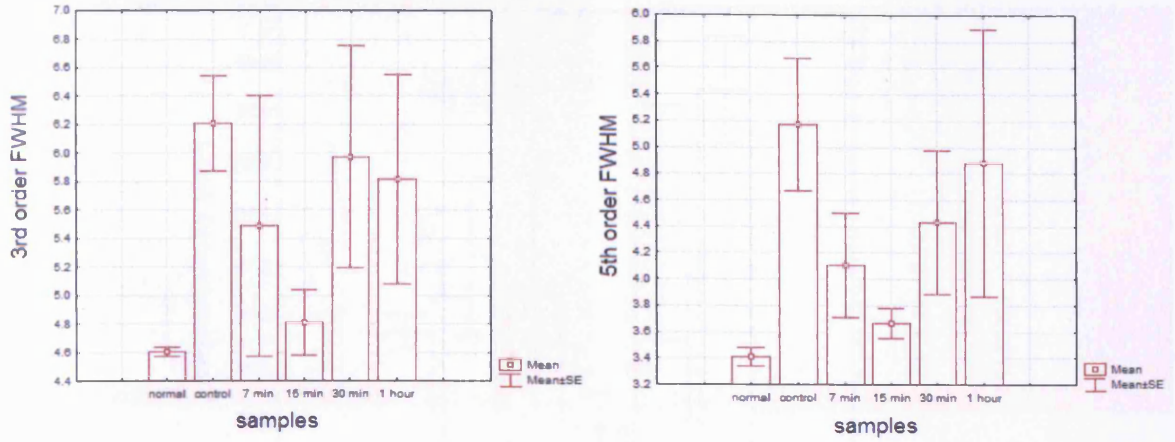

Figure 5.10. Bar charts derived from the analysis of the breadth of the diffraction peaks in the direction parallel to the meridian for the 3rd and 5th diffraction orders. Graphs show FWHM values for tendon samples treated with collagenases for different times; time of incubation is shown on the x-axis.

The analysis of the meridional reflection of the diffraction patterns showed an increase in axial periodicity from 67.2 nm in the control tendon up to 67.9 nm in tendon incubated with enzyme for 1 hour. Values calculated for axial periodicity are shown in Figure 5.11.

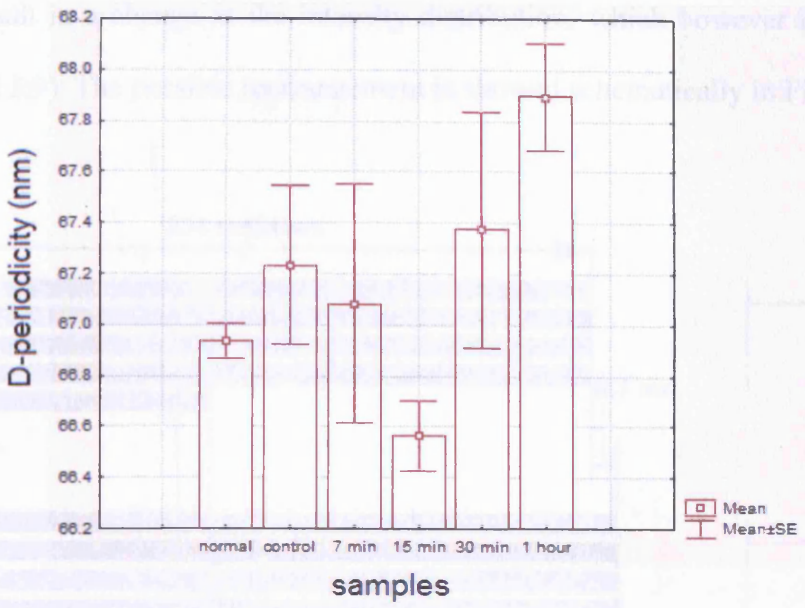

Figure 5.11. The axial periodicity values calculated from small angle X-ray diffraction images of MMP treated tendons.

5.4.3. Discussion

The aim of this study was to monitor the effects of MMPs on a model tissue, rat tail tendon, and provide information about possible molecular alterations in collagen structure. The analysis of SAXS patterns revealed a decrease in the diffraction intensity, which may suggest a loss of the crystalline coherence between the fibrils (i.e. a loss of order within collagen molecular structure). This was accompanied by a 0.7 nm increase in the D-periodicity in samples incubated with MMPs for 1 hour. This might have been caused by two possible mechanisms: relative slippage of the molecules (see section 1.2.4 in Chapter 1) or an increase in the axial rise per amino acid residue (from 0.286 nm to 0.288 nm) (see section 1.2.2 in Chapter 1). A relative slippage which would cause a 0.7 nm increase in axial periodicity would be accompanied by the change in amino-acid residues from 234 to 236 in a D-period.

This would result in a change in the intensity distribution, which however is not observed (Figure 5.8 and 5.9). The possible rearrangement is showed schematically in Figure 5.12.

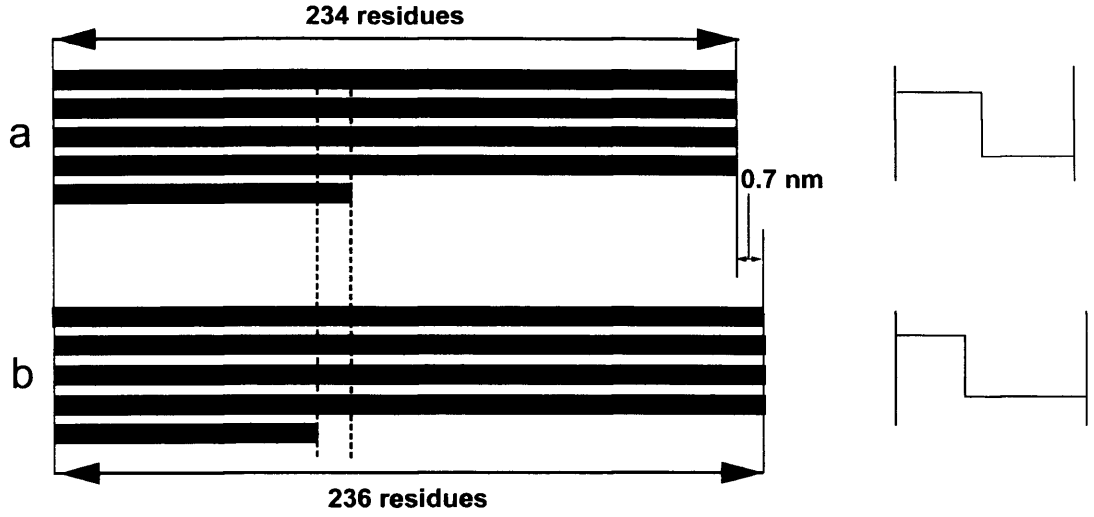

Figure 5.12. A schematic diagram showing the relative slippage of the collagen triple helices. This molecular rearrangement can cause a change in the number of amino-acid residues in a D-period from 234 (a) to 236 residues (b). This would be accompanied by an increase in the D-periodicity by 0.7 nm and a change in the electron density distribution (the projected step functions are shown on the right).

An increase in the D-period could be explained by breakages that might occur along collagen molecules; it is possible this can cause the elongation of collagen molecules (i.e. stretching within regions where breakage occurred) and therefore the elongation of the D-period.

It should be noted that the standard error values were very high, which suggests that the differences in the D-period between the samples may not be statistically significant. However, previous studies of cancerous breast tissues showed that the D-periodicity values (measured using SAXS) in cancer-invaded regions were higher than in healthy tissues

(Fernandez et al., 2002; Fernandez et al., 2004). Although reported differences were relatively small (0.3 and 0.2 nm), these findings, combined with the results described here, may suggest that the increase in the D-period can be related to the high levels of MMPs in the tissue.

Understanding the effects of MMPs on the collagen structure is an important issue, which can greatly benefit early detection and diagnosis of breast cancer. It has been reported that conventional mammography fails to diagnose about 20 % of cancers (Wang, 2003); therefore new, more efficient methods are needed. The study presented in this thesis showed that although MMPs treatment clearly reduced diffraction intensity of the tendon samples, the effect of the treatment on the axial periodicity is not clear. Further studies are needed that involve more samples (i.e. tendons incubated with MMPs) for statistically significant results. In the project presented here, rat tail tendon was used as a model tissue, therefore the observed effects are characteristic for type I collagen (major type found in rat tail tendon – see section 1.1.1.2). Since the breast tissue also contains type III collagen, the continuation of this study could also involve the use of normal breast tissue, which can be treated with MMPs for various amount of time. The breast tissue samples incubated with MMPs could also be compared to the tumour tissues to observe if there are differences between changes induced in collagen structure by the enzymes (incubation with MMPs) and changes that occur during tumour invasion.

6. The effects of UV-irradiation (λ=254nm) on collagen structure

6.1 Introduction

Ultraviolet light (UV) is well known to induce alterations in collagen-rich connective tissues and has been associated with symptoms such as premature skin aging and skin cancer (Fisher et al., 1997). It has also been used as a method of inducing crosslinking in collagen structure (Sionkowska, 2000; Wollensak et al., 2003). In biomaterial production, UV irradiation is a useful method of modifying the structure of collagen which could potentially improve physical, chemical and biological properties of the collagen biomaterial (Sionkowska and Wess, 2004; Sionkowska, 2006; Wang, 2006). In medicine, UV irradiation has been used to induce crosslinking in collagen structure and therefore improve corneal stiffness as a treatment of keratoconus, a disorder of the eye in which the cornea has an altered, conical shape causing distortion and reduced vision (Wollensak et al., 2003; Wollensak, 2006; Mencucci et al., 2007). Although UV irradiation is currently being used to modify collagen properties in biomaterial production and as a treatment for patients with keratoconus, the effects of UV light on the protein is still poorly understood. It is therefore essential to examine and describe the effects of UV light on collagen especially in order to gain control over the transformation process. This would be of great benefit in medicine, i.e. the exact UV dose can be calculated for patients with keratoconus, which will decrease the risk of harmful side effects of UV irradiation, and in biomaterial production, where collagen material with improved and controlled properties can be designed.

A series of experiments presented in this chapter were designed in order to examine the effects of UV light on collagen structure. The studies involved rat tail tendon and rat skin, which were used as a source of collagen; the alterations induced in the molecular structure of the protein were examined using small and wide angle X-ray diffraction. FTIR spectroscopy was also used to monitor conformational changes of the chemical environment within collagen structure in a response to UV treatment. Samples were irradiated in both hydrated and dry state in order to examine the effects of UV light on collagen in different environments. The knowledge gained from these structural and chemical studies can be used to guide new methods of enhancing the crosslinking process and optimise mechanical properties of collagen.

6.2. UV-irradiation of collagen

Ultraviolet light has a wavelength between 100 – 400 nm. The UV spectrum has been divided into subtypes: (1) UV A with wavelength between 400 nm – 315 nm, (2) UV B: 315 nm – 280 nm, (3) UV C: 280 nm – 100 nm (Diffey, 2002). In collagen molecules, only UVC irradiation is directly absorbed by the aromatic amino-acid residues: tyrosine and phenylalanine and by peptide bonds (McLaren and Shugar, 1964). The absorption of radiation above 290 nm wavelength by these species is negligible; therefore it would be unlikely to occur at irradiation with solar UV wavelengths that reach the earth's surface (i.e. 290 – 400 nm) (Gruijl, 2002). UV light with higher wavelengths (above 290 nm) affects biological molecules indirectly, i.e. by producing reactive oxygen species (ROS) (Afaq and Mukhtar, 2006). The studies presented in this thesis are focused on the examination of the effects of UVC light of λ=254 nm, since it is a wavelength directly absorbed by amino-acid

residues present in collagen molecules. The use of other wavelengths (i.e. above 290 nm) would have to involve the addition of photosensitizers such as riboflavin, used in a combined treatment of UVA/riboflavin proposed as a method of inducing crosslinking into collagen structure (Wollensak et al., 2003). This process is also poorly understood and the exact nature of crosslinking remains undefined.

The aromatic amino-acid residues (i.e. tyrosine and phenylalanine), which directly absorb UV light used in the studies presented here, are not found in the collagen triple helix but are present in telopeptides, which are non-helical ends of the molecule (section 1.1.1.3). However, there are only a small number of these residues in the collagen molecule, i.e. 5 tyrosine residues in the α1 chain (only found in the telopeptides) and 13 phenylalanine residues (found both in the telopeptides and in the main chain) (Protein Data Bank).

Upon UV irradiation, the following reactions could occur: (1) formation of tyrosine from phenylalanine, (2) formation of dityrosine and (3) dihydroxyphenylalanine (DOPA), the first product in melanin formation (Menter et al., 1995b). Figure 6.1 shows the possible products of photooxidation of amino acid residues in the collagen molecule.

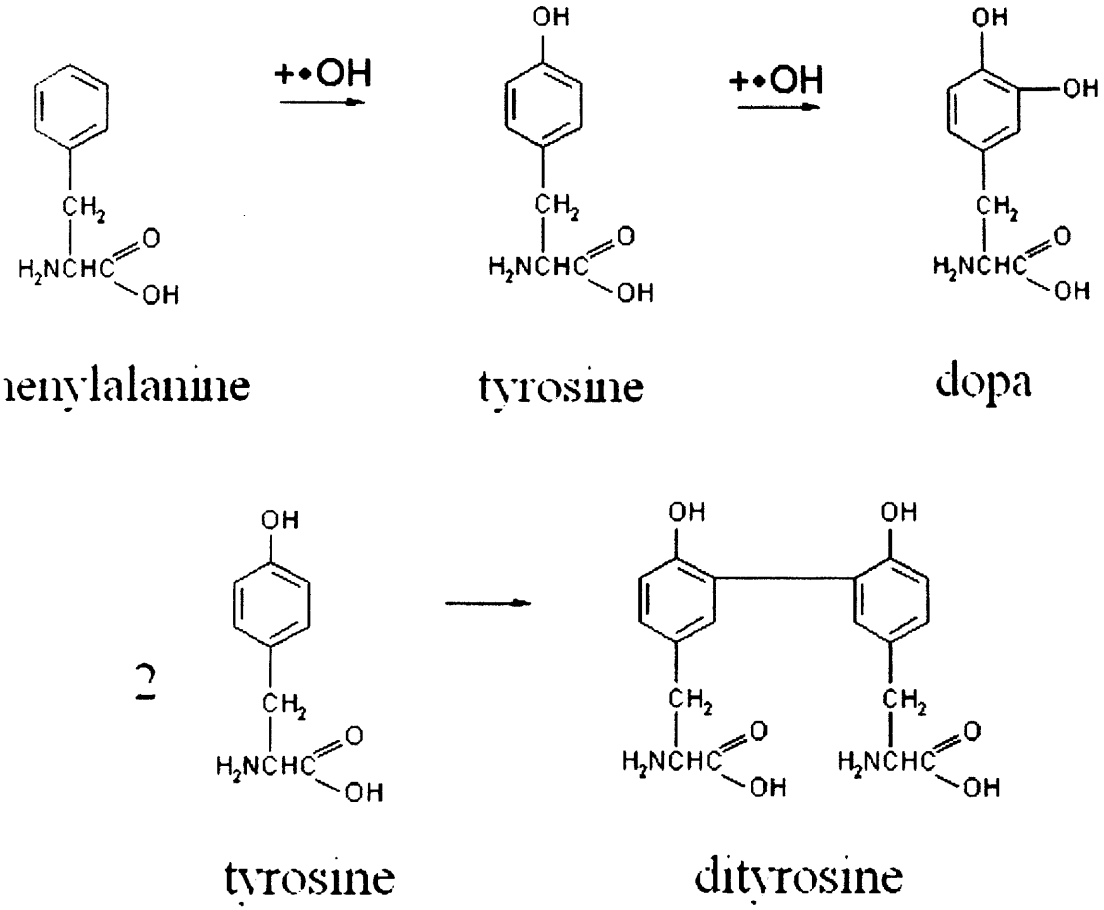

Figure 6.1. Photooxidation products of UV irradiated aromatic residues in collagen. Top: the oxidation of phenylalanine residues leads to the formation of tyrosine, which can be further oxidised forming DOPA. Bottom: two tyrosine residues can be crosslinked to form dityrosine (adapted from (Dyer, Bringans and Bryson, 2006)).

It is therefore apparent, that the photooxidation of aromatic amino-acid residues can lead to the formation of new crosslinks in collagen structure (i.e. dityrosine). The formation of the intermolecular crosslinks is accompanied by a rupture of hydrogen bonds which causes disorganization of the protein structure (Majewski et al., 2002; Sionkowska, 2005). UV irradiation in solution was reported to cause the appearance of free radicals in the water molecules that surround collagen. It has been suggested that when they interact with proline it

results in the appearance of the secondary free radicals which interacts with glycine residues causing chain scissions in collagen (Bailey et al., 1964; McLaren and Shugar, 1964; Weadock et al., 1995). The cleavage of peptide bonds was suggested to cause the formation of a local gelatine-like structure (Sudoh and Noda, 1972). Such structures would be potentially formed as a result of chain scissions, which occurred at sites along the collagen molecule and cause partial destabilization of the protein. However, due to the hydrogen bonding, the triple helical structure remains intact; this results in the formation of local, gelatine-like areas. The formation of an intermediate state prior to degradation, which is mainly triple helical but contains a number of chain scissions, was reported by Miles et al (Miles et al., 2000). The presence of this intermediate state was identified by differential scanning calorimetry and it was suggested that the chain scissions occur at random along the length of the molecule (Miles et al., 2000).

In summary, it is apparent that UV irradiation leads to complex changes within collagen structure. Two processes are suggested to be induced by UV light: crosslinking that can be potentially used as a method of improving collagen properties, and bond scissions, which lead to a degradation of the protein. It is therefore important to fully understand the mechanism of collagen transformation in response to UV light and rearrangements induced within its molecular structure, in order to control these two types of reactions. By controlling the irradiation conditions (i.e. irradiation time) it could be possible to enhance the degradative process (i.e. bond scissions) or crosslinking of collagen to obtain biomaterials with specific properties.

6.3. Material and methods

6.3.1. Sample preparation

Collagen was obtained from rat tail tendons. Dissected tendons were placed in phosphate-buffered saline (PBS) and irradiated in open Petri dishes using UVP Ultraviolet Shortwave Crosslinker (CX-2000) that emits light of 254 nm wavelength. The intensity of irradiation was 0.263 J/(cm^2min) and the distance between the lamp and the sample was approximately 10 cm. In addition to this, some tendons were dried overnight at room temperature and irradiated in a dry state in order to make a comparison of the effect of free water on collagen-UV interactions. Skin samples were dissected from rat tails. As the penetration of UV light at 254 nm through the tissues is very low (i.e. it is absorbed only by the outermost layers of skin) skin samples were irradiated at each side to increase the effect.

6.3.2. Acetic acid treatment

Sample fractions of all of the UV irradiated tendons were dissolved in 0.5 M acetic acid to observe the solubility of the samples. Collagen has been reported to swell in dilute acetic acid, lose its fibrillar appearance and dissolve into a viscous solution (Kessler, Rosen and Levenson, 1960). The formation of additional crosslinks may stabilize collagen fibrillar structure and result in the reduction of its solubility. The acetic acid treatment was therefore used in the study presented here as a method to indicate crosslinks formation.

6.3.3. Small-angle X-ray scattering (SAXS)

SAXS experiments were carried out at Daresbury Synchrotron Radiation Source, UK, station 2.1 (section 3.1.1.1). The camera was positioned at 5.5 m or 4.25 m from the specimen; the wavelength used was 0.154 nm. 2D scattering images were converted into linear plots of integrated intensity vs scattering vector q (1/nm) using FibreFix software (Rajkumar et al., 2005) (section 3.2.1). One dimensional profiles were then analyzed using PeakFit software (section 3.2.3) which allowed determination of the position, intensity and the width of the meridional diffraction peaks, as explained in Chapter 3.

Some measurements were also conducted using the Bruker NanoSTAR facility at Cardiff University with a sample to detector distance of 107.2 cm (section 3.1.2). Silver behenate was used as a calibration standard.

Rat tail tendon samples were kept under slight tension during the SAXS measurements.

6.3.4. Wide-angle X-ray scattering (WAXS)

Wide-angle X-ray scattering patterns were collected using the Bruker NanoSTAR facility at Cardiff University (section 3.1.2). A shorter sample to detector distance of 22 cm was used, which allowed the observation of reflections that correspond to the intermolecular spacing of the collagen molecules and the helical rise per residue distance of the collagen helix. Calcite was used as a calibration standard.

6.3.5. Electron Microscopy (EM)

Negative-stain electron micrographs were used to view the morphology of UV-irradiated collagen fibres. To obtain micrographs, tendons were placed in 1 ml of phosphate-buffered saline (pH 7.5) and homogenized. 100 µl of the homogenate was mixed with 100 µl of 2% phosphotungstic acid (PTA). 10 µl of the mix was then placed on a grid containing uranyl acetate and ultrastructural examination was carried out using a Philips 208 TEM (FEI Electron Optics, Eindhoven, The Netherlands) operated at 80 kV accelerating voltage at the Bioscience Department, Cardiff University.

6.3.6. Fourier Transform Infrared Spectroscopy (FTIR)

FTIR measurements were conducted to monitor the effects of UV-irradiation on the collagen backbone. FTIR analysis was carried out using Attenuated Total Reflectance-FTIR at The National Archives, London (section 2.2.4). Scans were collected in absorption mode at 32 scans per sample using a resolution of 4 cm^{-1} and analyzed using OMNIC software.

6.4. Results

Figure 6.2 shows control rat tail tendons and samples UV-irradiated for 24 hours in a hydrated state. It can be seen that after irradiation tissue becomes yellow and more coiled. When 0.5 M acetic acid was added to the UV-irradiated tendons, only samples that were irradiated for up to 6 hours were dissolved. Tendons irradiated for longer exposure times

retained their fibrillar appearance, indicating that additional crosslinks may have been formed in these samples.

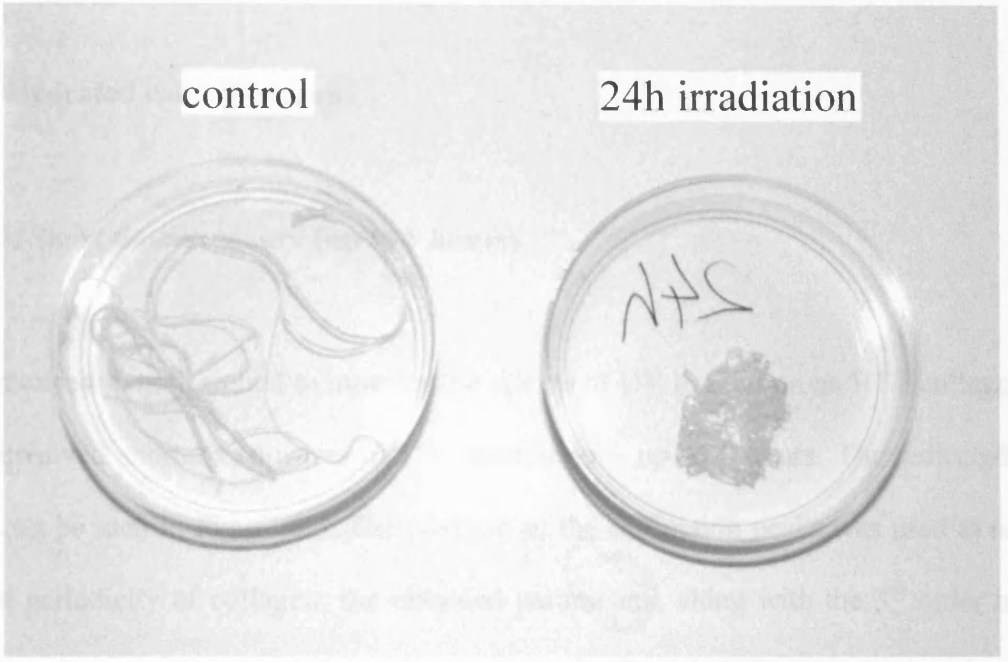

Figure 6.2. Rat tail tendon samples – control (left) and after 24 h of UV-irradiation (right). The yellowing of the tendons can be observed upon UV irradiation; tendons also appear to be more coiled and contain yellow photoproducts.

6.4.1. Small-angle X-ray scattering (SAXS)

SAXS measurements were conducted on rat tail tendons irradiated by UV light in a hydrated and a dried state. Typical X-ray exposure times were 30 seconds so none of the effects seen in Chapter 4 were believed to contribute. Various exposure times were used: from 5 minutes to 72 hours. The SAXS result section has been divided into two parts: the first part provides the results based on measurements on samples UV irradiated from 5 minutes to 8 hours (i.e. short time exposures), while the second part provides the results based on samples subjected

to longer exposure times (i.e. up to 47 and 72 hours for tendons irradiated in a hydrated and dried state, respectively).

6.4.1.1. Hydrated rat tail tendon

6.4.1.1.1. Short time exposure (up to 8 hours)

The first experiment designed to monitor the effects of UV irradiation on RTT collagen using SAXS involved shorter exposures of UV irradiation – up to 8 hours. The collected SAXS images can be seen in Figure 6.3. The position of the diffraction peaks was used to calculate the axial periodicity of collagen; the obtained parameters, along with the 3rd order intensity values, are shown in Figure 6.4. It can be seen that the D-periodicity was not found to change upon UV irradiation: the D-period value was 67 nm in normal tendons and 66.8 nm in tendon irradiated for 8 hours (Figure 6.4). The only effect observed on the SAXS patterns was the reduction of the diffraction orders intensity, which can indicate a loss of order within collagen structure. The intensities measured for the 3rd diffraction order are shown in Figure 6.4.

It can also be observed from diffraction images in Figure 6.3 that the meridional reflections collected from the UV-irradiated tendons appear as wide arcs. Since the UV-irradiated samples were found to be more coiled than control tendons, it is suggested that this effect (i.e. an increase in the breadth of the meridional reflections in the direction perpendicular to the axis) is due to the curvature of the sample rather than an alteration in the crimp level (see section 1.1.1.2).

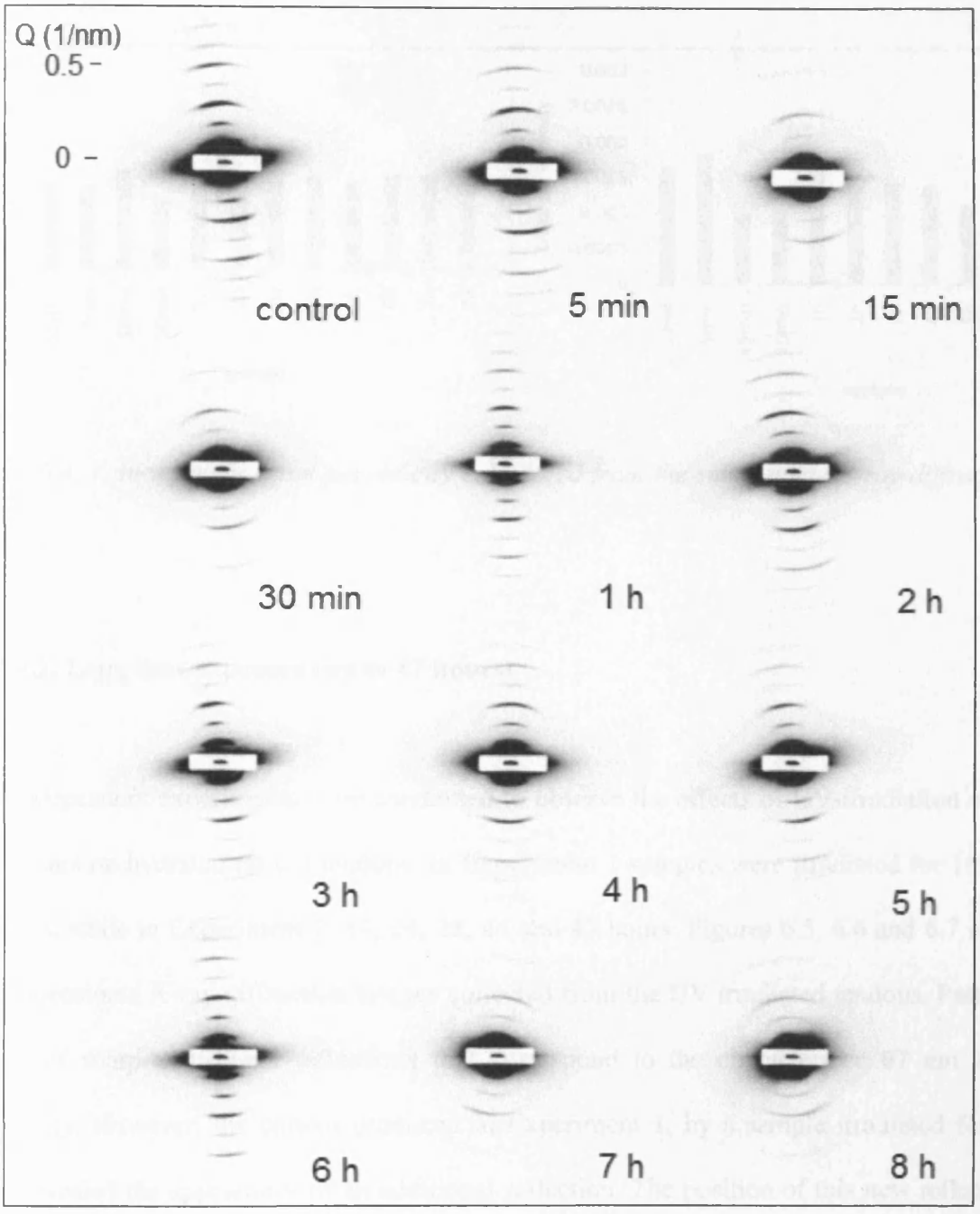

Figure 6.3. Small-angle X-ray diffraction images of UV-irradiated tendons collected at Daresbury Radiation Facility, UK. The series shows images collected from control tendons and samples irradiated from 5 minutes up to 8 hours. The effect of disorientation in UV-irradiated samples is probably due to the curvature of the sample, while the crimp level remains unchanged.

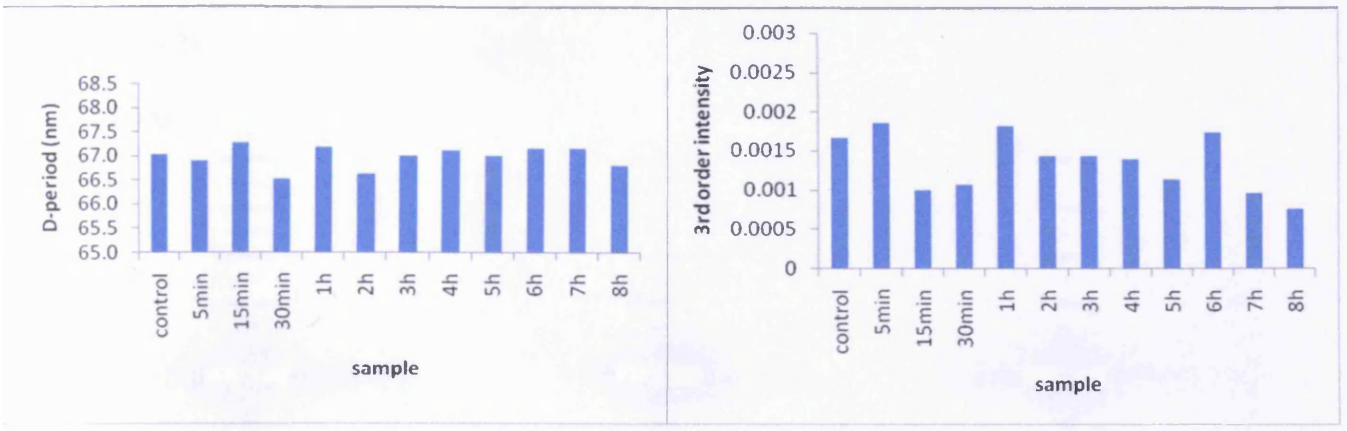

Figure 6.4. Values for the axial periodicity calculated from the small-angle X-ray diffraction patterns.

6.4.1.1.2. Long time exposure (up to 47 hours)

Two independent experiments were conducted to observe the effects of UV-irradiation of up to 47 hours on hydrated rat tail tendons. In Experiment 1 samples were irradiated for 18 and 24 hours, while in Experiment 2: 19, 24, 28, 44 and 47 hours. Figures 6.5, 6.6 and 6.7 show two-dimensional X-ray diffraction images collected from the UV irradiated tendons. Patterns consist of sharp meridional reflections that correspond to the characteristic 67 nm axial periodicity. However, the pattern produced in Experiment 1, by a sample irradiated for 18 hours revealed the appearance of an additional reflection. The position of this new reflection may correspond to the first diffraction order of a 20 nm periodicity. A zoomed-in section of the diffraction pattern is shown in Figure 6.6. The intensity of the new reflection is weak compared to the strong orders of the fundamental 67 nm periodicity, however, it is clearly visible on the diffraction pattern and on the corresponding linear profile (Figure 6.6). This

new reflection was also observed in Experiment 2, in the sample irradiated for 24 hours (Figure 6.7).

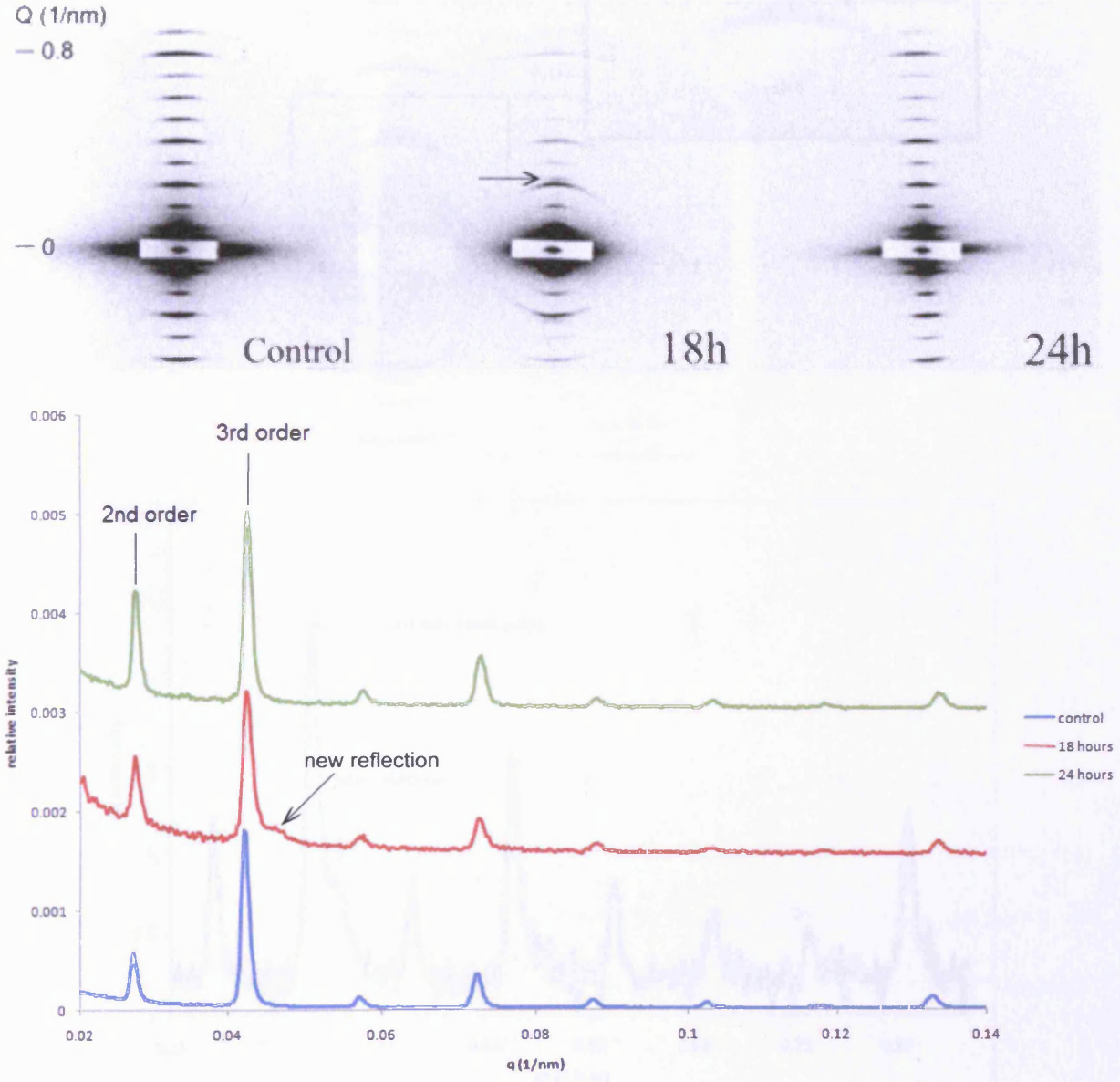

Figure 6.5. Top: Small-angle X-ray diffraction images of UV-irradiated tendons collected at Daresbury Radiation Facility, UK during Experiment 1 (a new reflection observed after 18 h of irradiation has been indicated by an arrow). Bottom: corresponding linear profiles showing the position and intensities of the diffraction peaks. The 2nd and the 3rd diffraction orders are indicated on the graphs.

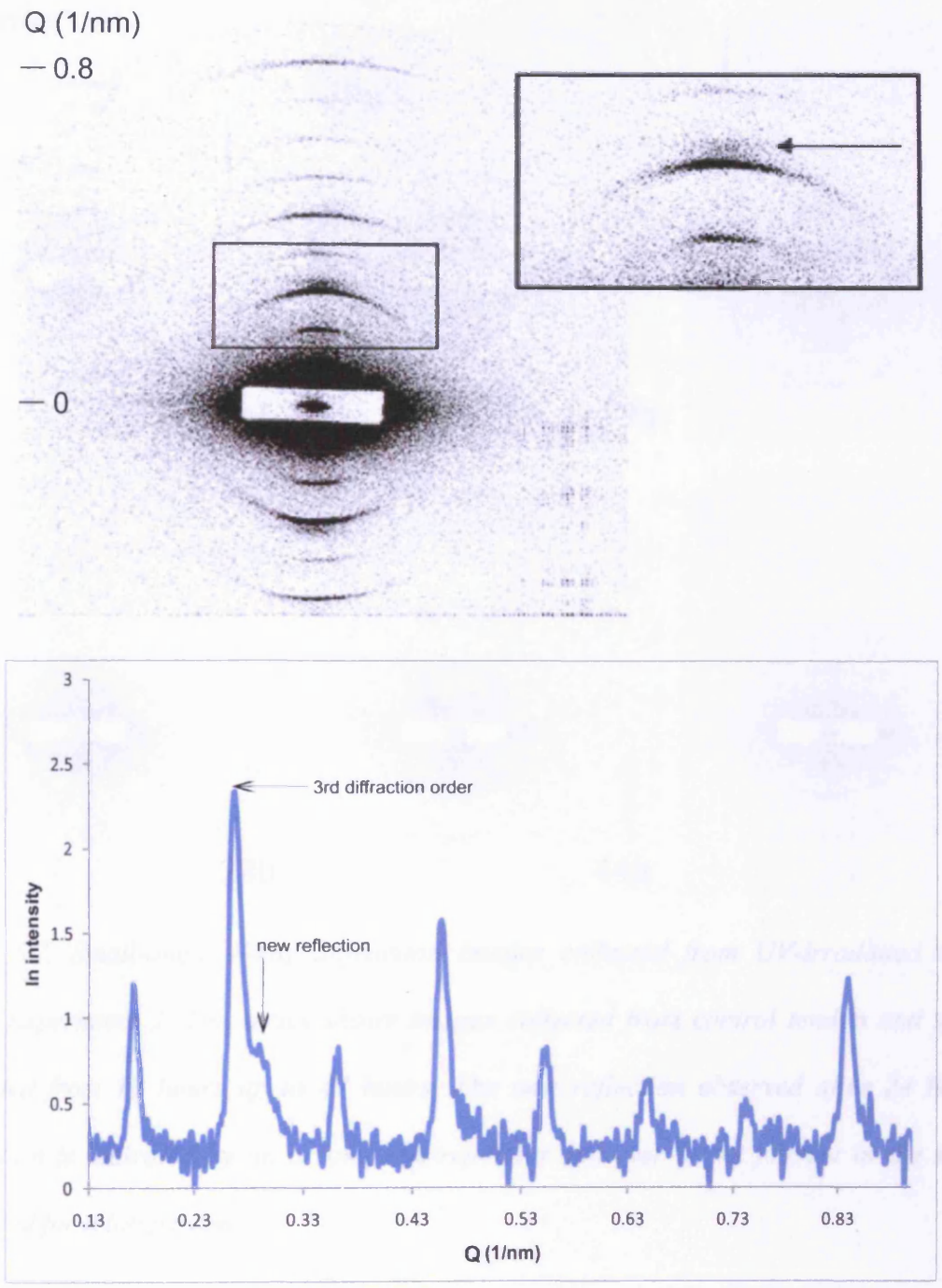

Figure 6.6. Top: an X-ray diffraction image of rat tail tendon UV-irradiated for 18 hours. A zoomed-in section shows the 3rd diffraction order and a new reflection (indicated by an arrow). Bottom: corresponding linear profile; the positions of the 3rd diffraction order and the new reflection are indicated on the graph.

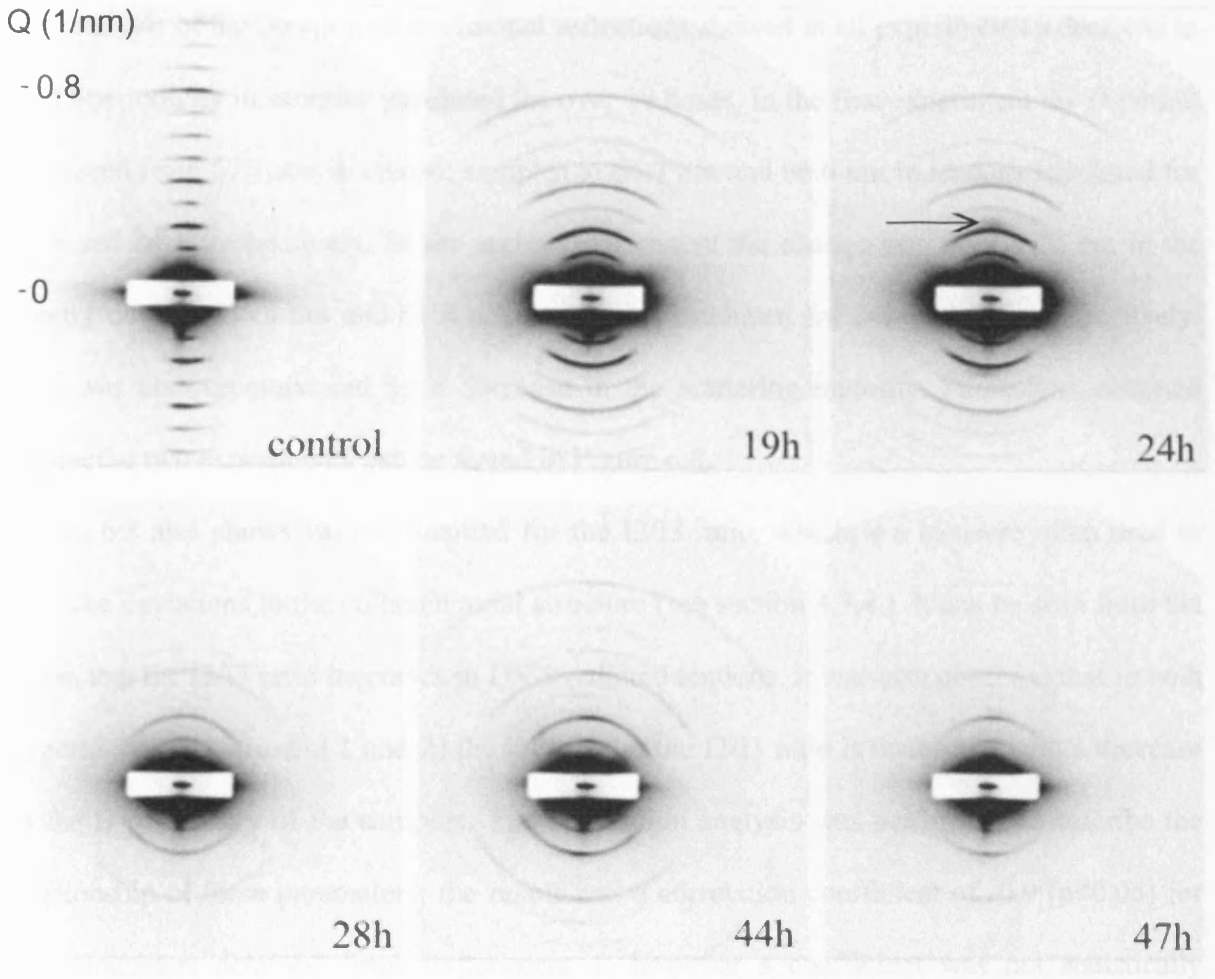

Figure 6.7. Small-angle X-ray diffraction images collected from UV-irradiated tendons during Experiment 2. The series shows images collected from control tendon and samples irradiated from 19 hours up to 47 hours. The new reflection observed after 24 hours of irradiation is indicated by an arrow. The reflection however is not present in the samples irradiated for a longer time.

The analysis of the position of meridional reflections showed in all experiments a decrease in the D-periodicity in samples irradiated for over 19 hours. In the first experiment the D-period decreased from 67.1 nm in control samples to 66.7 nm and 66.6 nm in tendons irradiated for 19 h and 24 h, respectively. In the second experiment the change was from 67.2 nm in the control down to 66.9 nm and 66.8 nm in samples irradiated for 24h and 47 h, respectively. This was also accompanied by a decrease in the scattering intensity. Parameters obtained during the two experiments can be found in Figure 6.8.

Figure 6.8 also shows values obtained for the I2/I3 ratio, which is a measure often used to describe deviations in the collagen axial structure (see section 4.3.4.). It can be seen from the graph that the I2/I3 ratio increases in UV irradiated tendons. It was also observed that in both experiments (Experiment 1 and 2) the increase in the I2/I3 ratio is connected with a decrease in the D-periodicity of the samples. The correlation analysis was performed to describe the relationship of these parameters; the result was a correlation coefficient of -0.9 ($p<0.05$) for the parameters obtained from Experiment 1, however a coefficient was not statistically significant for the parameters from Experiment 2 (correlation coefficient of -0.57, $p>0.05$).

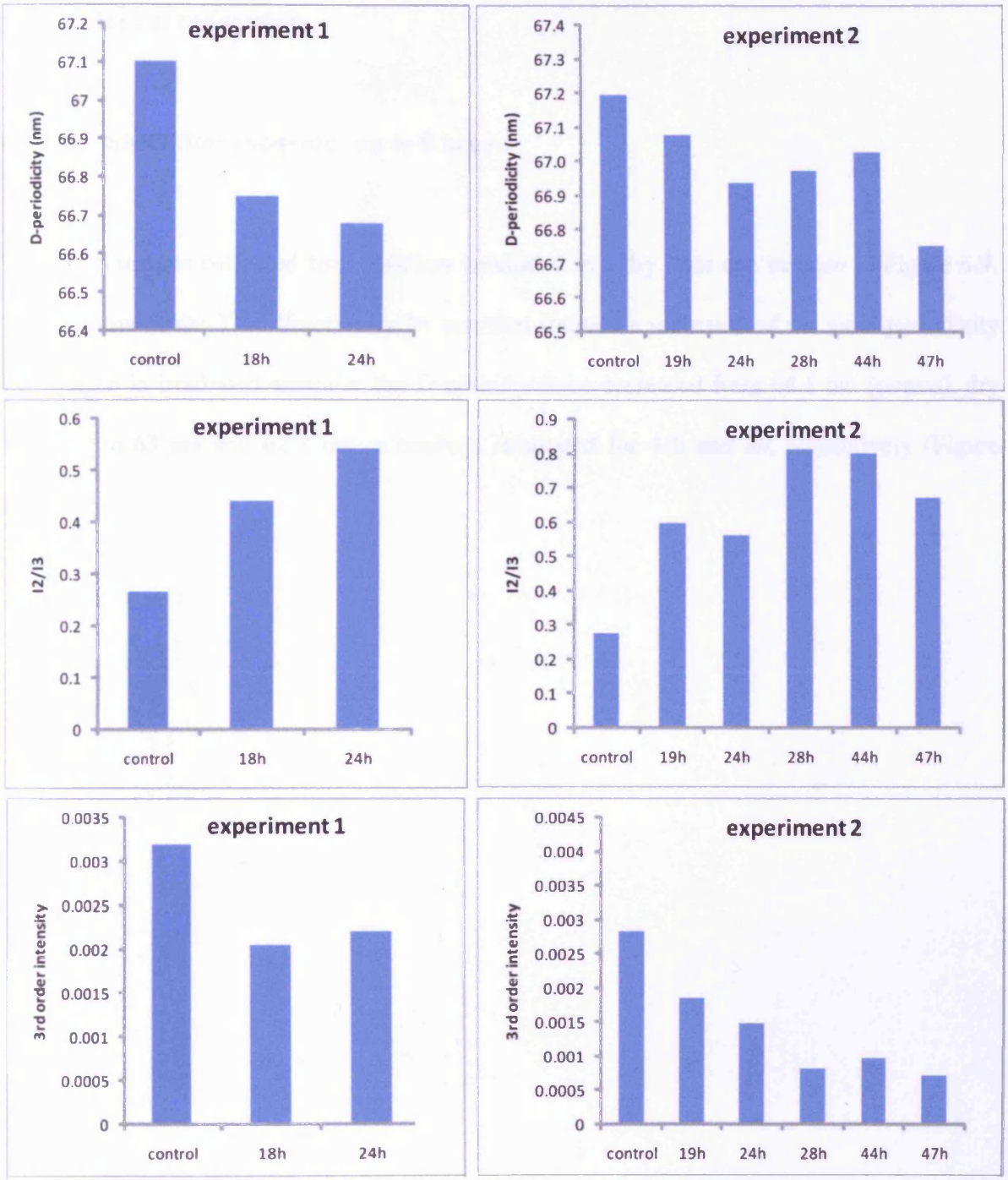

Figure 6.8. Values for the axial periodicity, the I2/I3 ratio and intensity of the 3rd diffraction order calculated from the small-angle X-ray diffraction patterns collected during Experiment 1 and 2.

6.4.1.2. Dry rat tail tendon

6.4.1.2.1. Short time exposure (up to 8 hours)

2D SAXS images collected from tendons irradiated in a dry state can be seen in Figure 6.9. The analysis of the 3rd diffraction order position showed a reduction of the axial periodicity of collagen in irradiated samples: the D-period values decreased from 64.1 nm (normal, dry tendons) to 63 nm and 62.7 nm in tendons irradiated for 4 h and 8h, respectively (Figure 6.10).

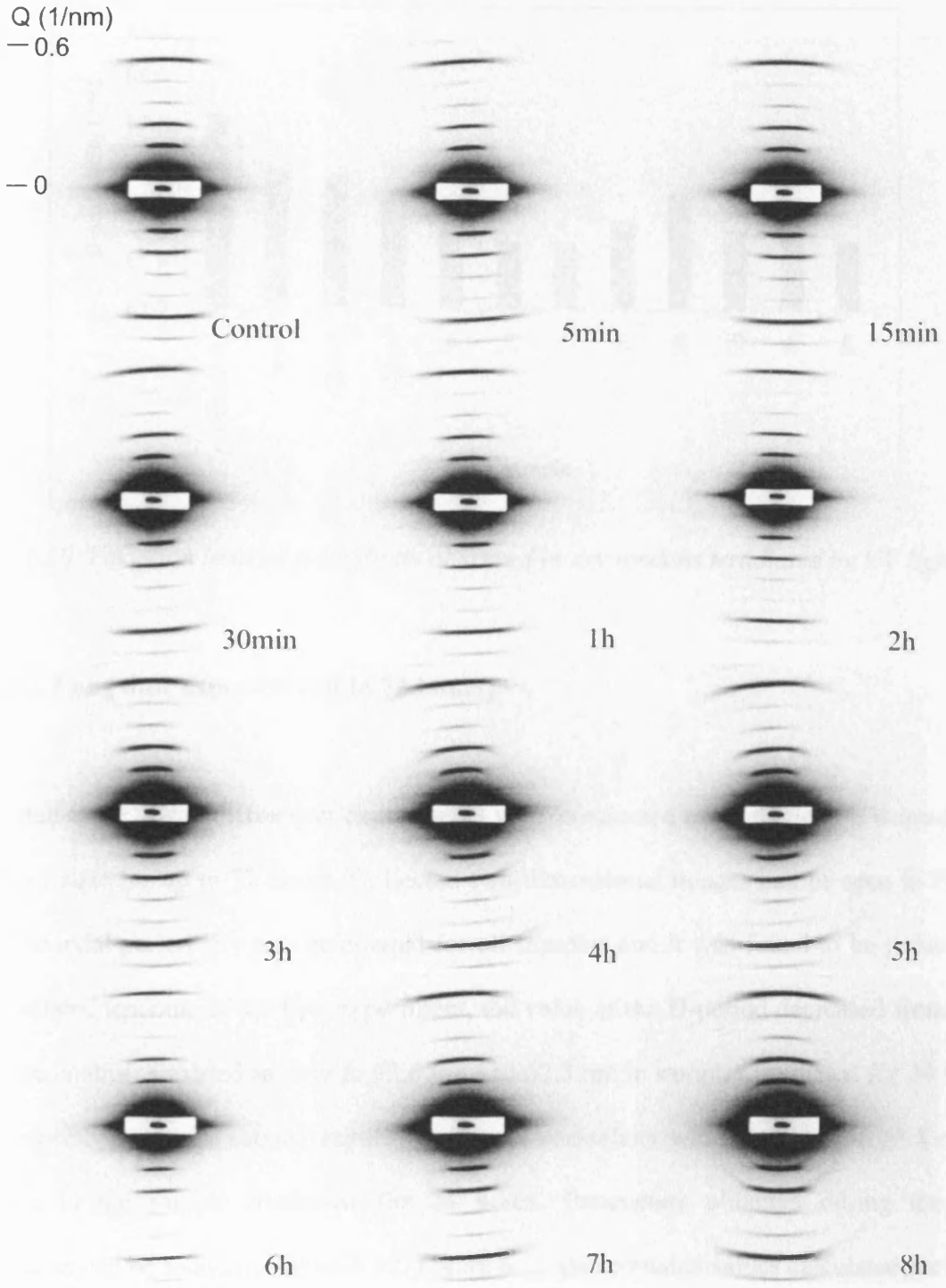

Figure 6.9. Small-angle X-ray diffraction images of UV-irradiated dry tendons collected at Daresbury Synchrotron Radiation Facility, UK. The series shows the diffraction images collected from control tendon and samples irradiated from 5 minutes up to 8 hours.

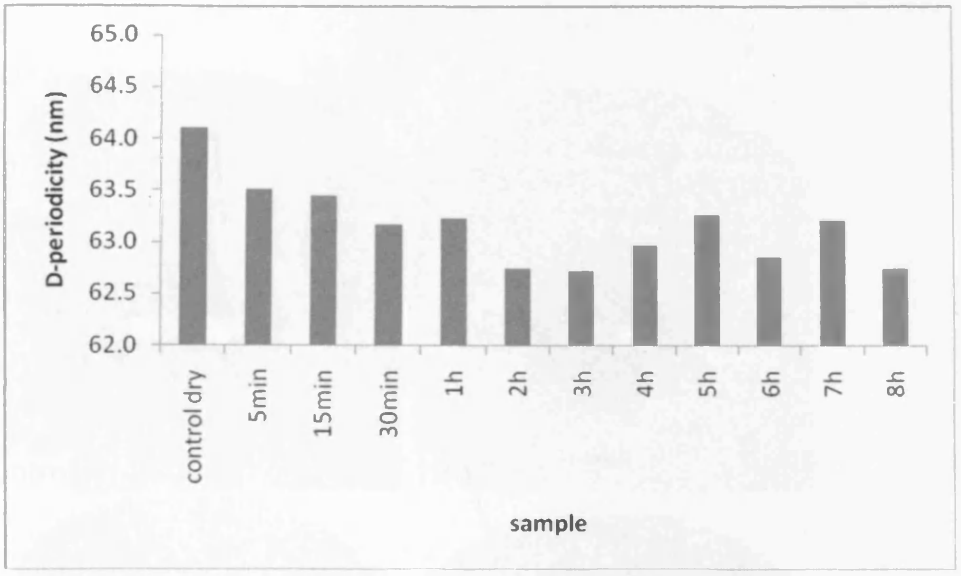

Figure 6.10. Variation in axial periodicity observed in dry tendons irradiated by UV light.

6.4.1.2.2. Long time exposure (up to 72 hours)

Two small-angle X-ray diffraction experiments were conducted using tendons UV-irradiated in the dry state for up to 72 hours. Collected two-dimensional images can be seen in Figure 6.11. The axial periodicity was calculated for all samples and it was found to be reduced in UV-irradiated tendons. In the first experiment, the value of the D-period decreased from 64.4 nm in the control, air dried sample to 63.6 nm and 62.3 nm in samples irradiated for 24 h and 72 h, respectively. In the second experiment, the D-periodicity was reduced from 63.8 nm to 61.2 nm in the sample irradiated for 24 hours. Parameters obtained during the two experiments can be found in Figure 6.12. Figure 6.12 also contains values calculated for I2/I3 ratio. A correlation analysis showed that there is no statistically significant relationship between these two parameters (the axial periodicity and the I2/I3 ratio).

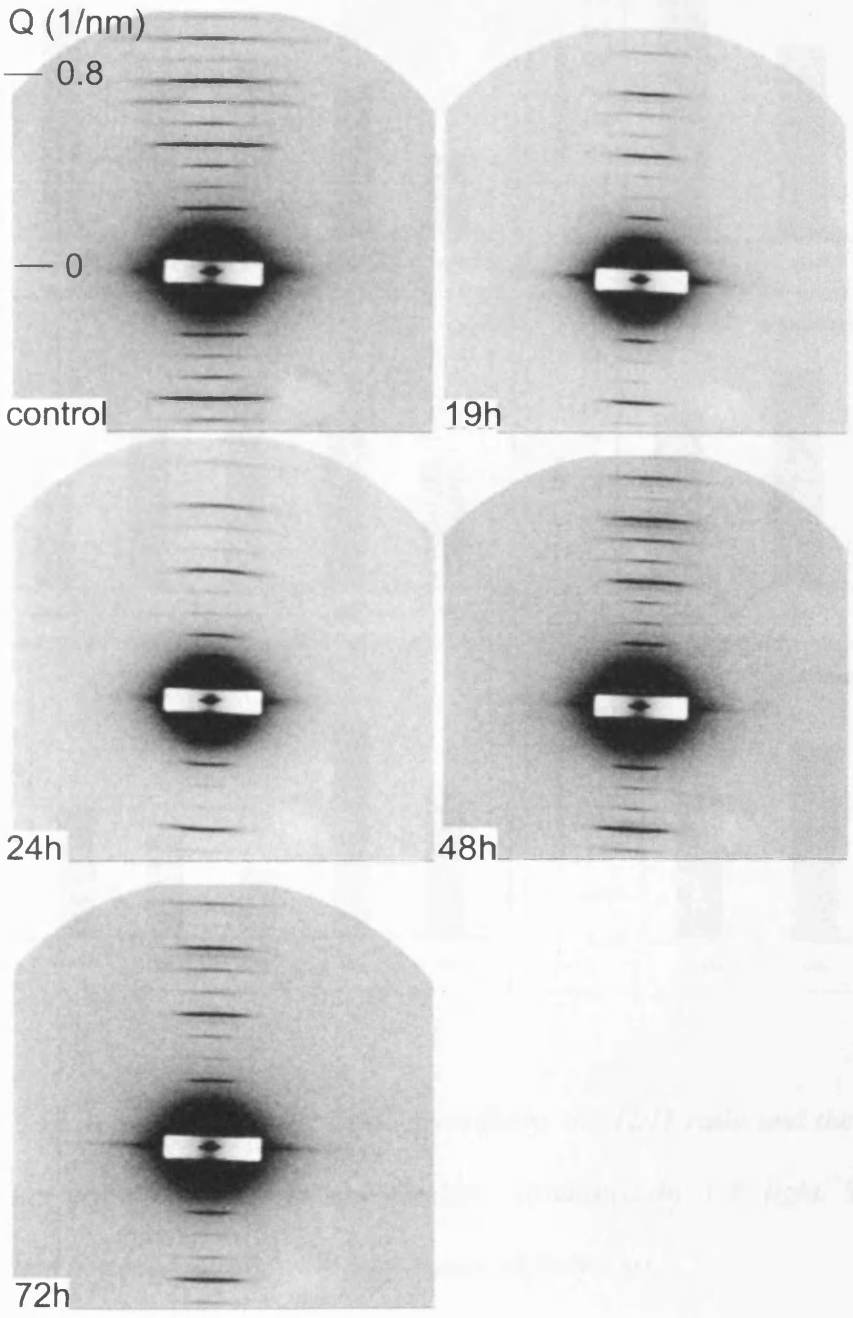

Figure 6.11. Small-angle X-ray diffraction images of UV-irradiated dry tendons collected at Daresbury Synchrotron Radiation Facility, UK. The series shows diffraction images collected from control tendons and samples irradiated for up to 72 hours.

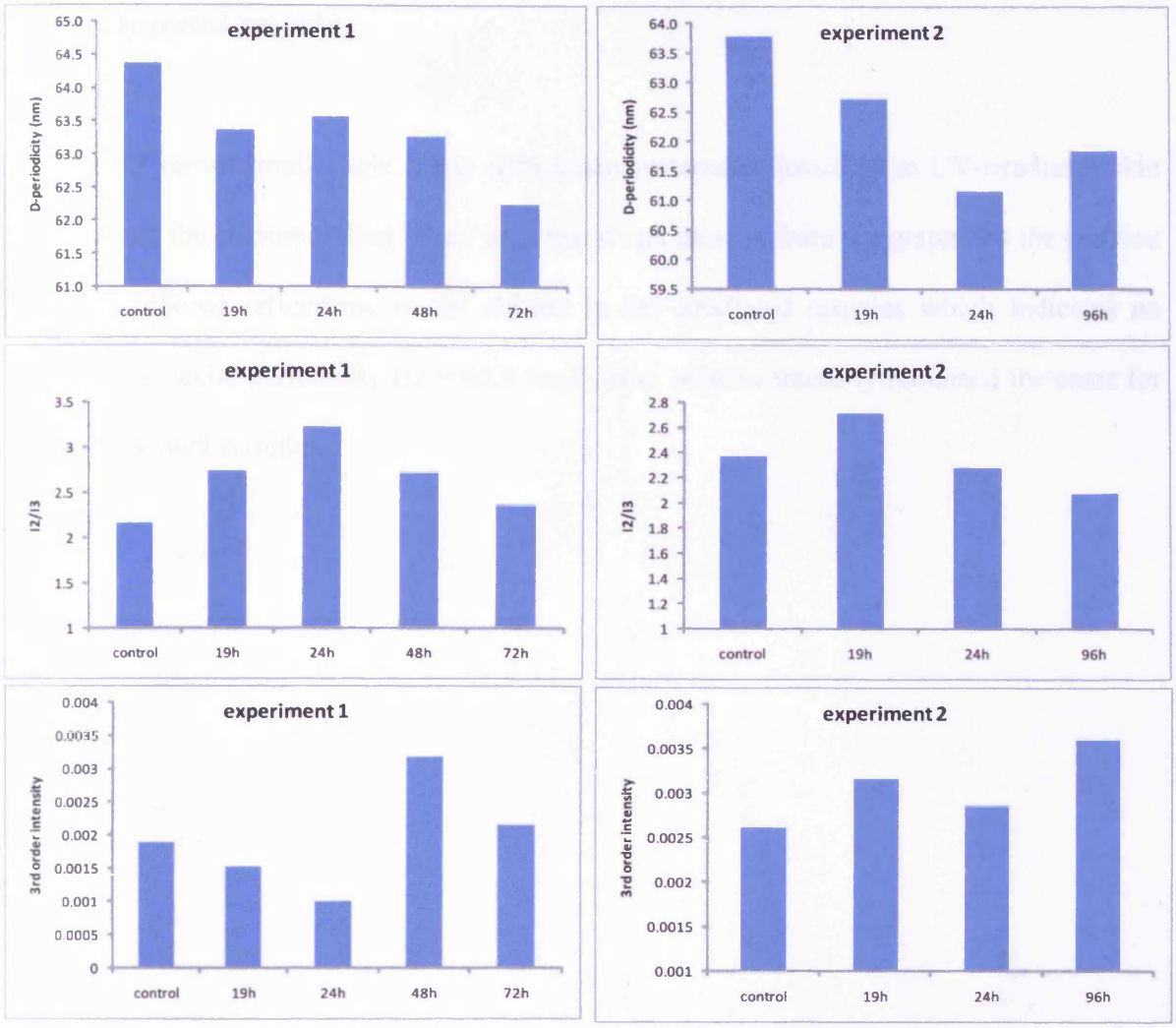

Figure 6.12. A variation in the axial periodicity, the I2/I3 ratio and the intensity of the 3rd diffraction order observed in dry tendons irradiated by UV light. The graphs present parameters obtained during two independent experiments.

6.4.1.3. Hydrated rat skin

Figure 6.13 shows small-angle X-ray diffraction patterns collected from UV-irradiated skin samples, and the corresponding linear profiles. It can be seen from the graph that the position of the meridional reflections is not shifted in the irradiated samples which indicates no change in the axial periodicity (D = 65.4 nm). Also, relative intensity remained the same for all UV-irradiated samples.

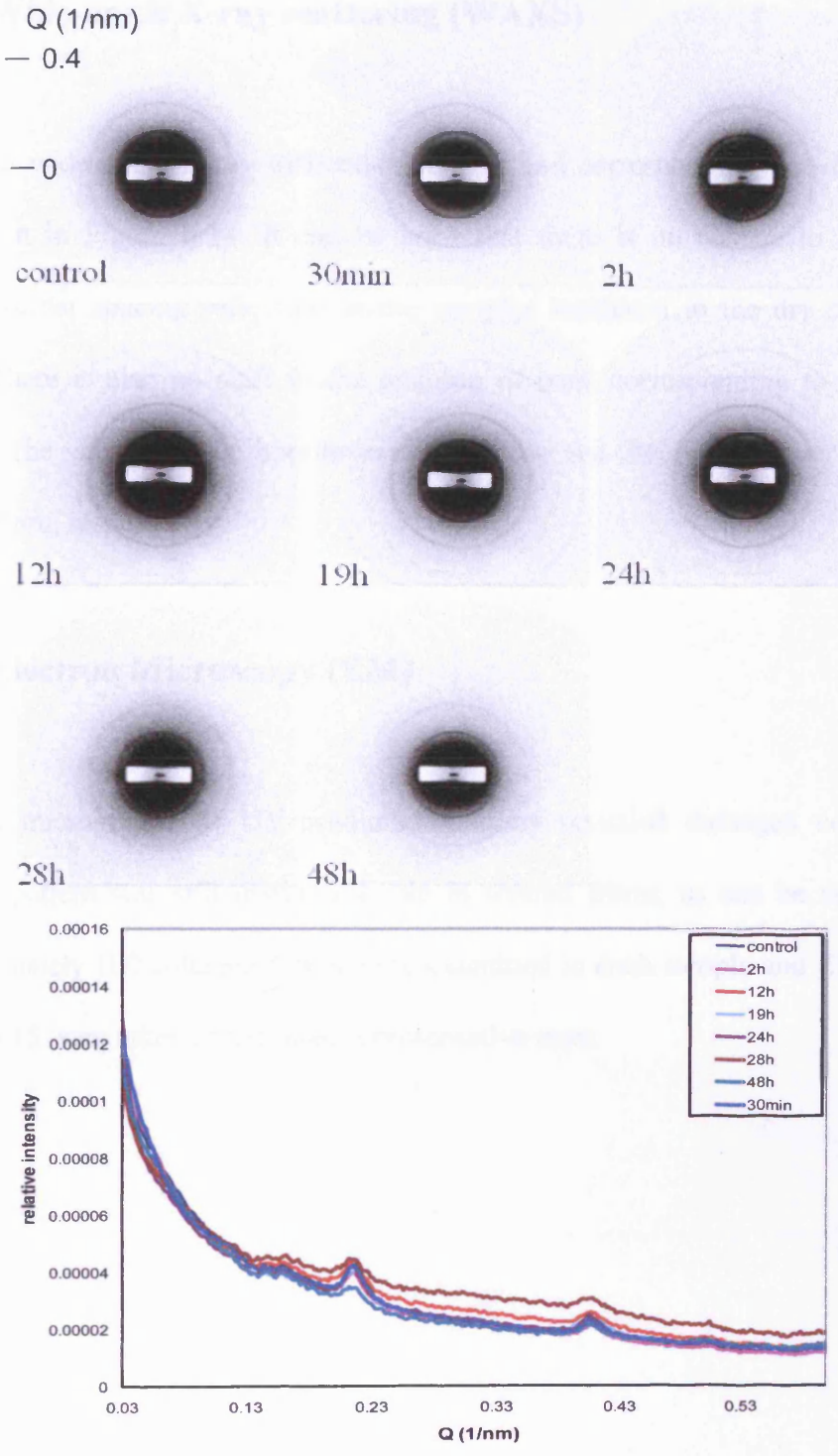

Figure 6.13. Top: Small-angle X-ray diffraction images of skin samples irradiated with UV light for up to 48 hours. Corresponding linear profiles are shown at the bottom.

6.4.2. Wide-angle X-ray scattering (WAXS)

Collected wide-angle X-ray diffraction images and corresponding one-dimensional profiles are shown in Figure 6.14. It can be seen that there is no change in the position of the intermolecular spacing reflection in the samples irradiated in the dry state from 19 to 72 hours. There is also no shift in the position of peak corresponding to the helical rise per residue. The values for the intermolecular spacing and the axial rise per residue are 1.2 nm and 0.28 nm, respectively.

6.4.3. Electron Microscopy (EM)

Electron micrographs of UV-irradiated tendons revealed damaged collagen fibres. The banding pattern was still distinguishable in treated fibres, as can be seen in Figure 6.15. Approximately 100 collagen fibres were examined in each sample and EM images shown in Figure 6.15 were taken of the most representative ones.

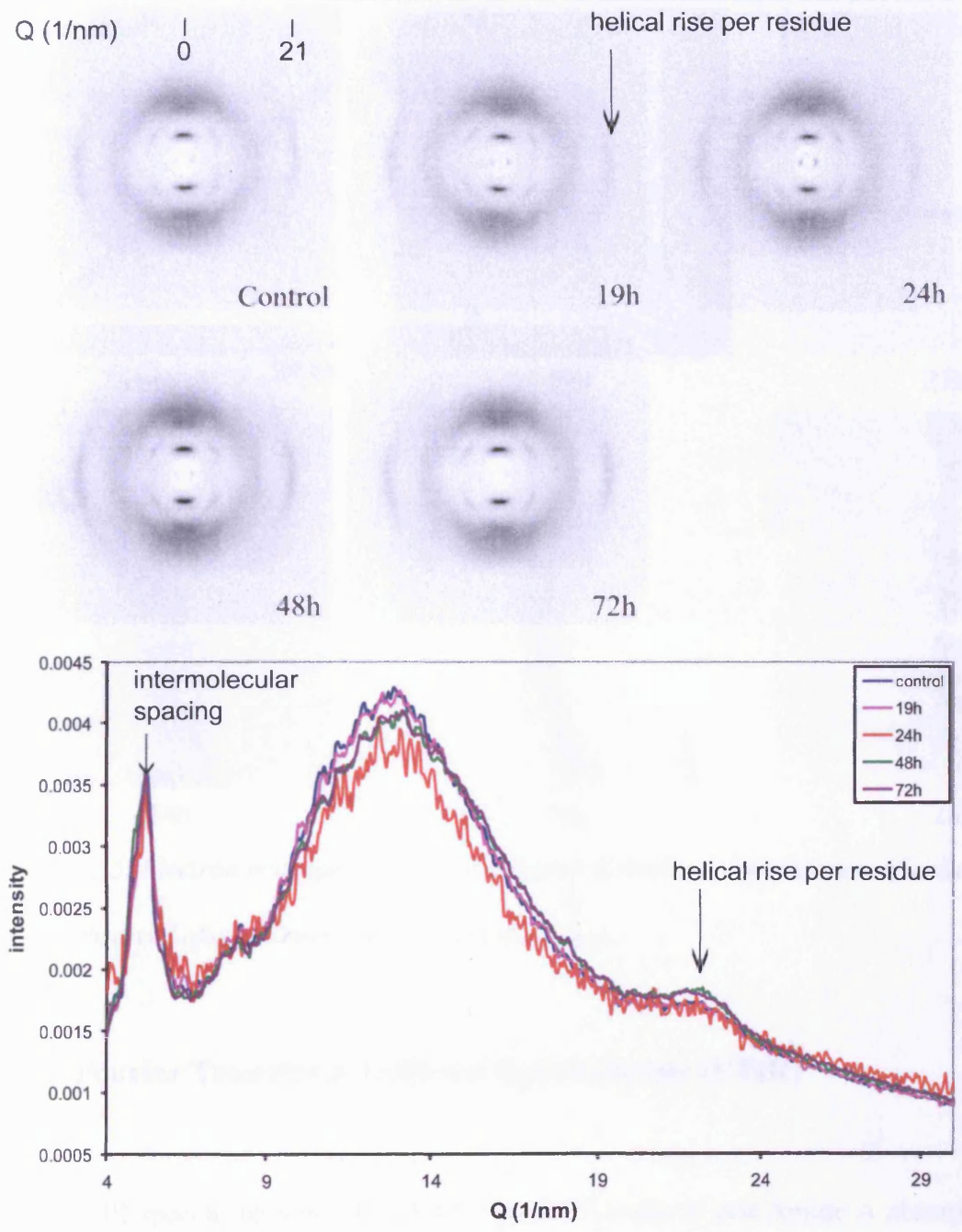

Figure 6.14. Wide-angle X-ray diffraction images of dry UV-irradiated tendons (top) and corresponding linear traces of intensity versus scattering vector q (1/nm) (bottom). The peaks corresponding to the intermolecular spacing (1.2 nm) and helical rise per residue (0.28 nm) are indicated on the graph.

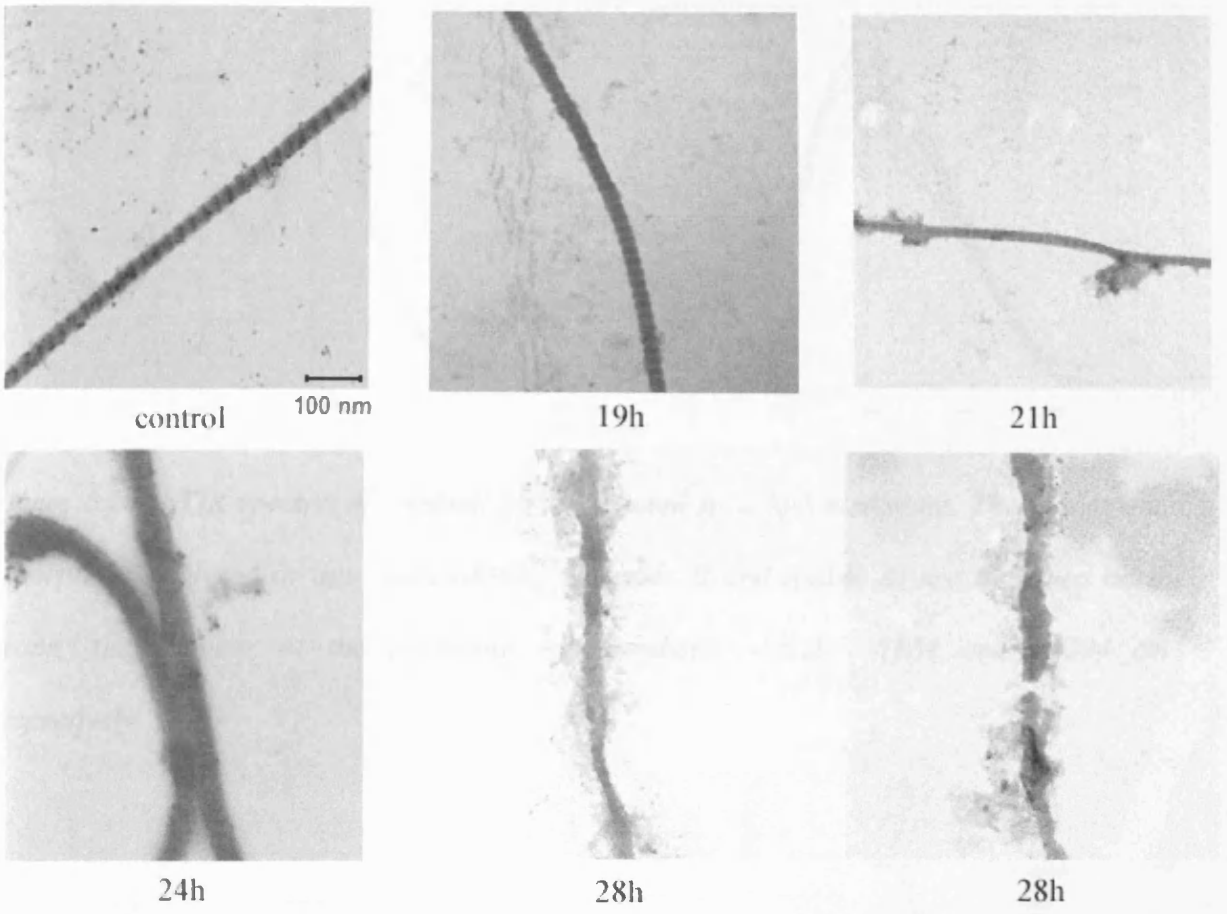

Figure 6.15. Electron micrographs of UV-irradiated tendons. Degradation of collagen fibrils can be observed after 28 hours of UV light treatment.

6.4.4. Fourier Transform Infrared Spectroscopy (FTIR)

In the FTIR spectra the positions of the Amide I, Amide II and Amide A absorptions were analyzed (see section 2.2.3). Figures 6.16 and 6.17 show spectra recorded for samples irradiated by UV-light in a hydrated and dry state, respectively.

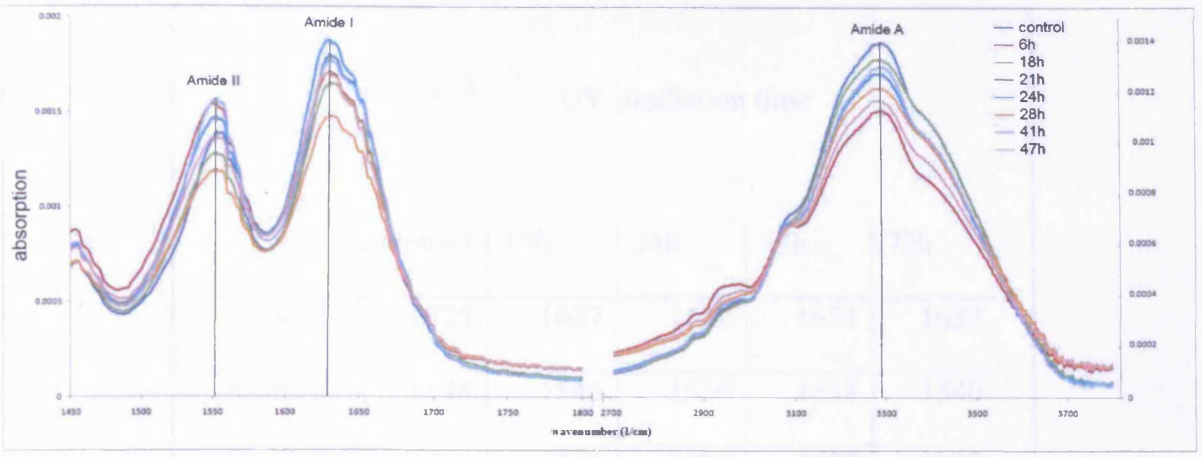

Figure 6.16. FTIR spectra of tendons UV-irradiated in a hydrated state. The fundamental absorptions analyzed in this study (Amide I, Amide II and Amide A) are indicated on the graph; they appear at the following wavenumbers: ≈1629, ≈1554 and ≈3294 cm^{-1} respectively.

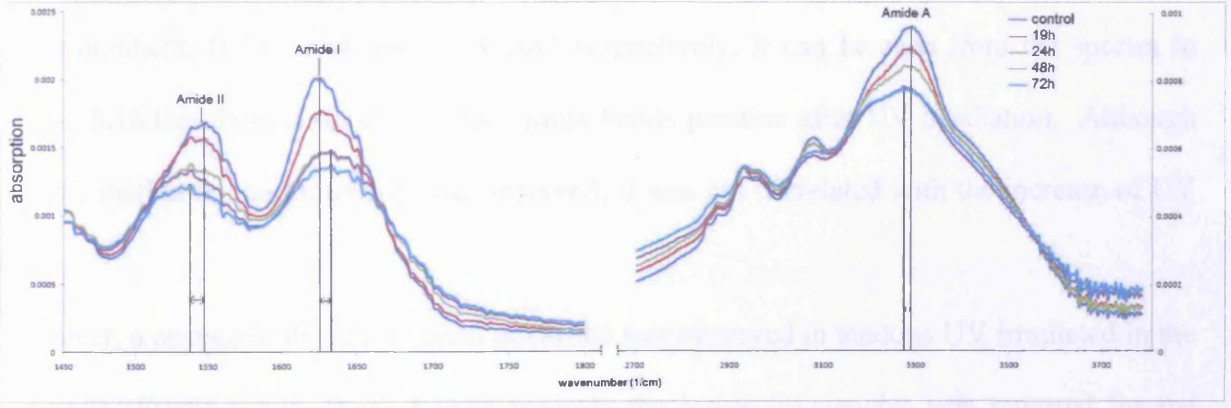

Figure 6.17. FTIR spectra of tendons UV-irradiated in a dry state. The fundamental absorptions analyzed in this study (Amide I, Amide II, Amide A) are indicated on the graph. The frequency shift of the amide bands is observed and have been indicated by arrows.

band	UV irradiation time				
	control	19h	24h	48h	72h
Amide I	1625	1627	1632	1634	1633
Amde II	1548	1546	1539	1538	1540
Amide A	3292	3290	3290	3282	3282

Table 6.1. Amide band frequencies of rat tail tendons UV irradiated in the dry state.

In the spectrum of untreated, hydrated tendon (control) the Amide I, II and A bands appear at wave numbers: 1629, 1554 and 3294 cm^{-1} respectively. It can be seen from the spectra in Figure 6.16 that there is no shift in the amide bands position after UV irradiation. Although some variation in band intensity was observed, it was not correlated with the increase of UV dose.

However, a change in the amide band positions was observed in tendons UV irradiated in the dry state (Figure 6.17). Here, a shift towards the lower frequencies was reported for the Amide II and Amide A bands, whereas the position of the Amide I band was observed to move to a higher frequency. The positions of these bands in UV irradiated tendons are listed in Table 6.1. It can be seen that a decrease in the Amide II ($\Delta\nu$ = 10 cm^{-1}) and an increase in the Amide I frequency ($\Delta\nu$ = 8 cm^{-1}) occurs in samples that were UV irradiated for over 24 hours; after that time the positions of the bands remain unchanged. The Amide A band was observed to shift by 10 cm^{-1} in samples UV irradiated for over 48 hours (Table 6.1). These

changes were also accompanied by a decrease in the intensities of all three amide bands, with the irradiation time (Figure 6.17).

6.5. Discussion

6.5.1. Irradiation in the hydrated state

The initial SAXS measurements were performed on tendons that were UV irradiated for up to 8 hours. The results showed that the only effect was a decrease in the diffraction intensity, which may suggest a loss of order within collagen fibrillar structure (Figure 6.4).

After obtaining these results, the UV dose was increased and tendons were treated for up to 47 hours in the hydrated state and up to 72 hours in the dry state. SAXS measurements conducted on tendons UV-irradiated in the hydrated state showed a decrease in the axial periodicity after 6 hours of treatment. This was accompanied by an increase in the I2/I3 ratio, which provides information about the electron density distribution (Figure 6.9). A statistical analysis of the relationship of these two parameters showed that there is a statistically significant negative correlation between them ($p<0.05$); however, the correlation was only significant for parameters obtained in Experiment 1 (i.e. hydrated tendons, long time exposure). A decrease in the axial periodicity that is accompanied by an increase in the I2/I3 ratio is observed during drying of collagen (see section 1.3.3). During drying, the removal of water results in an increase of the overlap region and a decrease in the gap region (Tomlin and Worthington, 1956; Chandross and Bear, 1973). This process leads to an alteration in the electron density distribution along the collagen fibril, and therefore changes in the diffraction orders intensities on the scattering pattern. However, in these experiments, tendons were kept

hydrated during UV irradiation and SAXS measurements so it is unlikely that the rearrangements result from the removal of water.

The FTIR measurements showed that there were no changes in the position of any of the analyzed bands (Amide I, Amide II and Amide A) after UV irradiation of tendons. This indicates that there is no alteration in the steric forces around the measured bonds and hence, there are no observable conformational changes in the collagen triple helix. Although the variation of the amide peak intensities was observed, it was not correlated with the increase of the UV dose. It should be noted that the amide bands have a complex contour and their intensity depends on the contributions of many overlapping component bands (Gonzalez and Wess, 2008). Therefore, in this study, the variation of the peak intensities was not taken into account when analysing the FTIR spectra.

6.5.2. Irradiation in the dry state

A decrease in the axial periodicity was also observed in tendons UV irradiated in the dry state (Figure 6.14). However, in this case, it was not accompanied by a change in the electron density distribution (represented as the I2/I3 ratio – see Figure 6.12). A decrease in the axial periodicity of collagen could be explained by a shortening of the collagen helix pitch (a reduction in the axial rise per amino acid residue – see section 1.3.1). If that was the underlying mechanism, then a change in the axial rise per residue would result in a shift of the corresponding peak on the wide-angle X-ray diffraction pattern. This, however, is not observed (section 6.4.2, Figure 6.14).

The FTIR measurements of tendons UV-irradiated in a dry state showed that the position of the Amide A (amide N–H stretching) and II (amide N–H bending and C–N stretching) bands

is shifted to the regions of lower wavenumber. This was accompanied by a movement of the Amide I band (amide C=O stretching) to the higher wavenumber (Table 6.1). Previous studies on the effects of UV light on collagen showed that the irradiation results in a shift of all three amide bands (Amide I, II and A) to the lower wavenumber (Kaminska and Sionkowska, 1995; Torikai and Shibata, 1999; Sionkowska, 2006). This shift was suggested to be due to the destruction of the hydrogen bonds and indicates the partial destruction of the collagen triple helical structure into the less ordered structure of a random coil. However, these studies were performed using dried collagen films and it has been suggested that the film preparation may induce some changes in the collagen structure (Kaminska and Sionkowska, 1995). It can be seen that the results presented here differ from these reported for the collagen films.

The position of the Amide I peak is observed to shift to a higher wavenumber (Table 6.1). A negative shift would indicate that a conformational change occurred within the triple helix structure and as a result the vibrational energy of the C=O bond is increased. This can be caused by the unfolding of the collagen triple helix and a change in the steric forces around the C=O bond (Yakimets et al., 2005; Gonzalez and Wess, 2008). Consequently, the shift of the Amide I band to the higher wavenumber can indicate a shortening of the triple helix, which would restrict the vibrations of the bond. This conformational change, observed here in the UV irradiated tendons can be linked to the crosslinks that are induced by UV light. This crosslinking would be formed inside the collagen helix, as proposed by (Sudoh and Noda, 1972; Menter et al., 1995a).

The amide II absorption band is highly dependent on the hydration and it has been reported to shift to the higher wavenumber upon gelatinization (Yakimets et al., 2005; Gonzalez and

Wess, 2008). Therefore, it can be suggested that the negative shift observed here is related to the increased tightening of the collagen triple helix.

The amide A absorption banding has been linked to the strength of the hydrogen bonds within the collagen triple helix and the upward shift of this band was reported in the thermally denaturated collagen (Liu et al., 1994). The shift to the lower wavenumber observed in the UV irradiated tendons (Table 6.1) would suggest that the hydrogen bonds are stronger in the treated samples.

The decrease in the D periodicity measured using SAXS and the changes in the positions of the Amide I, Amide II and Amide A absorptions from the FTIR spectra, that were observed upon UV irradiation, indicate that the conformational changes occurred within the collagen molecular structure. A negative shift of the Amide A and Amide II bands and the positive shift of the Amide I band indicate tightening of the collagen helix which can be caused by crosslinking induced by the UV light. The crosslinking would occur at the molecular level of the collagen structure.

6.5.3. A novel 20 nm periodicity

Apart from changes in the axial periodicity and diffraction intensities, another effect observed on the SAXS pattern after UV irradiation of hydrated rat tail tendons was the appearance of a new reflection in samples irradiated for 18-24 hours (Figure 6.6). This observation suggests the formation of a new 20 nm periodicity. It may be that UV-irradiation altered the collagen structure and a new structure was formed with a 20 nm axial periodicity. Similar reduction in the D-period was reported in a previous study, where it was induced by a dehydrothermal treatment, which is another method of inducing crosslinks into collagen. In that study, using

electron microscopy, the banding periodicity of collagen fibrils was found to be reduced by 50 % (Gorham et al., 1992). Fibrils with a similar, reduced banding repeat of approximately 22-23 nm were also observed in the embryonic tissues and in the proximal zone of the predentin from rat incisors, indicating that these unusual fibrils may represent the early stages of collagen formation (Randall et al., 1952; Beniash et al., 2000). The molecular structure of such fibrils is not clear and models proposed to explain it include a 1/3 D displacement of adjacent collagen molecules and binding of ions or macromolecules to the collagen (Beniash et al., 2000; Venturoni et al., 2003). The first explanation seems unlikely, since previous studies reported only very small displacements of collagen molecules, which were induced by strong forces: e.g. tissue elongation resulted in an increase in D-periodicity from 67 to 68.3 nm (Mosler et al., 1985); detailed information about this mechanism was provided in section 1.3.4 (relative slippage).

Another explanation for a new periodicity can be local alterations along collagen fibres, e.g. local unfolding of the collagen structure that occurs every 20 nm. Disorganization of collagen molecules and formation of local gelatine-like structure, at the points where chain scission occurred, has been suggested before (Bailey et al., 1964; Sudoh and Noda, 1972; Miles et al., 2000). Miles et al suggested that chain scissions occur randomly along the collagen molecule (Miles et al., 2000); however, it could be possible that initially, only specific regions of the collagen molecule become unfolded giving rise to a new 20 nm periodicity.

6.5.4. UV irradiation of skin

The irradiation of skin using UV light did not produce changes on the diffraction pattern (Figure 6.13). One explanation for this result could be limited penetration of the UV light of

λ=254 nm. The thickness of the skin samples was in the range of a few millimetres; it can be therefore assumed, that even though collagen molecules placed near the skin surface were affected by UV light, the majority of molecules in the samples remained unchanged. When X-rays pass through the tissue, they interact with many collagen fibres and the generated diffraction pattern provides average values from all fibres within the sample. It can be therefore concluded that to describe the effects of UV light on a thick tissue samples (i.e. skin) other techniques should be used, such as microfocus X-ray diffraction, which can provide information from thin sections of the biological samples. This technique uses intense X-ray beams of a micron size, which can be used to map thin sections of biological tissues and has been previously used for mapping the nanostructure in bones (Wess et al., 2001), eggshells (Lammie, Bain and Wess, 2005) and historical parchment (Kennedy et al., 2004). In case of the UV irradiated skin samples, it can prove useful for the analysis of changes in the collagen molecular structure in small sections – from the outer layer (the most exposed to the UV light) to the deeper sections, where UV penetration is much poorer.

6.6. Conclusions

The study showed that UV irradiation of up to 6 hours had little effect on rat tail tendons. Longer irradiation resulted in molecular changes and the effects were different depending on the environment in which the tendons were irradiated (i.e. in a hydrated or a dry state).

The results obtained from SAXS, WAXS and FTIR measurements indicate that UV light induces crosslinks in collagen structure; however, the nature of these newly formed crosslinks depends on the level of hydration of collagen. The FTIR measurements showed that in tendons UV irradiated in the dry state there are conformational changes in the collagen

triple helix. Together with the observed decrease in the axial periodicity it can be suggested that the crosslinks are induced in the collagen structure on the molecular level. During drying, the 3rd and 4th phases of water are removed from the collagen structure. These phases correspond to the free and transition water fractions (Bigi et al., 1987). It can be suggested that when the two water fractions are removed, collagen molecules are moved closer together, therefore there are more chances that intermolecular crosslinking occurs.

The results from FTIR measurements of tendons irradiated in the hydrated state indicate that there are no conformational changes upon UV light treatment. However, the irradiated tendons did not dissolve in acetic acid, which indicates that new crosslinks have formed. It can therefore be suggested that when water is present in the collagen structure, crosslinks are also formed, however, not on a molecular level but perhaps between collagen fibrils. It was also observed that the diffraction intensity was decreased in the tendons irradiated in a hydrated state, suggesting that there is a loss of order within the collagen structure. The degradation was also observed in UV irradiated tendons using EM (Figure 6.16). It can be therefore concluded that when water is present in collagen, crosslinks are formed on a different level than when water is removed; also, the presence of water during UV treatment is connected with partial degradation of collagen structure.

7. The effects of tissue extension on lateral packing of fibrillin-rich microfibrils

7.1. Introduction

Previous Result Chapters (Four – Six) have shown studies designed to monitor alterations induced by various external factors into the molecular structure of collagen. Since it is the most abundant protein in the animal body, collagen is often used as a model tissue to study fibrous proteins, and also in biomaterial production. It was therefore the main protein used in the studies described here. The second fibrous protein, used in the experiments presented in this thesis, fibrillin, is a more specific example of a biological polymer. It is usually found in elastin-containing tissues where it provides a structural lattice for elastin deposition. However, it can also be found in a pure form (i.e. without elastin) in zonular filaments (see section 1.1.2.1). Zonular filaments were therefore used as a source of fibrillin in the study presented here. These structures play a crucial role in the suspensory system of the lens and their elastic properties are important for accurate lens accommodation. The aim of this study was to understand the elastic response of fibrillin and in order to achieve this, hydrated fibrillin microbirils from zonular filament were subjected to a controlled tissue extension. A series of X-ray diffraction measurements were taken during tissue stretching to observe alterations in lateral packing of the microfibrils. Computer generated simulated patterns were used to fit the experimental X-ray scattering data and obtain the fibril diameter and lateral distance between the fibrils. The study described in this chapter has been conducted to give an insight into the molecular structure of microfibrils in intact tissue and it has major

implications for understanding the functionality and extensibility of fibrillin in connective tissues.

7.2. Models of fibrillin organization

The structure of microfibrils and their main component, fibrillin, has been described in Chapter 1. Since the arrangement of fibrillin monomers within microfibrils is still poorly understood, there have been several models proposed to explain its molecular organization (Figure 7.1). A 'folding/pleating model' proposes a head-to-toe parallel alignment of fibrillin monomers where molecules are highly folded and form characteristic beads (Figure 7.1a). This model was supported by an immunolocalization study which showed that monoclonal antibodies bind only once per bead period implying the presence of only one fibrillin molecule in a microfibril repeat (Reinhardt et al., 1996). Scanning transmission electron microscopy (STEM) mass distribution analysis of microfibrils revealed repeated minima and maxima which corresponded to the bead and interbead regions and it was suggested that the complex folding of molecules within the beads is responsible for the observed mass maximum. Another possibility was an interaction of other components that can be periodically attached to microfibrils and form observed asymmetric axial mass distribution (Sherratt et al., 1997). A combined study presented by Baldock et al showed a detailed explanation of the 'folded model' where it was proposed that a complex molecular folding of 160 nm fibrillin molecules allows reversible extension (Baldock et al., 2001). This packing arrangement could explain the appearance of different periodicities observed in extended fibrils and is believed to be the basis of fibrillin-rich microfibrils elasticity (Keene et al., 1991; Baldock et al., 2001; Sherratt et al., 2003). The molecular folded model was also

supported by a detailed analysis of the theoretical axial mass distribution (TAMD), where profiles calculated for the folded alignment fitted the observed microfibril mass maps (Kielty et al., 2005).

Another model suggested a staggered arrangement of individual molecules. In this arrangement it is possible that unfolded fibrillin monomers span over two or three interbead regions (Figure 7.1b and c). The model was supported by the results from nuclear magnetic resonance (NMR) study of the fibrillin-1 structure that implied parallel arrangement of extended monomers that contribute to two interbead regions with 50% overlap (Downing et al., 1996). It was also suggested that unfolded fibrillin molecules are aligned with a 12 nm overlap between successive molecules and a 1/3 stagger that would produce the observed 56 nm periodicity. Domain linker extensibility was suggested to be a basis of the elastic properties (Lee et al., 2004). However, it was noted that the flexibility of this site could not account for the extensions observed in microfibrils with 160 nm periodicity and the theoretical axial distribution calculated for this model was not in agreement with the observed mass profile (Kielty et al., 2005).

In a more recent study, recombinant overlapping fragments of fibrillin-1 were analyzed using solution small-angle X-ray scattering (SAXS) to provide detailed information on the shape of the domains and their organization in physiological conditions. The data from that study supported the folding model and provided a detailed compact arrangement of the fibrillin domains (Baldock et al., 2006). In comparison, another study based on EM and antibody binding analysis of extracted and digested microfibrils supported a staggered model with the C-terminal halves of the fibrillin molecule composing the core and N-terminal halves situated outside of the microfibril (Kuo et al., 2007). Figure 7.1 shows a schematic representation of the 'folded' and the 'staggered' model of fibrillin organization.

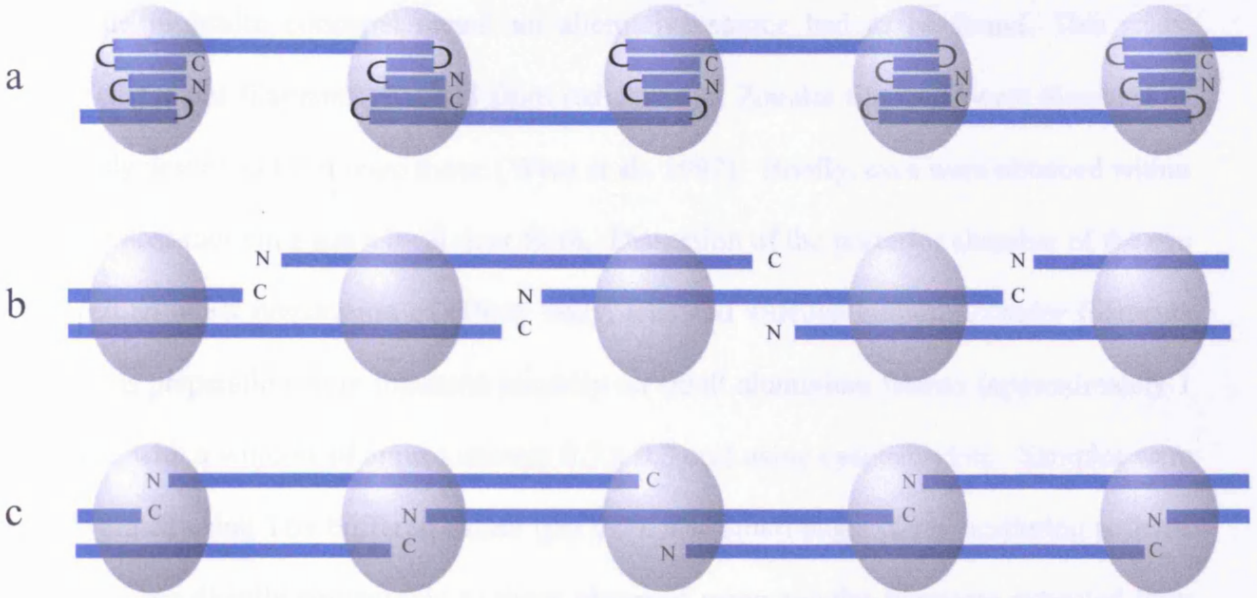

Figure 7.1. Models proposed for the organization of fibrillin molecules within microfibrils. In the 'folding/pleating' model fibrillin monomers are highly folded (a) while in the 'staggered' model unfolded molecules can span over two (b) or three (c) bead domains.

The fundamental packing models proposed are not interconvertible and are mutually incompatible. The study of the molecular packing within an intact tissue can help to discriminate between models since the molecular rearrangements required to impart the elastic response will reflect in changes in the electron density profile.

7.3. Material and methods

7.3.1. Sample preparation

Initial studies of mammalian zonular filaments were conducted using bovine ocular tissue (Wess et al., 19971998). Restrictions on the availability of bovine nervous tissue in recent

times due to health concerns meant an alternative source had to be found. This study examined zonular filaments obtained from red deer eye. Zonular filaments were dissected as previously described for bovine tissue (Wess et al., 1997). Briefly, eyes were obtained within 24 hours post-mortem from a local deer farm. Dissection of the posterior chamber of the eye produced an intact preparation of ciliary body, lens and vitreous humor. Zonular filaments within this preparation were mounted securely on small aluminium frames (approximately 1 x 0.5 cm, with a window of approximately 0.7 x 0.3 cm) using cyanoacrylate. Samples were kept hydrated using Tris buffered saline (pH 7.2). The small-angle X-ray scattering patterns obtained were directly comparable to those observed using zonular filaments extracted from both bovine and ovine eye. Most notably, the results demonstrate the existence of a periodic structure, indexing on an axial periodicity of 56.2 nm and a lateral spacing of 32.8 nm in the resting state.

7.3.2. Small-angle X-ray scattering

Small-angle X-ray scattering of zonular filaments was carried out on ID02 at the European Synchrotron Radiation Facility, Grenoble, France, using a 5 m sample to detector distance. Images were collected over 0.5 seconds on a Thomson X-ray Intensifier (TH 49-427) lens coupled to a FReLoN CCD camera (2048 x 2048 pixels). This detector has an active area of size 180 mm and a frame rate of 14 images (1024 x 1024 pixels) per second with a 14 bit nominal dynamic range. The wavelength of X-rays used was 0.1 nm. Each sample was covered on either side by (30 μm thick) mica sheets and maintained in a hydrated state using Tris buffered saline (pH 7.2) during data collection. The tissue was mounted on a mechanical stretching rig which allowed controlled tissue extension and the application of predetermined

stresses on the system. Images were obtained of tissue in the native, resting state and during extension up to 270 % of the original rest length.

7.3.3. X-ray data analysis

X-ray diffraction data were analyzed using CCP13 FibreFix software (Rajkumar et al., 2005). Two-dimensional images were converted into linear plots and calibrated using rat tail tendon standard of known 1/67 nm^{-1} meridional spacing. A typical diffraction image consists of meridional peaks that correspond to characteristic axial periodicity of fibrillin, and equatorial reflections that contain information about interfibrillar spacing and fibril diameter (Figure 7.2(a)). The analysis of the collected data is shown in Figure 7.3.

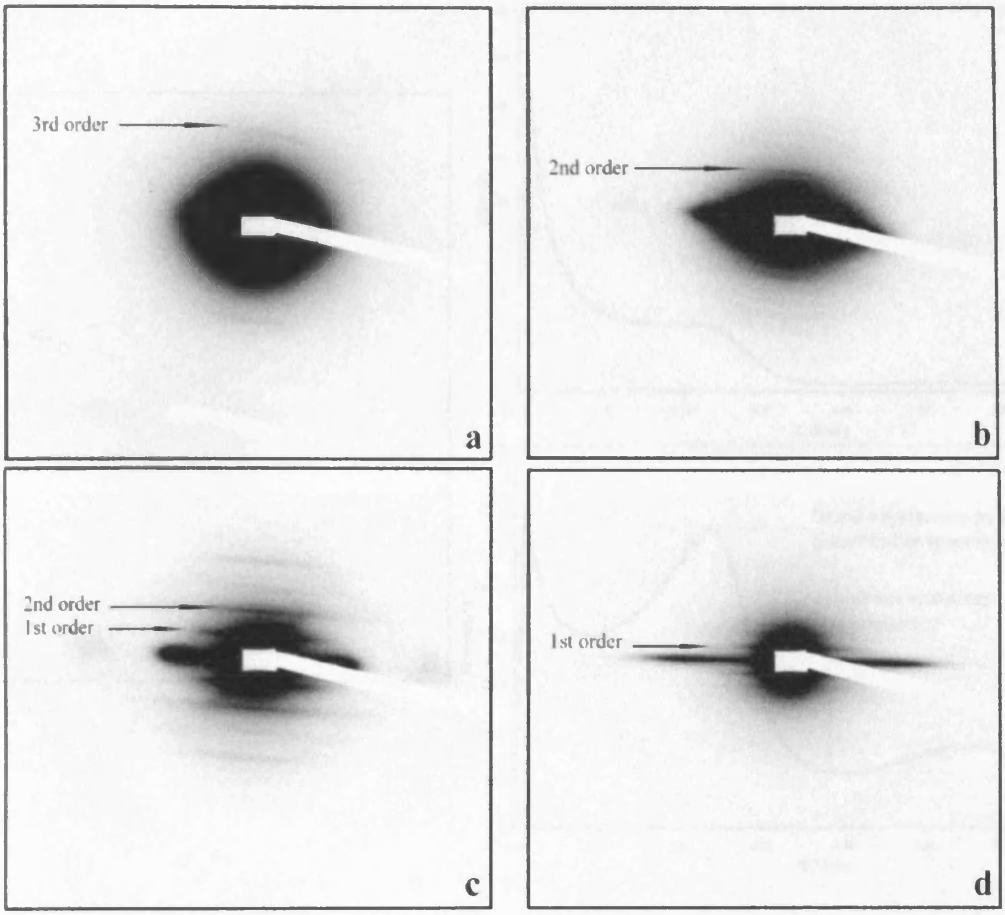

Figure 7.2. Diffraction images of fibrillin-rich microfibrils from zonular filaments in the native state (a) and following tissue extension b: 100%, c: 200%, d: 270%. Images were collected on beamline ID02 at the European Synchrotron Radiation Facility, Grenoble, France. A 5m sample to detector distance was used which made it possible to see low-angle meridional and equatorial reflections that contain information about axial and lateral packing of microfibrils. Arrows indicate the position of the meridional diffraction orders which can be seen to shift towards smaller angles in (d) and indicates an increase in the axial periodicity.

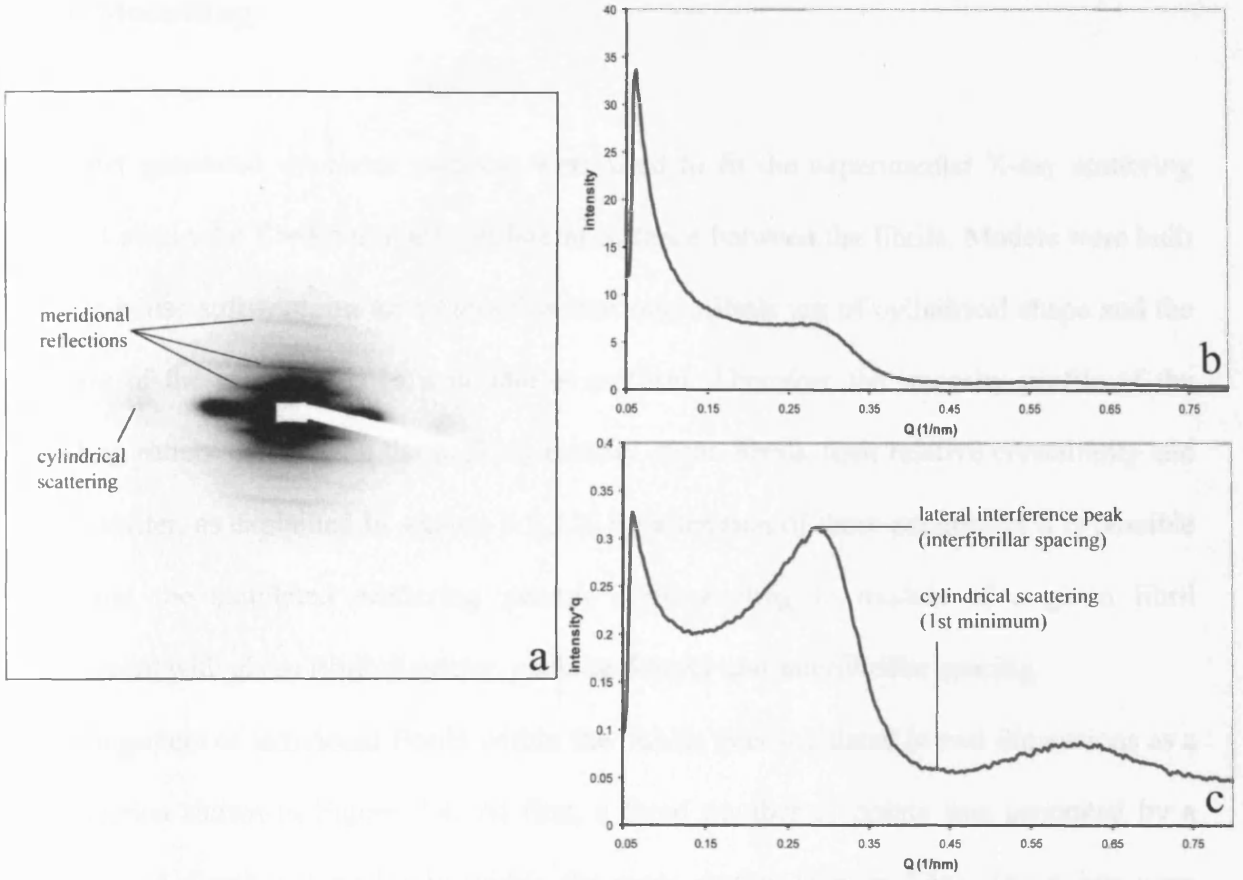

Figure 7.3. The analysis of an equatorial pattern from small-angle X-ray scattering images. (a): two-dimensional diffraction image collected at the beamline where meridional peaks and equatorial reflections can be observed; an integrated scan produced using FibreFix software is converted into a one-dimensional linear profile of scattering intensity against Q (Q = $4\pi\sin\theta/\lambda$) (b). Further numerical analysis involves multiplication of the intensity at each point of the linear data set by its distance from the centre. This results in a plot (c) where both lateral interference and cylindrical scattering peaks can be easily distinguished. The position of the interference peak is used to estimate spacing between microfibrils whilst the position of the 1st minimum of cylindrical scattering gives information about fibril diameter.

7.3.4. Modelling

Computer generated simulated patterns were used to fit the experimental X-ray scattering data and obtain the fibril diameter and lateral distance between the fibrils. Models were built using in-house software, on an assumption that microfibrils are of cylindrical shape and the diameter of the microfibrils in a bundle is uniform. Therefore the intensity profile of the scattering pattern depends on the packing density of the fibrils, their relative crystallinity and their diameter, as explained in section 3.1.3.2. By alteration of these parameters it is possible to control the simulated scattering pattern corresponding to models of a given fibril arrangement with given fibril diameter, packing density and interfibrillar spacing.

An arrangement of individual fibrils within the bundle was simulated in two dimensions as a cross section shown in Figure 7.4. At first, a fixed number of points was generated by a program and distributed randomly within the cross section (Figure 7.4a). The points were then moved in random directions using a series of Lennard-Jones potentials with specific interaction distances (see section 3.1.3.4). The result is shown in Figure 7.4b.

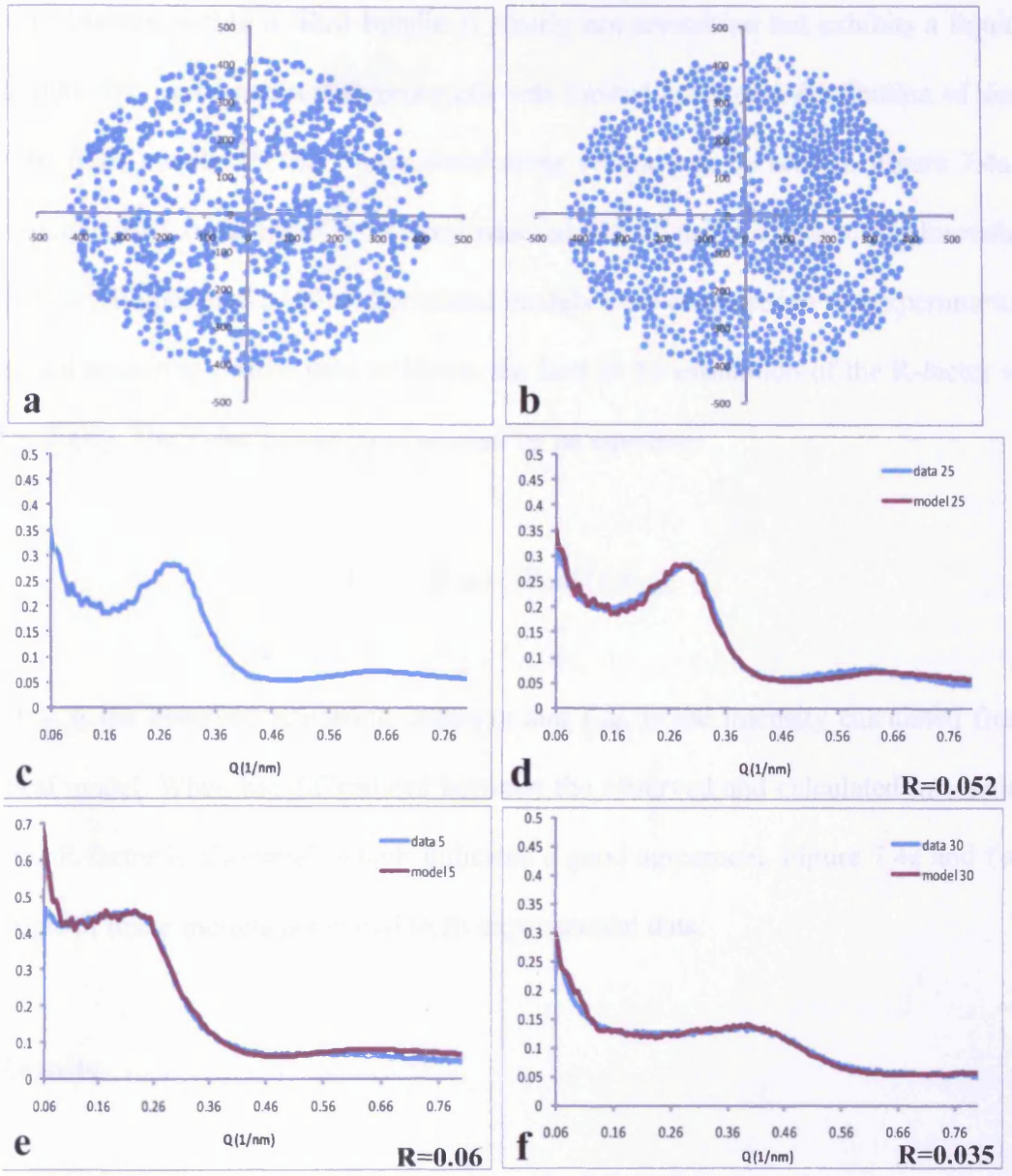

Figure 7.4. Modelling of the experimental data (a): a generated cross section of a fibril bundle – circles correspond to the microfibrils with uniform diameter and are distributed randomly within the bundle. Fibrils were randomly chosen and moved in a random direction resulting in (b). The change in the potential energy was calculated as described by (Hulmes et al., 1995). (c) shows a corresponding scattering pattern calculated using Fourier transformation. The theoretical profile was then compared to the experimental data (d). (e, f): two examples of theoretical (red lines) and observed (blue lines) scattering patterns that correspond to the fibril arrangement at ~30 % and 270 % tissue extension respectively. The R-factor values are shown on the graphs.

Since the structure within a fibril bundle is clearly not crystalline but exhibits a liquid like organization, the use of interaction potentials was limited to allow a distribution of disorder within the fibril bundle. A two dimensional cross section can be seen in Figure 7.4a. The scattering intensity from these structures was calculated using Fourier transformation as described by (Hulmes et al., 1995). Generated models were compared to the experimental one dimensional scattering profile data to obtain the best fit by estimation of the R-factor values (Rhodes, 2000). The R-factor can be expressed by an equation:

$$R = \Sigma \mid |F_{obs}| - |F_{calc}| \mid / |F_{obs}|$$

where F_{obs} is the observed scattering intensity and F_{calc} is the intensity calculated from the theoretical model. When the differences between the observed and calculated intensities are small, the R-factor is also small which indicates a good agreement. Figure 7.4e and f shows an example of linear models generated to fit experimental data.

7.4. Results

Small-angle X-ray scattering of rest length explanted zonular filaments revealed a series of meridional diffraction peaks that were truncated after the 8^{th} order and exhibit dominant 3^{rd} and 6^{th} orders. This is consistent with the presence of a regular array of microfibrils with a relative stagger of 56/3-nm, and indicates a higher level of order in microfibrillar assembly (Wess et al., 1998; Haston et al., 2003). The images obtained following tissue extension of deer eye zonular filaments are shown in Figure 7.2. Figure 7.2 (a) shows the scattering pattern of the tissue at the normal resting length, while images (b)-(d) correspond to the

pattern of the tissue in a series of extended states. Analysis of the data indicated that the microfibrils have a diameter of approximately 20.1 (+/- 0.6) nm and exhibit a lateral spacing of 32.8 (+/- 0.8) nm in the resting state. Both the equatorial and meridional peaks were spread over a range of 20 +/- 5 degrees in the resting state, indicating misalignment of the microfibrils within the tissue.

7.4.1. Changes in lateral packing

Figure 7.5 shows linear profiles of the integrated equatorial X-ray scattering intensity. The scattering curve can be described as resulting from the scattering of a cylinder i.e. it approximates to a Bessel function of the first kind which is sampled by an interference function due to the lateral packing of the cylinders in a liquid like manner. The position of the lateral molecular interference peak provides information about the packing distance between microfibrils. It can be seen that tissue extension causes a shift of the peak to a higher angle. This corresponds to a decrease in the interfibrillar spacing and indicates that fibrils have moved closer together. Changes were also observed in the position and shape of the linear scattering profile which is produced by the uniform diameter of the microfibrils. The presence of distinct minima in the scattering profile indicates that the distribution of fibril diameters is negligible for this system. The position of the first minimum of the scattering curve (corresponding to the Bessel function first minima – see Figure 7.5) can be used to estimate the microfibril diameter and it has been explained in Chapter 3 (section 3.1.3.2). During tissue extension the position of the minima in the scattering function was observed to move towards higher angles, this indicates a decrease of the microfibrillar diameter with strain. Calculated lateral spacing and microfibrillar diameter are detailed in Table 7.1. The

average distance between microfibrils changed from the initial value of 32.8 nm (+/- 0.8) observed in the resting state to 20.6 nm (+/- 0.6) at the 100 % extension and then further decreased down to 16.1 nm (+/- 0.4) when a 270 % macroscopic extension was applied. This was accompanied by alterations in microfibrillar diameter which were observed to decrease from 20.1 nm (+/- 0.6) down to 12.7 nm (+/- 0.2) at the 270 % extension. The significance of these changes is discussed in more detail below.

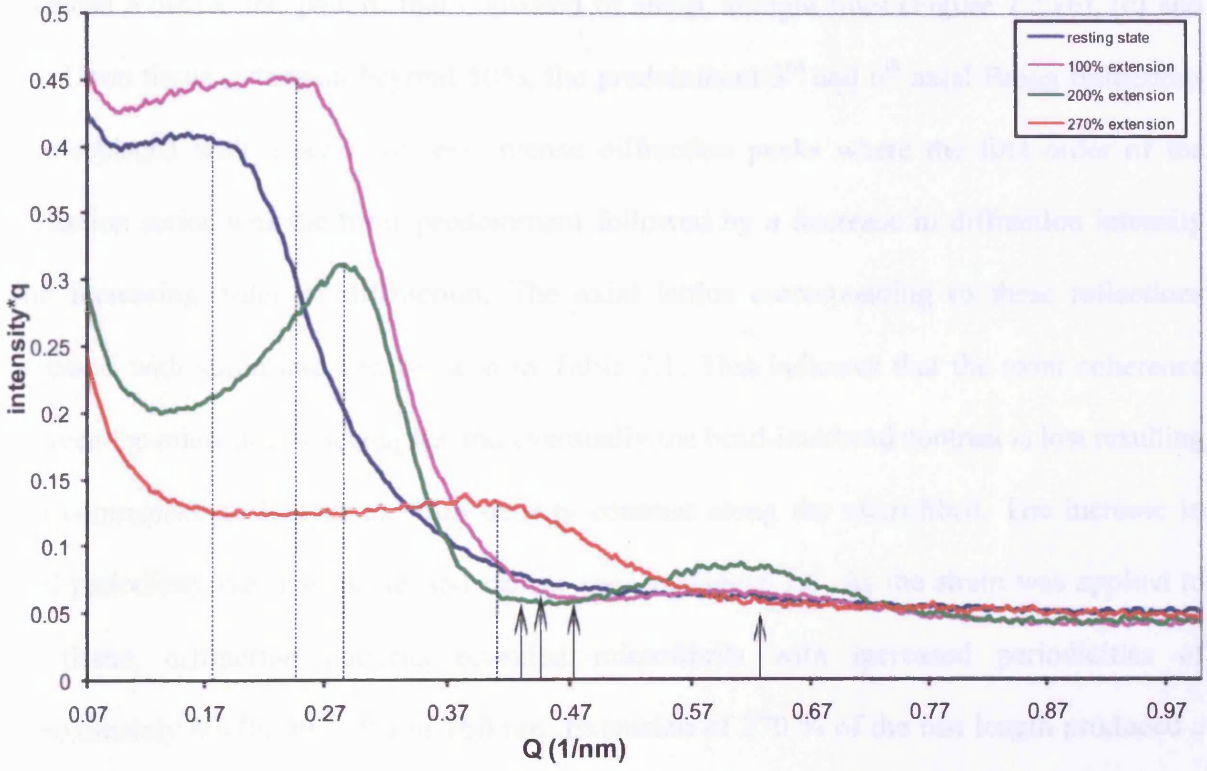

Figure 7.5. Linear traces of the integrated low-angle equatorial pattern, converted from two-dimensional diffraction images. A shift of the interference function peak can be observed towards higher angles which suggests a decrease in lateral spacing following tissue extension (dotted lines mark the position of the peak). Also, the 1st minimum of cylindrical scattering has moved indicating a gradual decrease in fibril diameter (arrows indicate the minimum).

7.4.2. Changes in axial structure

Figures 7.2 (b), (c) and (d) were obtained following the application of increasing strains to the tissue. Mis-orientation of the microfibrils in the resting tissue produces a diffraction pattern that consists of rings or arced reflections, as can be observed in Figure 7.2 (a). Application of strain resulted in an arrangement where microfibrils become more aligned and produced a diffraction pattern that consisted of sharp, straight lines (Figure 7.2 (b), (c) and (d)). Upon tissue extension beyond 50%, the predominant 3^{rd} and 6^{th} axial Bragg reflections were replaced with a series of less intense diffraction peaks where the first order of the diffraction series was the most predominant followed by a decrease in diffraction intensity with increasing order of diffraction. The axial lattice corresponding to these reflections increased with strain and can be seen in Table 7.1. This indicates that the axial coherence between the microfibrils decouples and eventually the bead-interbead contrast is lost resulting in a commensurate loss in electron density contrast along the microfibril. The increase in axial periodicity was non-linear and can be seen in Figure 7.6. As the strain was applied to the tissue, diffraction patterns revealed microfibrils with increased periodicities of approximately 60-70, 90-100 and 160 nm. Extension of 270 % of the rest length produced a periodicity of 160 nm, a value that was not previously observed using X-ray diffraction; extension beyond this level led to tissue failure.

group	n	periodicity (nm)	SE	interfibrillar spacing (nm)	SE	fibril diameter (nm)	SE
55-57	12	56.2	0.2	32.8	0.8	20.1	0.6
60-70	10	65.5	1.1	25.9	0.6	18.3	0.6
90-100	4	100.3	2.9	20.6	0.6	16.9	0.7
~160	2	161.5	4.4	16.1	0.4	12.7	0.2

Table 7.1. Values of lateral spacing, axial periodicity and fibril diameter for microfibrils during tissue extension. The observed structures can be divided into four groups: fibrils with an axial periodicity of 55-57 nm (resting state), 60-70 nm, 90-100 nm and ~160 nm. The data shown here were collected during several independent tissue extension experiments and the standard error values are included for each of the parameters.

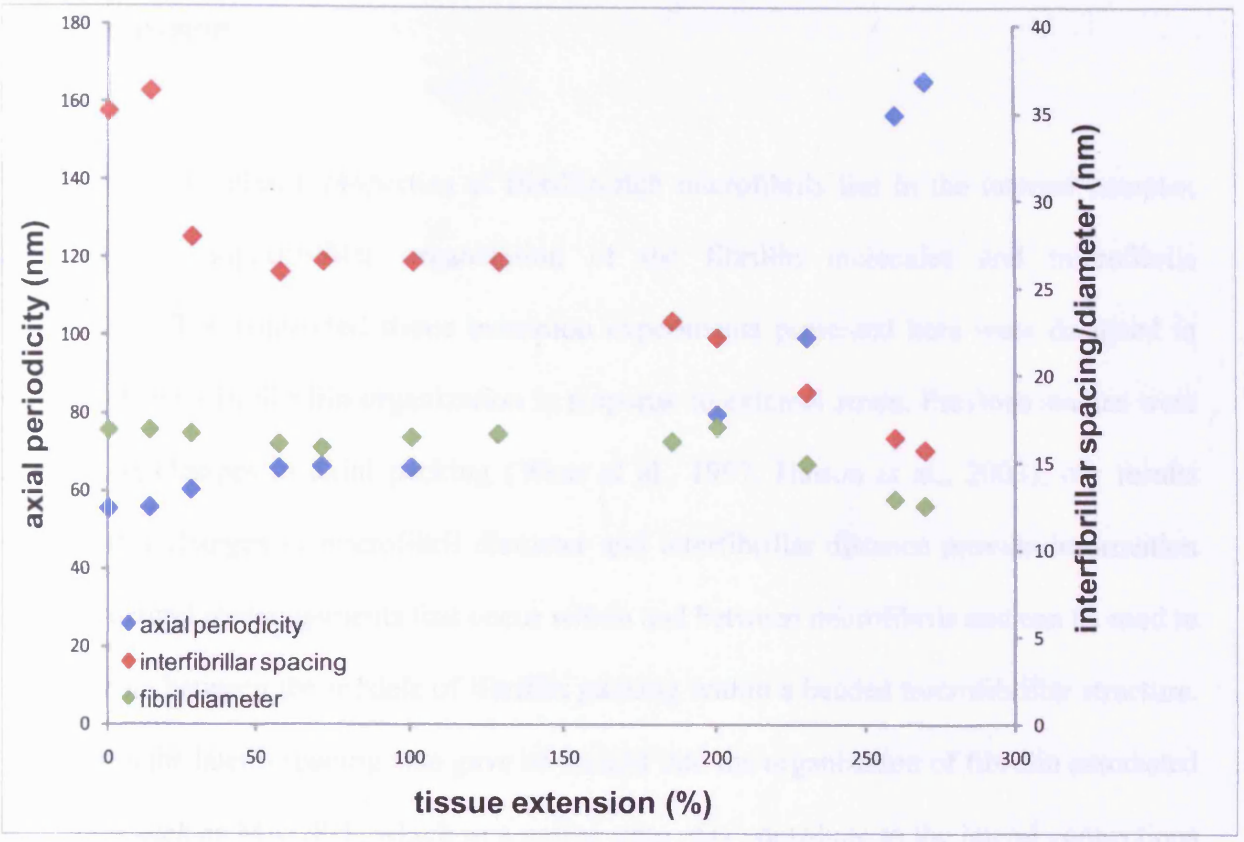

Figure 7.6. Variation of the axial periodicity, interfibrillar spacing and fibril diameter following tissue extension. The graph shows a non linear increase in periodicity during the extension which is accompanied by a decrease in the spacing between microfibrils. The axial periodicity gradually increases which is accompanied by a decrease in the average distance between microfibrils.

7.5. Discussion

The basis of the elastic properties of fibrillin-rich microfibrils lies in the internal complex structure and suprafibrillar organization of the fibrillin molecules and microfibrils respectively. The controlled tissue extension experiments presented here were designed to observe changes in fibrillin organization in response to external strain. Previous studies were focused on changes in axial packing (Wess et al., 1997; Haston et al., 2003); our results showed that changes in microfibril diameter and interfibrillar distance provide information about structural rearrangements that occur within and between microfibrils and can be used to discriminate between the models of fibrillin packing within a beaded microfibrillar structure. Changes in the lateral spacing also gave an insight into the organization of fibrillin associated molecules such as MAGP-1, which in a native state may contribute to the lateral connections between microfibrils (Gibson et al., 1996; Davis et al., 2002).

Previous studies on mechanical testing of mammalian zonular filaments indicated that the application of relatively low strains produces only minor changes in the fundamental axial periodicity of the microfibrils and that this process is fully reversible (Wess et al., 19971998). Tissue extension of up to 50 % revealed no apparent difference in the local three dimensional organisation within the microfibrils, as observed from the diffraction pattern and rearrangements were restricted to the realignment of microfibril bundles within the tissue. In contrast, the application of increasing forces resulted in a corresponding increase in the fundamental axial periodicity of individual microfibrils. Macroscopic tissue extension to 100 % of the rest length produced a fundamental axial periodicity of approximately 80 nm, whereas further extension to 150 % resulted in a periodicity of 100 nm (Wess et al., 1998; Haston et al., 2003). These correspond to microfibrillar metastable states which were

observed by electron microscopy and may reflect sequential molecular unfolding (Baldock et al., 2001). In the study presented here diffraction images were collected during tissue extension of up to 270 % which allowed a structure that is suggested to be a completely unfolded metastable state to be recorded. It should be noted that during full lens accommodation the ciliary body radius was observed to decrease by 0.3607 mm (for the 29-year old eye) (Burd, Judge and Flavell, 1999) and zonules were extended only by 3.4 % of the rest length (Sherratt et al., 2003). It is apparent that the applied strain used during mechanical testing greatly exceeds physiological extensions. However, the tensile state of the zonules in the unaccommodated eye is still unknown. It is possible that zonules in the physiological resting state do not have 56 nm periodicity observed in the explanted tissue, but they might be in one of the metastable states observed during mechanical stretching studies (e.g. with 80 or 100 nm periodicity). Therefore, to understand the underlying process, it is important to monitor the elastic response of fibrillin during the extension until tissue failure.

The diffraction experiments conducted here showed that the extension behaviour of all microfibrils bathed by the X-ray beam are generally identical. This points to a highly concerted behaviour of the microfibrillar interactions throughout a tissue and the basis for the connectivity between microfibrils and bundles of microfibrils deserves attention. It is also apparent that the macroscopic elasticity of a tissue requires interactions at the suprafibrillar level that cannot be measured by examining the properties of individual fibrils. The importance of the suprafibrillar arrangements was highlighted by Sherratt et al (Sherratt et al., 2003), where authors showed possible models of fibrillar bundle movements and their contributions to the elastic response. Furthermore the relationship of fibrillin-rich microfibrils with associated molecules may be a key to the interfibrillar interactions and these are lost on microfibrillar isolation. In the study presented here a non-invasive technique was used that

allows the study of proteins in their native state to give a further insight into their functionality and extensibility in connective tissues and to validate existing models of molecular organization of fibrillin within microfibrils.

Following tissue extension, a number of changes in supramolecular structure occurred as observed by small angle X-ray scattering. An increase in the fundamental axial periodicity of fibrillin-rich microfibrils following the application of strain to the tissue was previously documented (Wess et al., 1998; Haston et al., 2003), and can be seen from the images in Figure 7.2. This study was focused on the analysis of the equatorial pattern and corresponding lateral packing. It was observed that in the resting state the average distance between microfibrils was 32.8 nm (+/- 0.8), a value which is greater than the estimated fibril diameter of 20.1 nm (+/- 0.6). This implies that in the hydrated state a distance is maintained between the fibrils which may involve molecules associated with fibrillin. A candidate suggested for those interactions is MAGP-1, a glycoprotein associated with most fibrillin-rich microfibrils. Although it is an elastin-binding protein, it was also found in non-elastin zonular fibrils where it was specifically localized within the beads of the microfibrils (Gibson et al., 1996; Henderson et al., 1996). A recent study using a mass spectroscopy approach showed that MAGP-1 is the only molecule observed in the fundamental microfibrillar structure in addition to fibrillin (Cain et al., 2006). It was suggested that MAGP-1 may play a role in the stabilization of the head-to-tail organization of fibrillin molecules and may also be involved in lateral aggregation of microfibrils (Gibson et al., 1996). A study using quick-freeze deep-etch (QFDE) microscopy revealed a realistic view of the microfibril ultrastructure and showed small lateral filaments connecting microfibrils at regular intervals (Davis et al., 2002). These filaments were suggested to be aggregates of MAGP-1 which play an important role in the lateral organization of microfibrils.

In the present study the distance between microfibrils was reduced from 32.8 nm (+/- 0.8) to 16.1 nm (+/- 0.4) after an extension of 270 %. One explanation of this decrease can be a disruption in the lateral filaments that connect microfibrils. This was accompanied by a decrease in fibril diameter from approximately 20.1 nm (+/- 0.6) observed in the microfibrils in the resting state to 12.7 nm (+/- 0.2) after 270 % macroscopic extension. It is apparent, therefore, that extension of zonular filaments leads to a thinning of the microfibrils and a decrease in the space between them. This may reflect a sequential unfolding of the fibrillin molecules supporting a model of unstaggered fibrillin molecules compressed within the microfibril (Reinhardt et al., 1996; Baldock et al., 2001).

If we assume that each bead contains highly folded N and C termini of the adjacent fibrillin molecules, then applied extension will cause their unfolding. Each unfolding event would result in a decrease in fibril diameter, with a concomitant decrease in axial contrast as the molecule unfolds and the bead like properties and coherent suprafibrillar interactions are lost. The data from mass distribution studies during fibrillin extension suggest that the first unfolding event occurs in the interbead region of the microbril and that the beads unfold at periodicities over ~100 nm (Baldock et al., 2001). The unravelling of the interbead region would not result in a decrease in fibril diameter and in our present study we observed that the fibril diameter is already reduced at ~ 100 nm periodicity (Table 7.1). This may suggest that although the interbead region unfolds first, the unravelling of the bead region occurs earlier as proposed by Baldock et al (Baldock et al., 2001).

The unfolding of the beads may also disrupt associated MAGP-1 molecules, which are specifically associated with each microfibrillar bead (Henderson et al., 1996), and lateral filaments that connect microfibrils. This would allow microfibrils to be placed closer together. A simplified model of these rearrangements is shown in Figure 7.7(B). The

arrangement in a resting state corresponds to the folded model proposed by Baldock et al (Baldock et al., 2001) shown in Figure 7.7(i) and would give rise to the diffraction pattern observed in this study (Figure 7.2(a)). The bead-to-bead distance of 56 nm produces meridional reflections, where the 3rd order is strong due to the axial coherence between microfibrils. The applied strain causes unfolding of the microfibrils into a linear structure shown in Figure 7.7(f) which corresponds to the arrangement proposed by Baldock et al (Baldock et al., 2001) (Figure 7.7(iii)). The axial distance between two fibrillin molecules in this state would be 160 nm (the length of a single molecule) and the corresponding density distribution along the microfibril would produce weak meridional reflections of 160 nm periodicity on the diffraction pattern. This was also observed in this study (Figure 7.2(d)).

The analysis of the alterations induced in both axial and lateral packing by controlled tissue extension showed the appearance of metastable states formed during sequential fibrillin unfolding. These states correspond to concerted changes in molecular unfolding resulting in sequential changes in the microfibril to give axial periodicities of approximately 60-70, 90-100 and 160 nm and that are characterized by a non-linear reduction in fibril diameter and a decrease in interfibrillar spacing.

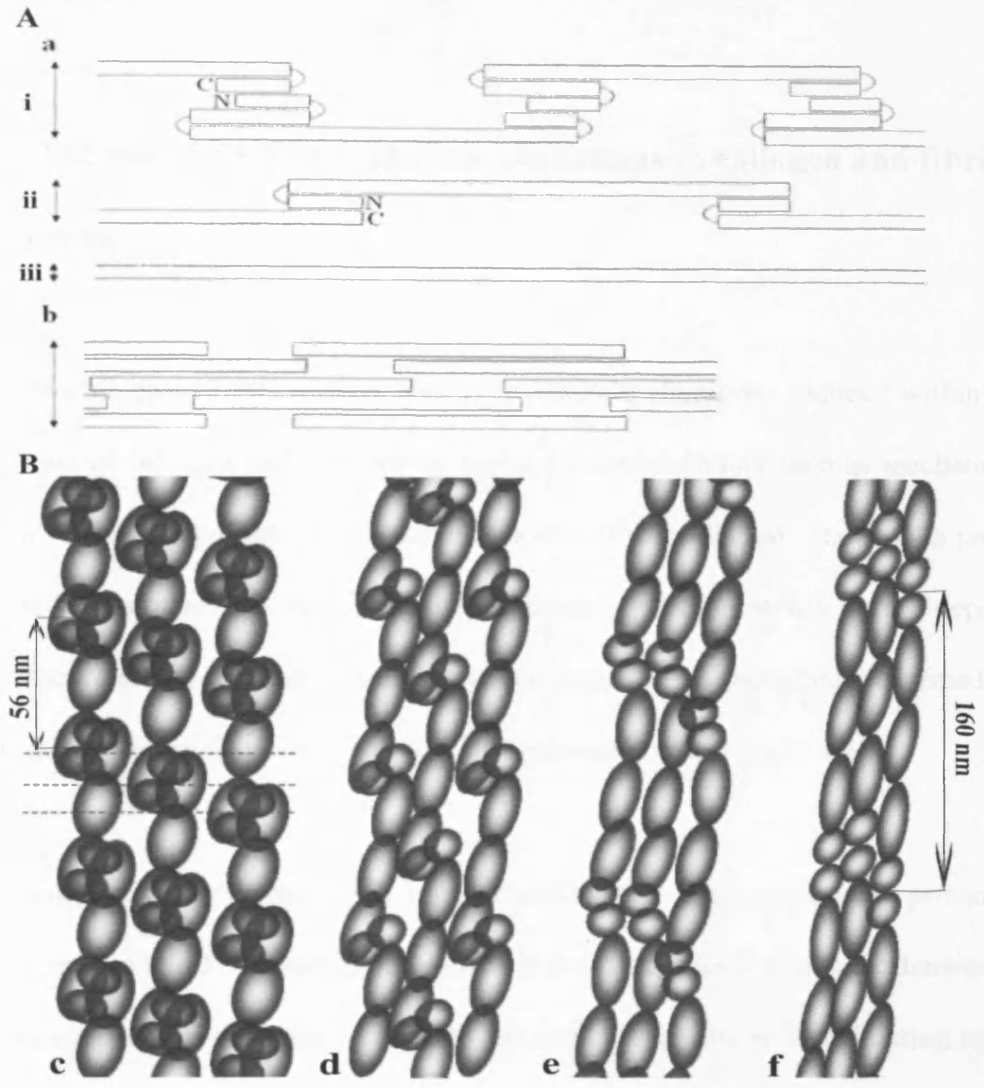

Figure 7.7. A: Two previously proposed models of fibrillin organization: a) in an intermolecular pleating/folding model (Baldock et al., 2001) sequential unfolding of the fibrillin molecules (i-iii) would result in a decrease in fibril diameter; b) in a 1/3 staggered model the basis of the elasticity lies in the extensibility of the domain linker (Lee et al., 2004), hence tissue extension would not cause a significant narrowing of the fibrils. B: A simplified model showing sequential unravelling of fibrillin, following macroscopic tissue extension. In a resting state (c), fibrillin monomers are highly folded within microfibrils. A 1/3 stagger of microfibrils that gives rise to the strong 3rd diffraction order is indicated by dotted lines. The external strain causes unfolding of the fibrillin molecules and therefore a decrease of their diameter (d-f). Unfolded microfibrils are narrower and placed closer together.

8. Conclusions

8.1. The use of SAXS to monitor alterations in collagen and fibrillin structure

The overall goal of this project was to investigate alterations induced within the molecular structure of collagen and fibrillin by various external factors such as mechanical stretching, an intensive X-ray dose, *in-situ* metastasis and UV irradiation. The results presented in this thesis proved that the nature of the molecular rearrangements varies depending on the treatment and that external factors can cause formation of metastable, intermediate structures. The main, previously unobserved findings presented in this thesis are:

- Fibrillin microfibrils with 160 nm periodicity that have never been previously observed using small-angle X-ray scattering, recorded during mechanical tissue extension.
- A novel collagen structure with an 80 nm axial periodicity recorded during an intense X-ray dose irradiation of collagen.
- Broadening of the diffraction peaks which indicates a wide distribution of D-periods within collagen fibrils that have been induced by an intense X-ray dose.
- A novel 20 nm periodic structure formed during UV irradiation of collagen.
- Changes in collagen fibril diameter and interfibrillar distance observed in breast cancer tissues.

Small angle X-ray scattering has proved useful to investigate molecular rearrangements within ordered axial and lateral packing of the two biopolymers. The aim of the studies presented here was to (1) examine different paths of collagen degradation and its transformation into gelatine, (2) examine the rearrangements that occur within fibrillin microfibils structure as a result of induced external strain and (3) to identify and describe intermediate, metastable states that may occur during the process. In order to achieve these objectives, collagen was subjected to various external factors: an intense X-ray dose (experiments described in Chapter Four), an enzymatic treatment (Chapter Five) and UV irradiation (Chapter Six). In addition, breast cancer tissues were analyzed, which provided information about the effects of *in-situ* metastasis on the collagen structure (Chapter Five). Results from the studies described in Chapter Four suggest that an intense X-ray dose causes local movements of water within the collagen structure and results in variations of the fundamental periodicity which have not been reported before. UV light was found to have a different effect on the collagen structure – a novel structure has been reported with an unusual 20 nm periodicity. Another effect of UV irradiation was formation of additional crosslinks, which caused conformational changes in collagen, identified using FTIR spectroscopy. The studies presented here showed that the degradation of collagen is a complex process; various external factors can induce specific rearrangements within the molecular structure of the protein which then results in the formation of novel, metastable states. The importance and benefits gained from the presented studies is discussed in sections 8.2-8.4 below.

In order to examine the effects of the external strain on the second biopolymer, fibrillin, zonular filaments (which contain high levels of fibrillin microfibrils without the presence of elastin and collagen) were subjected to the controlled tissue extension and SAXS

measurements were taken during this process (results presented in Chapter Seven). The aim of this study was to understand the molecular organization of fibrillin and the basis of its elastic properties. The results indicate intrafibrillar and interfibrillar reorganization in the elastic response and their importance is discussed in section 8.5 below.

In the studies presented in this thesis, two important biological polymers, collagen and fibrillin, have been subjected to extreme conditions (e.g. an intense X-ray dose, mechanical stretching up to 270 % of the original resting length). The proteins would not normally be exposed to such extreme treatments in physiological conditions, e.g. it is believed that fibrillin microfibrils are stretched only by 3.4 % of the resting length during full lens accommodation (Burd et al., 1999). However, it is important to examine the response of these proteins since this can lead to the understanding of the underlying molecular transformations, and therefore potentially be used to gain control over the transformation process. In the case of fibrillin it is essential to fully understand the lens accommodation system and explain why a protein with such elastic properties (i.e. ability to stretch up to 270 %) is not used to its full potential within the suspensory system of the lens. If the basis for elasticity can be understood and hence controlled, it has great potential in biomaterial production, e.g. improving properties of existing materials and in designing new materials with controlled biodegradative properties for tissue engineering.

8.2. Dynamic studies using SAXS

Small-angle X-ray scattering is a non-invasive technique that enables the examination of biological tissues under nearly physiological conditions. It also allows dynamic studies to be conducted, which would not be possible using, for example, electron microscopy techniques.

With regard to electron microscopy techniques, samples need to be treated (e.g. dehydrated or fixed) in order to view the structural features; it also means that the micrographs can only show the structure of the specimen at that certain moment i.e. before or after the treatment. However, using SAXS it is possible to examine explanted tissues *during* the treatment; therefore, it allows study of the simultaneous response of the protein to the external factor. It is also important to note that the changes observed on the SAXS patterns correspond to the molecular alterations in a large population of fibrils e.g. the change in the characteristic position and profile of the meridional reflections implies that the majority of fibrils undergo a change in the axial period.

In the studies presented in this thesis, SAXS was used to conduct two dynamic studies:

(1) the effects of an intense X-ray dose on the collagen structure (Chapter Four)

(2) controlled tissue extension of zonular filaments – which was designed to investigate the elastic response of fibrillin microfibrils (Chapter Seven).

The series of frames collected during the X-ray exposure of collagen permitted the examination of metastable states of collagen and showed previously unreported novel variations in its axial structure. Molecular rearrangements induced by an intense X-ray dose are novel and differ from those induced by other treatments such as stretching or drying. The study presented here shows the potential pitfalls of emergent techniques such as the X-ray photon correlation spectroscopy (XPCS) where intense X-ray illumination is used to examine the time dependent density fluctuations in a sample. The high level of hydration in biological samples means that radiation damage is of special importance. The results presented in this thesis showed that the use of an extremely bright X-ray beam enables the estimation of the

damage induced by X-rays as well as investigation of collagen dynamics. New opportunities can potentially emerge from these findings that could involve examination of fast dynamics in collagen using new light sources that are currently under development (i.e. X-ray free-electron lasers, X-FEL). X-FEL sources will be able to provide X-ray radiation with extremely intense and ultra short pulses (on the femtosecond scale), which have a potential to reduce the radiation damage induced in biological samples and would provide new opportunities to examine collagen dynamics.

The results and conclusions from the second dynamic study (i.e. controlled tissue extension of zonular filaments) are described in section 8.5 below. The important findings that resulted from both studies revealed the great potential of using SAXS to conduct dynamic studies and gave an insight into the rearrangements within the molecular structure of biological polymers.

8.3. Using SAXS as a diagnostic tool for breast cancer

Understanding the molecular alterations that occur within the collagen structure during tumour invasion is important for advancement in cancer diagnosis and treatment. It has been shown that metastasis is accompanied by a high expression of matrix metalloproteinases, which are enzymes that are responsible for collagen degradation. In the studies described in Chapter Five, rat tail tendon was used as a source of collagen and the aim was to describe effects of MMPs on this model tissue that contains mainly type I collagen. Tendons were exposed to the enzymatic treatment using Matrix Metalloproteinases and the results obtained suggest a loss of order within collagen axial structure.

In addition to the described experiments, normal and cancerous breast tissues were examined. The aim of this study was to identify the differences in the collagen structure between the two

types of tissues, which can have an important impact on the understanding of collagen degradation *in-situ*, during tumour invasion and for cancer diagnosis. Previous studies have shown differences in the axial periodicity and the diffraction intensity between normal and cancerous tissues; however the study presented here was focused on the analysis of the lateral organization of collagen. The results showed that both the diameter of collagen fibrils and the interfibrillar spacing values were higher in tumour samples; furthermore, these differences were observed at all temperatures examined (5°, 20°, 37° and 60°C).

However, it should be noted that the study described here was performed on a small set of samples; therefore, the results should be treated as initial findings, which need to be confirmed. Future studies should involve a greater number of samples for more statistically significant results. However, when confirmed, these finding will provide new insights into the understanding of collagen degradation induced by MMPs and will play an important role in advancing breast cancer diagnosis and treatment.

Future studies on the effects of MMPs on collagen molecular structure could also include a controlled incubation of normal breast tissues with enzymes (i.e. for various amounts of time). The breast tissue samples incubated with MMPs can also be compared to the tumour tissues to observe if there are differences between changes induced in collagen structure purely by enzymes (incubation of normal breast tissues with MMPs) and changes that occur during tumour invasion.

8.4. The effects of UV light on collagen structure

Chapter Six of this thesis introduced a combined study using SAXS, WAXS, FTIR and EM, designed to describe the effects of UV light on the collagen structure. UV irradiation is used both in biomaterial production (as a method of inducing crosslinking into collagen structure and therefore modifying the properties of collagen materials) and in medicine, where it is used as a method of increasing corneal stiffness as a treatment of keratoconus. Understanding the transformation that occurs within collagen structure during UV irradiation is crucial to control the process and could be used to improve chemical, physical and biological properties of collagen. In order to examine the effects of UV light on collagen, rat tail tendon and skin samples were subjected to UV treatment (i.e. UV exposures from 5 minutes up to 72 hours in both hydrated and dry states). The results suggest that UV light induces crosslinks in collagen structure and the nature of these newly formed crosslinks depends on the level of hydration of collagen. The conformational changes in the collagen triple helix were observed after the irradiation of the samples in the dry state, which was accompanied by a decrease in the axial periodicity. These results may indicate that the crosslinks have been induced in collagen at the molecular level. In comparison to samples irradiated in the dry state, different results were obtained from the examination of samples incubated in a hydrated state: no conformational changes were observed, therefore the formation of crosslinks on a different structural level was suggested, e.g. between collagen fibrils. The measurements also revealed the appearance of a novel, intermediate state that was formed during UV irradiation of hydrated tendons. The newly formed structure was characterized by an unusual 20 nm periodicity and could be a result of local unfolding of the ordered, triple helical structure of collagen. It can also be speculated that this new feature may be due to the modifications of

the suprafibrillar architecture. The identification of intermediate, metastable states that are formed during collagen degradation could be useful in biomaterials, since these structures may potentially have improved properties, compared to normal collagen.

Future studies on the effects of UV light on collagen could involve the use of microfocus X-ray diffraction on skin samples. This technique provides information from thin sections of the biological samples and in the case of UV irradiated skin it could prove useful to observe alterations induced in collagen structure in different layers of skin – from the outer layer (the most exposed to UV light) to the deeper sections, where UV penetration is much poorer. Future studies could also involve the use of additional techniques such as atomic force microscopy (AFM) to examine the nature of 20 nm periodicity intermediate formed during UV irradiation. AFM technique allows the analysis of the surface of a given material with a high-resolution and may potentially provide additional information about the novel structure.

8.5. Understanding fibrillin elasticity

The basis of the elastic properties of fibrillin microfibrils lies in the organization of the fibrillin molecules, which unfortunately is still poorly understood. Chapter Seven of this thesis presents an X-ray diffraction study of hydrated fibrillin-rich microfibrils from zonular filaments, which has been conducted to give an insight into the molecular structure of microfibrils in intact tissue. A series of measurements were taken during controlled tissue extension to observe alterations in the lateral packing of the microfibrils. The results suggest a non-linear correlation between the external strain and a decrease in fibril diameter and lateral spacing. This was accompanied by a non linear increase in the axial periodicity up to a

structure with a 160 nm periodicity, which is reported here for the first time using X-ray diffraction. The results obtained in this study suggest that the intermediate states observed reflect sequential unfolding of fibrillin and can explain the process of its reversible unravelling. These changes may reflect the unravelling of fibrillin from the complex folded arrangement to a linear structure and therefore the results of this study support a 'pleated/folded' model of fibrillin organization where fibrillin molecules are highly folded within the microfibril. The findings resulting from this study have major implications for understanding the functionality and extensibility of fibrillin in connective tissues.

Future studies on fibrillin microfibrils could concentrate on obtaining a signal from fibrillar zonules in an intact eye to examine the structure of fibrillin *in situ*. Since the tensile state of the zonules in the unaccommodated eye is still unknown, it is possible that zonules in the physiological resting state do not have a 56 nm periodicity observed in the explanted tissue, but they might be in one of the metastable states observed during mechanical stretching studies (e.g. with 80 or 100 nm periodicity). The SAXS measurement on the microfibrils *in-situ* (i.e. by removing cornea, but leaving zonular filaments still attached to the lenses) could help to understand the state of the zonules in the unaccomodated eye.

9. References

Afaq F, and Mukhtar H (2006) Botanical antioxidants in the prevention of photocarcinogenesis and photoaging. *Experimental Dermatology* 15: 678-684.

Ala-aho R, and Kahari V M (2005) Collagenases in cancer. *Biochimie* 87: 273-286.

Bailey A J, Rhodes D N, and Cater C W (1964) Irradiation-induced crosslinking of collagen. *Radiation Research* 22: 606-621.

Bailey A J, and Tromans W J (1964) Effects of ionizing radiation on the ultrastructure of collagen fibrils. *Radiation Research* 23: 145-155.

Baldock C, Koster A J, Ziese U, Rock M J, Sherratt M J, Kadler K E, Shuttleworth C A et al. (2001) The supramolecular organization of fibrillin-rich microfibrils. *Journal of Cell Biology* 152: 1045-1056.

Baldock C, Siegler V, Bax D V, Cain S A, Mellody K T, Marson A, Haston J L et al. (2006) Nanostructure of fibrillin-1 reveals compact conformation of EGF arrays and mechanism for extensibility. *Proceedings of the National Academy of Sciences* 103: 11922-11927.

Bard J B L (1990) The role of extracellular matrix in development. In: Hukins, D W L [ed.] *Connective tissue matrix. Part 2.* CRC Press.

Bass L S, Moazami N, Pocsidio J, Oz M C, LoGerfo P, and Treat M R (1992) Changes in Type I collagen following laser welding. *Lasers in Surgery and Medicine* 12: 500-505.

Bear R S (1944) X-ray diffraction studies on protein fibers: I. The large fiber-axis period of collagen. *Journal of the American Chemical Society* 66: 1297-1305

Bella J, Brodsky B, and Berman H M (1995) Hydration structure of a collagen peptide. *Structure* 3: 893-906.

Beniash E, Traub W, Veis A, and Weiner S (2000) A Transmission Electron Microscope study using vitrified ice sections of predentin: structural changes in the dentin collagenous matrix prior to mineralization. *Journal of Structural Biology* 132: 212–225.

Bernhard E J, Gruber S B, and Muschel R J (1994) Direct evidence linking expression of matrix metalloproteinase 9 (92-kDa gelatinase/collagenase) to the metastatic phenotype in transformed rat embryo cells. *Proceedings of the National Academy of Sciences USA* 91: 4293-4297.

Bigi A, Fishera A M, Roveri N, and Koch M H J (1987) Structural modifications of air-dried tendon collagen on heating. *International Journal of Biological Macromolecules* 9: 176-180.

Blattmann H, Gebbers J-O, Brauer-Krisch E, Bravin A, Duc G L, Burkard W, Michiel M D et al. (2005) Application of synchrotron X-rays to radiotherapy. *Nuclear Instruments and Methods in Physics Research A* 548: 17-22.

Bourge J L, Robert A M, Robert L, and Renard G (2007) Zonular fibers, multimolecular composition as related to function (elasticity) and pathology. *Pathologie Biologie* 55: 347-359.

Burd H J, Judge S J, and Flavell M J (1999) Mechanics of accommodation of the human eye. *Vision Research* 39: 1591-1595.

Burgeson R E, and Nimni M E (1992) Collagen types molecular structure and tissue distribution. *Clinical Orthopaedics and Related Research* 282: 250-272.

Cain S A, Morgan A, Sherratt M J, Ball S G, Shuttleworth C A, and Kielty C M (2006) Proteomic analysis of fibrillin-rich microfibrils. *Proteomics* 6: 111-122.

Chandross R J, and Bear R S (1973) Improved Profiles of Electron Density Distribution Along Collagen Fibrils. *Biophys. J.* 13: 1030-1048.

Cravioto H, and Lockwood R (1968) Long-spacing fibrous collagen in human acoustic nerve tumors. In vivo and in vitro observations. *J. Ultrastructure Research* 24: 70-85.

Crews P, Rodriguez J, and Jaspars M (1998) *Organic structure analysis*. New York: Oxford University Press US.

Davis E C (1994) Immunolocalization of microfibril and microfibril-associated proteins in the subendothelial matrix of the developing mouse aorta. *J Cell Sci* 107: 727-736.

Davis E C, Roth R A, Heuser J E, and Mecham R P (2002) Ultrastructural properties of ciliary zonule microfibrils. *Journal of Structural Biology* 139: 65-75.

Dehl R E (1970) Collagen: Mobile Water Content of Frozen Fibers. *Science* 170: 738-739.

Dietz H C, and Pyeritz R E (1995) Mutations in the human gene for fibrillin-1 (FBN1) in the Marfan syndrome and related disorders. *Hum. Mol. Genet.* 4: 1799-1809.

Diffey B L (2002) What is light? *Photodermatology, Photoimmunology & Photomedicine* 18: 68-74.

Dilmanian F A, Morris G M, Zhong N, Bacarian T, Hainfeld J F, Kalef-Ezra J, Brewington L J et al. (2003) Murine EMT- carcinoma: high therapeutic efficacy of microbeam radiation therapy. *Radiation Research* 159: 632-641.

Dilmanian F A, Qu Y, Liu S, Cool C D, Gilbert J, Hainfeld J F, Kruse C A et al. (2005) X-ray microbeams: Tumor therapy and central nervous system research. *Nucl Instrum Methods Phys Res A* 548: 30-37.

Downing A K, Knott V, Werner J M, Cardy C M, Campbell I D, and Handford P A (1996) Solution Structure of a Pair of Calcium-Binding Epidermal Growth Factor-like Domains: Implications for the Marfan Syndrome and Other Genetic Disorders. *Cell* 85: 597-605.

Duffy M J (1987) Do proteases play a role in cancer invasion and metastasis? *European Journal of Cancer and Clinical Oncology* 23: 583-589.

Duffy M J, Maguire T M, Hill A, McDermott E, and O'Higgins N (2000) Metalloproteinases: role in breast carcinogenesis, invasion and metastasis. *Breast Cancer Research* 2: 252-257.

Dyer J M, Bringans S D, and Bryson W G (2006) Characterisation of photo-oxidation products within photoyellowed wool proteins: tryptophan and tyrosine derived chromophores. *Photochem. Photobiol. Sci.* 5: 698–706.

Egeblad M, and Werb Z (2002) New functions for the matrix metalloproteinases in cancer progression. *Nature Reviews* 2: 161-174.

Fernandez M, Keyrilainen J, Karjalainen-Lindsberg M-L, Leidenius M, Smitten K v, Fiedler S, and Suortti P (2004) Human breast tissue characterisation with small-angle X-ray scattering. *Spectroscopy* 18: 167-176.

Fernandez M, Keyrilainen J, Serimaa R, Torkkeli M, Karjalainen-Lindsberg M-L, Tenhunen M, Thomlinson W et al. (2002) Small-angle X-ray scattering studies of human breast tissue samples. *Phys. Med. Biol.* 47: 577-592.

Fisher G J, Wang Z, Datta S C, Varani J, Kang S, and Voorhees J J (1997) Pathophysiology of premature skin aging induced by Ultraviolet light. *The New England Journal of medicine* 337: 1419-1429.

Folkhard W, Mosler E, Geercken W, Knorzen E, Nemetschek-Gansler H, and Nemetschek T (1987) Quantitative analysis of the molecular sliding mechanism in native tendon collagen time-resolved dynamic studies using synchrotron radiation. *International Journal of Biological Macromolecules* 9: 169-175.

Fraser R D B, and MacRae T P (1973) *Conformation in fibrous proteins*. Academic Press.

Fraser R D B, MacRae T P, and Suzuki E (1979) Chain conformation in the collagen molecule. *Journal of Molecular Biology* 129: 463-481.

Fratzl P (2003) Cellulose and collagen: from fibres to tissues. *Current Opinion in Colloid and Interface Science* 8: 32-39.

Fratzl P, Misof K, and Zizak I (1997) Fibrillar Structure and Mechanical Properties of Collagen. *Journal of Structural Biology* 122: 119-122.

Giacomoni P U, and D'Alessio P (1996) Open questions in photobiology IV. Photoaging of the skin. *Journal of Photochemistry and Photobiology B: Biology* 33: 267-272.

Gibson M A, Hatzinikolas G, Kumaratilake J S, Sandberg L B, Nicholl J K, Sutherland G R, and Cleary E G (1996) Further Characterization of Proteins Associated with Elastic Fiber Microfibrils Including the Molecular Cloning of MAGP-2 (MP25). *J. Biol. Chem.* 271: 1096-1103.

Glatter O, and Kratky O (1982) *Small-angle X-ray scattering.* Academic Press.

Goh K L, Hiller J, Haston J L, Holmes D F, Kadler K E, Murdoch A, Meakin J R et al. (2005) Analysis of collagen fibril diameter distribution in connective tissues using small-angle X-ray scattering. *Biochim Biophys Acta.* 1722: 183-188.

Gonzalez L, and Wess T J (2008) Use of Attenuated Total Reflection-Fourier Transform Infrared Spectroscopy to measure collagen degradation in historical parchments. *Applied Spectroscopy* 62: 1108-1114.

Gorham S D, Light N D, Diamond A M, Willins M J, Bailey A J, Wess T J, and Leslie N J (1992) Effect of chemical modifications on the susceptibility of collagen to proteolysis. II. Dehydrothermal crosslinking. *International Journal of Biological Macromolecules* 14: 129-137.

Grant R A, Cox R W, and Kent C M (1970) The effects of irradiation with high energy electrons on the structure and reactivity of native and cross-linked collagen fibres. *J. Cell Sci.* 7: 387-405.

Gruijl F R (2002) Photocarcinogenesis: UVA vs. UVB radiation. *Skin Pharmacology and Applied Skin Physiology* 15: 316-320.

Hammersley A P (1997) ESRF Internal Report. *Publication no ESRF97HA02T. Grenoble, France.*

Hammond C (1997) *The basics of crystallography and diffraction.* Oxford: Oxford University Press.

Handford P A, Downing A K, Reinhardt D P, and Sakai L Y (2000) Fibrillin: from domain structure to supramolecular assembly. *Matrix Biology* 19: 457-470.

Hansen K A, Weiss J A, and Barton J K (2002) Recruitment of tendon crimp with applied tensile strain. *Journal of Biomechanical Engineering* 124: 72-77.

Hanssen E, Franc S, and Garrone R (1998) Atomic force microscopy and modeling of natural elastic fibrillin polymers. *Biol. Cell* 90: 223-228.

Hanssen E, Hew F H, Moore E, and Gibson M A (2004) MAGP-2 Has Multiple Binding Regions on Fibrillins and Has Covalent Periodic Association with Fibrillin-containing Microfibrils. *J. Biol. Chem.* 279: 29185-29194.

Hasegawa T, Umemura J, and Yamada N (2005) Characterization of thin cast films of a trileucine-induced lipid by infrared multiple-angle incidence resolution spectrometry. *Journal of Molecular Structure* 735-736: 63-67.

Haston J L, Engelsen S B, Roessle M, Clerkson J, Blanch E W, Baldock C, Kielty C M et al. (2003) Raman microscopy and X-ray diffraction, a combined study of fibrillin-rich microfibrillar elasticity. *Journal of Biological Chemistry* 278: 41189-41197.

Hay E D (1991) *Cell biology of extracellular matrix*. Second ed. New York: Plenum Press.

Helliwell J R (2006) X-ray diffraction at Synchrotron Light sources.*Encyclopedia of Life Sciences*. Chichester: John Wiley & Sons, Ltd.

Henderson M, Polewski R, Fanning J C, and Gibson M A (1996) Microfibril-associated glycoprotein-1 (MAGP-1) is specifically located on the beads of the beaded-filament structure for fibrillin-containing microfibrils as visualized by the rotary shadowing technique. *J. Histochem. Cytochem.* 44: 1389-1397.

Holmes D F, and Kadler K E (2005) The Precision of Lateral Size Control in the Assembly of Corneal Collagen Fibrils. *Journal of Molecular Biology* 345: 773-784.

Hulmes D J S, Wess T J, Prockop D J, and Fratzl P (1995) Radial packing, order, and disorder in collagen fibrils. *Biophysical Journal* 68: 1661-1670.

Jozsa L, Kannus P, Balint J B, and Reffy A (1991) Three-dimensional ultrastructure of human tendons. *Acta Anat* 142: 306-312.

Judge D P, and Dietz H C (2005) Marfan's syndrome. *Lancet* 366: 1965-19761.

Kadler K E, Holmes D F, Trotter J A, and Chapman J A (1996) Collagen fibril formation. *Biochem. J.* 316: 1-11.

Kaminska A, and Sionkowska A (1995) Effect of UV radiation on the infrared spectra of collagen. *Polymer Degradation and Stability* 51: 19-26.

Kannus P (2000) Structure of the tendon connective tissue. *Scandinavian Journal of Medicine and Science in Sports* 10: 312–320.

Kastelic J, Galeski A, and Baer E (1978) The multicomposite structure of tendon. *Connective Tissue Research* 6: 11-23.

Kastelic J, Palley I, and Baer E (1980) A structure mechanical model for tendon crimping. *Journal of Biomechanics* 13: 887-893.

Keene D R, Maddox B K, Kuo H J, Sakai L Y, and Glanville R W (1991) Extraction of extendable beaded structures and their identification as fibrillin-containing extracellular matrix microfibrils. *J. Histochem. Cytochem.* 39: 441-449.

Kennedy C J, Hiller J C, Lammie D, Drakopoulos M, Vest M, Cooper M, Adderley W P et al. (2004) Microfocus X-ray diffraction of historical parchment reveals variations in structural features through parchment cross sections. *Nano Letters* 4: 1373-1380.

Kessler A, Rosen H, and Levenson S M (1960) Chromatographic fractionation of acetic acid-solubilized rat tail tendon collagen. *The Journal of Biological Chemistry* 235: 989-994.

Kielty C, Wess T J, Haston L, Ashworth J, Sherratt M, and Shuttleworth C (2002) Fibrillin-rich microfibrils: elastic biopolymers of the extracellular matrix. *Journal of Muscle Research and Cell Motility* 23: 581-596.

Kielty C M, Sherratt M J, Marson A, Baldock C, David A D P, and John M S (2005) Fibrillin Microfibrils. *Advances in Protein Chemistry* 70: 405-436.

Kielty C M, and Shuttleworth C A (1993) Synthesis and assembly of fibrillin by fibroblasts and smooth muscle cells. *J Cell Sci* 106: 167-173.

Kielty C M, and Shuttleworth C A (1995) Fibrillin-containing microfibrils: Structure and function in health and disease. *The International Journal of Biochemistry & Cell Biology* 27: 747-760.

Kim J K, Xu Y, Xu X, Keene D R, Gurusiddappa S, Liang X, Wary K K et al. (2005) A Novel Binding Site in Collagen Type III for Integrins {alpha}1{beta}1 and {alpha}2{beta}1. *J. Biol. Chem.* 280: 32512-32520.

Kuo C L, Isogai Z, Keene D R, Hazeki N, Ono R N, Sengle G, Peter Bachinger H et al. (2007) Effects of Fibrillin-1 Degradation on Microfibril Ultrastructure. *J. Biol. Chem.* 282: 4007-4020.

Lammie D, Bain M M, and Wess T J (2005) Microfocus X-ray scattering investigations of eggshell nanostructure. *Journal of Synchrotron Science* 12: 721-726.

Lee S S J, Knott V, Jovanovic J, Harlos K, Grimes J M, Choulier L, Mardon H J et al. (2004) Structure of the integrin binding fragment from fibrillin-1 gives new isights into microfibril organization. *Structure* 12: 717-729.

Lees S (1986) Water content in type I collagen tissues calculated from the generalized packing model. *International Journal of Biological Macromolecules* 8: 66-72.

Lin A C, and Goh M C (2002) Investigating the ultrastructure of fibrous long spacing collagen by parallel atomic force and transmission electron microscopy. *PROTEINS: Structure, Function, and Genetics* 49: 378-384.

Linsenmayer T F (1991) Collagen. In: Hay, E D [ed.] *Cell biology of extracellular matrix.* (Second edn.) New York: Plenum Press.

Liu Y, Cho R K, Sakuri K, Miura T, and Ozaki Y (1994) Studies on spectra/structure correlations in near-infrared spectra of proteins and polypeptides. Part I: A marker band for hydrogen bonds. *Applied Spectroscopy* 48: 1181-1295.

Lowy J, and Poulsen F R (1982) Time-resolved X-ray diffraction studies of the structural behaviour of myosin heads in a living contracting unstriated muscle. *Nature* 299: 308-312.

Lowy J, and Poulsen F R (1990) Studies of the diffuse x-ray scattering from contracting frog skeletal muscles. *Biophys. J.* 57: 977-985.

Majewski A J, Sanzari M, Cui H-L, and Torzilli P (2002) Effects of ultraviolet radiation on the type-I collagen protein triple helical structure: A method for measuring structural changes through optical activity. *Physical review E* 65.

Marchini M, Morocutti M, Ruggeri A, Koch M H J, Bigi A, and Roveri N (1986) Differences in the fibril structure of corneal and tendon collagen. An electron microscopy and X-ray diffraction investigation. *Connective Tissue Research* 15: 269-281.

Maxwell C A, Wess T J, and Kennedy C J (2006) X-ray Diffraction Study into the Effects of Liming on the Structure of Collagen. *Biomacromolecules* 7: 2321-2326.

McLaren A D, and Shugar D (1964) *Photochemistry of proteins and nucleic acids.* Pergamon Press.

Mecham R P, and Heuser J E (1991) The elastic fiber. In: Hay, E D [ed.] *Cell Biology of Extracellular Matrix.* (2nd edn.) Plenum Press, pp. 79-109.

Meek K M, Chapman J A, and Hardcastle R A (1979) The staining pattern of collagen fibrils. *Journal of Biological Chemistry* 254: 10710-10714.

Meek K M, Fullwood N J, Cooke P H, Elliott G F, Maurice D M, Quantock A J, Wall R S et al. (1991) Synchrotron x-ray diffraction studies of the cornea, with implications for stromal hydration. *Biophys. J.* 60: 467-474.

Meek K M, and Quantock A J (2001) The use of X-ray scattering techniques to determine corneal ultrastructure. *Progress in Retinal and Eye Research* 20: 93-137.

Mencucci R, Mazzotta C, Rossi F, Ponchietti C, Pini R, Baiocchi S, Caporossi A et al. (2007) Riboflavin and ultraviolet A collagen crosslinking: In vivo thermographic analysis of the corneal surface. *Journal of Cataract & Refractive Surgery* 33: 1005-1008.

Menter J M, Williamson G D, Carlyle K, Moore C L, and Willis I (1995a) Photochemistry of type I acid-soluble calf skin collagen: dependence on excitation wavelength. *Photochemistry and Photobiology* 62: 402-408.

Menter J M, Williamson G D, Carlyle K, Moore C L, and Willis I (1995b) Photochemistry of type I acid-soluble calf skin collagen: dependence on excitation wavelength. *Photochemistry and Photobiology* 62: 402-408.

Metcalfe A D, and Ferguson M W J (2007) Tissue engineering of replacement skin: the crossroads of biomaterials, wound healing, embryonic development, stem cells and regeneration. *Journal of The Royal Society Interface* 4: 413-437.

Miki H, Unno K, Park P, Ohno T, and Nakajima M (1993) Morphogenesis and origin of fibrous long-spacing collagen fibers in collagenase-treated mouse skin tissues. *Tissue and Cell* 25: 669-680.

Miles C A, Burjanadze T V, and Bailey A J (1995) The kinetics of the thermal denaturation of collagen in unrestrained rat tail tendon determined by differential scanning calorimetry. *J. Mol. Biol.* 245: 437-446.

Miles C A, and Ghelashvili M (1999) Polymer-in-a-box mechanism for the thermal stabilization of collagen molecules in fibers. *Biophysical Journal* 76: 3243-3252.

Miles C A, Sionkowska A, Hulin S L, Sims T J, Avery N C, and Bailey A J (2000) Identification of an intermediate state in the helix-coil. Degradation of collagen by ultraviolet light. *Journal of Biological Chemistry* 275: 33014-33020.

Mosler E, Folkhard W, Knorzer E, Nemetschek-Gansler H, and Nemetschek T (1985) Stress-induced molecular rearrangements in tendon collagen. *J. Mol. Biol.* 182: 589-596.

Newsome D A, Gross J, and Hassell J R (1982) Human corneal stroma contains three distinct collagens. *Invest. Ophthalmol. Vis. Sci.* 22: 376-381.

Nicholls S P, Gathercole L J, Keller A, and Shah J S (1983) Crimping in rat tail tendon collagen: morphology and transverse mechanical anisotropy. *International Journal of Biological Macromolecules* 5: 283-288.

Nollen G J, and Mulder B J M (2004) What is new in the Marfan syndrome? *International Journal of Cardiology* 97: 103-108.

Overall C M, and Lopez-Otin C (2002) Strategies for MMP inhibition in cancer: innovations for the post-trial era. *Nature Reviews* 2: 657-672.

Paige M F, Lin A C, and Goh M C (2002) Real-time enzymatic biodegradation of collagen fibrils monitored by atomic force microscopy. *International Biodeterioration and Biodegradation* 50: 1-10.

Paige M F, Rainey J K, and Goh M C (1998) Fibrous long spacing collagen ultrastructure elucidated by atomic force microscopy. *Biophysical Journal* 74: 3211-3216.

Pardo A, and Selman M (2005) MMP-1: the elder of the family. *The International Journal of Biochemistry and cell Biology* 37: 283-288.

Pavia D L, Lampman G M, and Kriz G S (1996) *Introduction to spectroscopy*. second ed. Harcourt Brace College Publishers.

Payne K J, and Veis A (1988) Fourier transform IR spectroscopy of collagen and gelatin solutions: deconvolution of the Amide I band for conformational studies. *Biopolymers* 27: 1749-1760.

Petruska J A, and Hodge A J (1964) A subunit model for the tropocollagen macromolecule. *Proceedings of the National Academy of Sciences* 51: 871-876.

Pineri M H, Escoubes M, and Roche G (1978) Water-collagen interactions: Calorimetric and mechanical experiments. *Biopolymers* 17: 2799-2815.

Price R I, Lees S, and Kirschner D A (1997) X-ray diffraction analysis of tendon collagen at ambient and cryogenic temperatures: role of hydration. *International Journal of Biological Macromolecules* 20: 23-33.

Pucci-Minafra I, Andriolo M, Basirico L, Alessandro R, Luparello C, Buccellato C, Garbelli R et al. (1998) Absence of regular alpha2(I) collagen chains in colon carcinoma biopsy fragments. *Carcinogenesis* 19: 575-584.

Pucci-Minafra I, Luparello C, Andriolo M, Basirico L, Aquino A, and Minafra S (1993) A new form of tumor and fetal collagen that binds laminin. *Biochemistry* 32: 7421-7427.

Purslow P, Wess T J, and Hukins D W L (1998) Collagen orientation and molecular spacing during creep and stress-relaxation in soft connective tissues. *The Journal of Experimental Biology* 201: 135-142.

Puxkandl R, Zizak I, Paris O, Keckes J, Tesch W, Bernstorff S, P P et al. (2002) Viscoelastic properties of collagen: synchrotron radiation investigations and structural model. *Phil. Trans. R. Soc. Lond. B* 357: 191-197.

Rajkumar G, Al-Khayat H A, Eakins F, He A, Knupp C, and Squire J M (2005) FibreFix – A New Integrated CCP13 Software Package. *Fibre Diffraction Review* 13: 11-18.

Randall J T, Fraser R D B, Jackson S, Martin A V W, and North A C T (1952) Aspects of collagen structure. *Nature* 169: 1029-1033.

Reinhardt D P, Keene D R, Corson G M, Poschl E, Bachinger H P, Gambee J E, and Sakai L Y (1996) Fibrillin-1: Organization in Microfibrils and Structural Properties. *Journal of Molecular Biology* 258: 104-116.

Rest M v d, and Garrone R (1991) Collagen family of proteins. *The FASEB Journal* 5: 2814-2823.

Rhodes G (2000) *Crystallography made crystal clear.* Second Edition ed. San Diego: Academic Press.

Ricard-Blum S, and Ruggiero F (2005) The collagen superfamily: from the extracellular matrix to the cell membrane. *Pathologie Biologie* 53: 430-442.

Rittie L, and Fisher G J (2002) UV-light-induced signal cascades and skin aging. *Ageing Research Reviews* 1: 705-720.

Rosso F, Marino G, Giordano A, Barbarisi M, Parmeggiani D, and Barbarisi A (2005) Smart materials as scaffolds for tissue engineering. *Journal of Cellular Physiology* 203: 465-470.

Round A R, Wilkinson S J, C.J. H, K.D. R, Glatter O, T.J W, and I.O. E (2005) A preliminary study of breast cancer diagnosis using laboratory based small angle x-ray scattering. *Physics in Medicine and Biology* 50: 1-10.

Saika S, Miyamoto T, Tanaka T, Ishida I, Ohnishi Y, and Ooshima A (2001) Collagens XII and XIV (FACITs) in capsular opacification and in cultured lens epithelial cells. *Current Eye Research* 23: 463–468.

Sakai L Y, Keene D R, and Engvall E (1986) Fibrillin, a new 350-kD glycoprotein, is a component of extracellular microfibrils. *J. Cell Biol.* 103: 2499-2509.

Sakai L Y, Keene D R, Glanville R W, and Bachinger H P (1991) Purification and partial characterization of fibrillin, a cysteine-rich structural component of connective tissue microfibrils. *J. Biol. Chem.* 266: 14763-14770.

Sandler U, and Wyler A (2000) Phase transitions in fiber materials. *Physical Review B* 61.

Sasaki N, and Odajima S (1996) Elongation mechanism of collagen fibrils and force-strain relations of tendon at each level of structural hierarchy. *Journal of Biomechanics* 29: 1131-1136.

Sasaki N, Shukunami N, Matsushima N, and Izumi Y (1999) Time-resolved X-ray diffraction from tendon collagen during creep using synchrotron radiation. *Journal of Biomechanics* 32: 285-292.

Senechal M (1995) *Quasicrystals and geometry*. Cambridge: Cambridge University Press.

Sherratt M J, Baldock C, Haston L J, Holmes D F, Jones C J P, Shuttleworth A C, Wess T J et al. (2003) Fibrillin Microfibrils are Stiff Reinforcing Fibres in Compliant Tissues. *Journal of Molecular Biology* 332: 183-193.

Sherratt M J, Holmes D F, Shuttleworth C A, and Kielty C M (1997) Scanning transmission electron microscopy mass analysis of fibrillin-containing microfibrils from foetal elastic tissues. *The International Journal of Biochemistry & Cell Biology* 29: 1063-1070.

Sherratt M J, Wess T J, Baldock C, Ashworth J L, Purslow P, Shuttleworth C A, and Kielty C M (2001) Fibrillin-rich microfibrils of the extracellular matrix: ultrastructure and assembly. *Micron* 32: 185-200.

Sionkowska A (2000) Modification of collagen films by ultraviolet irradiation. *Polymer Degradation and Stability* 68: 147-151.

Sionkowska A (2005) Thermal denaturation of UV-irradiated wet rat tail tendon collagen. *International Journal of Biological Macromolecules* 35: 145-149.

Sionkowska A (2006) The influence of UV light on collagen/polyethylene glycol blends. *Polymer Degradation and Stability* 91: 305-312.

Sionkowska A, and Wess T J (2004) Mechanical properties of UV irradiated rat tail tendon (RTT) collagen. *International Journal of Biological Macromolecules* 34: 9-12.

Sionkowska A, Wisniewski M, Skopinska J, Kennedy C J, and Wess T J (2004) Molecular interactions in collagen and chitosan blends. *Biomaterials* 25: 795-801.

Slatkin D N, Spanne P, Dilmanian F A, Gebbers J-O, and Laissue J A (1995) Subacute neuropathological effects of microplanar beams of x-rays from a synchrotron wiggler. *Proceedings of the National Academy of Sciences* 92: 8783-8787.

Somasundaran P (2006) *Encyclopeadia of Surface and Colloid Science*. New York: CRC Press.

Spoerl E, Huhle M, and Seiler T (1998) Induction of cross-links in corneal tissue. *Exp. Eye Res.* 66: 97-103.

Stinson R H, and Sweeny P R (1980) Skin collagen has an unusual d-spacing. *Biochim Biophys Acta.* 621: 158-161.

Sudoh K, and Noda H (1972) UV-irradiation of collagen and its effect on fibril reconstitution. *Connective Tissue Research* 1: 267-274.

Tomlin S G, and Worthington C R (1956) Low-angle X-ray diffraction patterns of collagen. *Proceedings of the Royal Society of London. Series A* 235: 189-201.

Torikai A, and Shibata H (1999) Effect of Ultraviolet radiation on photodegradation of collagen. *Journal of Applied Polymer Science* 73: 1259 - 1265.

Towns-Andrews E, Berry A, Bordas J, Mant G R, Murray P K, Roberts K, Sumner I et al. (1989) Time-resolved X-ray diffraction station: X-ray optics, detectors, and data acquisition. *Rev. Sci. Instrum.* 60: 2346-2349.

Venturoni M, Gutsmann T, Fantner G E, Kindt J H, and Hansma P K (2003) Investigations into the polymorphism of rat tail tendon fibrils using atomic force microscopy. *Biochemical and Biophysical Research Communications* 303: 508-513.

Wallace R N, Streeten B W, and Hanna R B (1991) Rotary shadowing of elastic system microfibrils in the ocular zonule, vitreous, and ligamentum nuchae. *Current Eye Research* 10: 99 - 109.

Wang J H C (2006) Mechanobiology of tendon. *Journal of Biomechanics* 39: 1563-1582.

Wang L (2003) Mammography and Beyond: Building Better Breast Cancer Screening Tests. *J. Natl. Cancer Inst.* 95: 344-346.

Wang X, Li X, and Yost M J (2005) Microtensile testing of collagen fibril for cardiovascular tissue engineering. *Journal of Biomedical Materials Research Part A* 74: 263-268.

Weadock K S, Miller E J, Bellincampi L D, Zawadsky J P, and Dunn M G (1995) Physical crosslinking of collagen fibers: Comparison of ultraviolet irradiation and dehydrothermal treatment. *Journal of Biomedical Materials Research* 29: 1373-1379.

Wess T J, Drakopoulos M, Snigirev A, Wouters J, Paris O, Fratzl P, Collins M et al. (2001) The use of small-angle X-ray diffraction studies for the analysis of structural features in archeological samples. *Archaeometry* 43: 117-129.

Wess T J, and Orgel J P (2000) Changes in collagen structure: drying, dehydrothermal treatment and relation to long term deterioration. *Thermochimica Acta* 365: 119-128.

Wess T J, Purslow P P, and Kielty C M (1997) Fibrillin-rich microfibrils: an X-ray diffraction study of the fundamental axial periodicity. *FEBS* 413: 424-428.

Wess T J, Purslow P P, and Kielty C M (1998) X-ray diffraction studies of fibrillin-rich microfibrils: effects of tissue extension on axial and lateral packing. *J Struct Biol.* 122: 123-127.

Williamson G K, and Hall W H (1953) X-ray line broadening from filed aluminium and wolfram. *Acta Metallurgica* 1: 22-31.

Wollensak G (2006) Crosslinking treatment of progressive keratoconus: new hope. . *Current Opinion in Ophthalmology.* 17: 356-360.

Wollensak G, Spoerl E, and Seiler T (2003) Riboflavin/ultraviolet-a-induced collagen crosslinking for the treatment of keratoconus. *American Journal of Ophthalmology* 135: 620-627.

Worthington C R, and Tomlin S G (1955) Small-angle X-ray diffraction patterns of collagen. *Nature* 175: 811.

Wright N T, and Humphrey J D (2002) Denaturation of collagen via heating: an irreversible rate process. *Annu. Rev. Biomed. Eng.* 4: 109-128.

Yakimets I, Wellner N, Smith A C, Wilson R H, Farhat I, and Mitchell J (2005) Mechanical properties with respect to water content of gelatin films in glassy state. *Polymer* 46: 12577-12585.

Yuan X, Werner J M, Lack J, Knott V, Handford P A, Campbell I D, and Downing A K (2002) Effects of the N2144S mutation on backbone dynamics of a TB-cbEGF domain pair from human fibrillin-1. *Journal of Molecular Biology* 316: 113-125.

Appendix 1

Publications

J. Glab, T. J. Wess (2008) Changes in the Molecular Packing of Fibrillin Microfibrils During Extension Indicate Intrafibrillar and Interfibrillar Reorganization in Elastic Response. J. Mol. Biol. 383: 1171–1180

J. Glab, T. J. Wess, K. Thomas (2009) X-Ray Scattering of Biomolecules. Encyclopedia of Nanoscience and Nanotechnology, American Scientific Publishers